Study on Probabilistic Image Processing by Extended Gauss-Markov Random Fields

Master's Thesis

Study on Probabilistic Image Processing by Extended Gauss-Markov Random Fields

Department of Applied Information Sciences,
Graduate School of Information Sciences,
TOHOKU University

Nicolas Morin
A7IM4501
(March 2010)

Contents

Chapter 1

Introduction

1.1 Background

In image restoration, we are interested in recovering an original image $\boldsymbol{f}$ from a degraded version of that image $\boldsymbol{g}$ in order to improve the quality of the degraded image. In our research, we consider the case where the original image is degraded by noise. Such a degradation can have various causes such as film grain, electronic noise or quantization and its impact is the most severe in low signal situations such as low-light photography or low-dose X-ray imaging.

Unfortunately, since there is no way to find the exact original image from the degraded image, we are concerned with finding the best possible estimate of the original image. To do so, we use probability as a tool and try to find a restored image which has a high probability of being very similar to the original image. In our research, we use Bayesian probability where we find the original image estimate $\widehat{\boldsymbol{f}}$ by defining a prior probability model for the original image $\Pr\{\boldsymbol{f}\}$ based on the expected structure of the image and a conditional probability model for the degraded image $\Pr\{\boldsymbol{g}|\boldsymbol{f}\}$ based on the way we assume the degraded image is generated from the original image. These allow us to define a posterior probability for the original image as a function of the degraded image $\Pr\{\boldsymbol{f}|\boldsymbol{g}\} \propto \Pr\{\boldsymbol{g}|\boldsymbol{f}\}\Pr\{\boldsymbol{f}\}$.

The basis for our models is the conditional autoregression model (CAR) defined by Molina in [1] and for which the exact expressions for the marginal likelihood and the restored image as a function of the degraded image and model hyperparameters was obtained by Tanaka and Inoue in [2] and [3] for binary and greyscale images and by Tanaka and Horiguchi in [4] for colour images in the *RGB* space. It is also interesting to note that probabilistic image processing is considered to have a close relationship to the spin glass theory in the field of statistical mechanics [5], which constitutes the inspiration for one of our proposed models.

1.2 Objectives

Our objective is to explore ways of extending the CAR model in order to improve its performance with regards to image correction for both greyscale and colour images. To do so, we investigate two extensions to the model: the extension to the second-neighbour interactions and the extension to the third-neighbour interactions. We are also interested in evaluating the computational complexity of the algorithms constructed using our extended models.

The motivation behind the extension to the second-neighbour interactions is that we expect such an extension to help preserve the edges in the corrected images. Indeed, Fan and Wu described an extension of the Ising model (a mathematical model of ferromagnetism in statistical mechanics used in spin glass theory, among others) to second-neighbour interactions in [6]. They showed that depending on the values of the parameters controlling first- and second-neighbour interactions, there can be three spin configurations of lowest energy. These configurations are the ferromagnetic, antiferromagnetic and superantiferromagnetic states and are illustrated in Fig. 1.1. Our hypothesis is that by similarly extending the CAR model to second-neighbour interactions, we can preserve diagonal edges by approaching the antiferromagnetic state or horizontal and vertical edges by approaching the superantiferromagnetic state.

The motivation behind the extension to the third-neighbour interactions is that cortical neural tissues are often modelled mathematically as neural fields. One such neural field which is used to model the

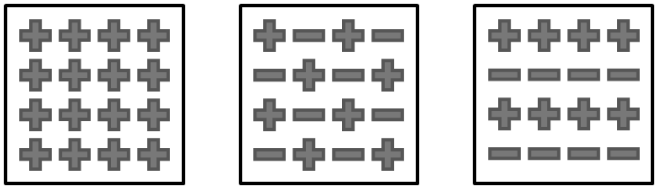

(a) $J > 2|J'|$ (b) $J < -2|J'|$ (c) $-|J| > 2J'$

Figure 1.1: Spin configurations of lowest energy for the Ising model with second-neighbour interactions. J and J' refer to the parameters controlling first- and second-neighbour interactions respectively. These parameters correspond to the hyperparameters α and α' in our second-neighbour interactions model. (a) Ferromagnetic state. $J > 2|J'|$. (b) Antiferromagnetic state. $J < -2|J'|$. (c) Superantiferromagnetic state. $-|J| > 2J'$.

human visual system is the lateral inhibition type field and is characterized by a weighting function giving a positive weight near to the origin and a negative or zero weight as we move away from the origin [7][8][9]. Here, a positive weight represents neuron stimulation and a negative weight represents neuron inhibition. Such a weighting function is called a mexican-hat weighting function and is illustrated in Fig. 1.2. Our hypothesis is that we can improve image correction by trying to reproduce a lateral inhibition type field. This is done by approximating the mexican-hat weighting function through the use of hyperparameters controlling the weights of the second- and third-neighbour pixel interactions relative to the weight of the nearest-neighbour pixel interactions as shown by the arrows in Fig 1.2.

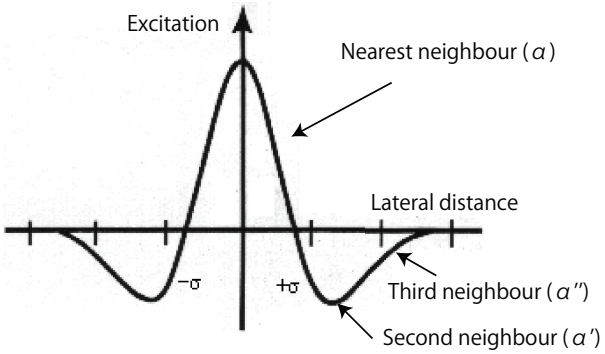

Figure 1.2: Mexican-hat weighting function. The x-axis represents lateral distance relative to the origin. The y-axis represents neuron excitation where positive values represent neuron stimulation and negative values represent neuron inhibition. The arrows represent the relative weights for nearest-, second- and third-neighbour pixel interactions which we expect can approximate a lateral inhibition type field. The values α, α' and α'' correspond to the hyperparameters controlling the pixel weights in our third-neighbour interactions model.

1.3 Structure

This thesis consists of 6 chapters. In chapter 2, we present an extended version of the CAR model to the second-neighbour interactions for greyscale image restoration. In chapter 3, we extend the model of chapter 2 to colour images. Chapter 4 presents a model with third-neighbour interactions for greyscale images and that model is also extended to colour images in chapter 5. Finally, we conclude in chapter 6 with a summary of our thesis and a description of future tasks related to our research.

Chapter 2

Solvable Probabilistic Model with Second-Neighbour Interaction for Grayscale Image Restoration

2.1 Chapter Outline

In this chapter, we shall describe the extension to the second-neighbour pixel interactions of the solvable probabilistic model for greyscale images originally proposed by Tanaka in [3]. We start with a detailed description of the model as well as the calculations involved in its formation. This is followed by the presentation of an image correction algorithm based on this model before concluding with a description of the numerical experiments we performed to evaluate this model.

2.2 Model Description

In this section we describe in detail the equations that form the basis of our solvable probabilistic model with second-neighbour interaction for grayscale image restoration. From these equations, we also derive mathematical expressions that can be used to implement an efficient image correction algorithm.

2.2.1 Image Model

We consider an image to be composed of a set of pixels on a square lattice. The lattice is defined as $\mathbf{V} \equiv \{(x,y)\,|x = 0,1,\ldots,V_x - 1, y = 0,1,\ldots,V_y - 1\}$ with $V_x = V_y$ so that the number of pixels in an image is defined as $|\mathbf{V}| = V_x \times V_y$. We also consider the lattice to be on a torus so that it satisfies the periodic boundary conditions. We define a pixel as a real value corresponding to the light intensity at that location on the lattice, so that we have the values $f_{x,y}$ and $g_{x,y}$ corresponding to the pixel (x,y) in the original and the degraded images respectively. Thus the configurations of the original and degraded images are represented by $\boldsymbol{f} = \{f_{x,y} \in \mathbb{R}|\,(x,y) \in \mathbf{V}\}$ and $\boldsymbol{g} = \{g_{x,y} \in \mathbb{R}|\,(x,y) \in \mathbf{V}\}$ respectively. We associate the random variables $\boldsymbol{F} = \{F_{x,y} \in \mathbb{R}|\,(x,y) \in \mathbf{V}\}$ and $\boldsymbol{G} = \{G_{x,y} \in \mathbb{R}|\,(x,y) \in \mathbf{V}\}$ to the original and degraded images respectively.

2.2.2 Degradation Process Model

The model for the image degradation is additive white Gaussian noise $N(0,\sigma^2)$ added independently to each pixel. Thus we have the conditional probability function

$$\Pr\{\boldsymbol{G} = \boldsymbol{g}|\boldsymbol{F} = \boldsymbol{f}, \sigma\} \equiv \frac{1}{Z_{\text{noise}}(\sigma)} \exp\left(-\frac{1}{2\sigma^2}\|\boldsymbol{g} - \boldsymbol{f}\|^2\right) \tag{2.1}$$

where

$$Z_{\text{noise}}(\sigma) \equiv \int \exp\left(-\frac{1}{2\sigma^2}\|\boldsymbol{z} - \boldsymbol{f}\|^2\right) d\boldsymbol{z}, \tag{2.2}$$

with $\int d\boldsymbol{z} \equiv \int_{-\infty}^{+\infty} \int_{-\infty}^{+\infty} \cdots \int_{-\infty}^{+\infty} \prod_{(x,y)\in\mathbf{V}} dz_{x,y}$, is the normalization constant and

$$\|\boldsymbol{g}-\boldsymbol{f}\|^2 \equiv \sum_{(x,y)\in\mathbf{V}} (g_{x,y}-f_{x,y})^2. \tag{2.3}$$

By substituting (2.3) into (2.2) and using the Gaussian integral formula, we can find the value of $Z_{\text{noise}}(\sigma)$ as follows:

$$\begin{aligned}
Z_{\text{noise}}(\sigma) &= \int \exp\left(-\frac{1}{2\sigma^2}\sum_{(x,y)\in\mathbf{V}} (z_{x,y}-f_{x,y})^2\right) d\boldsymbol{z} \\
&= \int \prod_{(x,y)\in\mathbf{V}} \exp\left(-\frac{1}{2\sigma^2}(z_{x,y}-f_{x,y})^2\right) d\boldsymbol{z} \\
&= \prod_{(x,y)\in\mathbf{V}} \int \exp\left(-\frac{1}{2\sigma^2}(z_{x,y}-f_{x,y})^2\right) dz_{x,y} \\
&= \prod_{(x,y)\in\mathbf{V}} \sqrt{2\pi\sigma^2} \\
&= \left(2\pi\sigma^2\right)^{\frac{|\mathbf{V}|}{2}}
\end{aligned} \tag{2.4}$$

2.2.3 A Priori Probability Density Function

We define the a priori probability density function (prior) that the original image $\boldsymbol{F}$ has a given configuration $\boldsymbol{f}$ as

$$\begin{aligned}
\Pr\{\boldsymbol{F}=\boldsymbol{f}|\alpha,\alpha'\} \equiv \frac{1}{Z_{\text{prior}}(\alpha,\alpha')} \exp\Bigg\{-\frac{1}{8}\Bigg(&\alpha \sum_{(x,y)\in\mathbf{V}} \left[(f_{x,y}-f_{x+1,y})^2 + (f_{x,y}-f_{x,y+1})^2\right] \\
&+ \alpha' \sum_{(x,y)\in\mathbf{V}} \left[(f_{x,y}-f_{x+1,y+1})^2 + (f_{x,y}-f_{x+1,y-1})^2\right]\Bigg)\Bigg\}
\end{aligned} \tag{2.5}$$

where α defines the correlation between nearest neighbour pixels, α' defines the correlation between second-neighbour pixels and

$$\begin{aligned}
Z_{\text{prior}}(\alpha,\alpha') \equiv \int \exp\Bigg\{-\frac{1}{8}\Bigg(&\alpha \sum_{(x,y)\in\mathbf{V}} \left[(z_{x,y}-z_{x+1,y})^2 + (z_{x,y}-z_{x,y+1})^2\right] + \\
&\alpha' \sum_{(x,y)\in\mathbf{V}} \left[(z_{x,y}-z_{x+1,y+1})^2 + (z_{x,y}-z_{x+1,y-1})^2\right]\Bigg)\Bigg\} d\boldsymbol{z},
\end{aligned} \tag{2.6}$$

with $\int d\boldsymbol{z} \equiv \int_{-\infty}^{+\infty} \int_{-\infty}^{+\infty} \cdots \int_{-\infty}^{+\infty} \prod_{(x,y)\in\mathbf{V}} dz_{x,y}$, is the normalization constant.

The prior can be rewritten using matrix notation as follows:

$$\begin{aligned}
&\Pr\{\boldsymbol{F}=\boldsymbol{f}|\alpha,\alpha'\} \\
&= \frac{1}{Z_{\text{prior}}(\alpha,\alpha')} \exp\Bigg\{-\frac{1}{8}\Bigg(\alpha \sum_{(x,y)\in\mathbf{V}} \left[(f_{x,y}-f_{x+1,y})^2 + (f_{x,y}-f_{x,y+1})^2 + \right. \\
&\left.\frac{\alpha'}{\alpha}\left\{(f_{x,y}-f_{x+1,y+1})^2 + (f_{x,y}-f_{x+1,y-1})^2\right\}\right]\Bigg)\Bigg\} \\
&= \frac{1}{Z_{\text{prior}}(\alpha,\alpha')} \exp\Bigg\{-\frac{1}{8}\Bigg(\alpha \sum_{(x,y)\in\mathbf{V}} \left[2f_{x,y}^2 - 2f_{x,y}f_{x+1,y} + f_{x+1,y}^2 - 2f_{x,y}f_{x,y+1} + \right. \\
&\left. f_{x,y+1}^2 + \frac{\alpha'}{\alpha}\left(2f_{x,y}^2 - 2f_{x,y}f_{x+1,y+1} + f_{x+1,y+1}^2 - 2f_{x,y}f_{x+1,y-1} + f_{x+1,y-1}^2\right)\right]\Bigg)\Bigg\}
\end{aligned}$$

$$
\begin{aligned}
=&\frac{1}{Z_{\text{prior}}(\alpha,\alpha')}\exp\left\{-\frac{1}{8}\left(\alpha\sum_{(x,y)\in\mathbf{V}}\left[4f_{x,y}^2-2f_{x,y}f_{x+1,y}-2f_{x,y}f_{x,y+1}+\right.\right.\right.\\
&\left.\left.\left.\frac{\alpha'}{\alpha}\left(4f_{x,y}^2-2f_{x,y}f_{x+1,y+1}-2f_{x,y}f_{x+1,y-1}\right)\right]\right)\right\}\\
=&\frac{1}{Z_{\text{prior}}(\alpha,\alpha')}\exp\left\{-\frac{1}{8}\left(\alpha\sum_{(x,y)\in\mathbf{V}}\left[4f_{x,y}^2-f_{x,y}f_{x+1,y}-f_{x+1,y}f_{x,y}-\right.\right.\right.\\
&f_{x,y}f_{x,y+1}-f_{x,y+1}f_{x,y}+\\
&\left.\left.\left.\frac{\alpha'}{\alpha}\left(4f_{x,y}^2-f_{x,y}f_{x+1,y+1}-f_{x+1,y+1}f_{x,y}-f_{x,y}f_{x+1,y-1}-f_{x+1,y-1}f_{x,y}\right)\right]\right)\right\}\\
=&\frac{1}{Z_{\text{prior}}(\alpha,\alpha')}\exp\left\{-\frac{1}{8}\left(\alpha\sum_{(x,y)\in\mathbf{V}}\left[4f_{x,y}^2-f_{x,y}f_{x+1,y}-f_{x,y}f_{x-1,y}-\right.\right.\right.\\
&f_{x,y}f_{x,y+1}-f_{x,y}f_{x,y-1}+\\
&\left.\left.\left.\frac{\alpha'}{\alpha}\left(4f_{x,y}^2-f_{x,y}f_{x+1,y+1}-f_{x,y}f_{x-1,y-1}-f_{x,y}f_{x+1,y-1}-f_{x,y}f_{x-1,y+1}\right)\right]\right)\right\}\\
=&\frac{1}{Z_{\text{prior}}(\alpha,\alpha')}\exp\left\{-\frac{1}{2}\alpha\boldsymbol{f}^T\boldsymbol{C}(\alpha,\alpha')\boldsymbol{f}\right\}
\end{aligned}
\tag{2.7}
$$

where $\boldsymbol{C}(\alpha,\alpha')$ is a $|\mathbf{V}|\times|\mathbf{V}|$ matrix where the $(x,y|x',y')$ elements are defined by

$$
\begin{aligned}
&\langle x,y|x',y'\rangle\equiv\delta_{x,x'}\delta_{y,y'}-\frac{1}{4}\delta_{x,x'+1}\delta_{y,y'}-\frac{1}{4}\delta_{x,x'-1}\delta_{y,y'}-\frac{1}{4}\delta_{x,x'}\delta_{y,y'+1}-\frac{1}{4}\delta_{x,x'}\delta_{y,y'-1}\\
&+\alpha_2\left[\delta_{x,x'}\delta_{y,y'}-\frac{1}{4}\delta_{x,x'+1}\delta_{y,y'+1}-\frac{1}{4}\delta_{x,x'-1}\delta_{y,y'-1}-\frac{1}{4}\delta_{x,x'+1}\delta_{y,y'-1}-\frac{1}{4}\delta_{x,x'-1}\delta_{y,y'+1}\right]\left[(x,y),(x',y')\in\mathbf{V}\right]
\end{aligned}
\tag{2.8}
$$

where $\delta_{a,b}$ is the Kronecker delta and we defined $\alpha_2\equiv\alpha'/\alpha$ to simplify notations, so that we can write $\boldsymbol{C}(\alpha,\alpha')\equiv\boldsymbol{C}(\alpha_2)$.

Similarly, $Z_{\text{prior}}(\alpha,\alpha')$ can be rewritten using matrix notation as

$$
Z_{\text{prior}}(\alpha,\alpha_2)\equiv\int\exp\left\{-\frac{1}{2}\alpha\boldsymbol{z}^T\boldsymbol{C}(\alpha_2)\boldsymbol{z}\right\}d\boldsymbol{z}
\tag{2.9}
$$

and subsequently, it can be simplified using the multidimensional Gaussian integral to give

$$
Z_{\text{prior}}(\alpha,\alpha_2)=\sqrt{\frac{(2\pi)^{|\mathbf{V}|}}{\alpha^{|\mathbf{V}|}\det(\boldsymbol{C}(\alpha_2))}}.
\tag{2.10}
$$

This model corresponds to an extension to the second-neighbour of the CAR model proposed by Molina in [1] and its energy function is:

$$
\frac{1}{8}\left(\alpha\sum_{(x,y)\in\mathbf{V}}\left[(f_{x,y}-f_{x+1,y})^2+(f_{x,y}-f_{x,y+1})^2\right]+\alpha'\sum_{(x,y)\in\mathbf{V}}\left[(f_{x,y}-f_{x+1,y+1})^2+(f_{x,y}-f_{x+1,y-1})^2\right]\right)
\tag{2.11}
$$

We note that $\boldsymbol{f}$ is a Gaussian Markov random field (GMRF) with mean $\mathbf{0}$ and precision matrix $\boldsymbol{Q}=\alpha\boldsymbol{C}(\alpha_2)$. In [10], Rue and Held derive the following properties for a GMRF $\boldsymbol{x}=(x_1,\ldots,x_n)^T$ with mean $\boldsymbol{\mu}$ and precision matrix $\boldsymbol{Q}>0$:

$$
\Pr(x_i|\boldsymbol{x}_{-i})\text{ is a normal distribution,}
\tag{2.12}
$$

$$
\mathrm{E}(x_i|\boldsymbol{x}_{-i})=\mu_i-\frac{1}{Q_{ii}}\sum_{j:j\sim i}Q_{ij}(x_j-\mu_j),
\tag{2.13}
$$

$$\mathrm{Prec}(x_i|\boldsymbol{x}_{-i}) = Q_{ii}, \tag{2.14}$$

$$\mathrm{Corr}(x_i, x_j|\boldsymbol{x}_{-ij}) = -\frac{Q_{ij}}{\sqrt{Q_{ii}Q_{jj}}}, \quad i \neq j \tag{2.15}$$

where $\mathrm{E}(x_i|\boldsymbol{x}_{-i})$ is the expected value of x_i given all other values of $\boldsymbol{x}$ (i.e. $\boldsymbol{x}_{-i} \equiv \{\boldsymbol{x} \backslash x_i\}$), $j : j \sim i$ means the values of j that are neighbors of i (i.e. $i \neq j$ and $\boldsymbol{Q}_{ij} \neq 0$), Prec is the precision and Corr is the correlation. Applying these properties to our model, we obtain the following:

$$\begin{aligned}
\mathrm{E}(f_{(x,y)}|\boldsymbol{f}_{-(x,y)}) &= \mu_{(x,y)} - \frac{1}{Q_{(x,y),(x,y)}} \sum_{(i,j):(i,j)\sim(x,y)} Q_{(x,y),(i,j)}(f_{(i,j)} - \mu_{(i,j)}) \\
&= -\frac{1}{\alpha + \alpha'} \sum_{(i,j):(i,j)\sim(x,y)} Q_{(x,y),(i,j)} f_{(i,j)} \\
&= -\frac{1}{\alpha + \alpha'} \big[-\alpha \left(\frac{1}{4} f_{(x+1,y)} + \frac{1}{4} f_{(x-1,y)} + \frac{1}{4} f_{(x,y+1)} + \frac{1}{4} f_{(x,y-1)} \right) \\
&\quad - \alpha' \left(\frac{1}{4} f_{(x+1,y+1)} + \frac{1}{4} f_{(x-1,y-1)} + \frac{1}{4} f_{(x+1,y-1)} + \frac{1}{4} f_{(x-1,y+1)} \right) \big] \\
&= \frac{1}{4(\alpha + \alpha')} \big[\alpha \left(f_{(x+1,y)} + f_{(x-1,y)} + f_{(x,y+1)} + f_{(x,y-1)} \right) \\
&\quad + \alpha' \left(f_{(x+1,y+1)} + f_{(x-1,y-1)} + f_{(x+1,y-1)} + f_{(x-1,y+1)} \right) \big]
\end{aligned} \tag{2.16}$$

and

$$\mathrm{Prec}(f_{(x,y)}|\boldsymbol{f}_{-(x,y)}) = \alpha + \alpha' \tag{2.17}$$

so that we have

$$\begin{aligned}
&\mathrm{Pr}(f_{(x,y)}|\boldsymbol{f}_{-(x,y)}) \sim N\Bigg(\frac{1}{4(\alpha + \alpha')} \\
&\times \left[\alpha \left(f_{(x+1,y)} + f_{(x-1,y)} + f_{(x,y+1)} + f_{(x,y-1)} \right) + \alpha' \left(f_{(x+1,y+1)} + f_{(x-1,y-1)} + f_{(x+1,y-1)} + f_{(x-1,y+1)} \right) \right], \\
&\qquad \frac{1}{\alpha + \alpha'} \Bigg).
\end{aligned} \tag{2.18}$$

Since $\boldsymbol{C}(\alpha_2)$ is a real symmetric matrix, it can be eigendecomposed to obtain

$$\boldsymbol{C}(\alpha_2) = \left(\boldsymbol{U}^{-1} \boldsymbol{\Lambda} \boldsymbol{U} \right) \tag{2.19}$$

where $\boldsymbol{U}$ is a unitary matrix with the eigenvectors of $\boldsymbol{C}(\alpha_2)$ as its column vectors. We shall use the DFT matrix defined as

$$\langle x, y|\boldsymbol{U}|p, q\rangle \equiv \frac{1}{\sqrt{|\mathbf{V}|}} \exp\left[-2\pi i \left(\frac{px}{V_x} + \frac{qy}{V_y} \right) \right], \tag{2.20}$$

$\boldsymbol{U}^{-1}$ is the conjugate transpose of $\boldsymbol{U}$, known as the inverse DFT matrix and defined as

$$\left\langle x, y|\boldsymbol{U}^{-1}|p, q\right\rangle \equiv \frac{1}{\sqrt{|\mathbf{V}|}} \exp\left[2\pi i \left(\frac{px}{V_x} + \frac{qy}{V_y} \right) \right] \tag{2.21}$$

and $\boldsymbol{\Lambda}$ is the diagonal matrix of the eigenvalues $\lambda(p, q)$ of $\boldsymbol{C}(\alpha_2)$.

We shall now find the value of $\boldsymbol{\Lambda}$ for $\boldsymbol{U}$ by using the eigenvalue equation

$$\boldsymbol{M}\boldsymbol{u}_{(x,y)} = \lambda(x, y)\boldsymbol{u}_{(x,y)} \tag{2.22}$$

for every $(x, y) \in \mathbf{V}$. Here $\boldsymbol{u}_{(x,y)}$ is the column vector (x, y) of $\boldsymbol{U}$ and $\lambda(x, y)$ is the corresponding eigenvalue. To simplify our calculations, we shall split $\boldsymbol{C}(\alpha_2)$ into the sum of matrices $\boldsymbol{A}$ and $\boldsymbol{B}$ as follows

$$\langle x, y|\boldsymbol{A}|x', y'\rangle \equiv \delta_{x,x'}\delta_{y,y'} - \frac{1}{4}\delta_{x,x'+1}\delta_{y,y'} - \frac{1}{4}\delta_{x,x'-1}\delta_{y,y'} - \frac{1}{4}\delta_{x,x'}\delta_{y,y'+1} - \frac{1}{4}\delta_{x,x'}\delta_{y,y'-1}, \tag{2.23}$$

$$\langle x,y|\boldsymbol{B}|x',y'\rangle \equiv$$
$$\alpha_2\big[\delta_{x,x'}\delta_{y,y'} - \frac{1}{4}\delta_{x,x'+1}\delta_{y,y'+1} - \frac{1}{4}\delta_{x,x'-1}\delta_{y,y'-1} - \frac{1}{4}\delta_{x,x'+1}\delta_{y,y'-1} - \frac{1}{4}\delta_{x,x'-1}\delta_{y,y'+1}\big]. \quad (2.24)$$

We then have

$$\begin{aligned}
\boldsymbol{C}(\alpha_2) &= \boldsymbol{A}+\boldsymbol{B}\\
\boldsymbol{U}^{-1}\boldsymbol{\Lambda}\boldsymbol{U} &= \boldsymbol{A}+\boldsymbol{B}\\
\boldsymbol{\Lambda} &= \boldsymbol{U}(\boldsymbol{A}+\boldsymbol{B})\boldsymbol{U}^{-1}\\
\boldsymbol{\Lambda} &= \boldsymbol{U}\boldsymbol{A}\boldsymbol{U}^{-1}+\boldsymbol{U}\boldsymbol{B}\boldsymbol{U}^{-1}\\
\boldsymbol{\Lambda} &= \boldsymbol{\Lambda}_A+\boldsymbol{\Lambda}_B, \qquad (2.25)
\end{aligned}$$

so we can find the value of $\boldsymbol{\Lambda}$ by finding the values of $\boldsymbol{\Lambda}_A$ and $\boldsymbol{\Lambda}_B$.

We start with $\boldsymbol{\Lambda}_A$. We shall use the fact that the elements of $\boldsymbol{A}$ are such that

$$a_{(p,q),(r,s)} = \begin{cases} 1 & \text{if } (p,q)=(r,s),\\ -\frac{1}{4} & \text{if } (p,q)=(r-1,s),\\ -\frac{1}{4} & \text{if } (p,q)=(r+1,s),\\ -\frac{1}{4} & \text{if } (p,q)=(r,s-1),\\ -\frac{1}{4} & \text{if } (p,q)=(r,s+1)\\ 0 & \text{for every other case.}\end{cases} \quad (2.26)$$

Line (r,s) of equation (2.22) can be rewritten as follows:

$$\sum_{(p,q)\in\mathbf{V}} a_{(p,q),(r,s)}u_{(x,y),(p,q)} = \lambda_a(x,y)u_{(x,y),(r,s)} \quad (2.27)$$

so by using the values of (2.26) into equation (2.27) we obtain

$$\begin{aligned}
u_{(x,y),(r,s)} - \left(\frac{1}{4}u_{(x,y),(r-1,s)} + \frac{1}{4}u_{(x,y),(r+1,s)} + \frac{1}{4}u_{(x,y),(r,s-1)} + \frac{1}{4}u_{(x,y),(r,s+1)}\right)&\\
= \lambda_a(x,y)u_{(x,y),(r,s)}&\\
\therefore -\frac{1}{4}\left(u_{(x,y),(r-1,s)} + u_{(x,y),(r+1,s)} + u_{(x,y),(r,s-1)} + u_{(x,y),(r,s+1)}\right) = (\lambda_a(x,y)-1)\,u_{(x,y),(r,s)}&\\
\therefore -\frac{1}{4\sqrt{|\mathbf{V}|}}\left\{\exp\left[-2\pi i\left(\frac{x(r-1)}{V_x}+\frac{ys}{V_y}\right)\right] + \exp\left[-2\pi i\left(\frac{x(r+1)}{V_x}+\frac{ys}{V_y}\right)\right]&\\
+ \exp\left[-2\pi i\left(\frac{xr}{V_x}+\frac{y(s-1)}{V_y}\right)\right] + \exp\left[-2\pi i\left(\frac{xr}{V_x}+\frac{y(s+1)}{V_y}\right)\right]\right\}&\\
= (\lambda_a(x,y)-1)\,\frac{1}{\sqrt{|\mathbf{V}|}}\exp\left[-2\pi i\left(\frac{xr}{V_x}+\frac{ys}{V_y}\right)\right]&\\
\therefore -\frac{1}{4}\exp\left[2\pi i\left(\frac{xr}{V_x}+\frac{ys}{V_y}\right)\right]\left\{\exp\left[-2\pi i\left(\frac{x(r-1)}{V_x}+\frac{ys}{V_y}\right)\right] + \exp\left[-2\pi i\left(\frac{x(r+1)}{V_x}+\frac{ys}{V_y}\right)\right]&\\
+ \exp\left[-2\pi i\left(\frac{xr}{V_x}+\frac{y(s-1)}{V_y}\right)\right] + \exp\left[-2\pi i\left(\frac{xr}{V_x}+\frac{y(s+1)}{V_y}\right)\right]\right\}&\\
= \lambda_a(x,y) - 1&\\
\therefore -\frac{1}{4}\left\{\exp\left[-2\pi i\frac{-x}{V_x}\right] + \exp\left[-2\pi i\frac{x}{V_x}\right] + \exp\left[-2\pi i\frac{-y}{V_y}\right] + \exp\left[-2\pi i\frac{y}{V_y}\right]\right\}&\\
= \lambda_a(x,y) - 1&\\
\therefore 1 - \frac{1}{4}\left\{\cos\left(\frac{2\pi x}{V_x}\right) + i\sin\left(\frac{2\pi x}{V_x}\right) + \cos\left(-\frac{2\pi x}{V_x}\right) + i\sin\left(-\frac{2\pi x}{V_x}\right)\right.&\\
\left. + \cos\left(\frac{2\pi y}{V_y}\right) + i\sin\left(\frac{2\pi y}{V_y}\right) + \cos\left(-\frac{2\pi y}{V_y}\right) + i\sin\left(-\frac{2\pi y}{V_y}\right)\right\}&\\
= \lambda_a(x,y)&
\end{aligned}$$

$$\therefore \lambda_a(x,y) = 1 - \frac{1}{2}\cos\left(\frac{2\pi x}{V_x}\right) - \frac{1}{2}\cos\left(\frac{2\pi y}{V_y}\right). \tag{2.28}$$

Similarly, we find the values of $\boldsymbol{\Lambda}_B$ by using the fact that the elements of $\boldsymbol{B}$ are such that

$$b_{(p,q),(r,s)} = \begin{cases} \alpha_2 & \text{if } (p,q) = (r,s) \\ -\frac{1}{4}\alpha_2 & \text{if } (p,q) = (r+1,s+1) \\ -\frac{1}{4}\alpha_2 & \text{if } (p,q) = (r-1,s-1) \\ -\frac{1}{4}\alpha_2 & \text{if } (p,q) = (r+1,s-1) \\ -\frac{1}{4}\alpha_2 & \text{if } (p,q) = (r-1,s+1) \\ 0 & \text{for every other case.} \end{cases} \tag{2.29}$$

Line (r,s) of equation (2.22) can be rewritten as follows:

$$\sum_{(p,q)\in\mathbf{V}} b_{(p,q),(r,s)} u_{(x,y),(p,q)} = \lambda_b(x,y) u_{(x,y),(r,s)} \tag{2.30}$$

so by using the values of (2.29) into equation (2.30) we obtain

$$\begin{aligned}
&\alpha_2\left[u_{(x,y),(r,s)} - \frac{1}{4}\left(u_{(x,y),(r+1,s+1)} + u_{(x,y),(r-1,s-1)} + u_{(x,y),(r+1,s-1)} + u_{(x,y),(r-1,s+1)}\right)\right] \\
&\qquad = \lambda_b(x,y) u_{(x,y),(r,s)} \\
&\therefore -\frac{\alpha_2}{4}\left[\left(u_{(x,y),(r+1,s+1)} + u_{(x,y),(r-1,s-1)} + u_{(x,y),(r+1,s-1)} + u_{(x,y),(r-1,s+1)}\right)\right] \\
&\qquad = \left(\lambda_b(x,y) - \alpha_2\right) u_{(x,y),(r,s)} \\
&\therefore -\frac{\alpha_2}{4\sqrt{|\mathbf{V}|}}\left\{\exp\left[-2\pi i\left(\frac{x(r+1)}{V_x} + \frac{y(s+1)}{V_y}\right)\right] + \exp\left[-2\pi i\left(\frac{x(r-1)}{V_x} + \frac{y(s-1)}{V_y}\right)\right]\right. \\
&\qquad \left. + \exp\left[-2\pi i\left(\frac{x(r+1)}{V_x} + \frac{y(s-1)}{V_y}\right)\right] + \exp\left[-2\pi i\left(\frac{x(r-1)}{V_x} + \frac{y(s+1)}{V_y}\right)\right]\right\} \\
&\qquad = \left(\lambda_b(x,y) - \alpha_2\right)\frac{1}{\sqrt{|\mathbf{V}|}}\exp\left[-2\pi i\left(\frac{xr}{V_x} + \frac{ys}{V_y}\right)\right] \\
&\qquad \therefore -\exp\left[2\pi i\left(\frac{xr}{V_x} + \frac{ys}{V_y}\right)\right] \\
&\times\frac{\alpha_2}{4}\left\{\exp\left[-2\pi i\left(\frac{x(r+1)}{V_x} + \frac{y(s+1)}{V_y}\right)\right] + \exp\left[-2\pi i\left(\frac{x(r-1)}{V_x} + \frac{y(s-1)}{V_y}\right)\right]\right. \\
&\qquad \left. + \exp\left[-2\pi i\left(\frac{x(r+1)}{V_x} + \frac{y(s-1)}{V_y}\right)\right] + \exp\left[-2\pi i\left(\frac{x(r-1)}{V_x} + \frac{y(s+1)}{V_y}\right)\right]\right\} \\
&\qquad = \lambda_b(x,y) - \alpha_2 \\
&\therefore -\frac{\alpha_2}{4}\left\{\exp\left[-2\pi i(\frac{x}{V_x} + \frac{y}{V_y})\right] + \exp\left[-2\pi i(-\frac{x}{V_x} - \frac{y}{V_y})\right]\right. \\
&\qquad \left. + \exp\left[-2\pi i(\frac{x}{V_x} - \frac{y}{V_y})\right] + \exp\left[-2\pi i(-\frac{x}{V_x} + \frac{y}{V_y})\right]\right\} \\
&\qquad = \lambda_b(x,y) - \alpha_2 \\
&\qquad \therefore \alpha_2\left\{1 - \frac{1}{4}\left[\cos\left(-2\pi(\frac{x}{V_x} + \frac{y}{V_y})\right) + i\sin\left(-2\pi(\frac{x}{V_x} + \frac{y}{V_y})\right)\right.\right. \\
&+ \cos\left(2\pi(\frac{x}{V_x} + \frac{y}{V_y})\right) + i\sin\left(2\pi(\frac{x}{V_x} + \frac{y}{V_y})\right) + \cos\left(-2\pi(\frac{x}{V_x} - \frac{y}{V_y})\right) + i\sin\left(2\pi(\frac{x}{V_x} - \frac{y}{V_y})\right) \\
&\qquad \left.\left. + \cos\left(2\pi(\frac{x}{V_x} - \frac{y}{V_y})\right) + i\sin\left(2\pi(\frac{x}{V_x} - \frac{y}{V_y})\right)\right]\right\} = \lambda_b(x,y) \\
&\therefore \lambda_b(x,y) = \alpha_2\left[1 - \frac{1}{2}\cos\left(2\pi(\frac{x}{V_x} + \frac{y}{V_y})\right) - \frac{1}{2}\cos\left(2\pi(\frac{x}{V_x} - \frac{y}{V_y})\right)\right].
\end{aligned} \tag{2.31}$$

Using the results of (2.28) and (2.31), we find

$$\lambda(p,q) = \lambda_a(p,q) + \lambda_b(p,q)$$
$$= 1 - \frac{1}{2}\cos\left(\frac{2\pi p}{V_x}\right) - \frac{1}{2}\cos\left(\frac{2\pi q}{V_y}\right) + \alpha_2\left[1 - \frac{1}{2}\cos\left(2\pi(\frac{p}{V_x} + \frac{q}{V_y})\right) - \frac{1}{2}\cos\left(2\pi(\frac{p}{V_x} - \frac{q}{V_y})\right)\right] \quad (2.32)$$

so we have

$$\mathbf{\Lambda} \equiv \sum_{(p,q)\in\mathbf{V}}\left(1 - \frac{1}{2}\cos\left(\frac{2\pi p}{V_x}\right) - \frac{1}{2}\cos\left(\frac{2\pi q}{V_y}\right) + \right.$$
$$\left.\alpha_2\left[1 - \frac{1}{2}\cos\left(2\pi(\frac{p}{V_x} + \frac{q}{V_y})\right) - \frac{1}{2}\cos\left(2\pi(\frac{p}{V_x} - \frac{q}{V_y})\right)\right]\right)\boldsymbol{J}^{pq,pq} \quad (2.33)$$

which is the diagonal matrix of the eigenvalues $\lambda(p,q)$ of $\boldsymbol{C}(\alpha_2)$ where $\boldsymbol{J}^{pq,pq}$ is the $|\boldsymbol{V}| \times |\boldsymbol{V}|$ single-entry matrix.

Using the results of this eigendecomposition, we can rewrite the expression of $Z_{\text{prior}}(\alpha, \alpha_2)$ given in (2.10) as

$$Z_{\text{prior}}(\alpha,\alpha_2) = \left(\frac{2\pi}{\alpha}\right)^{\frac{|\mathbf{V}|}{2}} \prod_{(p,q)\in\mathbf{V}} \lambda(p,q)^{-\frac{1}{2}} \quad (2.34)$$

2.2.4 A Posteriori Probability Density Function

The a posteriori probability density function of having an original image configuration $\boldsymbol{f}$ given a degraded image $\boldsymbol{g}$ is found by applying Bayes' theorem as follows:

$$\begin{aligned}\Pr\{\boldsymbol{F} = \boldsymbol{f}|\boldsymbol{G} = \boldsymbol{g}, \alpha, \alpha_2, \sigma\} &= \frac{\Pr\{\boldsymbol{G} = \boldsymbol{g}|\boldsymbol{F} = \boldsymbol{f}, \sigma\}\Pr\{\boldsymbol{F} = \boldsymbol{f}|\alpha, \alpha_2\}}{\Pr\{\boldsymbol{G} = \boldsymbol{g}|\alpha, \alpha_2, \sigma\}} \\ &= \frac{\Pr\{\boldsymbol{G} = \boldsymbol{g}|\boldsymbol{F} = \boldsymbol{f}, \sigma\}\Pr\{\boldsymbol{F} = \boldsymbol{f}|\alpha, \alpha_2\}}{\int \Pr\{\boldsymbol{G} = \boldsymbol{g}|\boldsymbol{F} = \boldsymbol{z}, \sigma\}\Pr\{\boldsymbol{F} = \boldsymbol{z}|\alpha, \alpha_2\}\, d\boldsymbol{z}}\end{aligned} \quad (2.35)$$

where $\Pr\{\boldsymbol{G} = \boldsymbol{g}|\alpha, \alpha_2, \sigma\} = \int \Pr\{\boldsymbol{G} = \boldsymbol{g}|\boldsymbol{F} = \boldsymbol{z}, \sigma\}\Pr\{\boldsymbol{F} = \boldsymbol{z}|\alpha, \alpha_2\}\, d\boldsymbol{z}$ is called the evidence.

Using (2.1) and (2.7), the function can be rewritten as follows:

$$\Pr\{\boldsymbol{F} = \boldsymbol{f}|\boldsymbol{G} = \boldsymbol{g}, \alpha, \alpha_2, \sigma\} =$$
$$\frac{\frac{1}{Z_{\text{noise}}(\sigma)}\exp\left(-\frac{1}{2\sigma^2}\sum_{(x,y)\in\mathbf{V}}(g_{x,y} - f_{x,y})^2\right) \times \frac{1}{Z_{\text{prior}}(\alpha,\alpha_2)}\exp\left\{-\frac{1}{2}\alpha\boldsymbol{f}^T\boldsymbol{C}(\alpha_2)\,\boldsymbol{f}\right\}}{\int \frac{1}{Z_{\text{noise}}(\sigma)}\exp\left(-\frac{1}{2\sigma^2}\sum_{(x,y)\in\mathbf{V}}(g_{x,y} - z_{x,y})^2\right) \times \frac{1}{Z_{\text{prior}}(\alpha,\alpha_2)}\exp\left\{-\frac{1}{2}\alpha\boldsymbol{z}^T\boldsymbol{C}(\alpha_2)\,\boldsymbol{z}\right\} d\boldsymbol{z}}. \quad (2.36)$$

Since Z_{noise} and Z_{prior} are not dependant on $\boldsymbol{z}$, they can be taken out of the integral in the denominator and cancel out with the numerator, so we have

$$\Pr\{\boldsymbol{F} = \boldsymbol{f}|\boldsymbol{G} = \boldsymbol{g}, \alpha, \alpha_2, \sigma\} = \frac{1}{Z_{\text{posterior}}(\boldsymbol{g}, \alpha, \alpha_2, \sigma)}\exp\left[-H(\boldsymbol{f}|\boldsymbol{g}, \alpha, \alpha_2, \sigma)\right] \quad (2.37)$$

where

$$Z_{\text{posterior}}(\boldsymbol{g}, \alpha, \alpha_2, \sigma) = \int \exp\left[-H(\boldsymbol{z}|\boldsymbol{g}, \alpha, \alpha_2, \sigma)\right] d\boldsymbol{z} \quad (2.38)$$

and

$$H(\boldsymbol{f}|\boldsymbol{g}, \alpha, \alpha_2, \sigma) = \frac{1}{2\sigma^2}\sum_{(x,y)\in\mathbf{V}}(g_{x,y} - f_{x,y})^2 + \frac{1}{2}\alpha\boldsymbol{f}^T\boldsymbol{C}(\alpha_2)\,\boldsymbol{f}. \quad (2.39)$$

We can simplify calculations by grouping all element of $\boldsymbol{f}$ in H in one single term as follows

$$H(\boldsymbol{f}|\boldsymbol{g}, \alpha, \alpha_2, \sigma) = \frac{1}{2\sigma^2}(\boldsymbol{g} - \boldsymbol{f})^T(\boldsymbol{g} - \boldsymbol{f}) + \frac{1}{2}\boldsymbol{f}^T\alpha\boldsymbol{C}(\alpha_2)\,\boldsymbol{f}$$

$$
\begin{aligned}
&= \frac{1}{2\sigma^2}\left[\boldsymbol{f}^T\boldsymbol{f} - \boldsymbol{f}^T\boldsymbol{g} - \boldsymbol{g}^T\boldsymbol{f} + \boldsymbol{g}^T\boldsymbol{g}\right] + \frac{1}{2}\boldsymbol{f}^T\alpha\boldsymbol{C}\left(\alpha_2\right)\boldsymbol{f} \\
&= \frac{1}{2\sigma^2}\left(\boldsymbol{f}^T\boldsymbol{f} - \boldsymbol{f}^T\boldsymbol{g} - \boldsymbol{g}^T\boldsymbol{f} + \sigma^2\boldsymbol{f}^T\alpha\boldsymbol{C}\left(\alpha_2\right)\boldsymbol{f}\right) + \frac{1}{2\sigma^2}\boldsymbol{g}^T\boldsymbol{g} \\
&= \frac{1}{2\sigma^2}\left(\boldsymbol{f}^T\boldsymbol{f} - \boldsymbol{f}^T\boldsymbol{g} - \boldsymbol{g}^T\boldsymbol{f} + \sigma^2\boldsymbol{f}^T\alpha\boldsymbol{C}\left(\alpha_2\right)\boldsymbol{f}\right) \\
&\quad + \frac{1}{2\sigma^2}\boldsymbol{g}^T\left(\boldsymbol{I} + \sigma^2\alpha\boldsymbol{C}\left(\alpha_2\right)\right)\left(\boldsymbol{I} + \sigma^2\alpha\boldsymbol{C}\left(\alpha_2\right)\right)^{-1}\boldsymbol{g} \\
&= \frac{1}{2\sigma^2}\left[\boldsymbol{f}^T\boldsymbol{f} - \boldsymbol{f}^T\boldsymbol{g} - \boldsymbol{g}^T\boldsymbol{f} + \sigma^2\boldsymbol{f}^T\alpha\boldsymbol{C}\left(\alpha_2\right)\boldsymbol{f}\right] \\
&\quad + \frac{1}{2\sigma^2}\boldsymbol{g}^T\left[\left(\boldsymbol{I} + \sigma^2\alpha\boldsymbol{C}\left(\alpha_2\right)\right)^{-1} + \sigma^2\alpha\boldsymbol{C}\left(\alpha_2\right)\left(\boldsymbol{I} + \sigma^2\alpha\boldsymbol{C}\left(\alpha_2\right)\right)^{-1}\right]\boldsymbol{g} \\
&= \frac{1}{2\sigma^2}\left[\boldsymbol{f}^T\boldsymbol{f} - \boldsymbol{f}^T\boldsymbol{g} - \boldsymbol{g}^T\boldsymbol{f} + \boldsymbol{f}^T\left(\sigma^2\alpha\boldsymbol{C}\left(\alpha_2\right)\right)\boldsymbol{f}\right] \\
&\quad + \frac{1}{2\sigma^2}\boldsymbol{g}^T\left(\boldsymbol{I} + \sigma^2\alpha\boldsymbol{C}\left(\alpha_2\right)\right)^{-1}\boldsymbol{g} + \frac{1}{2}\boldsymbol{g}^T\alpha\boldsymbol{C}\left(\alpha_2\right)\left(\boldsymbol{I} + \sigma^2\alpha\boldsymbol{C}\left(\alpha_2\right)\right)^{-1}\boldsymbol{g} \\
&= \frac{1}{2\sigma^2}\left[\boldsymbol{f}^T\left(\boldsymbol{I} + \sigma^2\alpha\boldsymbol{C}\left(\alpha_2\right)\right)\boldsymbol{f} - \boldsymbol{f}^T\boldsymbol{g} - \boldsymbol{g}^T\boldsymbol{f} + \boldsymbol{g}^T\left(\boldsymbol{I} + \sigma^2\alpha\boldsymbol{C}\left(\alpha_2\right)\right)^{-1}\boldsymbol{g}\right] \\
&\quad + \frac{1}{2}\boldsymbol{g}^T\alpha\boldsymbol{C}\left(\alpha_2\right)\left(\boldsymbol{I} + \sigma^2\alpha\boldsymbol{C}\left(\alpha_2\right)\right)^{-1}\boldsymbol{g} \\
&= \frac{1}{2\sigma^2}[\boldsymbol{f}^T\left(\boldsymbol{I} + \sigma^2\alpha\boldsymbol{C}\left(\alpha_2\right)\right)\boldsymbol{f} - \boldsymbol{f}^T\left(\boldsymbol{I} + \sigma^2\alpha\boldsymbol{C}\left(\alpha_2\right)\right)\left(\boldsymbol{I} + \sigma^2\alpha\boldsymbol{C}\left(\alpha_2\right)\right)^{-1}\boldsymbol{g} \\
&\quad - \boldsymbol{g}^T\left(\boldsymbol{I} + \sigma^2\alpha\boldsymbol{C}\left(\alpha_2\right)\right)^{-1}\left(\boldsymbol{I} + \sigma^2\alpha\boldsymbol{C}\left(\alpha_2\right)\right)\boldsymbol{f} + \boldsymbol{g}^T\left(\boldsymbol{I} + \sigma^2\alpha\boldsymbol{C}\left(\alpha_2\right)\right)^{-1}\boldsymbol{g}] \\
&\quad + \frac{1}{2}\boldsymbol{g}^T\alpha\boldsymbol{C}\left(\alpha_2\right)\left(\boldsymbol{I} + \sigma^2\alpha\boldsymbol{C}\left(\alpha_2\right)\right)^{-1}\boldsymbol{g} \\
&= \frac{1}{2\sigma^2}\left[\boldsymbol{f} - \left(\boldsymbol{I} + \sigma^2\alpha\boldsymbol{C}\left(\alpha_2\right)\right)^{-1}\boldsymbol{g}\right]^T\left(\boldsymbol{I} + \sigma^2\alpha\boldsymbol{C}\left(\alpha_2\right)\right) \\
&\quad \times \left[\boldsymbol{f} - \left(\boldsymbol{I} + \sigma^2\alpha\boldsymbol{C}\left(\alpha_2\right)\right)^{-1}\boldsymbol{g}\right] + \frac{1}{2}\boldsymbol{g}^T\alpha\boldsymbol{C}\left(\alpha_2\right)\left(\boldsymbol{I} + \sigma^2\alpha\boldsymbol{C}\left(\alpha_2\right)\right)^{-1}\boldsymbol{g}
\end{aligned}
\tag{2.40}
$$

where we made use of the fact that $\left(\boldsymbol{I} + \sigma^2\alpha\boldsymbol{C}\left(\alpha_2\right)\right)$ is symmetric.

Using the eigendecomposition described in (2.19), we can rewrite the second term of (2.40) as follows

$$
\begin{aligned}
&\frac{1}{2}\boldsymbol{g}^T\alpha\boldsymbol{C}\left(\alpha_2\right)\left(\boldsymbol{I} + \sigma^2\alpha\boldsymbol{C}\left(\alpha_2\right)\right)^{-1}\boldsymbol{g} \\
=&\frac{1}{2}\boldsymbol{g}^T\alpha\left(\boldsymbol{U}^{-1}\boldsymbol{\Lambda}\boldsymbol{U}\right)\left[\boldsymbol{I} + \sigma^2\alpha\left(\boldsymbol{U}^{-1}\boldsymbol{\Lambda}\boldsymbol{U}\right)\right]^{-1}\boldsymbol{g} \\
=&\frac{1}{2}\boldsymbol{g}^T\boldsymbol{U}^{-1}\alpha\boldsymbol{\Lambda}\boldsymbol{U}\left[\boldsymbol{U}^{-1}\boldsymbol{I}\boldsymbol{U} + \sigma^2\boldsymbol{U}^{-1}\alpha\boldsymbol{\Lambda}\boldsymbol{U}\right]^{-1}\boldsymbol{g} \\
=&\frac{1}{2}\boldsymbol{g}^T\boldsymbol{U}^{-1}\alpha\boldsymbol{\Lambda}\boldsymbol{U}\left[\boldsymbol{U}^{-1}\left(\boldsymbol{I} + \sigma^2\alpha\boldsymbol{\Lambda}\right)\boldsymbol{U}\right]^{-1}\boldsymbol{g} \\
=&\frac{1}{2}\boldsymbol{g}^T\boldsymbol{U}^{-1}\alpha\boldsymbol{\Lambda}\left(\boldsymbol{I} + \sigma^2\alpha\boldsymbol{\Lambda}\right)^{-1}\boldsymbol{U}\boldsymbol{g} \\
=&\frac{1}{2}\overrightarrow{G}^{\dagger}\alpha\boldsymbol{\Lambda}\left(\boldsymbol{I} + \sigma^2\alpha\boldsymbol{\Lambda}\right)^{-1}\overrightarrow{G} \\
=&\frac{1}{2}\sum_{(p,q)\in\mathbf{V}} G^{\dagger}_{p,q}\alpha\lambda\left(p,q\right)\left(1 + \sigma^2\alpha\lambda\left(p,q\right)\right)^{-1}G_{p,q}
\end{aligned}
\tag{2.41}
$$

where

$$
G_{p,q} \equiv \frac{1}{\sqrt{|\mathbf{V}|}}\sum_{(x,y)\in\mathbf{V}} g_{x,y}\exp\left[-2\pi i\left(\frac{px}{V_x} + \frac{qy}{V_y}\right)\right] \tag{2.42}
$$

and

$$
G^{\dagger}_{p,q} \equiv \frac{1}{\sqrt{|\mathbf{V}|}}\sum_{(x,y)\in\mathbf{V}} g_{x,y}\exp\left[2\pi i\left(\frac{px}{V_x} + \frac{qy}{V_y}\right)\right]. \tag{2.43}
$$

Here we note that $G_{p,q}$ corresponds to $(\boldsymbol{U}\boldsymbol{g})_{p,q}$ where $(\boldsymbol{U}\boldsymbol{g})$ is the DFT of $\boldsymbol{g}$. Similarly for $\overrightarrow{G}^{\dagger}$ using $(\boldsymbol{g}^T\boldsymbol{U}^{-1})$, the inverse DFT.

From the above, we conclude that

$$H\left(\boldsymbol{f}|\boldsymbol{g},\alpha,\alpha_2,\sigma\right)=\frac{1}{2\sigma^2}\left[\boldsymbol{f}-\left(\boldsymbol{I}+\sigma^2\alpha\boldsymbol{C}\left(\alpha_2\right)\right)^{-1}\boldsymbol{g}\right]^T\left(\boldsymbol{I}+\sigma^2\alpha\boldsymbol{C}\left(\alpha_2\right)\right)\left[\boldsymbol{f}-\left(\boldsymbol{I}+\sigma^2\alpha\boldsymbol{C}\left(\alpha_2\right)\right)^{-1}\boldsymbol{g}\right]+\frac{1}{2}\sum_{(p,q)\in\mathbf{V}}G_{p,q}^{\dagger}\alpha\lambda\left(p,q\right)\left(1+\sigma^2\alpha\lambda\left(p,q\right)\right)^{-1}G_{p,q}. \quad (2.44)$$

Using the variable substitution $\boldsymbol{x}=\left[\boldsymbol{z}-\left(\boldsymbol{I}+\sigma^2\alpha\boldsymbol{C}\left(\alpha_2\right)\right)^{-1}\boldsymbol{g}\right]$ and $d\boldsymbol{z}=d\boldsymbol{x}$, $Z_{\text{posterior}}$ can be rewritten as

$$Z_{\text{posterior}}=\int\exp\Bigg\{-\frac{1}{2\sigma^2}\boldsymbol{x}^T\left(\boldsymbol{I}+\sigma^2\alpha\boldsymbol{C}\left(\alpha_2\right)\right)\boldsymbol{x}-\frac{1}{2}\sum_{(p,q)\in\mathbf{V}}G_{p,q}^{\dagger}\alpha\lambda\left(p,q\right)\left(1+\sigma^2\alpha\lambda\left(p,q\right)\right)^{-1}G_{p,q}\Bigg\}d\boldsymbol{x} \quad (2.45)$$

which, using the multidimensional Gaussian integral becomes

$$Z_{\text{posterior}}=\left(2\pi\sigma^2\right)^{\frac{|\mathbf{V}|}{2}}\left\{\det\left(\boldsymbol{I}+\sigma^2\alpha\boldsymbol{C}\left(\alpha_2\right)\right)\right\}^{-\frac{1}{2}}\times\exp\left\{-\frac{1}{2}\sum_{(p,q)\in\mathbf{V}}G_{p,q}^{\dagger}\alpha\lambda\left(p,q\right)\left(1+\sigma^2\alpha\lambda\left(p,q\right)\right)^{-1}G_{p,q}\right\}. \quad (2.46)$$

The determinant in equation (2.46) can be rewritten as follows:

$$\begin{aligned}&\det\left(\boldsymbol{I}+\alpha\sigma^2\boldsymbol{C}\left(\alpha_2\right)\right)\\&=\det\left(\boldsymbol{U}^{-1}\boldsymbol{I}\boldsymbol{U}+\boldsymbol{U}^{-1}\alpha\sigma^2\boldsymbol{\Lambda}\boldsymbol{U}\right)\\&=\det\left[\boldsymbol{U}^{-1}\left(\boldsymbol{I}+\alpha\sigma^2\boldsymbol{\Lambda}\right)\boldsymbol{U}\right]\\&=\det\left(\boldsymbol{I}+\alpha\sigma^2\boldsymbol{\Lambda}\right)\\&=\prod_{(p,q)\in\mathbf{V}}\left(1+\alpha\sigma^2\lambda(p,q)\right).\end{aligned} \quad (2.47)$$

So equation (2.46) can be transformed into

$$Z_{\text{posterior}}=\left(2\pi\sigma^2\right)^{\frac{|\mathbf{V}|}{2}}\left\{\prod_{(p,q)\in\mathbf{V}}\left(1+\alpha\sigma^2\lambda(p,q)\right)\right\}^{-\frac{1}{2}}\times\exp\left\{-\frac{1}{2}\sum_{(p,q)\in\mathbf{V}}G_{p,q}^{\dagger}\alpha\lambda\left(p,q\right)\left(1+\sigma^2\alpha\lambda\left(p,q\right)\right)^{-1}G_{p,q}\right\}. \quad (2.48)$$

2.2.5 Restored Image Equation

In our model, the estimated restored image configuration is given by the expected value of the a posteriori probability function. This gives us the following restored image equation:

$$\widehat{\boldsymbol{f}}\equiv\int\boldsymbol{z}\Pr\left\{\boldsymbol{F}=\boldsymbol{z}|\boldsymbol{G}=\boldsymbol{g},\alpha,\alpha_2,\sigma\right\}d\boldsymbol{z} \quad (2.49)$$

where the integral is performed over every image configuration $\boldsymbol{z}$ (range of $]-\infty,+\infty[$ for each pixel element) and $\widehat{\boldsymbol{f}}$ is our restored image.

Using (2.37) we obtain

$$\widehat{\boldsymbol{f}}=\frac{1}{Z_{\text{posterior}}\left(\boldsymbol{g},\alpha,\alpha_2,\sigma\right)}\int\boldsymbol{z}\exp\left[-H\left(\boldsymbol{z}|\boldsymbol{g},\alpha,\alpha_2,\sigma\right)\right]d\boldsymbol{z} \quad (2.50)$$

which, using the results of (2.44) and (2.46) is rewritten as

$$\begin{aligned}
\widehat{\boldsymbol{f}} &= \frac{1}{(2\pi\sigma^2)^{\frac{|\mathbf{V}|}{2}} \det\left(\sigma^2\boldsymbol{\Sigma}^{-1}\right)^{-1/2} \exp\left\{-\frac{1}{2}\sum_{(p,q)\in\mathbf{V}}\left[G^{\dagger}_{p,q}\alpha\lambda(\alpha_2,p,q)\left(1+\sigma^2\alpha\lambda(\alpha_2,p,q)\right)^{-1}G_{p,q}\right]\right\}} \\
&\quad\times\int \boldsymbol{z}\exp\Bigg(-\frac{1}{2\sigma^2}\left[\boldsymbol{z}-\boldsymbol{\mu}\right]^T\sigma^2\boldsymbol{\Sigma}^{-1}\left[\boldsymbol{z}-\boldsymbol{\mu}\right] \\
&\qquad-\frac{1}{2}\sum_{(p,q)\in\mathbf{V}}\left[G^{\dagger}_{p,q}\alpha\lambda(\alpha_2,p,q)\left(1+\sigma^2\alpha\lambda(\alpha_2,p,q)\right)^{-1}G_{p,q}\right]\Bigg)d\boldsymbol{z} \\
&= \frac{1}{(2\pi\sigma^2)^{\frac{|\mathbf{V}|}{2}}\left(\sigma^2\right)^{-\frac{|\mathbf{V}|}{2}}\det\left(\boldsymbol{\Sigma}\right)^{1/2}}\int \boldsymbol{z}\exp\left(-\frac{1}{2}\left[\boldsymbol{z}-\boldsymbol{\mu}\right]^T\boldsymbol{\Sigma}^{-1}\left[\boldsymbol{z}-\boldsymbol{\mu}\right]\right)d\boldsymbol{z} \\
&= \frac{1}{(2\pi)^{\frac{|\mathbf{V}|}{2}}\det\left(\boldsymbol{\Sigma}\right)^{1/2}}\int \boldsymbol{z}\exp\left(-\frac{1}{2}\left[\boldsymbol{z}-\boldsymbol{\mu}\right]^T\boldsymbol{\Sigma}^{-1}\left[\boldsymbol{z}-\boldsymbol{\mu}\right]\right)d\boldsymbol{z} \qquad (2.51)
\end{aligned}$$

with $\boldsymbol{\mu} \equiv \left(\boldsymbol{I}+\sigma^2\alpha\boldsymbol{C}\left(\alpha_2\right)\right)^{-1}\boldsymbol{g}$ and $\boldsymbol{\Sigma}^{-1} \equiv \frac{1}{\sigma^2}\left(\boldsymbol{I}+\sigma^2\alpha\boldsymbol{C}\left(\alpha_2\right)\right)$, which corresponds to the expected value equation of a multivariate Gaussian distribution. Using that fact, we conclude that

$$\widehat{\boldsymbol{f}} = \mathbf{E}[\boldsymbol{z}] = \boldsymbol{\mu} = \left(\boldsymbol{I}+\sigma^2\alpha\boldsymbol{C}\left(\alpha_2\right)\right)^{-1}\boldsymbol{g}. \qquad (2.52)$$

However, it is impractical to compute the inverse of such a large matrix, so we use the eigendecomposition of (2.19) to simplify the equation as follows:

$$\begin{aligned}
\widehat{\boldsymbol{f}} &= \left[\boldsymbol{I}+\sigma^2\alpha\left(\boldsymbol{U}^{-1}\boldsymbol{\Lambda}\boldsymbol{U}\right)\right]^{-1}\boldsymbol{g} \\
&= \boldsymbol{U}^{-1}\left(\boldsymbol{I}+\sigma^2\alpha\boldsymbol{\Lambda}\right)^{-1}\boldsymbol{U}\boldsymbol{g} \\
&= \boldsymbol{U}^{-1}\left(\boldsymbol{I}+\sigma^2\alpha\boldsymbol{\Lambda}\right)^{-1}\overrightarrow{G} \qquad (2.53)
\end{aligned}$$

Here we note that this corresponds to the inverse DFT of $\left(\boldsymbol{I}+\sigma^2\alpha\boldsymbol{\Lambda}\right)^{-1}\overrightarrow{G}$ where $\overrightarrow{G}$ is itself the DFT of the degraded image. $\left(\boldsymbol{I}+\sigma^2\alpha\boldsymbol{\Lambda}\right)^{-1}$ can also easily be computed since it is the inverse of a diagonal matrix.

2.2.6 Hyperparameters Estimation

As we saw in section 2.2.5, the restored image equation depends on the values of the hyperparameters σ, α and α_2. The selection of those values shall be done by fixing the value of α_2 and choosing values for σ and α that maximize the evidence (or likelihood) of equation (2.35). Such a method is known as Maximum Likelihood Estimation (MLE).

Using (2.35) with (2.1), (2.7) and (2.37), we find that the evidence is given by

$$\begin{aligned}
\Pr\left\{\boldsymbol{G}=\boldsymbol{g}|\alpha,\alpha_2,\sigma\right\} &= \frac{\Pr\left\{\boldsymbol{G}=\boldsymbol{g}|\boldsymbol{F}=\boldsymbol{f},\sigma\right\}\Pr\left\{\boldsymbol{F}=\boldsymbol{f}|\alpha,\alpha_2\right\}}{\Pr\left\{\boldsymbol{F}=\boldsymbol{f}|\boldsymbol{G}=\boldsymbol{g},\alpha,\alpha_2,\sigma\right\}} \\
&= \frac{\frac{1}{Z_{\text{noise}}(\sigma)}\exp\left(-\frac{1}{2\sigma^2}\left\|\boldsymbol{g}-\boldsymbol{f}\right\|^2\right)\frac{1}{Z_{\text{prior}}(\alpha,\alpha_2)}\exp\left\{-\frac{1}{2}\alpha\boldsymbol{f}^T\boldsymbol{C}\left(\alpha_2\right)\boldsymbol{f}\right\}}{\frac{1}{Z_{\text{posterior}}(\boldsymbol{g},\alpha,\alpha_2,\sigma)}\exp\left\{-\frac{1}{2\sigma^2}\left\|\boldsymbol{g}-\boldsymbol{f}\right\|^2-\frac{1}{2}\alpha\boldsymbol{f}^T\boldsymbol{C}\left(\alpha_2\right)\boldsymbol{f}\right\}} \\
&= \frac{Z_{\text{posterior}}(\boldsymbol{g},\alpha,\alpha_2,\sigma)}{Z_{\text{noise}}(\sigma)Z_{\text{prior}}(\alpha,\alpha_2)}. \qquad (2.54)
\end{aligned}$$

We can simplify the calculations by finding the maximum of the log of the evidence, which gives us

$$(\widehat{\alpha},\widehat{\sigma}) = \arg\max_{\alpha,\sigma}\left[\ln Z_{\text{posterior}}(\boldsymbol{g},\alpha,\alpha_2,\sigma) - \ln Z_{\text{noise}}(\sigma) - \ln Z_{\text{prior}}(\alpha,\alpha_2)\right]$$

$$
\begin{aligned}
&= \arg\max_{\alpha,\sigma}\Bigg[\frac{|\mathbf{V}|}{2}\ln(2\pi\sigma^2) - \frac{1}{2}\sum_{(p,q)\in\mathbf{V}}\ln\left(1+\alpha\sigma^2\lambda(\alpha_2,p,q)\right) \\
&\quad - \frac{1}{2}\sum_{(p,q)\in\mathbf{V}} G_{p,q}^{\dagger}\alpha\lambda(\alpha_2,p,q)\left(1+\sigma^2\alpha\lambda(\alpha_2,p,q)\right)^{-1} G_{p,q} - \frac{|\mathbf{V}|}{2}\ln(2\pi\sigma^2) \\
&\quad - \frac{|\mathbf{V}|}{2}\ln(2\pi) + \frac{|\mathbf{V}|}{2}\ln\alpha + \frac{1}{2}\sum_{(p,q)\in\mathbf{V}}\ln\lambda(\alpha_2,p,q)\Bigg] \\
&= \arg\max_{\alpha,\sigma}\Bigg[-\frac{|\mathbf{V}|}{2}\ln(2\pi) + \frac{|\mathbf{V}|}{2}\ln\alpha - \frac{1}{2}\sum_{(p,q)\in\mathbf{V}}\ln\left(1+\alpha\sigma^2\lambda(\alpha_2,p,q)\right) \\
&\quad - \frac{1}{2}\sum_{(p,q)\in\mathbf{V}} G_{p,q}^{\dagger}\alpha\lambda(\alpha_2,p,q)\left(1+\sigma^2\alpha\lambda(\alpha_2,p,q)\right)^{-1} G_{p,q} + \frac{1}{2}\sum_{(p,q)\in\mathbf{V}}\ln\lambda(\alpha_2,p,q)\Bigg]
\end{aligned}
\tag{2.55}
$$

where $\widehat{\alpha}$ and $\widehat{\sigma}$ are the estimated values of the hyperparameters α and σ respectively.

We notice that, due to the last term of (2.55), the values of $\lambda(\alpha_2,p,q)$ must be non-negative, which imposes some restrictions on the allowed values of α_2. Thus, by substituting $\theta = \frac{2\pi p}{V_x}$ and $\phi = \frac{2\pi q}{V_y}$ into equation (2.32), we have

$$
\begin{aligned}
\lambda(\alpha_2,\theta,\phi) &= 1 - \frac{1}{2}\cos\theta - \frac{1}{2}\cos\phi + \alpha_2\left(1 - \frac{1}{2}\cos(\theta+\phi) - \frac{1}{2}\cos(\theta-\phi)\right) \\
&= 1 - \frac{1}{2}\cos\theta - \frac{1}{2}\cos\phi \\
&\quad + \alpha_2\left(1 - \frac{1}{2}\left(\cos\theta\cos\phi - \sin\theta\sin\phi\right) - \frac{1}{2}\left(\cos\theta\cos\phi + \sin\theta\sin\phi\right)\right) \\
&= 1 - \frac{1}{2}\cos\theta - \frac{1}{2}\cos\phi + \alpha_2\left(1 - \cos\theta\cos\phi\right)
\end{aligned}
$$

therefore it follows that

$$
\begin{aligned}
1 - \frac{1}{2}\cos\theta - \frac{1}{2}\cos\phi + \alpha_2\left(1-\cos\theta\cos\phi\right) &\geq 0 \\
\alpha_2\left(1-\cos\theta\cos\phi\right) &\geq -1 + \frac{1}{2}\cos\theta + \frac{1}{2}\cos\phi.
\end{aligned}
\tag{2.56}
$$

Here we note that

$$
1 - \cos\theta\cos\phi \geq 0\,(\forall\phi,\theta)\,, \tag{2.57}
$$

$$
1 - \cos\theta\cos\phi = 0 \leftrightarrow (\cos\theta = \cos\phi = 1) \vee (\cos\theta = \cos\phi = -1)\,. \tag{2.58}
$$

If we take the case $\cos\theta = \cos\phi = 1$ and apply it to (2.56), we have

$$
0 \geq 0 \tag{2.59}
$$

so there is no restriction on α_2 in that case. Similarly, there is no restriction on α_2 when $\cos\theta = \cos\phi = -1$ since equation (2.56) then yields

$$
0 \geq -2. \tag{2.60}
$$

For the remaining cases, applying the property (2.57) to equation (2.56) allows us to write

$$
\alpha_2 \geq \frac{-1 + \frac{1}{2}\cos\theta + \frac{1}{2}\cos\phi}{1 - \cos\theta\cos\phi}. \tag{2.61}
$$

We now search for the maximum value of the right side of (2.61) by finding its partial derivatives. Setting the derivative according to θ to 0 yields

$$
\frac{-\frac{1}{2}\sin\theta\left(1-\cos\theta\cos\phi\right) - \sin\theta\cos\phi\left(-1 + \frac{1}{2}\cos\theta + \frac{1}{2}cos\phi\right)}{\left(1-\cos\theta\cos\phi\right)^2} = 0.
$$

Since we are not taking into account the case where the denominator is 0, we can write

$$-\frac{1}{2}\sin\theta\left(1-\cos\theta\cos\phi\right)-\sin\theta\cos\phi\left(-1+\frac{1}{2}\cos\theta+\frac{1}{2}cos\phi\right)=0$$
$$-\frac{1}{2}\sin\theta+\frac{1}{2}\sin\theta\cos\theta\cos\phi+\sin\theta\cos\phi-\frac{1}{2}\sin\theta\cos\theta\cos\phi-\frac{1}{2}\sin\theta\cos^2\phi=0$$
$$\sin\theta\left(\cos^2\phi-2\cos\phi+1\right)=0. \tag{2.62}$$

Therefore we have extrema for $\theta=0$ and $\theta=\pi$. By noticing that equation (2.61) is symmetrical with regards to θ and ϕ, we conclude that the derivative according to ϕ will yield extrema for $\phi=0$ and $\phi=\pi$. These results allow us to conclude that the extrema are located at $(\cos\theta,\cos\phi)=(1,1),(1,-1),(-1,1),(-1,-1)$. Since the right side of equation (2.61) becomes $-\infty$ for cases 1 and 4, we conclude that these are minima and that cases 2 and 3 are therefore maxima. For both cases 2 and 3, equation (2.61) yields

$$\alpha_2\geq-\frac{1}{2} \tag{2.63}$$

which defines the validity range of α_2.

Using equation (2.55), we find the value of $\widehat{\sigma}$ by solving the equation $\frac{d}{d\widehat{\sigma}^2}\ln(\Pr\{\boldsymbol{G}=\boldsymbol{g}|\widehat{\alpha},\alpha_2,\widehat{\sigma}\})=0$ as follows

$$\begin{aligned}
0&=-\frac{1}{2}\left\{\sum_{(p,q)\in\mathbf{V}}\frac{\widehat{\alpha}\lambda(\alpha_2,p,q)}{1+\widehat{\alpha}\widehat{\sigma}^2\lambda(\alpha_2,p,q)}\right\}-\frac{1}{2}\left\{\sum_{(p,q)\in\mathbf{V}}-\frac{G_{p,q}^{\dagger}\widehat{\alpha}^2\lambda(\alpha_2,p,q)^2G_{p,q}}{\left(1+\widehat{\alpha}\widehat{\sigma}^2\lambda(\alpha_2,p,q)\right)^2}\right\}\\
&=-\frac{1}{2\widehat{\sigma}^2}\left\{\sum_{(p,q)\in\mathbf{V}}\frac{\widehat{\alpha}\widehat{\sigma}^2\lambda(\alpha_2,p,q)}{1+\widehat{\alpha}\widehat{\sigma}^2\lambda(\alpha_2,p,q)}\right\}+\frac{1}{2}\left\{\sum_{(p,q)\in\mathbf{V}}G_{p,q}^{\dagger}\left(\frac{\widehat{\alpha}\lambda(\alpha_2,p,q)}{1+\widehat{\alpha}\widehat{\sigma}^2\lambda(\alpha_2,p,q)}\right)^2G_{p,q}\right\}\\
&=-\frac{1}{2\widehat{\sigma}^2}\left\{\sum_{(p,q)\in\mathbf{V}}\frac{-1+1+\widehat{\alpha}\widehat{\sigma}^2\lambda(\alpha_2,p,q)}{1+\widehat{\alpha}\widehat{\sigma}^2\lambda(\alpha_2,p,q)}\right\}\\
&\quad+\frac{1}{2}\left\{\sum_{(p,q)\in\mathbf{V}}G_{p,q}^{\dagger}\left(\frac{\widehat{\alpha}\lambda(\alpha_2,p,q)}{1+\widehat{\alpha}\widehat{\sigma}^2\lambda(\alpha_2,p,q)}\right)^2G_{p,q}\right\}\\
&=-\frac{1}{2\widehat{\sigma}^2}\left\{\sum_{(p,q)\in\mathbf{V}}\frac{-1}{1+\widehat{\alpha}\widehat{\sigma}^2\lambda(\alpha_2,p,q)}\right\}-\frac{1}{2\widehat{\sigma}^2}\left\{\sum_{(p,q)\in\mathbf{V}}1\right\}\\
&\quad+\frac{1}{2}\left\{\sum_{(p,q)\in\mathbf{V}}G_{p,q}^{\dagger}\left(\frac{\widehat{\alpha}\lambda(\alpha_2,p,q)}{1+\widehat{\alpha}\widehat{\sigma}^2\lambda(\alpha_2,p,q)}\right)^2G_{p,q}\right\}\\
\frac{|\mathbf{V}|}{2\widehat{\sigma}^2}&=\frac{1}{2\widehat{\sigma}^2}\left\{\sum_{(p,q)\in\mathbf{V}}\frac{1}{1+\widehat{\alpha}\widehat{\sigma}^2\lambda(\alpha_2,p,q)}\right\}+\frac{1}{2}\left\{\sum_{(p,q)\in\mathbf{V}}G_{p,q}^{\dagger}\left(\frac{\widehat{\alpha}\lambda(\alpha_2,p,q)}{1+\widehat{\alpha}\widehat{\sigma}^2\lambda(\alpha_2,p,q)}\right)^2G_{p,q}\right\}\\
\widehat{\sigma}^2&=\frac{\widehat{\sigma}^2}{|\mathbf{V}|}\sum_{(p,q)\in\mathbf{V}}\left\{\frac{1}{1+\widehat{\alpha}\widehat{\sigma}^2\lambda(\alpha_2,p,q)}+\widehat{\sigma}^2G_{p,q}^{\dagger}\left(\frac{\widehat{\alpha}\lambda(\alpha_2,p,q)}{1+\widehat{\alpha}\widehat{\sigma}^2\lambda(\alpha_2,p,q)}\right)^2G_{p,q}\right\}.
\end{aligned} \tag{2.64}$$

Similarly, we find the value $\widehat{\alpha}$ by solving the equation $\frac{d}{d\widehat{\alpha}}\ln(\Pr\{\boldsymbol{G}=\boldsymbol{g}|\widehat{\alpha},\alpha_2,\widehat{\sigma}\})=0$ as follows

$$\begin{aligned}
0&=\frac{|\mathbf{V}|}{2}\frac{1}{\widehat{\alpha}}-\frac{1}{2}\left\{\sum_{(p,q)\in\mathbf{V}}\frac{\widehat{\sigma}^2\lambda(\alpha_2,p,q)}{1+\widehat{\alpha}\widehat{\sigma}^2\lambda(\alpha_2,p,q)}\right\}\\
&\quad-\frac{1}{2}\left\{\sum_{(p,q)\in\mathbf{V}}G_{p,q}^{\dagger}\lambda(\alpha_2,p,q)G_{p,q}\left[\frac{1+\widehat{\alpha}\widehat{\sigma}^2\lambda(\alpha_2,p,q)-\widehat{\alpha}\widehat{\sigma}^2\lambda(\alpha_2,p,q)}{\left(1+\widehat{\alpha}\widehat{\sigma}^2\lambda(\alpha_2,p,q)\right)^2}\right]\right\}\\
\frac{|\mathbf{V}|}{\widehat{\alpha}}&=\sum_{(p,q)\in\mathbf{V}}\left\{\frac{\widehat{\sigma}^2\lambda(\alpha_2,p,q)}{1+\widehat{\alpha}\widehat{\sigma}^2\lambda(\alpha_2,p,q)}+\frac{G_{p,q}^{\dagger}\lambda(\alpha_2,p,q)G_{p,q}}{\left(1+\widehat{\alpha}\widehat{\sigma}^2\lambda(\alpha_2,p,q)\right)^2}\right\}
\end{aligned}$$

$$\widehat{\alpha}^{-1} = \frac{1}{|\mathbf{V}|} \sum_{(p,q)\in\mathbf{V}} \left\{ \frac{\widehat{\sigma}^2 \lambda(\alpha_2, p, q)}{1 + \widehat{\alpha}\widehat{\sigma}^2 \lambda(\alpha_2, p, q)} + \frac{G_{p,q}^{\dagger} \lambda(\alpha_2, p, q) G_{p,q}}{\left(1 + \widehat{\alpha}\widehat{\sigma}^2 \lambda(\alpha_2, p, q)\right)^2} \right\} \tag{2.65}$$

When actually computing the value of the log of the evidence given in (2.55), we notice that the value of the last term diverges when $\lambda(\alpha_2, p, q) = 0$. To get around this problem, we take advantage of the fact that we have a large number of pixels to approximate the discrete sum using an integral as follows: $\frac{1}{|\mathbf{V}|} \sum_{(p,q)\in\mathbf{V}} \approx \frac{1}{4\pi^2} \int_0^{2\pi} d\theta \int_0^{2\pi} d\phi$ with $\theta = \frac{2\pi q}{V_y}$ and $\phi = \frac{2\pi p}{V_x}$. Using this approximation and the integral formula

$$\int_0^{2\pi} \log\left(a + b\cos x\right) dx = 2\pi \log \frac{1}{2}\left(a + \sqrt{a^2 - b^2}\right) \quad (a \geq |b|) \tag{2.66}$$

from [11], the term can be rewritten as follows:

$$\begin{aligned}
&\frac{|\mathbf{V}|}{2} \frac{1}{|\mathbf{V}|} \sum_{(p,q)\in\mathbf{V}} \ln \lambda(\alpha_2, p, q) \\
&\approx \frac{|\mathbf{V}|}{2} \frac{1}{4\pi^2} \int_0^{2\pi} \int_0^{2\pi} \ln \lambda(\alpha_2, \theta, \phi) d\theta d\phi \\
&= \frac{|\mathbf{V}|}{2} \frac{1}{4\pi^2} \int_0^{2\pi} \int_0^{2\pi} \ln \left[1 - \frac{1}{2}\cos\theta - \frac{1}{2}\cos\phi + \alpha_2 - \frac{1}{2}\alpha_2 \cos(\theta + \phi) - \frac{1}{2}\alpha_2 \cos(\theta - \phi)\right] d\theta d\phi \\
&= \frac{|\mathbf{V}|}{2} \frac{1}{4\pi^2} \int_0^{2\pi} \int_0^{2\pi} \ln \Bigg[1 - \frac{1}{2}\cos\theta - \frac{1}{2}\cos\phi \\
&\quad + \alpha_2 - \frac{1}{2}\alpha_2 \left(\cos\theta\cos\phi - \sin\theta\sin\phi + \cos\theta\cos\phi + \sin\theta\sin\phi\right)\Bigg] d\theta d\phi \\
&= \frac{|\mathbf{V}|}{2} \frac{1}{4\pi^2} \int_0^{2\pi} \int_0^{2\pi} \ln \left[1 - \frac{1}{2}\cos\theta - \frac{1}{2}\cos\phi + \alpha_2 - \alpha_2\cos\theta\cos\phi\right] d\theta d\phi \\
&= \frac{|\mathbf{V}|}{2} \frac{1}{4\pi^2} \int_0^{2\pi} \int_0^{2\pi} \ln \left[1 - \frac{1}{2}\cos\phi + \alpha_2 - \frac{1}{2}\cos\theta\left(1 + 2\alpha_2\cos\phi\right)\right] d\theta d\phi \\
&= \frac{|\mathbf{V}|}{2} \frac{1}{4\pi^2} \int_0^{2\pi} \int_0^{2\pi} \ln \left[\frac{1}{2}(1 + 2\alpha_2\cos\phi)\left(\frac{2 - \cos\phi + 2\alpha_2}{1 + 2\alpha_2\cos\phi} - \cos\theta\right)\right] d\theta d\phi \\
&= \frac{|\mathbf{V}|}{2} \frac{1}{4\pi^2} \int_0^{2\pi} \int_0^{2\pi} \ln \left[\frac{1}{2}(1 + 2\alpha_2\cos\phi)\right] d\theta d\phi \\
&\quad + \frac{|\mathbf{V}|}{2} \frac{1}{4\pi^2} \int_0^{2\pi} \int_0^{2\pi} \ln \left(\frac{2 - \cos\phi + 2\alpha_2}{1 + 2\alpha_2\cos\phi} - \cos\theta\right) d\theta d\phi \\
&= \frac{|\mathbf{V}|}{2} \frac{1}{4\pi^2} \int_0^{2\pi} 2\pi \ln \left[\frac{1}{2}(1 + 2\alpha_2\cos\phi)\right] d\phi \\
&\quad + \frac{|\mathbf{V}|}{2} \frac{1}{4\pi^2} \int_0^{2\pi} 2\pi \ln \left[\frac{1}{2}\left(\frac{2 - \cos\phi + 2\alpha_2}{1 + 2\alpha_2\cos\phi} + \sqrt{\left(\frac{2 - \cos\phi + 2\alpha_2}{1 + 2\alpha_2\cos\phi}\right)^2 - 1}\right)\right] d\phi \\
&= \frac{|\mathbf{V}|}{2} \frac{1}{2\pi} \int_0^{2\pi} \ln \left[\frac{1}{4}(1 + 2\alpha_2\cos\phi)\left(\frac{2 - \cos\phi + 2\alpha_2}{1 + 2\alpha_2\cos\phi} + \sqrt{\left(\frac{2 - \cos\phi + 2\alpha_2}{1 + 2\alpha_2\cos\phi}\right)^2 - 1}\right)\right] d\phi \\
&= \frac{|\mathbf{V}|}{2} \frac{1}{2\pi} \int_0^{2\pi} \ln \left[\frac{1}{4}\left(2 - \cos\phi + 2\alpha_2 + \sqrt{\left(2 - \cos\phi + 2\alpha_2\right)^2 - (1 + 2\alpha_2\cos\phi)^2}\right)\right] d\phi \\
&\approx \frac{|\mathbf{V}|}{2} \frac{1}{V_y} \sum_{p=0}^{V_x - 1} \left(\ln \frac{1}{4}\right) + \frac{|\mathbf{V}|}{2} \frac{1}{V_y} \sum_{p=0}^{V_x - 1} \Bigg(2 - \cos\left(\frac{2\pi p}{V_x}\right) + 2\alpha_2 \\
&\quad + \sqrt{\left(2 - \cos\left(\frac{2\pi p}{V_x}\right) + 2\alpha_2\right)^2 - \left(1 + 2\alpha_2\cos\left(\frac{2\pi p}{V_x}\right)\right)^2}\Bigg)
\end{aligned} \tag{2.67}$$

$$\approx \frac{V_x^2}{2}\ln\frac{1}{4} + \frac{V_x}{2}\sum_{p=0}^{V_x-1}\ln\left(2-\cos\left(\frac{2\pi p}{V_x}\right)+2\alpha_2 + \sqrt{\left(2-\cos\left(\frac{2\pi p}{V_x}\right)+2\alpha_2\right)^2-\left(1+2\alpha_2\cos\left(\frac{2\pi p}{V_x}\right)\right)^2}\right). \tag{2.68}$$

We now find the values of α_2 for which the condition of (2.66) is respected at line (2.67), for any value of ϕ. From line (2.67) we have $a = \frac{2-\cos\phi+2\alpha_2}{1+2\alpha_2\cos\phi}$ and $b = -1$. So the condition of (2.66) is

$$a \geq |b| \leftrightarrow \frac{2-\cos\phi+2\alpha_2}{1+2\alpha_2\cos\phi} \geq 1. \tag{2.69}$$

We see that the condition is respected for $-0.5 < \alpha_2 < 0.5$ since we then have

$$\begin{aligned} a \geq |b| &\leftrightarrow 2-\cos\phi+2\alpha_2 \geq 1+2\alpha_2\cos\phi \\ &\leftrightarrow 1+2\alpha_2 \geq \cos\phi(1+2\alpha_2) \\ &\leftrightarrow 1 \geq \cos\phi. \end{aligned} \tag{2.70}$$

The condition is also respected for $\alpha_2 = -0.5$ since we then have

$$\begin{aligned} a \geq |b| &\leftrightarrow \frac{2-\cos\phi-1}{1-\cos\phi} \geq 1 \\ &\leftrightarrow 1 \geq 1. \end{aligned} \tag{2.71}$$

The condition is not respected in the case of $\alpha_2 < -0.5$ since for $\phi = 0$, we have

$$\begin{aligned} a \geq |b| &\leftrightarrow 2+2\alpha_2 \geq 1 \\ &\leftrightarrow \alpha_2 \geq -0.5. \end{aligned} \tag{2.72}$$

The state of the condition is unknown for $\alpha_2 = 0.5$ since its value diverges for $\phi = \pi$:

$$\frac{2-\cos\phi+2\alpha_2}{1+2\alpha_2\cos\phi} = \frac{4}{0}. \tag{2.73}$$

The condition is not respected in the case of $\alpha_2 > 0.5$ since for such a value, with $\phi = \pi$, we have

$$\begin{aligned} a \geq |b| &\leftrightarrow \frac{3+2\alpha_2}{1-2\alpha_2} \geq 1 \\ &\leftrightarrow 3+2\alpha_2 \leq 1-2\alpha_2 \\ &\leftrightarrow 4\alpha_2 \leq -2 \\ &\leftrightarrow \alpha_2 \leq -0.5. \end{aligned} \tag{2.74}$$

We also note that in the case of $\alpha_2 = -0.5$, in equation (2.68), we try to evaluate $\ln 0$ for the term in the sum where $p = 0$, so we need to reject the case where $\alpha_2 = -0.5$.

We shall therefore restrict the range of α_2 to

$$-0.5 < \alpha_2 < 0.5 \tag{2.75}$$

in our experiments.

2.3 Algorithm

In this section, we describe an image restoration algorithm based on our image restoration model. We use a fixed point iteration algorithm [12] to find our maximum likelihood estimates for the hyperparameters α and σ. As we saw in section 2.2.6, the extremum values for the hyperparameters α and σ can be expressed in the form of the simultaneous recursive equations $\alpha(r) = f(\alpha(r-1), \sigma(r-1))$ and $\sigma(r) = g(\alpha(r-1), \sigma(r-1))$. Therefore, in our algorithm, we find new values of $\widehat{\alpha}$ and $\widehat{\sigma}$ by applying their current

values to equations (2.64) and (2.65) and repeat that process until the algorithm converges. We shall assume that the algorithm has converged once we achieve the following 2 halting criteria:

$$e_1(r) = \left|\frac{a(r) - a(r-1)}{a(r-1)}\right| + \left|\frac{b(r) - b(r-1)}{b(r-1)}\right| < 10^{-4} \tag{2.76}$$

$$e_2(r) = \left|\frac{c(r) - c(r-1)}{c(r-1)}\right| < 10^{-4} \tag{2.77}$$

where $a(x)$, $b(x)$ and $c(x)$ are the values of $\widehat{\alpha}$, $\widehat{\sigma}^2$ and the log of evidence, respectively, at iteration x of the algorithm and r and $r-1$ are the current and previous iterations of the algorithm, respectively.

2.3.1 Algorithm Steps

Following are the steps of the practical algorithm.

Step 1.

(i) Compute the DFT of the degraded image to obtain the value of G. We note here that $G^\dagger$ is simply the complex conjugate of G so it does not need to be computed explicitly.

(ii) Compute the values of $\lambda(\alpha_2, p, q)$ using equation (2.33).

(iii) Initialize $a(0)$ to 0.0001

(iv) Initialize $b(0)$ to 10000.

(v) Initialize r to 0.

Step 2.

(i) Update $r \leftarrow r + 1$.

(ii) Using equation (2.65), update

$$a(r) \leftarrow \left(\frac{1}{|\mathbf{V}|}\sum_{(p,q)\in\mathbf{V}}\left\{\frac{b(r-1)\lambda(\alpha_2,p,q)}{1+a(r-1)b(r-1)\lambda(\alpha_2,p,q)} + \frac{G^\dagger_{p,q}G_{p,q}\lambda(\alpha_2,p,q)}{\left(1+a(r-1)b(r-1)\lambda(\alpha_2,p,q)\right)^2}\right\}\right)^{-1}. \tag{2.78}$$

(iii) Using equation (2.64), update

$$b(r) \leftarrow \frac{b(r-1)}{|\mathbf{V}|}\sum_{(p,q)\in\mathbf{V}}\left\{\frac{1}{1+a(r-1)b(r-1)\lambda(\alpha_2,p,q)} + b(r-1)G^\dagger_{p,q}G_{p,q}\left(\frac{a(r-1)\lambda(\alpha_2,p,q)}{1+a(r-1)b(r-1)\lambda(\alpha_2,p,q)}\right)^2\right\}. \tag{2.79}$$

(iv) Using equations (2.55) and (2.68), update

$$\begin{aligned} c(r) \leftarrow & -\frac{|\mathbf{V}|}{2}\ln 2\pi + \frac{|\mathbf{V}|}{2}\ln a(r) - \frac{1}{2}\sum_{(p,q)\in\mathbf{V}}\ln\left(1+a(r)b(r)\lambda(\alpha_2,p,q)\right) \\ & - \frac{1}{2}\sum_{(p,q)\in\mathbf{V}}G^\dagger_{p,q}G_{p,q}\frac{a(r)\lambda(\alpha_2,p,q)}{1+a(r)b(r)\lambda(\alpha_2,p,q)} + \frac{V_x^2}{2}\ln\frac{1}{4} \\ & + \frac{V_x}{2}\sum_{p=0}^{V_x-1}\ln\left(2-\cos\left(\frac{2\pi p}{V_x}\right)+2\alpha_2+\sqrt{\left(2-\cos\left(\frac{2\pi p}{V_x}\right)+2\alpha_2\right)^2-\left(1+2\alpha_2\cos\left(\frac{2\pi p}{V_x}\right)\right)^2}\right). \end{aligned} \tag{2.80}$$

Here we note that since $\overrightarrow{G}^\dagger$ is the conjugate transpose of $\overrightarrow{G}$, we can write $G_{p,q} = a + bi$ and $G^\dagger_{p,q} = a - bi$, so that $G^\dagger_{p,q}G_{p,q}$ is simply $a^2 + b^2$.

Step 3.

(i) Check the termination conditions of equations (2.76) and (2.77).

(ii) If the termination conditions are fulfilled, proceed to step 4. Otherwise go back to step 2.

Step 4.

(i) Update $\widehat{\alpha} \leftarrow a(r)$.

(ii) Update $\widehat{\sigma} \leftarrow \sqrt{b(r)}$.

(iii) Compute the values of $\left(1 + \widehat{\sigma}^2 \lambda(p,q)\,\widehat{\alpha}\right)^{-1} G_{p,q}$ for each p and q.

(iv) Apply the inverse DFT to the above values to obtain the restored image as described in (2.53).

2.3.2 Computational Complexity

We now analyse the complexity of our algorithm using the Big O notation. Here n is the number of pixels in the image, so $n = |\mathbf{V}|$.

Step 1 DFT computation using the FFT algorithm: $O(n \log n)$.

Step 2 Computation of $\widehat{\alpha}(r)$: $O(n)$.
Computation of $\widehat{\sigma}(r)$: $O(n)$.
Computation of the log of evidence: $O(n)$.
Total: $O(n)$.

Step 3 Computation of $e_1(r)$: $O(1)$.
Computation of $e_2(r)$: $O(1)$.
Total: $O(1)$.

Step 4 Computation of the values to be used in the inverse DFT: $O(n)$.
Restored image computation using the FFT algorithm: $O(n \log n)$.
Total: $O(n \log n)$.

This gives a total complexity of $O(n \log n)$.

2.4 Numerical Experiments

In this section, we present the numerical experiments we performed to evaluate our model as well as the results of these experiments. We also discuss these results.

2.4.1 Experiments

We applied our program to the original 256x256 pixels 8-bit grayscale images $\boldsymbol{f}$ presented in Fig.2.1. We first degraded the original images using additive white Gaussian noise with mean 0 and standard deviation $\sigma = 20$ and $\sigma = 40$ to produce 10 degraded images $\boldsymbol{g}$ for each original image and noise value. Examples of the degraded images are presented in Fig.2.2. We then applied our restoration algorithm to the degraded images to obtain the restored images $\widehat{\boldsymbol{f}}$. Examples of the resulting restored images are shown in Fig.2.12 to Fig.2.22.

2.4.2 Experimental Results

Our results are generated by fixing the value of $\alpha_2 = \frac{\alpha'}{\alpha}$ and applying our model to restore each set of 10 degraded images described in section 2.4.1 to obtain restored image sets containing 10 restored images for each value of α_2, σ and each original image.

We then measure the value of the the mean square error (MSE) and the mean structural similarity index (MSSIM) between the original image and the restored image as well as the log of evidence for each restored image. These measurements allow us to calculate the sample mean and sample standard

(a) Boat. (b) Lenna. (c) Mandrill.

Figure 2.1: Original images $\boldsymbol{f}$ used for the experiments.

deviation (s) of the MSE, MSSIM and log of evidence for each set of restored images. The sample standard deviation is defined in equation (2.82).

The MSE is used as a measure of the efficiency of our correction and is considered to be the dominant quantitative performance metric in the field of signal processing [13]. The MSE between two images $\boldsymbol{x}$ and $\boldsymbol{y}$ is defined as

$$\mathrm{MSE}(\mathrm{x},\mathrm{y}) = \frac{1}{|\mathbf{V}|}\sum_{\mathrm{i}\in\mathbf{V}}\left(\mathrm{x_i}-\mathrm{y_i}\right)^2. \tag{2.81}$$

The MSSIM is also used as a measure of the efficiency of our correction and is considered to yield results that are generally closer to the human perception of image fidelity and quality [13]. To measure the MSSIM, we use the method suggested in [14] and [15]. In particular, we use the suggested window defined as an 11x11 circular-symmetric Gaussian weighting function with standard deviation of 1.5. We note here that a higher value of the MSSIM indicates that the images being compared have a generally higher structural similarity and that the maximal value of 1.0 can only be attained if both images are identical.

We note here that the sample standard deviation is defined as

$$s = \sqrt{\frac{1}{N-1}\sum_{i=1}^{N}\left(x_i-\overline{x}\right)^2}. \tag{2.82}$$

Here N is the size of the sample and $\overline{x}$ is the sample mean defined as $\overline{x} = \frac{1}{N}\sum_{i=1}^{N} x_i$.

Figures 2.3, 2.4 and 2.5 show superpositions of 2 curves. The first curve (+ marks) shows, for various values of α_2, the values of the sample mean for the MSE, with error bars representing s. The second curve (x marks) shows the same statistics for the log of the evidence. By looking at these figures, we observe that an increase of the evidence is accompanied very closely by a decrease of the MSE in the case of the Boat image and is accompanied loosely by a decrease of the MSE in the case of the Mandrill image. However, we observe the opposite phenomenon in the case of the Lenna image, where an increase of the evidence is accompanied by an increase of the MSE. These results can be observed for the 2 noise levels used for our experiments.

Figures 2.6, 2.7 and 2.8 show superpositions of 2 curves. The first curve (+ marks) shows, for various values of α_2, the values of the sample mean for the estimated values of $\widehat{\alpha}$, with error bars representing s. The second curve (x marks) shows the same statistics for the estimated values of $\widehat{\sigma}^2$. By looking at these figures, we observe that an increase of the value of α_2 is accompanied by a decrease of both $\widehat{\alpha}$ and $\widehat{\sigma}^2$ for all images and noise levels.

Figures 2.9, 2.10 and 2.11 show superpositions of 2 curves. The first curve (+ marks) shows, for various values of α_2, the values of the sample mean for the MSE, with error bars representing s. The second curve (x marks) shows the same statistics for the estimated values of $\widehat{\sigma}^2$. By looking at these figures, we observe that the lowest values of the MSE occur for the values of α_2 where the estimated value of $\widehat{\sigma}^2$ is close to the actual value of σ^2 for all images and noise levels.

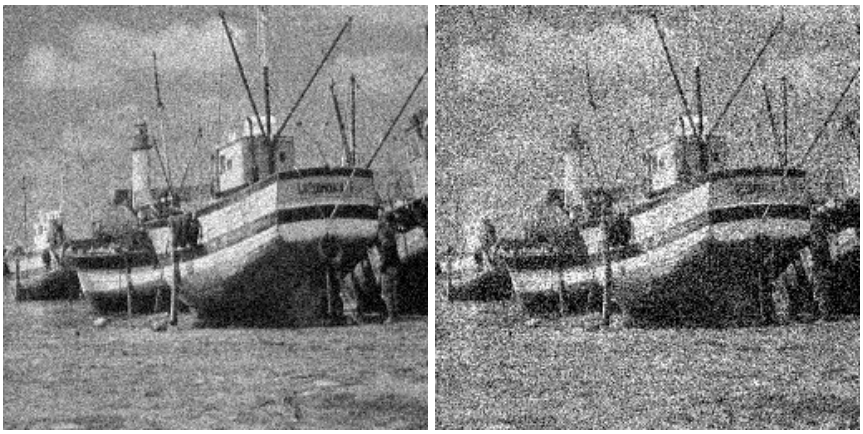

(a) Boat, $\sigma = 20$.

(b) Boat, $\sigma = 40$.

(c) Lenna, $\sigma = 20$.

(d) Lenna, $\sigma = 40$.

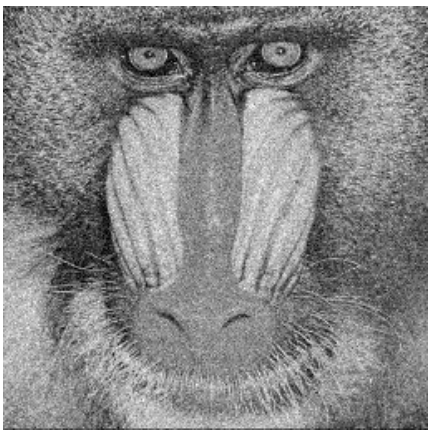

(e) Mandrill $\sigma = 20$.

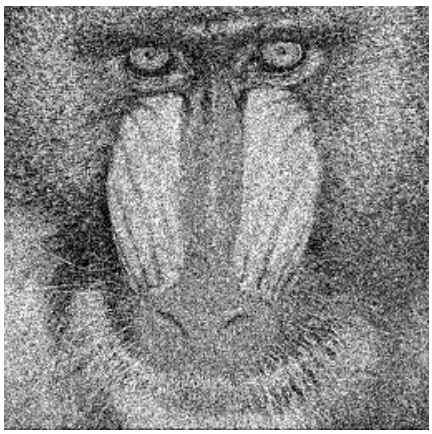

(f) Mandrill $\sigma = 40$.

Figure 2.2: Degraded images $\boldsymbol{g}$ used for the experiments. Degradation process is additive white Gaussian noise with mean 0 and standard deviation σ. (a) and (b) are generated from the original image in Figure 2.1a by setting $\sigma = 20$ and $\sigma = 40$, respectively. (c) and (d) are generated from the original image in Figure 2.1b. (e) and (f) are generated from the original image in Figure 2.1c.

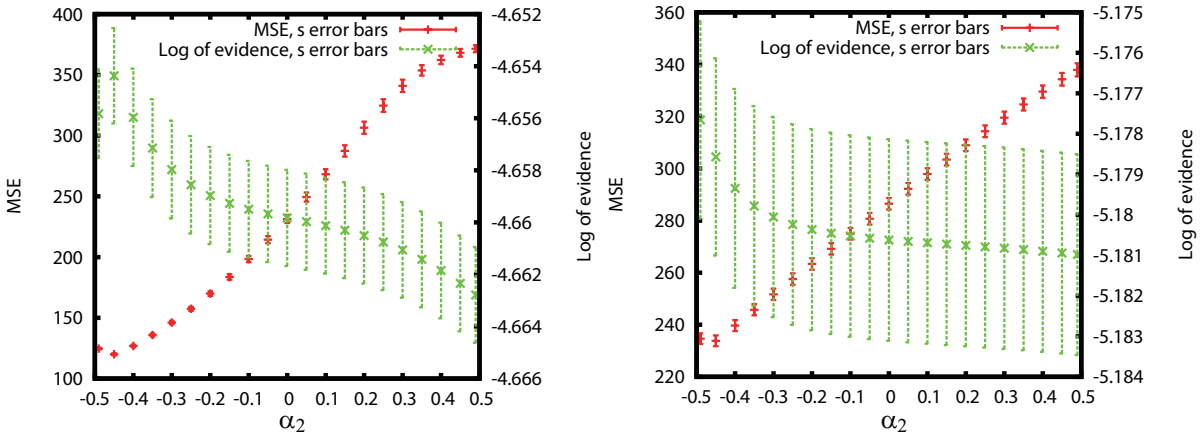

(a) $\sigma = 20$. (b) $\sigma = 40$.

Figure 2.3: Mean square error $\mathrm{MSE}(\boldsymbol{f}, \widehat{\boldsymbol{f}})$ (+ marks) and the log of evidence $\log \Pr\{\boldsymbol{G} = \boldsymbol{g} | \widehat{\alpha}, \alpha_2, \widehat{\sigma}\}$ (x marks) for the restored versions of the Boat image (Fig. 2.1a). The degraded images were generated with noise levels of $\sigma = 20$ in (a) and $\sigma = 40$ in (b). The estimates $\widehat{\alpha}$ and $\widehat{\sigma}$ are obtained by maximizing $\log \Pr\{\boldsymbol{G} = \boldsymbol{g} | \alpha, \alpha_2, \sigma\}$ with respect to α and σ for each fixed value of α_2. Here, the restored image $\widehat{\boldsymbol{f}}$ is defined as $\widehat{\boldsymbol{f}}(\widehat{\alpha}, \alpha_2, \widehat{\sigma})$ for each value of α_2. The values shown are the sample mean values ($\overline{x}$) of the 10 degraded images for each noise level with error bars corresponding to the sample standard deviation (s).

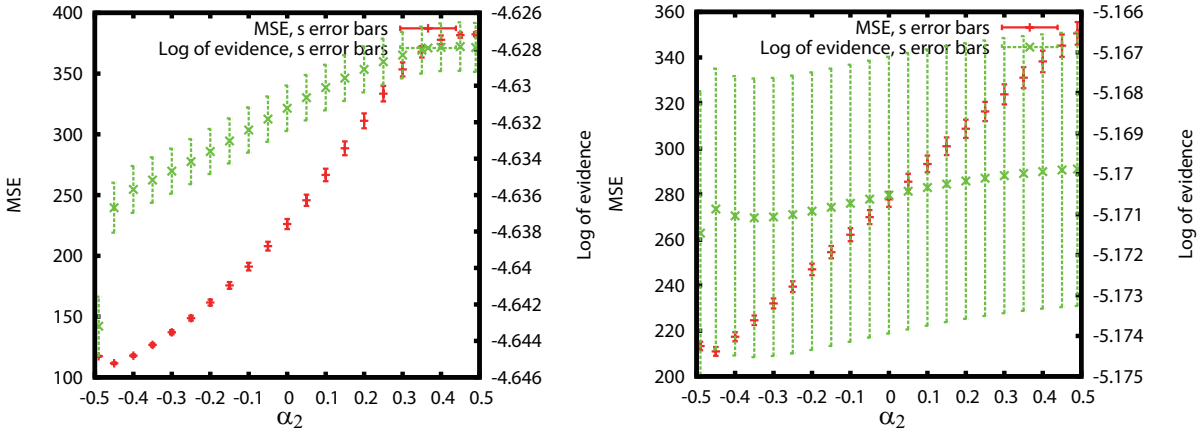

(a) $\sigma = 20$. (b) $\sigma = 40$.

Figure 2.4: Mean square error $\mathrm{MSE}(\boldsymbol{f}, \widehat{\boldsymbol{f}})$ (+ marks) and the log of evidence $\log \Pr\{\boldsymbol{G} = \boldsymbol{g} | \widehat{\alpha}, \alpha_2, \widehat{\sigma}\}$ (x marks) for the restored versions of the Lenna image (Fig. 2.1b). The degraded images were generated with noise levels of $\sigma = 20$ in (a) and $\sigma = 40$ in (b). The estimates $\widehat{\alpha}$ and $\widehat{\sigma}$ are obtained by maximizing $\log \Pr\{\boldsymbol{G} = \boldsymbol{g} | \alpha, \alpha_2, \sigma\}$ with respect to α and σ for each fixed value of α_2. Here, the restored image $\widehat{\boldsymbol{f}}$ is defined as $\widehat{\boldsymbol{f}}(\widehat{\alpha}, \alpha_2, \widehat{\sigma})$ for each value of α_2. The values shown are the sample mean values ($\overline{x}$) of the 10 degraded images for each noise level with error bars corresponding to the sample standard deviation (s).

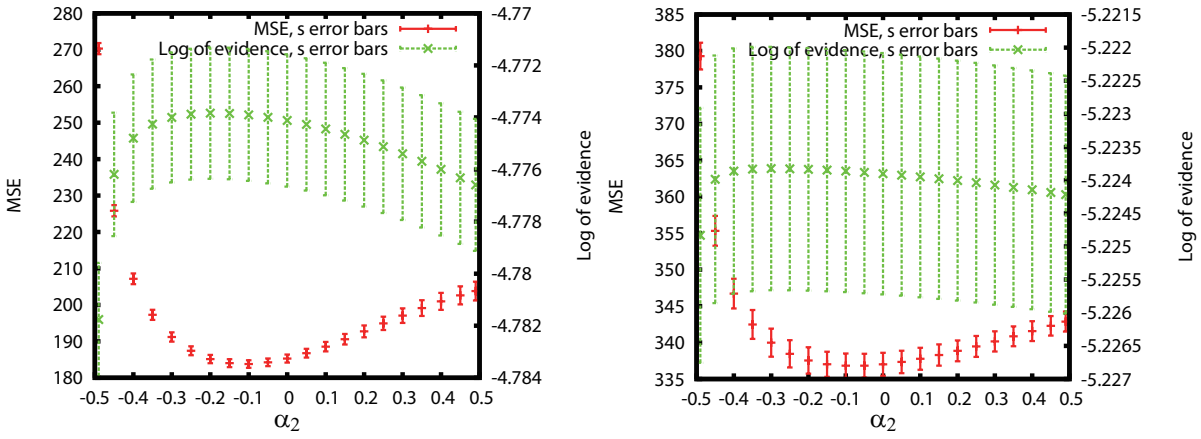

(a) $\sigma = 20$. (b) $\sigma = 40$.

Figure 2.5: Mean square error MSE$(\boldsymbol{f}, \widehat{\boldsymbol{f}})$ (+ marks) and the log of evidence $\log \Pr\{\boldsymbol{G} = \boldsymbol{g} | \widehat{\alpha}, \alpha_2, \widehat{\sigma}\}$ (x marks) for the restored versions of the Mandrill image (Fig. 2.1c). The degraded images were generated with noise levels of $\sigma = 20$ in (a) and $\sigma = 40$ in (b). The estimates $\widehat{\alpha}$ and $\widehat{\sigma}$ are obtained by maximizing $\log \Pr\{\boldsymbol{G} = \boldsymbol{g} | \alpha, \alpha_2, \sigma\}$ with respect to α and σ for each fixed value of α_2. Here, the restored image $\widehat{\boldsymbol{f}}$ is defined as $\widehat{\boldsymbol{f}}(\widehat{\alpha}, \alpha_2, \widehat{\sigma})$ for each value of α_2. The values shown are the sample mean values $(\overline{x})$ of the 10 degraded images for each noise level with error bars corresponding to the sample standard deviation (s).

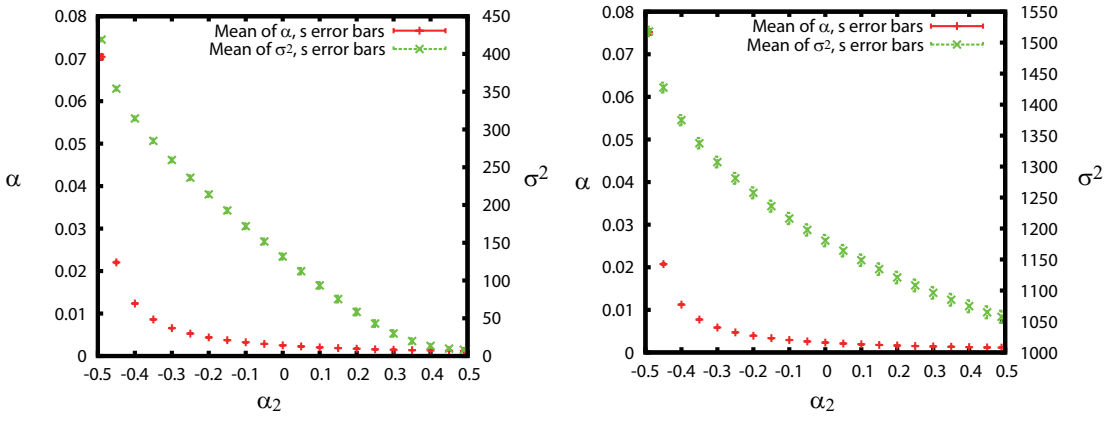

(a) $\sigma = 20$. (b) $\sigma = 40$.

Figure 2.6: Estimates $\widehat{\alpha}$ (+ marks) and $\widehat{\sigma}^2$ (x marks) obtained from the degraded versions of the Boat image (Fig. 2.1a) for various values of α_2. The degraded images were generated with noise levels of $\sigma = 20$ in (a) and $\sigma = 40$ in (b). The estimates are determined so as to maximize $\log \Pr\{\boldsymbol{G} = \boldsymbol{g} | \alpha, \alpha_2, \sigma\}$ with respect to α and σ for each fixed value of α_2. The values shown are the sample mean values $(\overline{x})$ of the 10 degraded images for each noise level with error bars corresponding to the sample standard deviation (s).

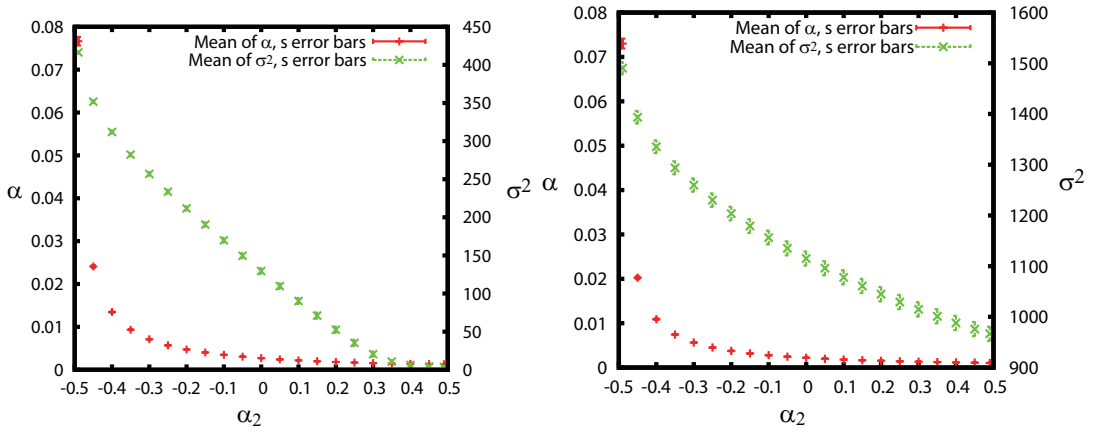

(a) $\sigma = 20$. (b) $\sigma = 40$.

Figure 2.7: Estimates $\widehat{\alpha}$ (+ marks) and $\widehat{\sigma}^2$ (x marks) obtained from the degraded versions of the Lenna image (Fig. 2.1b) for various values of α_2. The degraded images were generated with noise levels of $\sigma = 20$ in (a) and $\sigma = 40$ in (b). The estimates are determined so as to maximize $\log \Pr\{\boldsymbol{G} = \boldsymbol{g}|\alpha, \alpha_2, \sigma\}$ with respect to α and σ for each fixed value of α_2. The values shown are the sample mean values ($\overline{x}$) of the 10 degraded images for each noise level with error bars corresponding to the sample standard deviation (s).

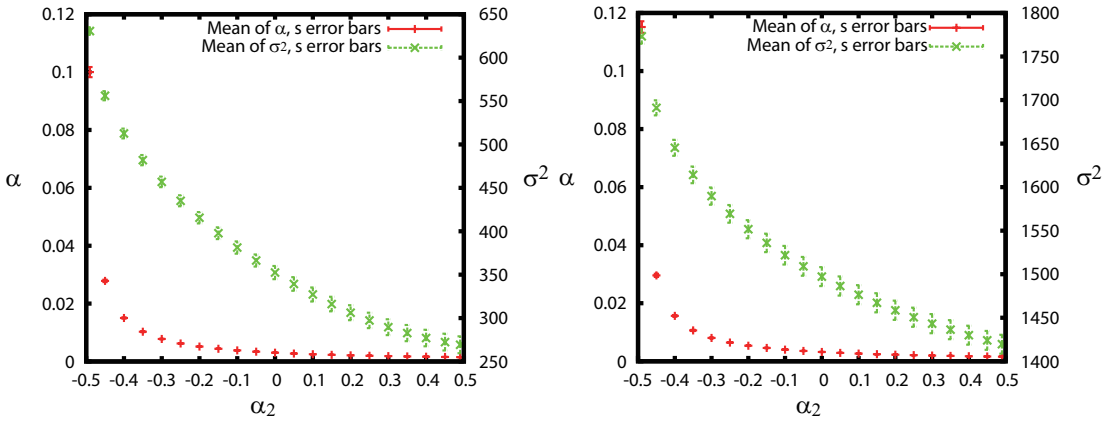

(a) $\sigma = 20$. (b) $\sigma = 40$.

Figure 2.8: Estimates $\widehat{\alpha}$ (+ marks) and $\widehat{\sigma}^2$ (x marks) obtained from the degraded versions of the Mandrill image (Fig. 2.1c) for various values of α_2. The degraded images were generated with noise levels of $\sigma = 20$ in (a) and $\sigma = 40$ in (b). The estimates are determined so as to maximize $\log \Pr\{\boldsymbol{G} = \boldsymbol{g}|\alpha, \alpha_2, \sigma\}$ with respect to α and σ for each fixed value of α_2. The values shown are the sample mean values ($\overline{x}$) of the 10 degraded images for each noise level with error bars corresponding to the sample standard deviation (s).

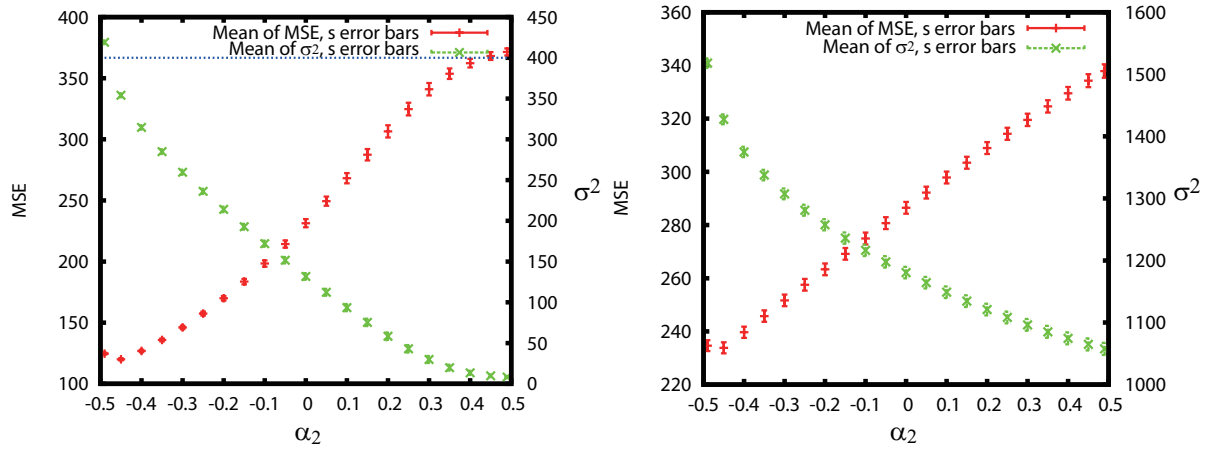

(a) $\sigma = 20$. (b) $\sigma = 40$.

Figure 2.9: Mean square error MSE($\boldsymbol{f}, \widehat{\boldsymbol{f}}$) (+ marks) and estimate $\widehat{\sigma}^2$ (x marks) for the restored versions of the Boat image (Fig. 2.1a). The degraded images were generated with noise levels of $\sigma = 20$ in (a) and $\sigma = 40$ in (b). The estimate $\widehat{\sigma}$ is obtained by maximizing $\log \Pr\{\boldsymbol{G} = \boldsymbol{g} | \alpha, \alpha_2, \sigma\}$ with respect to α and σ for each fixed value of α_2. Here, the restored image $\widehat{\boldsymbol{f}}$ is defined as $\widehat{\boldsymbol{f}}\,(\widehat{\alpha}, \alpha_2, \widehat{\sigma})$ for each value of α_2. The values shown are the sample mean values ($\overline{x}$) of the 10 degraded images for each noise level with error bars corresponding to the sample standard deviation (s).

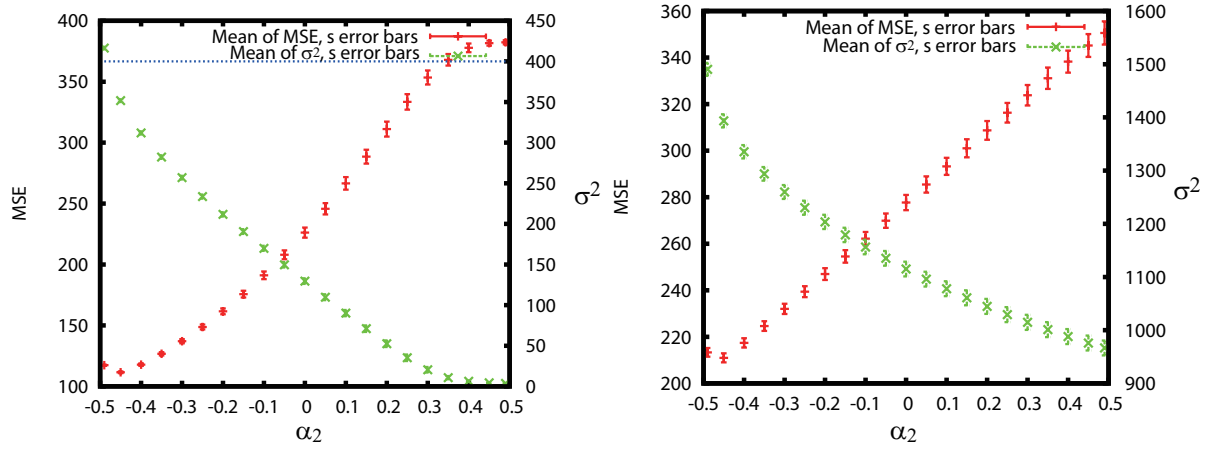

(a) $\sigma = 20$. (b) $\sigma = 40$.

Figure 2.10: Mean square error MSE($\boldsymbol{f}, \widehat{\boldsymbol{f}}$) (+ marks) and estimate $\widehat{\sigma}^2$ (x marks) for the restored versions of the Lenna image (Fig. 2.1b). The degraded images were generated with noise levels of $\sigma = 20$ in (a) and $\sigma = 40$ in (b). The estimate $\widehat{\sigma}$ is obtained by maximizing $\log \Pr\{\boldsymbol{G} = \boldsymbol{g} | \alpha, \alpha_2, \sigma\}$ with respect to α and σ for each fixed value of α_2. Here, the restored image $\widehat{\boldsymbol{f}}$ is defined as $\widehat{\boldsymbol{f}}\,(\widehat{\alpha}, \alpha_2, \widehat{\sigma})$ for each value of α_2. The values shown are the sample mean values ($\overline{x}$) of the 10 degraded images for each noise level with error bars corresponding to the sample standard deviation (s).

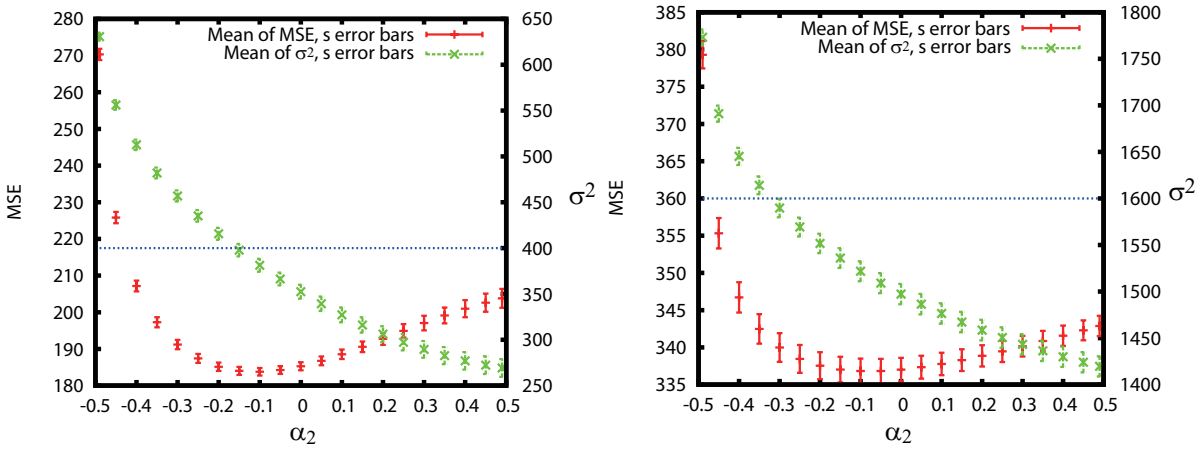

(a) $\sigma = 20$. (b) $\sigma = 40$.

Figure 2.11: Mean square error MSE($\boldsymbol{f}, \widehat{\boldsymbol{f}}$) (+ marks) and estimate $\widehat{\sigma}^2$ (x marks) for the restored versions of the Mandrill image (Fig. 2.1c). The degraded images were generated with noise levels of $\sigma = 20$ in (a) and $\sigma = 40$ in (b). The estimate $\widehat{\sigma}$ is obtained by maximizing $\log \Pr\{\boldsymbol{G} = \boldsymbol{g} | \alpha, \alpha_2, \sigma\}$ with respect to α and σ for each fixed value of α_2. Here, the restored image $\widehat{\boldsymbol{f}}$ is defined as $\widehat{\boldsymbol{f}}(\widehat{\alpha}, \alpha_2, \widehat{\sigma})$ for each value of α_2. The values shown are the sample mean values ($\overline{x}$) of the 10 degraded images for each noise level with error bars corresponding to the sample standard deviation (s).

Figures 2.12 to 2.22 show some results of the application of the next neighbour extension algorithm to the Boat, Lenna and Mandrill greyscale images for noise values of $\sigma = 20$ and $\sigma = 40$.

We only show the results for values of α_2 of -0.49, +0.49, 0.0, for the value producing the smallest MSE, namely $\alpha_2 = -0.45$ for Boat and Lenna, and $\alpha_2 = -0.1$ for Mandrill, as well as for the value producing the highest MSSIM, namely $\alpha_2 = -0.49$ for Boat and Lenna, as well as $\alpha_2 = -0.15$ and $\alpha_2 = 0.05$ for Mandrill with noise levels of $\sigma = 20$ and $\sigma = 40$ respectively. Also, only one restored image from the set of 10 is shown.

We observe that the resulting images are more blurry for low values of α_2 and that they become gradually less blurry, but more noisy, as α_2 increases. This can be explained by the previous observations where we saw that, as α_2 increases, the approximated values of $\widehat{\alpha}$ and $\widehat{\sigma}$ decrease, causing our model to assume that the noise level is lower and that correlation between neighbouring pixels is also low. As a consequence, less correction is applied, causing less blurring, but also leaving more noise in the corrected image. We also notice some improved horizontal and vertical edge preservation accompanied by grid-like artefacts in the restored images with a value of α_2 lower than -0.4. This is due to the fact that in such cases, our model approaches the superantiferromagnetic state, as shown in Fig. 1.1c

(a) Degraded Image. MSE=378. MSSIM=0.4978.

(b) Restored. $\alpha_2 = -0.49$. MSE=124. MSSIM=0.7461.

(c) Restored. $\alpha_2 = -0.45$. MSE=120. MSSIM=0.7270.

(d) Restored. $\alpha_2 = 0.0$. MSE=236. MSSIM=0.5760.

(e) Restored. $\alpha_2 = 0.49$. MSE=374. MSSIM=0.4994.

Figure 2.12: Restored images $\widehat{\boldsymbol{f}}(\boldsymbol{g}, \widehat{\alpha}, \alpha_2, \widehat{\sigma})$ obtained by means of the proposed Gauss-Markov random field model for one of the degraded versions of the Boat image (Fig. 2.1a). The degraded image was generated with a noise level of $\sigma = 20$, has $\mathrm{MSE}(\boldsymbol{f}, \boldsymbol{g}) = 378$, $\mathrm{MSSIM}(\boldsymbol{f}, \boldsymbol{g}) = 0.4978$, and is shown in (a). (b) $\alpha_2 = -0.49$, $\mathrm{MSE}(\boldsymbol{f}, \widehat{\boldsymbol{f}}(\boldsymbol{g}, \widehat{\alpha}, \alpha_2, \widehat{\sigma})) = 124$, $\mathrm{MSSIM}(\boldsymbol{f}, \widehat{\boldsymbol{f}}(\boldsymbol{g}, \widehat{\alpha}, \alpha_2, \widehat{\sigma})) = 0.7641$. (c) $\alpha_2 = -0.45$, $\mathrm{MSE}(\boldsymbol{f}, \widehat{\boldsymbol{f}}(\boldsymbol{g}, \widehat{\alpha}, \alpha_2, \widehat{\sigma})) = 120$, $\mathrm{MSSIM}(\boldsymbol{f}, \widehat{\boldsymbol{f}}(\boldsymbol{g}, \widehat{\alpha}, \alpha_2, \widehat{\sigma})) = 0.7270$. (d) $\alpha_2 = 0.0$, $\mathrm{MSE}(\boldsymbol{f}, \widehat{\boldsymbol{f}}(\boldsymbol{g}, \widehat{\alpha}, \alpha_2, \widehat{\sigma})) = 236$, $\mathrm{MSSIM}(\boldsymbol{f}, \widehat{\boldsymbol{f}}(\boldsymbol{g}, \widehat{\alpha}, \alpha_2, \widehat{\sigma})) = 0.5760$. (e) $\alpha_2 = 0.49$, $\mathrm{MSE}(\boldsymbol{f}, \widehat{\boldsymbol{f}}(\boldsymbol{g}, \widehat{\alpha}, \alpha_2, \widehat{\sigma})) = 374$, $\mathrm{MSSIM}(\boldsymbol{f}, \widehat{\boldsymbol{f}}(\boldsymbol{g}, \widehat{\alpha}, \alpha_2, \widehat{\sigma})) = 0.4994$.

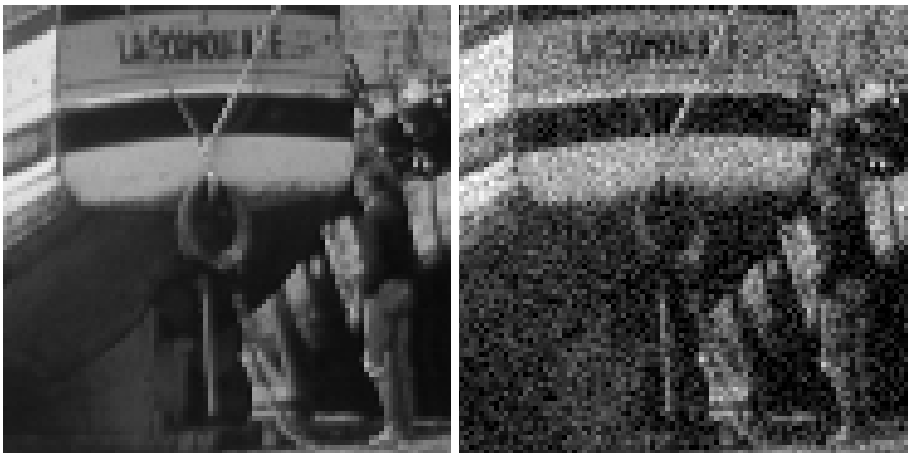

(a) Original Image. (b) Degraded Image. MSE=378. MSSIM=0.4978.

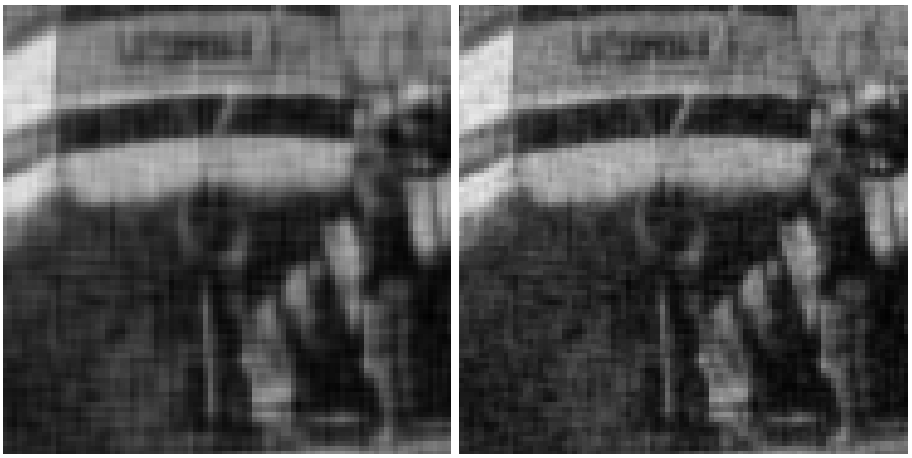

(c) Restored. $\alpha_2 = -0.49$. MSE=124. MSSIM=0.7461 (d) Restored. $\alpha_2 = -0.45$. MSE=120. MSSIM=0.7270

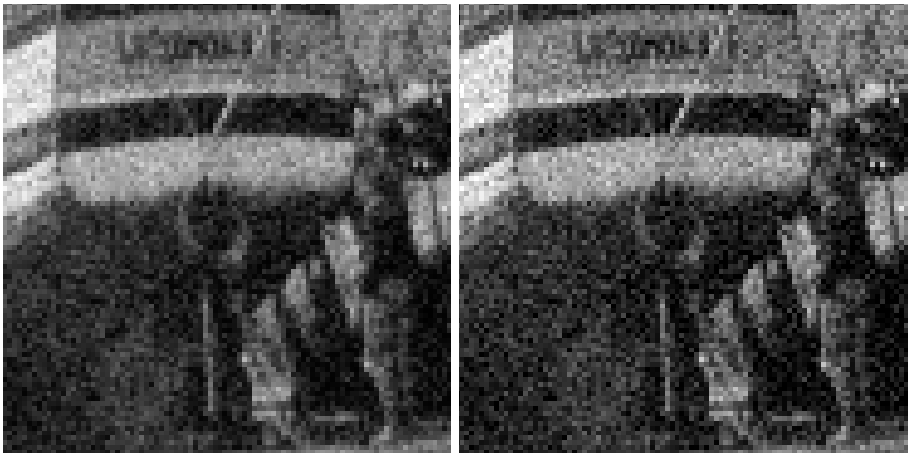

(e) Restored. $\alpha_2 = 0.0$. MSE=236. MSSIM=0.5760 (f) Restored. $\alpha_2 = 0.49$. MSE=374. MSSIM=0.4994

Figure 2.13: Details of the original image $\boldsymbol{f}$ in Fig. 2.1a, the degraded image $\boldsymbol{g}$ in Fig. 2.12a and the restored images $\widehat{\boldsymbol{f}}(\boldsymbol{g}, \widehat{\alpha}, \alpha_2, \widehat{\sigma})$ in Fig. 2.12. (a) Original image $\boldsymbol{f}$ in Fig. 2.1a. (b) Degraded image $\boldsymbol{g}$ in Fig. 2.12a. (c) Restored image $\widehat{\boldsymbol{f}}(\boldsymbol{g}, \widehat{\alpha}, \alpha_2, \widehat{\sigma})$ in Fig. 2.12b. (d) Restored image $\widehat{\boldsymbol{f}}(\boldsymbol{g}, \widehat{\alpha}, \alpha_2, \widehat{\sigma})$ in Fig. 2.12c. (e) Restored image $\widehat{\boldsymbol{f}}(\boldsymbol{g}, \widehat{\alpha}, \alpha_2, \widehat{\sigma})$ in Fig. 2.12d. (f) Restored image $\widehat{\boldsymbol{f}}(\boldsymbol{g}, \widehat{\alpha}, \alpha_2, \widehat{\sigma})$ in Fig. 2.12e.

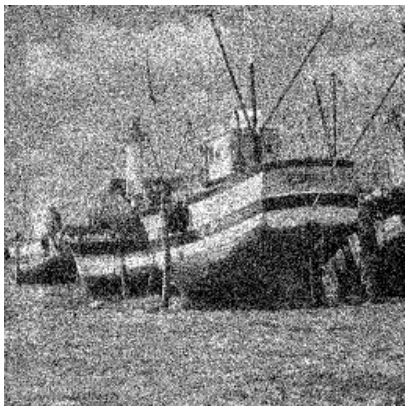

(a) Degraded Image. MSE=1486. MSSIM=0.2641.

(b) Restored. $\alpha_2 = -0.49$. MSE=236. MSSIM=0.6189.

(c) Restored. $\alpha_2 = -0.45$. MSE=235. MSSIM=0.6056.

(d) Restored. $\alpha_2 = 0.0$. MSE=286. MSSIM=0.5298.

(e) Restored. $\alpha_2 = 0.49$. MSE=336. MSSIM=0.4883.

Figure 2.14: Restored images $\widehat{\boldsymbol{f}}(\boldsymbol{g}, \widehat{\alpha}, \alpha_2, \widehat{\sigma})$ obtained by means of the proposed Gauss-Markov random field model for one of the degraded versions of the Boat image (Fig. 2.1a). The degraded image was generated with a noise level of $\sigma = 40$, has $\mathrm{MSE}(\boldsymbol{f}, \boldsymbol{g}) = 1486$, $\mathrm{MSSIM}(\boldsymbol{f}, \boldsymbol{g}) = 0.2641$ and is shown in (a). (b) $\alpha_2 = -0.49$, $\mathrm{MSE}(\boldsymbol{f}, \widehat{\boldsymbol{f}}(\boldsymbol{g}, \widehat{\alpha}, \alpha_2, \widehat{\sigma})) = 236$, $\mathrm{MSSIM}(\boldsymbol{f}, \widehat{\boldsymbol{f}}(\boldsymbol{g}, \widehat{\alpha}, \alpha_2, \widehat{\sigma})) = 0.6189$. (c) $\alpha_2 = -0.45$, $\mathrm{MSE}(\boldsymbol{f}, \widehat{\boldsymbol{f}}(\boldsymbol{g}, \widehat{\alpha}, \alpha_2, \widehat{\sigma})) = 235$, $\mathrm{MSSIM}(\boldsymbol{f}, \widehat{\boldsymbol{f}}(\boldsymbol{g}, \widehat{\alpha}, \alpha_2, \widehat{\sigma})) = 0.6056$. (d) $\alpha_2 = 0.0$, $\mathrm{MSE}(\boldsymbol{f}, \widehat{\boldsymbol{f}}(\boldsymbol{g}, \widehat{\alpha}, \alpha_2, \widehat{\sigma})) = 286$, $\mathrm{MSSIM}(\boldsymbol{f}, \widehat{\boldsymbol{f}}(\boldsymbol{g}, \widehat{\alpha}, \alpha_2, \widehat{\sigma})) = 0.5298$. (e) $\alpha_2 = 0.49$, $\mathrm{MSE}(\boldsymbol{f}, \widehat{\boldsymbol{f}}(\boldsymbol{g}, \widehat{\alpha}, \alpha_2, \widehat{\sigma})) = 336$, $\mathrm{MSSIM}(\boldsymbol{f}, \widehat{\boldsymbol{f}}(\boldsymbol{g}, \widehat{\alpha}, \alpha_2, \widehat{\sigma})) = 0.4883$.

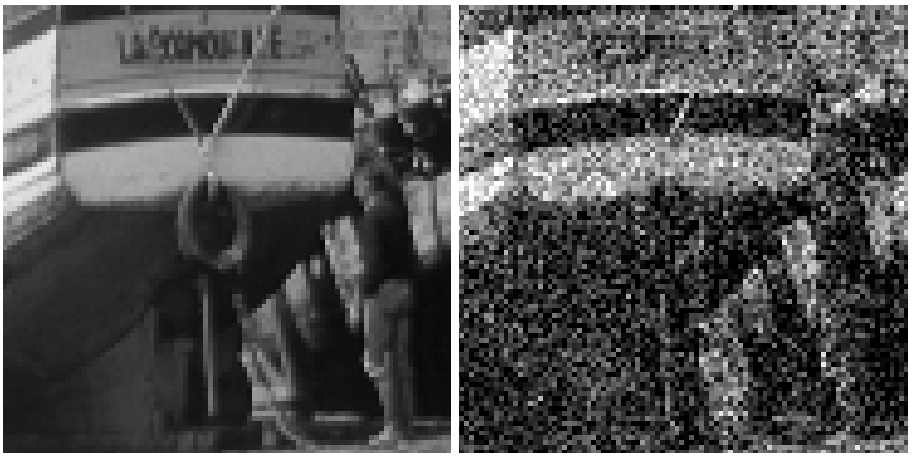

(a) Original Image. (b) Degraded Image. MSE=1486. MSSIM=0.2641.

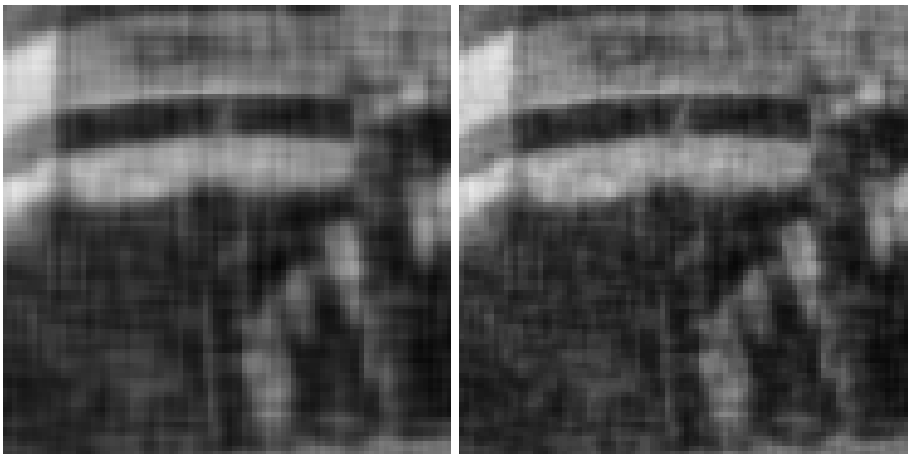

(c) Restored. $\alpha_2 = -0.49$. MSE=236. MSSIM=0.6189. (d) Restored. $\alpha_2 = -0.45$. MSE=235. MSSIM=0.6056.

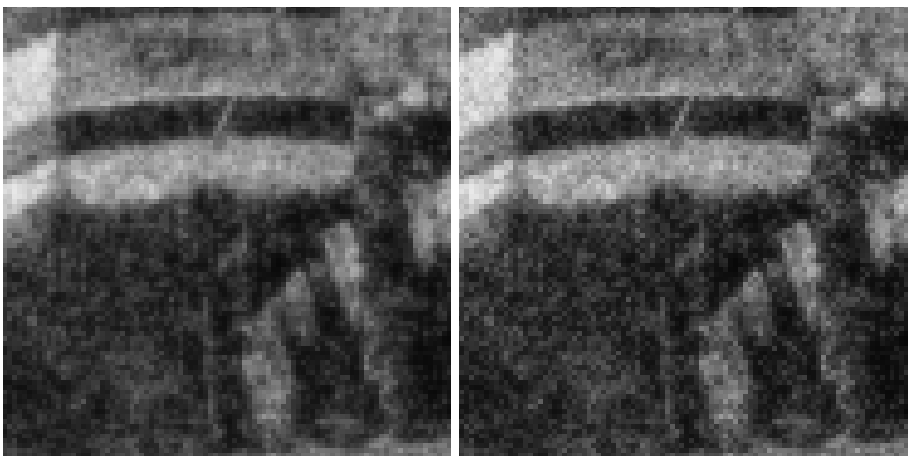

(e) Restored. $\alpha_2 = 0.0$. MSE=286. MSSIM=0.5298. (f) Restored. $\alpha_2 = 0.49$. MSE=336. MSSIM=0.4883.

Figure 2.15: Details of the original image $\boldsymbol{f}$ in Fig. 2.1a, the degraded image $\boldsymbol{g}$ in Fig. 2.14a and the restored images $\widehat{\boldsymbol{f}}(\boldsymbol{g}, \widehat{\alpha}, \alpha_2, \widehat{\sigma})$ in Fig. 2.14. (a) Original image $\boldsymbol{f}$ in Fig. 2.1a. (b) Degraded image $\boldsymbol{g}$ in Fig. 2.14a. (c) Restored image $\widehat{\boldsymbol{f}}(\boldsymbol{g}, \widehat{\alpha}, \alpha_2, \widehat{\sigma})$ in Fig. 2.14b. (d) Restored image $\widehat{\boldsymbol{f}}(\boldsymbol{g}, \widehat{\alpha}, \alpha_2, \widehat{\sigma})$ in Fig. 2.14c. (e) Restored image $\widehat{\boldsymbol{f}}(\boldsymbol{g}, \widehat{\alpha}, \alpha_2, \widehat{\sigma})$ in Fig. 2.14d. (f) Restored image $\widehat{\boldsymbol{f}}(\boldsymbol{g}, \widehat{\alpha}, \alpha_2, \widehat{\sigma})$ in Fig. 2.14e.

(a) Degraded Image. MSE=383. MSSIM=0.4453.

(b) Restored. $\alpha_2 = -0.49$. MSE=117. MSSIM=0.7393.

(c) Restored. $\alpha_2 = -0.45$. MSE=111. MSSIM=0.7133.

(d) Restored. $\alpha_2 = 0.0$. MSE=223. MSSIM=0.5375.

(e) Restored. $\alpha_2 = 0.49$. MSE=383. MSSIM=0.4454.

Figure 2.16: Restored images $\widehat{\boldsymbol{f}}(\boldsymbol{g}, \widehat{\alpha}, \alpha_2, \widehat{\sigma})$ obtained by means of the proposed Gauss-Markov random field model for one of the degraded versions of the Lenna image (Fig. 2.1b). The degraded image was generated with a noise level of $\sigma = 20$, has $\mathrm{MSE}(\boldsymbol{f}, \boldsymbol{g}) = 383$, $\mathrm{MSSIM}(\boldsymbol{f}, \boldsymbol{g}) = 0.4453$ and is shown in (a). (b) $\alpha_2 = -0.49$, $\mathrm{MSE}(\boldsymbol{f}, \widehat{\boldsymbol{f}}(\boldsymbol{g}, \widehat{\alpha}, \alpha_2, \widehat{\sigma})) = 117$, $\mathrm{MSSIM}(\boldsymbol{f}, \widehat{\boldsymbol{f}}(\boldsymbol{g}, \widehat{\alpha}, \alpha_2, \widehat{\sigma})) = 0.7393$. (c) $\alpha_2 = -0.45$, $\mathrm{MSE}(\boldsymbol{f}, \widehat{\boldsymbol{f}}(\boldsymbol{g}, \widehat{\alpha}, \alpha_2, \widehat{\sigma})) = 111$, $\mathrm{MSSIM}(\boldsymbol{f}, \widehat{\boldsymbol{f}}(\boldsymbol{g}, \widehat{\alpha}, \alpha_2, \widehat{\sigma})) = 0.7133$. (d) $\alpha_2 = 0.0$, $\mathrm{MSE}(\boldsymbol{f}, \widehat{\boldsymbol{f}}(\boldsymbol{g}, \widehat{\alpha}, \alpha_2, \widehat{\sigma})) = 223$, $\mathrm{MSSIM}(\boldsymbol{f}, \widehat{\boldsymbol{f}}(\boldsymbol{g}, \widehat{\alpha}, \alpha_2, \widehat{\sigma})) = 0.5375$. (e) $\alpha_2 = 0.49$, $\mathrm{MSE}(\boldsymbol{f}, \widehat{\boldsymbol{f}}(\boldsymbol{g}, \widehat{\alpha}, \alpha_2, \widehat{\sigma})) = 383$, $\mathrm{MSSIM}(\boldsymbol{f}, \widehat{\boldsymbol{f}}(\boldsymbol{g}, \widehat{\alpha}, \alpha_2, \widehat{\sigma})) = 0.4454$.

(a) Original Image. (b) Degraded Image. MSE=383. MSSIM=0.4453.

(c) Restored. $\alpha_2 = -0.49$. MSE=117. MSSIM=0.7393. (d) Restored. $\alpha_2 = -0.45$. MSE=111. MSSIM=0.7133.

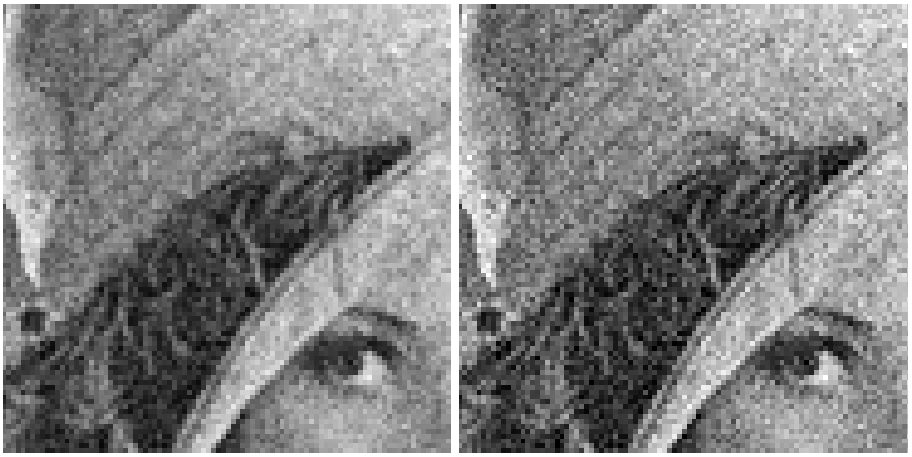

(e) Restored. $\alpha_2 = 0.0$. MSE=223. MSSIM=0.5375. (f) Restored. $\alpha_2 = 0.49$. MSE=383. MSSIM=0.4454.

Figure 2.17: Details of the original image $\boldsymbol{f}$ in Fig. 2.1b, the degraded image $\boldsymbol{g}$ in Fig. 2.16a and the restored images $\widehat{\boldsymbol{f}}(\boldsymbol{g}, \widehat{\alpha}, \alpha_2, \widehat{\sigma})$ in Fig. 2.16. (a) Original image $\boldsymbol{f}$ in Fig. 2.1b. (b) Degraded image $\boldsymbol{g}$ in Fig. 2.16a. (c) Restored image $\widehat{\boldsymbol{f}}(\boldsymbol{g}, \widehat{\alpha}, \alpha_2, \widehat{\sigma})$ in Fig. 2.16b. (d) Restored image $\widehat{\boldsymbol{f}}(\boldsymbol{g}, \widehat{\alpha}, \alpha_2, \widehat{\sigma})$ in Fig. 2.16c. (e) Restored image $\widehat{\boldsymbol{f}}(\boldsymbol{g}, \widehat{\alpha}, \alpha_2, \widehat{\sigma})$ in Fig. 2.16d. (f) Restored image $\widehat{\boldsymbol{f}}(\boldsymbol{g}, \widehat{\alpha}, \alpha_2, \widehat{\sigma})$ in Fig. 2.16e.

(a) Degraded Image. MSE=1462. MSSIM=0.2383.

(b) Restored. $\alpha_2 = -0.49$. MSE=214. MSSIM=0.6331.

(c) Restored. $\alpha_2 = -0.45$. MSE=212. MSSIM=0.6085.

(d) Restored. $\alpha_2 = 0.0$. MSE=279. MSSIM=0.5041.

(e) Restored. $\alpha_2 = 0.49$. MSE=351. MSSIM=0.4500.

Figure 2.18: Restored images $\widehat{\boldsymbol{f}}(\boldsymbol{g}, \widehat{\alpha}, \alpha_2, \widehat{\sigma})$ obtained by means of the proposed Gauss-Markov random field model for one of the degraded versions of the Lenna image (Fig. 2.1b). The degraded image was generated with a noise level of $\sigma = 40$, has $\mathrm{MSE}(\boldsymbol{f}, \boldsymbol{g}) = 1462$, $\mathrm{MSSIM}(\boldsymbol{f}, \boldsymbol{g}) = 0.2383$ and is shown in (a). (b) $\alpha_2 = -0.49$, $\mathrm{MSE}(\boldsymbol{f}, \widehat{\boldsymbol{f}}(\boldsymbol{g}, \widehat{\alpha}, \alpha_2, \widehat{\sigma})) = 214$, $\mathrm{MSSIM}(\boldsymbol{f}, \widehat{\boldsymbol{f}}(\boldsymbol{g}, \widehat{\alpha}, \alpha_2, \widehat{\sigma})) = 0.6331$. (c) $\alpha_2 = -0.45$, $\mathrm{MSE}(\boldsymbol{f}, \widehat{\boldsymbol{f}}(\boldsymbol{g}, \widehat{\alpha}, \alpha_2, \widehat{\sigma})) = 212$, $\mathrm{MSSIM}(\boldsymbol{f}, \widehat{\boldsymbol{f}}(\boldsymbol{g}, \widehat{\alpha}, \alpha_2, \widehat{\sigma})) = 0.6085$. (d) $\alpha_2 = 0.0$, $\mathrm{MSE}(\boldsymbol{f}, \widehat{\boldsymbol{f}}(\boldsymbol{g}, \widehat{\alpha}, \alpha_2, \widehat{\sigma})) = 279$, $\mathrm{MSSIM}(\boldsymbol{f}, \widehat{\boldsymbol{f}}(\boldsymbol{g}, \widehat{\alpha}, \alpha_2, \widehat{\sigma})) = 0.5041$. (e) $\alpha_2 = 0.49$, $\mathrm{MSE}(\boldsymbol{f}, \widehat{\boldsymbol{f}}(\boldsymbol{g}, \widehat{\alpha}, \alpha_2, \widehat{\sigma})) = 351$, $\mathrm{MSSIM}(\boldsymbol{f}, \widehat{\boldsymbol{f}}(\boldsymbol{g}, \widehat{\alpha}, \alpha_2, \widehat{\sigma})) = 0.4500$.

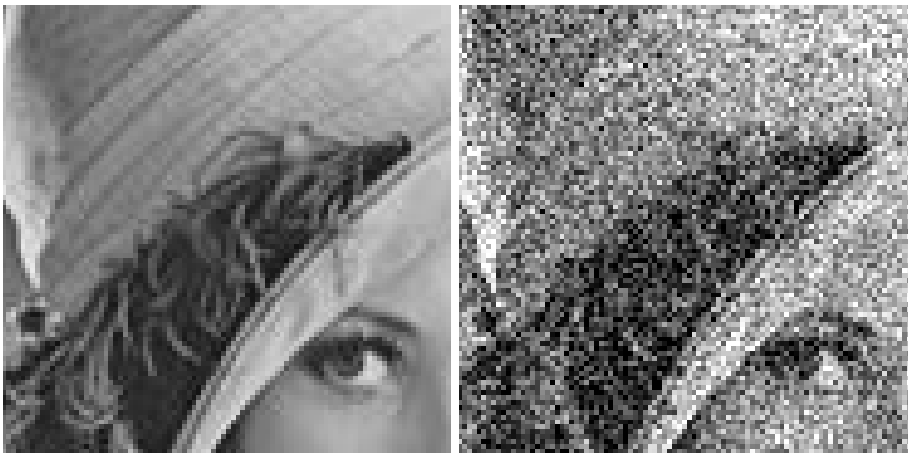

(a) Original Image.

(b) Degraded Image. MSE=1462. MSSIM=0.2383.

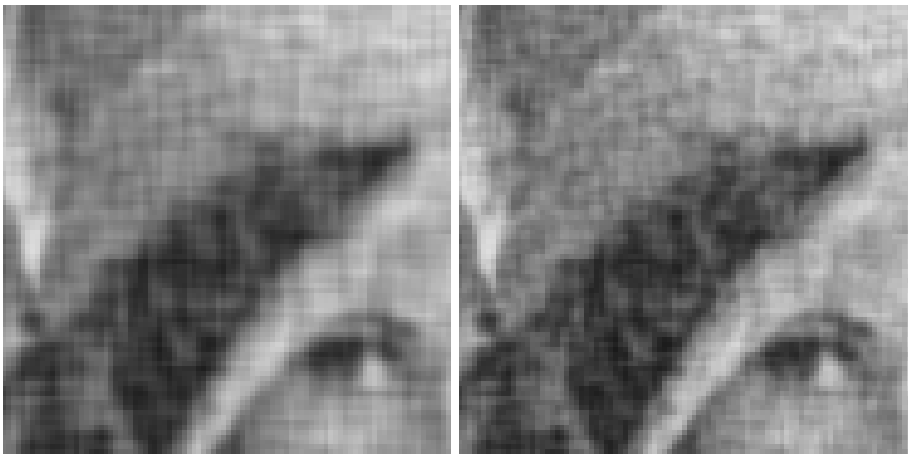

(c) Restored. $\alpha_2 = -0.49$. MSE=214. MSSIM=0.6331.

(d) Restored. $\alpha_2 = -0.45$. MSE=212. MSSIM=0.6085.

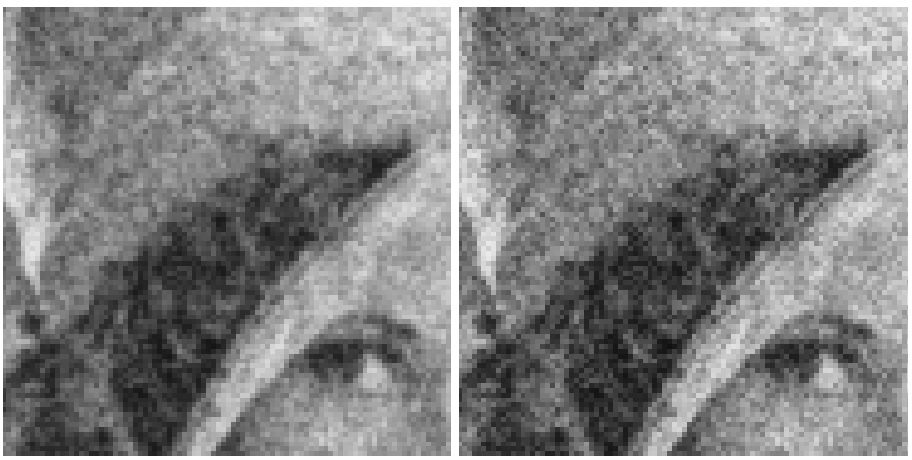

(e) Restored. $\alpha_2 = 0.0$. MSE=279. MSSIM=0.5041.

(f) Restored. $\alpha_2 = 0.49$. MSE=351. MSSIM=0.4500.

Figure 2.19: Details of the original image $\boldsymbol{f}$ in Fig. 2.1b, the degraded image $\boldsymbol{g}$ in Fig. 2.18a and the restored images $\widehat{\boldsymbol{f}}(\boldsymbol{g}, \widehat{\alpha}, \alpha_2, \widehat{\sigma})$ in Fig. 2.18. (a) Original image $\boldsymbol{f}$ in Fig. 2.1b. (b) Degraded image $\boldsymbol{g}$ in Fig. 2.18a. (c) Restored image $\widehat{\boldsymbol{f}}(\boldsymbol{g}, \widehat{\alpha}, \alpha_2, \widehat{\sigma})$ in Fig. 2.18b. (d) Restored image $\widehat{\boldsymbol{f}}(\boldsymbol{g}, \widehat{\alpha}, \alpha_2, \widehat{\sigma})$ in Fig. 2.18c. (e) Restored image $\widehat{\boldsymbol{f}}(\boldsymbol{g}, \widehat{\alpha}, \alpha_2, \widehat{\sigma})$ in Fig. 2.18d. (f) Restored image $\widehat{\boldsymbol{f}}(\boldsymbol{g}, \widehat{\alpha}, \alpha_2, \widehat{\sigma})$ in Fig. 2.18e.

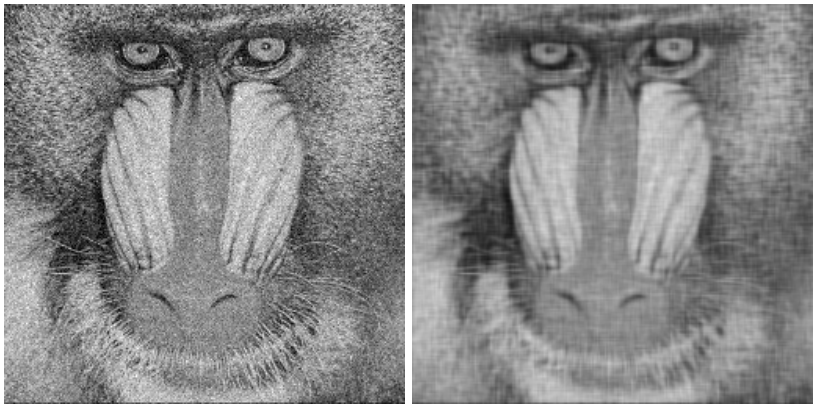

(a) Degraded Image. MSE=385. MSSIM=0.6065.

(b) Restored. $\alpha_2 = -0.49$. MSE=272. MSSIM=0.6099.

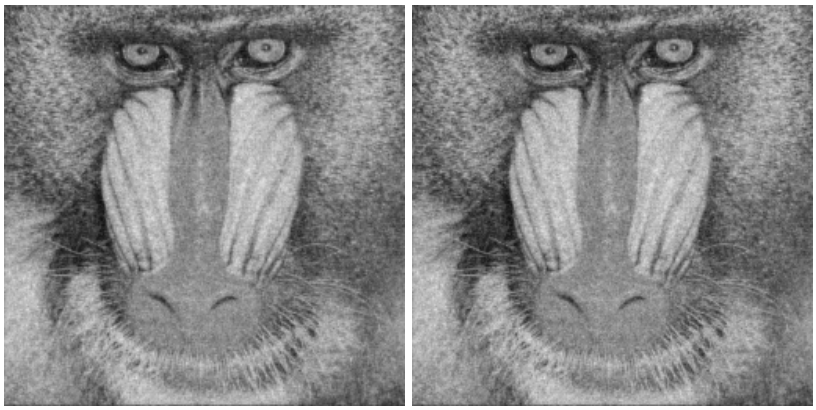

(c) Restored. $\alpha_2 = -0.15$. MSE=185.0. MSSIM=0.7153.

(d) Restored. $\alpha_2 = -0.1$. MSE=184.6. MSSIM=0.7150.

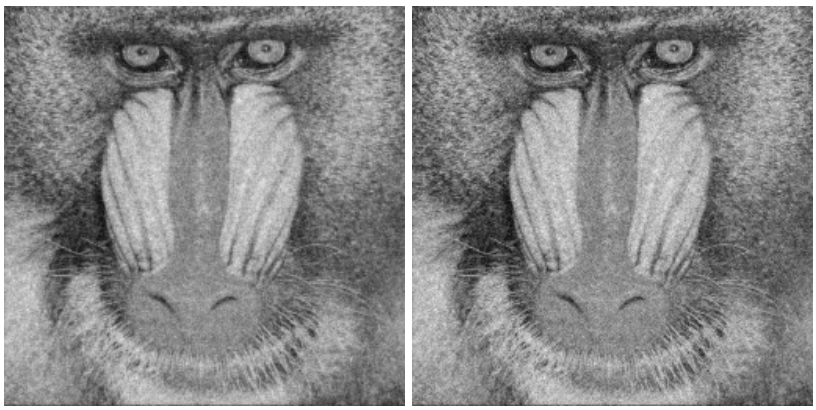

(e) Restored. $\alpha_2 = 0.0$. MSE=186. MSSIM=0.7126.

(f) Restored. $\alpha_2 = 0.49$. MSE=203. MSSIM=0.6959.

Figure 2.20: Restored images $\widehat{\boldsymbol{f}}(\boldsymbol{g}, \widehat{\alpha}, \alpha_2, \widehat{\sigma})$ obtained by means of the proposed Gauss-Markov random field model for one of the degraded versions of the Mandrill image (Fig. 2.1c). The degraded image was generated with a noise level of $\sigma = 20$, has $\text{MSE}(\boldsymbol{f}, \boldsymbol{g}) = 385$, $\text{MSSIM}(\boldsymbol{f}, \boldsymbol{g}) = 0.6065$ and is shown in (a). (b) $\alpha_2 = -0.49$, $\text{MSE}(\boldsymbol{f}, \widehat{\boldsymbol{f}}(\boldsymbol{g}, \widehat{\alpha}, \alpha_2, \widehat{\sigma})) = 272$, $\text{MSSIM}(\boldsymbol{f}, \widehat{\boldsymbol{f}}(\boldsymbol{g}, \widehat{\alpha}, \alpha_2, \widehat{\sigma})) = 0.6099$. (c) $\alpha_2 = -0.15$, $\text{MSE}(\boldsymbol{f}, \widehat{\boldsymbol{f}}(\boldsymbol{g}, \widehat{\alpha}, \alpha_2, \widehat{\sigma})) = 185.0$, $\text{MSSIM}(\boldsymbol{f}, \widehat{\boldsymbol{f}}(\boldsymbol{g}, \widehat{\alpha}, \alpha_2, \widehat{\sigma})) = 0.7153$. (d) $\alpha_2 = -0.1$, $\text{MSE}(\boldsymbol{f}, \widehat{\boldsymbol{f}}(\boldsymbol{g}, \widehat{\alpha}, \alpha_2, \widehat{\sigma})) = 184.6$, $\text{MSSIM}(\boldsymbol{f}, \widehat{\boldsymbol{f}}(\boldsymbol{g}, \widehat{\alpha}, \alpha_2, \widehat{\sigma})) = 0.7150$. (e) $\alpha_2 = 0.0$, $\text{MSE}(\boldsymbol{f}, \widehat{\boldsymbol{f}}(\boldsymbol{g}, \widehat{\alpha}, \alpha_2, \widehat{\sigma})) = 186$, $\text{MSSIM}(\boldsymbol{f}, \widehat{\boldsymbol{f}}(\boldsymbol{g}, \widehat{\alpha}, \alpha_2, \widehat{\sigma})) = 0.7126$. (f) $\alpha_2 = 0.49$, $\text{MSE}(\boldsymbol{f}, \widehat{\boldsymbol{f}}(\boldsymbol{g}, \widehat{\alpha}, \alpha_2, \widehat{\sigma})) = 203$, $\text{MSSIM}(\boldsymbol{f}, \widehat{\boldsymbol{f}}(\boldsymbol{g}, \widehat{\alpha}, \alpha_2, \widehat{\sigma})) = 0.6959$.

(a) Original Image.

(b) Degraded Image. MSE=385. MSSIM=0.6065.

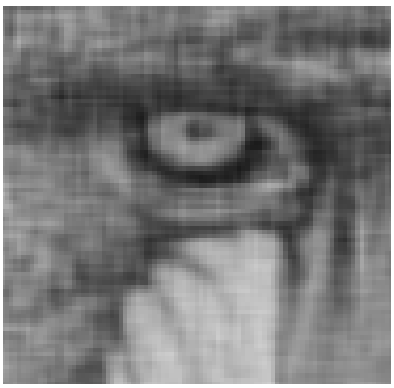

(c) Restored. $\alpha_2 = -0.49$. MSE=272. MSSIM=0.6099.

(d) Restored. $\alpha_2 = -0.15$. MSE=185.0. MSSIM=0.7153.

(e) Restored. $\alpha_2 = -0.1$. MSE=184.6. MSSIM=0.7150.

(f) Restored. $\alpha_2 = 0.0$. MSE=186. MSSIM=0.7126.

(g) Restored. $\alpha_2 = 0.49$. MSE=203. MSSIM=0.6959.

Figure 2.21: Details of the original image $\boldsymbol{f}$ in Fig. 2.1c, the degraded image $\boldsymbol{g}$ in Fig. 2.20a and the restored images $\widehat{\boldsymbol{f}}(\boldsymbol{g}, \widehat{\alpha}, \alpha_2, \widehat{\sigma})$ in Fig. 2.20. (a) Original image $\boldsymbol{f}$ in Fig. 2.1c. (b) Degraded image $\boldsymbol{g}$ in Fig. 2.20a. (c) Restored image $\widehat{\boldsymbol{f}}(\boldsymbol{g}, \widehat{\alpha}, \alpha_2, \widehat{\sigma})$ in Fig. 2.20b. (d) Restored image $\widehat{\boldsymbol{f}}(\boldsymbol{g}, \widehat{\alpha}, \alpha_2, \widehat{\sigma})$ in Fig. 2.20c. (e) Restored image $\widehat{\boldsymbol{f}}(\boldsymbol{g}, \widehat{\alpha}, \alpha_2, \widehat{\sigma})$ in Fig. 2.20d. (f) Restored image $\widehat{\boldsymbol{f}}(\boldsymbol{g}, \widehat{\alpha}, \alpha_2, \widehat{\sigma})$ in Fig. 2.20e. (g) Restored image $\widehat{\boldsymbol{f}}(\boldsymbol{g}, \widehat{\alpha}, \alpha_2, \widehat{\sigma})$ in Fig. 2.20f.

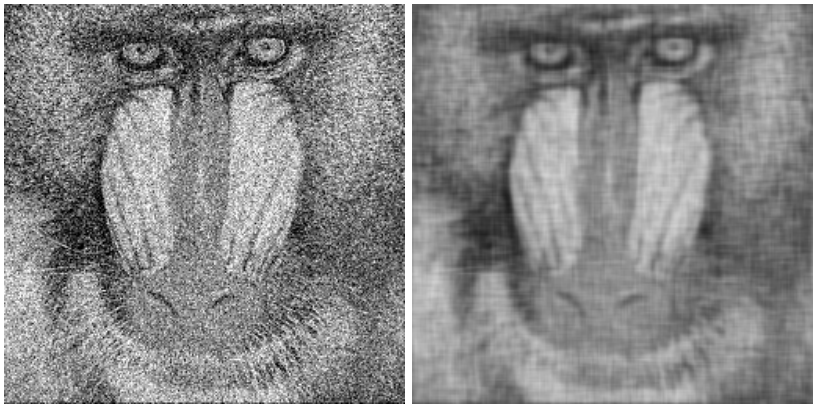

(a) Degraded Image. MSE=1518. MSSIM=0.3364.

(b) Restored. $\alpha_2 = -0.49$. MSE=380. MSSIM=0.4776.

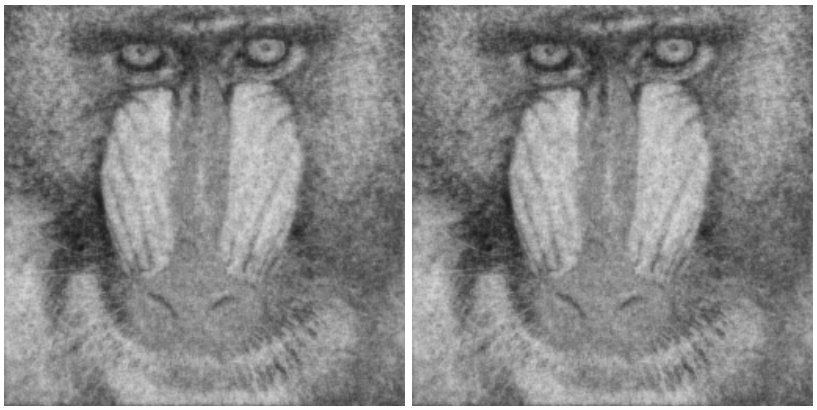

(c) Restored. $\alpha_2 = -0.05$. MSE=335.1. MSSIM=0.5438.

(d) Restored. $\alpha_2 = 0.0$. MSE=335.2. MSSIM=0.54402.

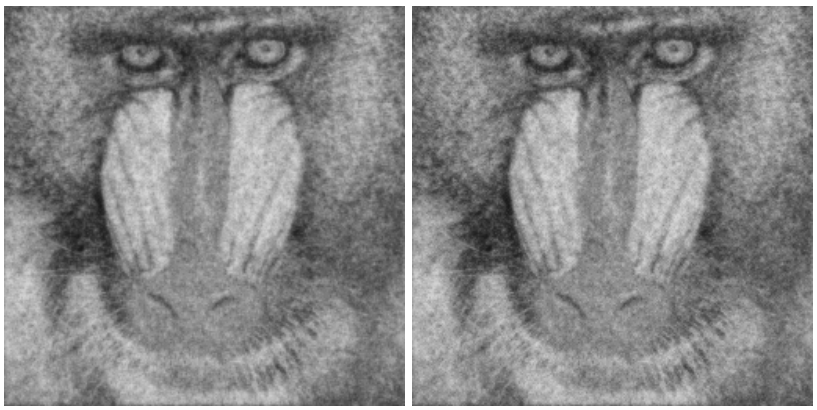

(e) Restored. $\alpha_2 = 0.05$. MSE=335.5. MSSIM=0.54403

(f) Restored. $\alpha_2 = 0.49$. MSE=341. MSSIM=0.5410

Figure 2.22: Restored images $\widehat{\boldsymbol{f}}(\boldsymbol{g}, \widehat{\alpha}, \alpha_2, \widehat{\sigma})$ obtained by means of the proposed Gauss-Markov random field model for one of the degraded versions of the Mandrill image (Fig. 2.1c). The degraded image was generated with a noise level of $\sigma = 40$, has $\mathrm{MSE}(\boldsymbol{f}, \boldsymbol{g}) = 1518$, $\mathrm{MSSIM}(\boldsymbol{f}, \boldsymbol{g}) = 0.3364$ and is shown in (a). (b) $\alpha_2 = -0.49$, $\mathrm{MSE}(\boldsymbol{f}, \widehat{\boldsymbol{f}}(\boldsymbol{g}, \widehat{\alpha}, \alpha_2, \widehat{\sigma})) = 380$, $\mathrm{MSSIM}(\boldsymbol{f}, \widehat{\boldsymbol{f}}(\boldsymbol{g}, \widehat{\alpha}, \alpha_2, \widehat{\sigma})) = 0.4776$. (c) $\alpha_2 = -0.05$, $\mathrm{MSE}(\boldsymbol{f}, \widehat{\boldsymbol{f}}(\boldsymbol{g}, \widehat{\alpha}, \alpha_2, \widehat{\sigma})) = 335.1$, $\mathrm{MSSIM}(\boldsymbol{f}, \widehat{\boldsymbol{f}}(\boldsymbol{g}, \widehat{\alpha}, \alpha_2, \widehat{\sigma})) = 0.5438$. (d) $\alpha_2 = 0.0$, $\mathrm{MSE}(\boldsymbol{f}, \widehat{\boldsymbol{f}}(\boldsymbol{g}, \widehat{\alpha}, \alpha_2, \widehat{\sigma})) = 335.2$, $\mathrm{MSSIM}(\boldsymbol{f}, \widehat{\boldsymbol{f}}(\boldsymbol{g}, \widehat{\alpha}, \alpha_2, \widehat{\sigma})) = 0.54402$. (e) $\alpha_2 = 0.05$, $\mathrm{MSE}(\boldsymbol{f}, \widehat{\boldsymbol{f}}(\boldsymbol{g}, \widehat{\alpha}, \alpha_2, \widehat{\sigma})) = 335.5$, $\mathrm{MSSIM}(\boldsymbol{f}, \widehat{\boldsymbol{f}}(\boldsymbol{g}, \widehat{\alpha}, \alpha_2, \widehat{\sigma})) = 0.54403$. (f) $\alpha_2 = 0.49$, $\mathrm{MSE}(\boldsymbol{f}, \widehat{\boldsymbol{f}}(\boldsymbol{g}, \widehat{\alpha}, \alpha_2, \widehat{\sigma})) = 341$, $\mathrm{MSSIM}(\boldsymbol{f}, \widehat{\boldsymbol{f}}(\boldsymbol{g}, \widehat{\alpha}, \alpha_2, \widehat{\sigma})) = 0.5410$.

(a) Original Image.

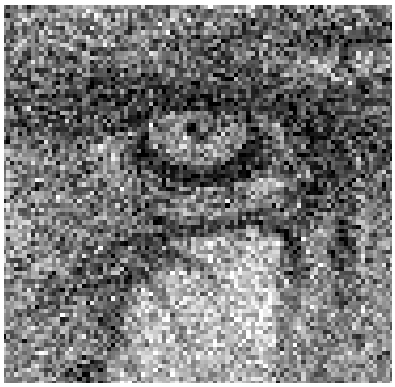

(b) Degraded Image. MSE=1518. MSSIM=0.3364.

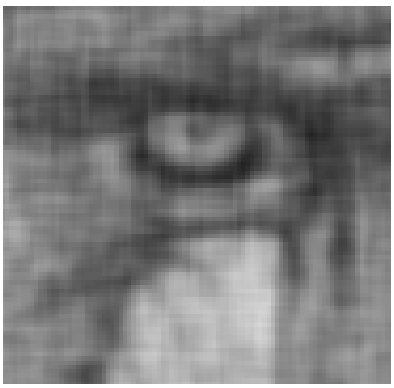

(c) Restored. $\alpha_2 = -0.49$. MSE=380. MSSIM=0.4776

(d) Restored. $\alpha_2 = -0.05$. MSE=335.1. MSSIM=0.5438

(e) Restored. $\alpha_2 = 0.0$. MSE=335.2. MSSIM=0.54402

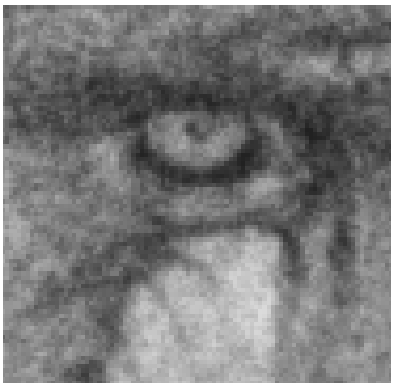

(f) Restored. $\alpha_2 = 0.05$. MSE=335.5. MSSIM=0.54403

(g) Restored. $\alpha_2 = 0.49$. MSE=341. MSSIM=0.5410

Figure 2.23: Details of the original image $\boldsymbol{f}$ in Fig. 2.1c, the degraded image $\boldsymbol{g}$ in Fig. 2.22a and the restored images $\widehat{\boldsymbol{f}}(\boldsymbol{g}, \widehat{\alpha}, \alpha_2, \widehat{\sigma})$ in Fig. 2.22. (a) Original image $\boldsymbol{f}$ in Fig. 2.1c. (b) Degraded image $\boldsymbol{g}$ in Fig. 2.22a. (c) Restored image $\widehat{\boldsymbol{f}}(\boldsymbol{g}, \widehat{\alpha}, \alpha_2, \widehat{\sigma})$ in Fig. 2.22b. (d) Restored image $\widehat{\boldsymbol{f}}(\boldsymbol{g}, \widehat{\alpha}, \alpha_2, \widehat{\sigma})$ in Fig. 2.22c. (e) Restored image $\widehat{\boldsymbol{f}}(\boldsymbol{g}, \widehat{\alpha}, \alpha_2, \widehat{\sigma})$ in Fig. 2.22d. (f) Restored image $\widehat{\boldsymbol{f}}(\boldsymbol{g}, \widehat{\alpha}, \alpha_2, \widehat{\sigma})$ in Fig. 2.22e. (g) Restored image $\widehat{\boldsymbol{f}}(\boldsymbol{g}, \widehat{\alpha}, \alpha_2, \widehat{\sigma})$ in Fig. 2.22f.

2.5 Chapter Summary

In this chapter, we described our solvable probabilistic model for greyscale images using second-neighbour pixel interactions. We derived the mathematical expressions related to this model and proposed an algorithm based on these results. Finally, we presented the results of numerical experiments using our algorithm and confirmed that, with a good choice of the hyperparameter α_2, we can obtain better image correction results by using our extension to the second-neighbour pixel interactions than by using the original model which only takes the next-neighbour pixel interactions into account. In particular, we saw that by using negative values of α_2, this model allows a better preservation of horizontal and vertical edges in the images, but at the same time, it introduces horizontal and vertical line artefacts in the images.

Chapter 3

Solvable Probabilistic Model with Second-Neighbour Interaction for Colour Image Restoration

3.1 Chapter Outline

In this chapter, we shall describe the extension to the second-neighbour pixel interactions of the solvable probabilistic model for colour images originally proposed by Tanaka and Horiguchi in [4]. We start with a detailed description of the model as well as the calculations involved in its formation. This is followed by the presentation of an image correction algorithm based on this model before concluding with a description of the numerical experiments we performed to evaluate this model. We note that this model constitutes an extension to colour images of the model described in Chapter 2.

3.2 Model Description

In this section we describe in detail the equations that form the basis of our solvable probabilistic model with second-neighbour interaction for colour image restoration. From these equations, we also derive mathematical expressions that can be used to implement an efficient image correction algorithm.

3.2.1 Image Model

We consider an image to be composed of a set of pixels on a square lattice. The lattice is defined as $\mathbf{V} \equiv \{(x,y)\,|x = 0,1,\ldots,Vx-1, y = 0,1,\ldots,Vy-1\}$ with $Vx = Vy$ so that the number of pixels in an image is defined as $|\mathbf{V}| = Vx^2$. We also consider the lattice to be on a torus so that it satisfies the periodic boundary conditions. We define a pixel as a vector consisting of three real values corresponding the light intensity in the three components of the RGB colour model at that location on the lattice. Thus we have the vectors

$$\boldsymbol{f}_{x,y} \equiv \begin{pmatrix} f_{x,y,\mathrm{red}} \\ f_{x,y,\mathrm{green}} \\ f_{x,y,\mathrm{blue}} \end{pmatrix} \quad \text{and} \quad \boldsymbol{g}_{x,y} \equiv \begin{pmatrix} g_{x,y,\mathrm{red}} \\ g_{x,y,\mathrm{green}} \\ g_{x,y,\mathrm{blue}} \end{pmatrix}$$

corresponding to the pixel (x,y) in the original and the degraded images respectively. We define the colour set $\mathbf{K} \equiv \{\mathrm{red},\mathrm{green},\mathrm{blue}\}$ corresponding to the three colour planes of the image. Thus the configurations of the original and degraded images are represented by $\boldsymbol{f} = \{f_{x,y,\kappa} \in \mathbb{R}|\,(x,y) \in \mathbf{V}, \kappa \in \mathbf{K}\}$ and $\boldsymbol{g} = \{g_{x,y,\kappa} \in \mathbb{R}|\,(x,y) \in \mathbf{V}, \kappa \in \mathbf{K}\}$ respectively. We associate the random variables

$$\boldsymbol{F} = \{F_{x,y,\kappa} \in \mathbb{R}|\,(x,y) \in \mathbf{V}, \kappa \in \mathbf{K}\} \quad \text{and} \quad \boldsymbol{G} = \{G_{x,y,\kappa} \in \mathbb{R}|\,(x,y) \in \mathbf{V}, \kappa \in \mathbf{K}\}$$

to the original and degraded images respectively.

3.2.2 Degradation Process Model

The model for the image degradation is additive white Gaussian noise $N(0, \sigma^2)$ added independently to each color component of each pixel. Thus we have the conditional probability function

$$\Pr\{\boldsymbol{G} = \boldsymbol{g} | \boldsymbol{F} = \boldsymbol{f}, \sigma\} \equiv \frac{1}{Z_{\text{noise}}(\sigma)} \exp\left(-\frac{1}{2\sigma^2} \|\boldsymbol{g} - \boldsymbol{f}\|^2\right) \tag{3.1}$$

where

$$Z_{\text{noise}}(\sigma) \equiv \int \exp\left(-\frac{1}{2\sigma^2} \|\boldsymbol{z} - \boldsymbol{f}\|^2\right) d\boldsymbol{z}, \tag{3.2}$$

with $\int d\boldsymbol{z} \equiv \int_{-\infty}^{+\infty} \int_{-\infty}^{+\infty} \cdots \int_{-\infty}^{+\infty} \prod_{(x,y)\in\mathbf{V}} \prod_{\kappa\in\mathbf{K}} dz_{x,y,\kappa}$, is the normalization constant and

$$\|\boldsymbol{g} - \boldsymbol{f}\|^2 \equiv \sum_{(x,y)\in\mathbf{V}} \sum_{\kappa\in\mathbf{K}} (g_{x,y,\kappa} - f_{x,y,\kappa})^2. \tag{3.3}$$

By substituting (3.3) into (3.2) and using the Gaussian integral formula, we can find the value of $Z_{\text{noise}}(\sigma)$ as follows:

$$\begin{aligned}
Z_{\text{noise}}(\sigma) &= \int \exp\left(-\frac{1}{2\sigma^2} \sum_{(x,y)\in\mathbf{L}} \sum_{\kappa\in\mathbf{K}} (g_{x,y,\kappa} - f_{x,y,\kappa})^2\right) d\boldsymbol{z} \\
&= \int \prod_{(x,y)\in\mathbf{V}} \prod_{\kappa\in\mathbf{K}} \exp\left(-\frac{1}{2\sigma^2} (z_{x,y,\kappa} - f_{x,y,\kappa})^2\right) d\boldsymbol{z} \\
&= \prod_{(x,y)\in\mathbf{V}} \prod_{\kappa\in\mathbf{K}} \int \exp\left(-\frac{1}{2\sigma^2} (z_{x,y,\kappa} - f_{x,y,\kappa})^2\right) dz_{x,y,\kappa} \\
&= \prod_{(x,y)\in\mathbf{V}} \prod_{\kappa\in\mathbf{K}} \sqrt{2\pi\sigma^2} \\
&= \left(2\pi\sigma^2\right)^{\frac{3|\mathbf{V}|}{2}}
\end{aligned} \tag{3.4}$$

3.2.3 A Priori Probability Density Function

We define the a priori probability density function (prior) that the original image $\boldsymbol{F}$ has a given configuration $\boldsymbol{f}$ as

$$\begin{aligned}
&\Pr\{\boldsymbol{F} = \boldsymbol{f} | \boldsymbol{\alpha}, \boldsymbol{\alpha}'\} \equiv \frac{1}{Z_{\text{prior}}(\boldsymbol{\alpha}, \boldsymbol{\alpha}')} \exp\Bigg\{-\frac{1}{8} \\
&\times \sum_{\kappa\in\mathbf{K}} \sum_{\kappa'\in\mathbf{K}} \Bigg(\alpha_{\kappa,\kappa'} \sum_{(x,y)\in\mathbf{V}} [(f_{x,y,\kappa} - f_{x+1,y,\kappa})(f_{x,y,\kappa'} - f_{x+1,y,\kappa'}) + (f_{x,y,\kappa} - f_{x,y+1,\kappa})(f_{x,y,\kappa'} - f_{x,y+1,\kappa'})] \\
&+\alpha'_{\kappa,\kappa'} \sum_{(x,y)\in\mathbf{V}} [(f_{x,y,\kappa} - f_{x+1,y+1,\kappa})(f_{x,y,\kappa'} - f_{x+1,y+1,\kappa'}) + (f_{x,y,\kappa} - f_{x+1,y-1,\kappa})(f_{x,y,\kappa'} - f_{x+1,y-1,\kappa'})]\Bigg)\Bigg\}
\end{aligned} \tag{3.5}$$

where

$$\boldsymbol{\alpha} \equiv \begin{pmatrix} \alpha_{red,red} & \alpha_{red,green} & \alpha_{red,blue} \\ \alpha_{green,red} & \alpha_{green,green} & \alpha_{green,blue} \\ \alpha_{blue,red} & \alpha_{blue,green} & \alpha_{blue,blue} \end{pmatrix} \tag{3.6}$$

is a hyperparameter expressing the correlation between the colour components of nearest neighbour pixels and is assumed to be symmetric, $\boldsymbol{\alpha}' \equiv \alpha_2 \boldsymbol{\alpha}$ is a hyperparameter expressing the correlation between the colour components of second-neighbour pixels and

$$Z_{\text{prior}}(\boldsymbol{\alpha},\boldsymbol{\alpha}') \equiv \int \exp\Bigg\{-\frac{1}{8}\sum_{\kappa\in\mathbf{K}}\sum_{\kappa'\in\mathbf{K}} \Bigg(\alpha_{\kappa,\kappa'}\sum_{(x,y)\in\mathbf{V}}[(f_{x,y,\kappa}-f_{x+1,y,\kappa})(f_{x,y,\kappa'}-f_{x+1,y,\kappa'})+(f_{x,y,\kappa}-f_{x,y+1,\kappa})(f_{x,y,\kappa'}-f_{x,y+1,\kappa'})] + \alpha'_{\kappa,\kappa'}\sum_{(x,y)\in\mathbf{V}}\big[(f_{x,y,\kappa}-f_{x+1,y+1,\kappa})(f_{x,y,\kappa'}-f_{x+1,y+1,\kappa'})+ (f_{x,y,\kappa}-f_{x+1,y-1,\kappa})(f_{x,y,\kappa'}-f_{x+1,y-1,\kappa'})\big]\Bigg)\Bigg\}d\boldsymbol{z} \quad (3.7)$$

with $\int d\boldsymbol{z} \equiv \int_{-\infty}^{+\infty}\int_{-\infty}^{+\infty}\dots\int_{-\infty}^{+\infty}\prod_{(x,y)\in\mathbf{V}}\prod_{\kappa\in\mathbf{K}} dz_{x,y,\kappa}$, is the normalization constant.

The exponential components of equation (3.5) can be rewritten using matrix notation as follows:

$$\begin{aligned}
&-\frac{1}{8}\sum_{\kappa\in\mathbf{K}}\sum_{\kappa'\in\mathbf{K}} \\
&\Bigg(\alpha_{\kappa,\kappa'}\sum_{(x,y)\in\mathbf{V}}[(f_{x,y,\kappa}-f_{x+1,y,\kappa})(f_{x,y,\kappa'}-f_{x+1,y,\kappa'})+(f_{x,y,\kappa}-f_{x,y+1,\kappa})(f_{x,y,\kappa'}-f_{x,y+1,\kappa'})] \\
&+\alpha'_{\kappa,\kappa'}\sum_{(x,y)\in\mathbf{V}}\Big[(f_{x,y,\kappa}-f_{x+1,y+1,\kappa})(f_{x,y,\kappa'}-f_{x+1,y+1,\kappa'}) \\
&+(f_{x,y,\kappa}-f_{x+1,y-1,\kappa})(f_{x,y,\kappa'}-f_{x+1,y-1,\kappa'})\Big]\Bigg) \\
=&-\frac{1}{8}\sum_{\kappa\in\mathbf{K}}\sum_{\kappa'\in\mathbf{K}}\alpha_{\kappa,\kappa'}\sum_{(x,y)\in\mathbf{V}} 2f_{x,y,\kappa}f_{x,y,\kappa'}-f_{x,y,\kappa}f_{x+1,y,\kappa'}-f_{x+1,y,\kappa}f_{x,y,\kappa'}+f_{x+1,y,\kappa}f_{x+1,y,\kappa'} \\
&-f_{x,y,\kappa}f_{x,y+1,\kappa'}-f_{x,y+1,\kappa}f_{x,y,\kappa'}+f_{x,y+1,\kappa}f_{x,y+1,\kappa'} \\
&+\alpha_2\Big[2f_{x,y,\kappa}f_{x,y,\kappa'}-f_{x,y,\kappa}f_{x+1,y+1,\kappa'}-f_{x+1,y+1,\kappa}f_{x,y,\kappa'}+f_{x+1,y+1,\kappa}f_{x+1,y+1,\kappa'} \\
&-f_{x,y,\kappa}f_{x+1,y-1,\kappa'}-f_{x+1,y-1,\kappa}f_{x,y,\kappa'}+f_{x+1,y-1,\kappa}f_{x+1,y-1,\kappa'}\Big] \\
=&-\frac{1}{8}\sum_{\kappa\in\mathbf{K}}\sum_{\kappa'\in\mathbf{K}}\alpha_{\kappa,\kappa'} \\
&\times\sum_{(x,y)\in\mathbf{V}} 4f_{x,y,\kappa}f_{x,y,\kappa'}-f_{x,y,\kappa}f_{x+1,y,\kappa'}-f_{x,y,\kappa}f_{x-1,y,\kappa'}-f_{x,y,\kappa}f_{x,y+1,\kappa'}-f_{x,y,\kappa}f_{x,y-1,\kappa'} \\
&+\alpha_2\Big[4f_{x,y,\kappa}f_{x,y,\kappa'}-f_{x,y,\kappa}f_{x+1,y+1,\kappa'}-f_{x,y,\kappa}f_{x-1,y-1,\kappa'}-f_{x,y,\kappa}f_{x+1,y-1,\kappa'}-f_{x,y,\kappa}f_{x-1,y+1,\kappa'}\Big] \\
=&-\frac{1}{2}\sum_{\kappa\in\mathbf{K}}\sum_{\kappa'\in\mathbf{K}}\alpha_{\kappa,\kappa'}\boldsymbol{f}^T\boldsymbol{C}(\alpha_2,\kappa,\kappa')\boldsymbol{f} \qquad (3.8)
\end{aligned}$$

where $\boldsymbol{C}(\alpha_2,\kappa,\kappa')$ is a $3|\mathbf{V}|\times 3|\mathbf{V}|$ matrix where the $(x,y,\mu|x',y',\mu')$ elements are defined by

$$\begin{aligned}
\langle x,y,\mu|x',y',\mu'\rangle \equiv \delta_{\kappa,\mu}\delta_{\kappa',\mu'}\Bigg(&\delta_{x,x'}\delta_{y,y'}-\frac{1}{4}\delta_{x,x'+1}\delta_{y,y'}-\frac{1}{4}\delta_{x,x'-1}\delta_{y,y'}-\frac{1}{4}\delta_{x,x'}\delta_{y,y'+1}-\frac{1}{4}\delta_{x,x'}\delta_{y,y'-1} \\
&+\alpha_2\left[\delta_{x,x'}\delta_{y,y'}-\frac{1}{4}\delta_{x,x'+1}\delta_{y,y'+1}-\frac{1}{4}\delta_{x,x'-1}\delta_{y,y'-1}-\frac{1}{4}\delta_{x,x'+1}\delta_{y,y'-1}-\frac{1}{4}\delta_{x,x'-1}\delta_{y,y'+1}\right]\Bigg) \\
&[(x,y),(x',y')\in\mathbf{V},\mu,\mu'\in\mathbf{K}] \qquad (3.9)
\end{aligned}$$

where $\delta_{a,b}$ is the Kronecker delta.

Thus equation (3.5) can be rewritten as

$$\Pr\{\boldsymbol{F}=\boldsymbol{f}|\boldsymbol{\alpha},\alpha_2\} \equiv \frac{1}{Z_{\text{prior}}(\boldsymbol{\alpha},\alpha_2)}\exp\left(-\frac{1}{2}\sum_{\kappa\in\mathbf{K}}\sum_{\kappa'\in\mathbf{K}}\alpha_{\kappa,\kappa'}\boldsymbol{f}^T\boldsymbol{C}(\alpha_2,\kappa,\kappa')\boldsymbol{f}\right) \qquad (3.10)$$

with

$$Z_{\text{prior}}(\boldsymbol{\alpha}, \alpha_2) \equiv \int \exp\left(-\frac{1}{2}\sum_{\kappa\in\mathbf{K}}\sum_{\kappa'\in\mathbf{K}} \alpha_{\kappa,\kappa'} \boldsymbol{z}^T \boldsymbol{C}(\alpha_2, \kappa, \kappa')\, \boldsymbol{z}\right) d\boldsymbol{z}. \tag{3.11}$$

This model corresponds to an extension to the second-neighbour interactions of the multichannel CAR model proposed by Tanaka and Horiguchi in [4] and its energy function is

$$\begin{aligned}\frac{1}{8}\sum_{\kappa\in\mathbf{K}}\sum_{\kappa'\in\mathbf{K}}\Bigg(&\alpha_{\kappa,\kappa'} \\ &\times \sum_{(x,y)\in\mathbf{V}} \left[(f_{x,y,\kappa} - f_{x+1,y,\kappa})(f_{x,y,\kappa'} - f_{x+1,y,\kappa'}) + (f_{x,y,\kappa} - f_{x,y+1,\kappa})(f_{x,y,\kappa'} - f_{x,y+1,\kappa'})\right] \\ +\alpha'_{\kappa,\kappa'} \sum_{(x,y)\in\mathbf{V}} &\Big[(f_{x,y,\kappa} - f_{x+1,y+1,\kappa})(f_{x,y,\kappa'} - f_{x+1,y+1,\kappa'}) + (f_{x,y,\kappa} - f_{x+1,y-1,\kappa})(f_{x,y,\kappa'} - f_{x+1,y-1,\kappa'})\Big]\Bigg)\end{aligned} \tag{3.12}$$

We note that $\boldsymbol{f}$ is a Multivariate Gaussian Markov random field with dimension 3 (MGMRF$_3$), with mean $\mathbf{0}$ and precision matrix $\boldsymbol{Q} = \sum_{\kappa\in\mathbf{K}}\sum_{\kappa'\in\mathbf{K}} \alpha_{\kappa,\kappa'}\boldsymbol{C}(\alpha_2, \kappa, \kappa')$. In [10], Rue and Held derive the following properties for a MGMRF$_p$ $\boldsymbol{x} = \left(\boldsymbol{x}_1^T, \ldots, \boldsymbol{x}_n^T\right)^T$ with mean $\boldsymbol{\mu}$ and precision matrix $\boldsymbol{Q} > 0$ where $\dim(\boldsymbol{x}_i) = p$:

$$\Pr(\boldsymbol{x}_i|\boldsymbol{x}_{-i}) \text{ is a normal distribution} \tag{3.13}$$

$$\mathrm{E}(\boldsymbol{x}_i|\boldsymbol{x}_{-i}) = \boldsymbol{\mu}_i - \boldsymbol{Q}_{ii}^{-1}\sum_{j:j\sim i} \boldsymbol{Q}_{ij}(\boldsymbol{x}_j - \boldsymbol{\mu}_j) \tag{3.14}$$

$$\mathrm{Prec}(\boldsymbol{x}_i|\boldsymbol{x}_{-i}) = \boldsymbol{Q}_{ii} \tag{3.15}$$

where $\mathrm{E}(\boldsymbol{x}_i|\boldsymbol{x}_{-i})$ is the expected value of $\boldsymbol{x}_i$ given all other values of $\boldsymbol{x}$ (i.e. $\boldsymbol{x}_{-i} \equiv \{\boldsymbol{x}\backslash x_i\}$), $j : j \sim i$ means the values of j that are neighbors of i (i.e. $i \neq j$ and $\boldsymbol{Q}_{ij} \neq \mathbf{0}$), Prec is the precision matrix and is the inverse of the covariance matrix. Applying these properties to our model, we obtain the following:

$$\begin{aligned}\mathrm{E}(\boldsymbol{f}_{(x,y)}|\boldsymbol{f}_{-(x,y)}) &= \boldsymbol{\mu}_{(x,y)} - \boldsymbol{Q}_{(x,y),(x,y)}^{-1}\sum_{(i,j):(i,j)\sim(x,y)} \boldsymbol{Q}_{(x,y),(i,j)}(\boldsymbol{f}_{(i,j)} - \boldsymbol{\mu}_{(i,j)}) \\ &= -(\boldsymbol{\alpha}+\boldsymbol{\alpha}')^{-1}\sum_{(i,j):(i,j)\sim(x,y)} \boldsymbol{Q}_{(x,y),(i,j)}\boldsymbol{f}_{(i,j)} \\ &= -(\boldsymbol{\alpha}+\boldsymbol{\alpha}')^{-1}\left[-\boldsymbol{\alpha}\left(\frac{1}{4}\boldsymbol{f}_{(x+1,y)} + \frac{1}{4}\boldsymbol{f}_{(x-1,y)} + \frac{1}{4}\boldsymbol{f}_{(x,y+1)} + \frac{1}{4}\boldsymbol{f}_{(x,y-1)}\right)\right. \\ &\quad \left. -\boldsymbol{\alpha}'\left(\frac{1}{4}\boldsymbol{f}_{(x+1,y+1)} + \frac{1}{4}\boldsymbol{f}_{(x+1,y-1)} + \frac{1}{4}\boldsymbol{f}_{(x-1,y+1)} + \frac{1}{4}\boldsymbol{f}_{(x-1,y-1)}\right)\right] \\ &= \frac{1}{4}(\boldsymbol{\alpha}+\boldsymbol{\alpha}')^{-1}\left[\boldsymbol{\alpha}\left(\boldsymbol{f}_{(x+1,y)} + \boldsymbol{f}_{(x-1,y)} + \boldsymbol{f}_{(x,y+1)} + \boldsymbol{f}_{(x,y-1)}\right)\right. \\ &\quad \left. +\boldsymbol{\alpha}'\left(\boldsymbol{f}_{(x+1,y+1)} + \boldsymbol{f}_{(x+1,y-1)} + \boldsymbol{f}_{(x-1,y+1)} + \boldsymbol{f}_{(x-1,y-1)}\right)\right]\end{aligned} \tag{3.16}$$

and

$$\mathrm{Prec}(\boldsymbol{f}_{(x,y)}|\boldsymbol{f}_{-(x,y)}) = \boldsymbol{\alpha} + \boldsymbol{\alpha}' \tag{3.17}$$

so that we have

$$\begin{aligned}\Pr(\boldsymbol{f}_{(x,y)}|\boldsymbol{f}_{-(x,y)}) \sim N\Bigg(&\frac{1}{4}(\boldsymbol{\alpha}+\boldsymbol{\alpha}')^{-1}\left[\boldsymbol{\alpha}\left(\boldsymbol{f}_{(x+1,y)} + \boldsymbol{f}_{(x-1,y)} + \boldsymbol{f}_{(x,y+1)} + \boldsymbol{f}_{(x,y-1)}\right)\right. \\ &\left. +\boldsymbol{\alpha}'\left(\boldsymbol{f}_{(x+1,y+1)} + \boldsymbol{f}_{(x+1,y-1)} + \boldsymbol{f}_{(x-1,y+1)} + \boldsymbol{f}_{(x-1,y-1)}\right)\right], (\boldsymbol{\alpha}+\boldsymbol{\alpha}')^{-1}\Bigg).\end{aligned} \tag{3.18}$$

So our model is such that the probability distribution for the value of one pixel given all the other pixels is a Gaussian distribution with expected value equal to a weighted average of the values of its nearest and second neighbours and covariance between the colour planes equal to $(\boldsymbol{\alpha}+\boldsymbol{\alpha}')^{-1}$.

To simplify calculations, $\boldsymbol{C}(\alpha_2,\kappa,\kappa')$ can be decomposed as follows:

$$\boldsymbol{C}(\alpha_2,\kappa,\kappa') = \boldsymbol{D}(\alpha_2)\otimes\boldsymbol{J}^{\kappa,\kappa'} \tag{3.19}$$

where $\otimes$ is the Kronecker product, $\boldsymbol{J}^{\kappa,\kappa'}$ is the single-entry 3x3 matrix, with 1 at position (κ,κ') and zero elsewhere and $\boldsymbol{D}(\alpha_2)$ is a $|\mathbf{V}|\times|\mathbf{V}|$ matrix where the $(x,y|x',y')$ elements are defined by

$$\begin{aligned}\langle x,y|x',y'\rangle \equiv{}& \delta_{x,x'}\delta_{y,y'} - \frac{1}{4}\delta_{x,x'+1}\delta_{y,y'} - \frac{1}{4}\delta_{x,x'-1}\delta_{y,y'} - \frac{1}{4}\delta_{x,x'}\delta_{y,y'+1} - \frac{1}{4}\delta_{x,x'}\delta_{y,y'-1}\\ &+\alpha_2\left(\delta_{x,x'}\delta_{y,y'} - \frac{1}{4}\delta_{x,x'+1}\delta_{y,y'+1} - \frac{1}{4}\delta_{x,x'+1}\delta_{y,y'-1} - \frac{1}{4}\delta_{x,x'-1}\delta_{y,y'+1} - \frac{1}{4}\delta_{x,x'-1}\delta_{y,y'-1}\right)\\ &[(x,y),(x',y')\in\mathbf{V}]\,.\end{aligned} \tag{3.20}$$

Here, we observe that $\boldsymbol{D}(\alpha_2)$ is identical to the matrix $\boldsymbol{C}(\alpha_2)$ defined in equation (2.8). We can then use the eigendecomposition of equation (2.19) to obtain

$$\boldsymbol{D} = \left(\boldsymbol{U}^{-1}\boldsymbol{\Lambda}\boldsymbol{U}\right) \tag{3.21}$$

where $\boldsymbol{U}$ is the DFT matrix defined as

$$\langle x,y|\boldsymbol{U}|p,q\rangle \equiv \frac{1}{\sqrt{|\mathbf{V}|}}\exp\left[-2\pi i\left(\frac{px}{V_x}+\frac{qy}{V_y}\right)\right], \tag{3.22}$$

$\boldsymbol{U}^{-1}$ is the conjugate transpose of $\boldsymbol{U}$, known as the inverse DFT matrix and defined as

$$\left\langle x,y|\boldsymbol{U}^{-1}|p,q\right\rangle \equiv \frac{1}{\sqrt{|\mathbf{V}|}}\exp\left[2\pi i\left(\frac{px}{V_x}+\frac{qy}{V_y}\right)\right] \tag{3.23}$$

and

$$\begin{aligned}\boldsymbol{\Lambda} \equiv \sum_{(p,q)\in\mathbf{V}}\Bigg(&1-\frac{1}{2}\cos\left(\frac{2\pi p}{V_x}\right)-\frac{1}{2}\cos\left(\frac{2\pi q}{V_y}\right)+\\ &\alpha_2\left[1-\frac{1}{2}\cos\left(2\pi(\frac{p}{V_x}+\frac{q}{V_y})\right)-\frac{1}{2}\cos\left(2\pi(\frac{p}{V_x}-\frac{q}{V_y})\right)\right]\Bigg)\boldsymbol{J}^{pq,pq}\end{aligned} \tag{3.24}$$

is the diagonal matrix of the eigenvalues $\lambda(\alpha_2,p,q)$ of $\boldsymbol{D}$ where $\boldsymbol{J}^{pq,pq}$ is the $|\mathbf{L}|\times|\mathbf{L}|$ single-entry matrix.

We can simplify the expression of Z_{prior}. Since $\boldsymbol{z}$ in equation (3.11) is not dependent on κ and κ', we can take $\boldsymbol{z}$ and $\boldsymbol{z}^T$ outside of the sums. We can then apply the multidimensional Gaussian integral to the equation followed by the decompositions of (3.19) and (3.21) to obtain

$$\begin{aligned}Z_{\text{prior}}(\boldsymbol{\alpha},\alpha_2) &= \int\exp\left(-\frac{1}{2}\boldsymbol{z}^T\left[\sum_{\kappa\in\mathbf{K}}\sum_{\kappa'\in\mathbf{K}}\alpha_{\kappa,\kappa'}\boldsymbol{C}(\alpha_2,\kappa,\kappa')\right]\boldsymbol{z}\right)d\boldsymbol{z}\\ &= (2\pi)^{\frac{3|\mathbf{V}|}{2}}\left\{\det\left(\sum_{\kappa\in\mathbf{K}}\sum_{\kappa'\in\mathbf{K}}\alpha_{\kappa,\kappa'}\boldsymbol{C}(\alpha_2,\kappa,\kappa')\right)\right\}^{-\frac{1}{2}}\\ &= (2\pi)^{\frac{3|\mathbf{V}|}{2}}\left\{\det\left[\sum_{\kappa\in\mathbf{K}}\sum_{\kappa'\in\mathbf{K}}\alpha_{\kappa,\kappa'}\left(\left[\boldsymbol{U}^{-1}\boldsymbol{\Lambda}\boldsymbol{U}\right]\otimes\boldsymbol{J}^{\kappa,\kappa'}\right)\right]\right\}^{-\frac{1}{2}}\\ &= (2\pi)^{\frac{3|\mathbf{V}|}{2}}\left\{\det\left[\left(\boldsymbol{U}^{-1}\boldsymbol{\Lambda}\boldsymbol{U}\right)\otimes\sum_{\kappa\in\mathbf{K}}\sum_{\kappa'\in\mathbf{K}}\left(\alpha_{\kappa,\kappa'}\boldsymbol{J}^{\kappa,\kappa'}\right)\right]\right\}^{-\frac{1}{2}}\\ &= (2\pi)^{\frac{3|\mathbf{V}|}{2}}\left\{\det\left[\left(\boldsymbol{U}^{-1}\boldsymbol{\Lambda}\boldsymbol{U}\right)\otimes\boldsymbol{\alpha}\right]\right\}^{-\frac{1}{2}}\end{aligned}$$

$$
\begin{aligned}
&= (2\pi)^{\frac{3|\mathbf{V}|}{2}} \left\{ \left[\det\left(\boldsymbol{U}^{-1}\boldsymbol{\Lambda}\boldsymbol{U}\right)\right]^3 \left[\det\left(\boldsymbol{\alpha}\right)\right]^{|\mathbf{V}|} \right\}^{-\frac{1}{2}} \\
&= (2\pi)^{\frac{3|\mathbf{V}|}{2}} \left\{ \left[\det\left(\boldsymbol{\Lambda}\right)\right]^3 \left[\det\left(\boldsymbol{\alpha}\right)\right]^{|\mathbf{V}|} \right\}^{-\frac{1}{2}} \\
&= (2\pi)^{\frac{3|\mathbf{V}|}{2}} \left\{ \prod_{(p,q)\in\mathbf{V}} \lambda\left(\alpha_2, p, q\right)^3 \det\boldsymbol{\alpha} \right\}^{-\frac{1}{2}}. \qquad (3.25)
\end{aligned}
$$

3.2.4 A Posteriori Probability Density Function

The a posteriori probability density function of having an original image configuration $\boldsymbol{f}$ given a degraded image $\boldsymbol{g}$ is found by applying Bayes' theorem as follows:

$$
\begin{aligned}
\Pr\left\{\boldsymbol{F}=\boldsymbol{f}|\boldsymbol{G}=\boldsymbol{g},\boldsymbol{\alpha},\alpha_2,\sigma\right\} &= \frac{\Pr\left\{\boldsymbol{G}=\boldsymbol{g}|\boldsymbol{F}=\boldsymbol{f},\sigma\right\}\Pr\left\{\boldsymbol{F}=\boldsymbol{f}|\boldsymbol{\alpha},\alpha_2\right\}}{\Pr\left\{\boldsymbol{G}=\boldsymbol{g}|\boldsymbol{\alpha},\alpha_2,\sigma\right\}} \\
&= \frac{\Pr\left\{\boldsymbol{G}=\boldsymbol{g}|\boldsymbol{F}=\boldsymbol{f},\sigma\right\}\Pr\left\{\boldsymbol{F}=\boldsymbol{f}|\boldsymbol{\alpha},\alpha_2\right\}}{\int \Pr\left\{\boldsymbol{G}=\boldsymbol{g}|\boldsymbol{F}=\boldsymbol{z},\sigma\right\}\Pr\left\{\boldsymbol{F}=\boldsymbol{z}|\boldsymbol{\alpha},\alpha_2\right\}d\boldsymbol{z}}
\end{aligned} \qquad (3.26)
$$

where $\Pr\left\{\boldsymbol{G}=\boldsymbol{g}|\boldsymbol{\alpha},\alpha_2,\sigma\right\} = \int \Pr\left\{\boldsymbol{G}=\boldsymbol{g}|\boldsymbol{F}=\boldsymbol{z},\sigma\right\}\Pr\left\{\boldsymbol{F}=\boldsymbol{z}|\boldsymbol{\alpha},\alpha_2\right\}d\boldsymbol{z}$ is called the evidence.

Using (3.1) and (3.10), the function can be rewritten as follows:

$$
\begin{aligned}
&\Pr\left\{\boldsymbol{F}=\boldsymbol{f}|\boldsymbol{G}=\boldsymbol{g},\boldsymbol{\alpha},\alpha_2,\sigma\right\} = \\
&\qquad \frac{1}{Z_{\text{noise}}\left(\sigma\right)}\exp\left(-\frac{1}{2\sigma^2}\sum_{(x,y)\in\mathbf{V}}\sum_{\kappa\in\mathbf{K}}\left(g_{x,y,\kappa}-f_{x,y,\kappa}\right)^2\right) \\
&\quad \times \frac{1}{Z_{\text{prior}}\left(\boldsymbol{\alpha},\alpha_2\right)}\exp\left\{-\frac{1}{2}\sum_{\kappa\in\mathbf{K}}\sum_{\kappa'\in\mathbf{K}}\alpha_{\kappa,\kappa'}\boldsymbol{f}^T\boldsymbol{C}\left(\alpha_2,\kappa,\kappa'\right)\boldsymbol{f}\right\} \\
&\quad \div \left[\int \frac{1}{Z_{\text{noise}}\left(\sigma\right)}\exp\left(-\frac{1}{2\sigma^2}\sum_{(x,y)\in\mathbf{V}}\sum_{\kappa\in\mathbf{K}}\left(g_{x,y,\kappa}-z_{x,y,\kappa}\right)^2\right)\right. \\
&\qquad \left. \times \frac{1}{Z_{\text{prior}}\left(\boldsymbol{\alpha},\alpha_2\right)}\exp\left\{-\frac{1}{2}\sum_{\kappa\in\mathbf{K}}\sum_{\kappa'\in\mathbf{K}}\alpha_{\kappa,\kappa'}\boldsymbol{z}^T\boldsymbol{C}\left(\alpha_2,\kappa,\kappa'\right)\boldsymbol{z}\right\}d\boldsymbol{z}\right]. \qquad (3.27)
\end{aligned}
$$

Since Z_{noise} and Z_{prior} are not dependant on $\boldsymbol{z}$, they can be taken out of the integral in the denominator and cancel out with the numerator, so we have

$$
\Pr\left\{\boldsymbol{F}=\boldsymbol{f}|\boldsymbol{G}=\boldsymbol{g},\boldsymbol{\alpha},\alpha_2,\sigma\right\} = \frac{1}{Z_{\text{posterior}}\left(\boldsymbol{g},\boldsymbol{\alpha},\alpha_2,\sigma\right)}\exp\left[-H\left(\boldsymbol{f}|\boldsymbol{g},\boldsymbol{\alpha},\alpha_2,\sigma\right)\right] \qquad (3.28)
$$

where

$$
Z_{\text{posterior}}\left(\boldsymbol{g},\boldsymbol{\alpha},\alpha_2,\sigma\right) = \int \exp\left[-H\left(\boldsymbol{z}|\boldsymbol{g},\boldsymbol{\alpha},\alpha_2,\sigma\right)\right]d\boldsymbol{z} \qquad (3.29)
$$

and

$$
H\left(\boldsymbol{f}|\boldsymbol{g},\boldsymbol{\alpha},\alpha_2,\sigma\right) = \frac{1}{2\sigma^2}\sum_{(x,y)\in\mathbf{V}}\sum_{\kappa\in\mathbf{K}}\left(g_{x,y,\kappa}-f_{x,y,\kappa}\right)^2 + \frac{1}{2}\boldsymbol{f}^T\left(\sum_{\kappa\in\mathbf{K}}\sum_{\kappa'\in\mathbf{K}}\alpha_{\kappa,\kappa'}\boldsymbol{C}\left(\alpha_2,\kappa,\kappa'\right)\right)\boldsymbol{f}. \qquad (3.30)
$$

We can simplify calculations by grouping all element of $\boldsymbol{f}$ in H in one single term as follows

$$
\begin{aligned}
H\left(\boldsymbol{f}|\boldsymbol{g},\boldsymbol{\alpha},\alpha_2,\sigma\right) &= \frac{1}{2\sigma^2}\left(\boldsymbol{f}-\boldsymbol{g}\right)^T\left(\boldsymbol{f}-\boldsymbol{g}\right) + \frac{1}{2}\boldsymbol{f}^T\left(\sum_{\kappa\in\mathbf{K}}\sum_{\kappa'\in\mathbf{K}}\alpha_{\kappa,\kappa'}\boldsymbol{C}\left(\alpha_2,\kappa,\kappa'\right)\right)\boldsymbol{f} \\
&= \frac{1}{2\sigma^2}\left[\boldsymbol{f}^T\boldsymbol{f}-\boldsymbol{f}^T\boldsymbol{g}-\boldsymbol{g}^T\boldsymbol{f}+\boldsymbol{g}^T\boldsymbol{g}\right] + \frac{1}{2}\boldsymbol{f}^T\left(\sum_{\kappa\in\mathbf{K}}\sum_{\kappa'\in\mathbf{K}}\alpha_{\kappa,\kappa'}\boldsymbol{C}\left(\alpha_2,\kappa,\kappa'\right)\right)\boldsymbol{f}
\end{aligned}
$$

$$
\begin{aligned}
&= \frac{1}{2\sigma^2}\left[\boldsymbol{f}^T\boldsymbol{f} - \boldsymbol{f}^T\boldsymbol{g} - \boldsymbol{g}^T\boldsymbol{f} + \sigma^2\boldsymbol{f}^T\left(\sum_{\kappa\in\mathbf{K}}\sum_{\kappa'\in\mathbf{K}}\alpha_{\kappa,\kappa'}\boldsymbol{C}\left(\alpha_2,\kappa,\kappa'\right)\right)\boldsymbol{f}\right] + \frac{1}{2\sigma^2}\boldsymbol{g}^T\boldsymbol{g} \\
&= \frac{1}{2\sigma^2}\left[\boldsymbol{f}^T\boldsymbol{f} - \boldsymbol{f}^T\boldsymbol{g} - \boldsymbol{g}^T\boldsymbol{f} + \sigma^2\boldsymbol{f}^T\left(\sum_{\kappa\in\mathbf{K}}\sum_{\kappa'\in\mathbf{K}}\alpha_{\kappa,\kappa'}\boldsymbol{C}\left(\alpha_2,\kappa,\kappa'\right)\right)\boldsymbol{f}\right] \\
&\quad + \frac{1}{2\sigma^2}\boldsymbol{g}^T\left(\boldsymbol{I} + \sigma^2\sum_{\kappa\in\mathbf{K}}\sum_{\kappa'\in\mathbf{K}}\alpha_{\kappa,\kappa'}\boldsymbol{C}\left(\alpha_2,\kappa,\kappa'\right)\right) \\
&\quad \times \left(\boldsymbol{I} + \sigma^2\sum_{\kappa\in\mathbf{K}}\sum_{\kappa'\in\mathbf{K}}\alpha_{\kappa,\kappa'}\boldsymbol{C}\left(\alpha_2,\kappa,\kappa'\right)\right)^{-1}\boldsymbol{g} \\
&= \frac{1}{2\sigma^2}\left[\boldsymbol{f}^T\boldsymbol{f} - \boldsymbol{f}^T\boldsymbol{g} - \boldsymbol{g}^T\boldsymbol{f} + \sigma^2\boldsymbol{f}^T\left(\sum_{\kappa\in\mathbf{K}}\sum_{\kappa'\in\mathbf{K}}\alpha_{\kappa,\kappa'}\boldsymbol{C}\left(\alpha_2,\kappa,\kappa'\right)\right)\boldsymbol{f}\right] \\
&\quad + \frac{1}{2\sigma^2}\boldsymbol{g}^T\left[\left(\boldsymbol{I} + \sigma^2\sum_{\kappa\in\mathbf{K}}\sum_{\kappa'\in\mathbf{K}}\alpha_{\kappa,\kappa'}\boldsymbol{C}\left(\alpha_2,\kappa,\kappa'\right)\right)^{-1}\right. \\
&\quad \left. + \sigma^2\left(\sum_{\kappa\in\mathbf{K}}\sum_{\kappa'\in\mathbf{K}}\alpha_{\kappa,\kappa'}\boldsymbol{C}\left(\alpha_2,\kappa,\kappa'\right)\right)\left(\boldsymbol{I} + \sigma^2\sum_{\kappa\in\mathbf{K}}\sum_{\kappa'\in\mathbf{K}}\alpha_{\kappa,\kappa'}\boldsymbol{C}\left(\alpha_2,\kappa,\kappa'\right)\right)^{-1}\right]\boldsymbol{g} \\
&= \frac{1}{2\sigma^2}\left[\boldsymbol{f}^T\boldsymbol{f} - \boldsymbol{f}^T\boldsymbol{g} - \boldsymbol{g}^T\boldsymbol{f} + \boldsymbol{f}^T\left(\sigma^2\sum_{\kappa\in\mathbf{K}}\sum_{\kappa'\in\mathbf{K}}\alpha_{\kappa,\kappa'}\boldsymbol{C}\left(\alpha_2,\kappa,\kappa'\right)\right)\boldsymbol{f}\right] \\
&\quad + \frac{1}{2\sigma^2}\boldsymbol{g}^T\left(\boldsymbol{I} + \sigma^2\sum_{\kappa\in\mathbf{K}}\sum_{\kappa'\in\mathbf{K}}\alpha_{\kappa,\kappa'}\boldsymbol{C}\left(\alpha_2,\kappa,\kappa'\right)\right)^{-1}\boldsymbol{g} \\
&\quad + \frac{1}{2}\boldsymbol{g}^T\left(\sum_{\kappa\in\mathbf{K}}\sum_{\kappa'\in\mathbf{K}}\alpha_{\kappa,\kappa'}\boldsymbol{C}\left(\alpha_2,\kappa,\kappa'\right)\right)\left(\boldsymbol{I} + \sigma^2\sum_{\kappa\in\mathbf{K}}\sum_{\kappa'\in\mathbf{K}}\alpha_{\kappa,\kappa'}\boldsymbol{C}\left(\alpha_2,\kappa,\kappa'\right)\right)^{-1}\boldsymbol{g} \\
&= \frac{1}{2\sigma^2}\left[\boldsymbol{f}^T\left(\boldsymbol{I} + \sigma^2\sum_{\kappa\in\mathbf{K}}\sum_{\kappa'\in\mathbf{K}}\alpha_{\kappa,\kappa'}\boldsymbol{C}\left(\alpha_2,\kappa,\kappa'\right)\right)\boldsymbol{f} - \boldsymbol{f}^T\boldsymbol{g} - \boldsymbol{g}^T\boldsymbol{f}\right. \\
&\quad \left. + \boldsymbol{g}^T\left(\boldsymbol{I} + \sigma^2\sum_{\kappa\in\mathbf{K}}\sum_{\kappa'\in\mathbf{K}}\alpha_{\kappa,\kappa'}\boldsymbol{C}\left(\alpha_2,\kappa,\kappa'\right)\right)^{-1}\boldsymbol{g}\right] \\
&\quad + \frac{1}{2}\boldsymbol{g}^T\left(\sum_{\kappa\in\mathbf{K}}\sum_{\kappa'\in\mathbf{K}}\alpha_{\kappa,\kappa'}\boldsymbol{C}\left(\alpha_2,\kappa,\kappa'\right)\right)\left(\boldsymbol{I} + \sigma^2\sum_{\kappa\in\mathbf{K}}\sum_{\kappa'\in\mathbf{K}}\alpha_{\kappa,\kappa'}\boldsymbol{C}\left(\alpha_2,\kappa,\kappa'\right)\right)^{-1}\boldsymbol{g} \\
&= \frac{1}{2\sigma^2}\left[\boldsymbol{f}^T\left(\boldsymbol{I} + \sigma^2\sum_{\kappa\in\mathbf{K}}\sum_{\kappa'\in\mathbf{K}}\alpha_{\kappa,\kappa'}\boldsymbol{C}\left(\alpha_2,\kappa,\kappa'\right)\right)\boldsymbol{f}\right. \\
&\quad - \boldsymbol{f}^T\left(\boldsymbol{I} + \sigma^2\sum_{\kappa\in\mathbf{K}}\sum_{\kappa'\in\mathbf{K}}\alpha_{\kappa,\kappa'}\boldsymbol{C}\left(\alpha_2,\kappa,\kappa'\right)\right)\left(\boldsymbol{I} + \sigma^2\sum_{\kappa\in\mathbf{K}}\sum_{\kappa'\in\mathbf{K}}\alpha_{\kappa,\kappa'}\boldsymbol{C}\left(\alpha_2,\kappa,\kappa'\right)\right)^{-1}\boldsymbol{g} \\
&\quad - \boldsymbol{g}^T\left(\boldsymbol{I} + \sigma^2\sum_{\kappa\in\mathbf{K}}\sum_{\kappa'\in\mathbf{K}}\alpha_{\kappa,\kappa'}\boldsymbol{C}\left(\alpha_2,\kappa,\kappa'\right)\right)^{-1}\left(\boldsymbol{I} + \sigma^2\sum_{\kappa\in\mathbf{K}}\sum_{\kappa'\in\mathbf{K}}\alpha_{\kappa,\kappa'}\boldsymbol{C}\left(\alpha_2,\kappa,\kappa'\right)\right)\boldsymbol{f} \\
&\quad \left. + \boldsymbol{g}^T\left(\boldsymbol{I} + \sigma^2\sum_{\kappa\in\mathbf{K}}\sum_{\kappa'\in\mathbf{K}}\alpha_{\kappa,\kappa'}\boldsymbol{C}\left(\alpha_2,\kappa,\kappa'\right)\right)^{-1}\boldsymbol{g}\right] \\
&\quad + \frac{1}{2}\boldsymbol{g}^T\left(\sum_{\kappa\in\mathbf{K}}\sum_{\kappa'\in\mathbf{K}}\alpha_{\kappa,\kappa'}\boldsymbol{C}\left(\alpha_2,\kappa,\kappa'\right)\right)\left(\boldsymbol{I} + \sigma^2\sum_{\kappa\in\mathbf{K}}\sum_{\kappa'\in\mathbf{K}}\alpha_{\kappa,\kappa'}\boldsymbol{C}\left(\alpha_2,\kappa,\kappa'\right)\right)^{-1}\boldsymbol{g}
\end{aligned}
$$

$$
\begin{aligned}
&= \frac{1}{2\sigma^2}\left[\boldsymbol{f} - \left(\boldsymbol{I} + \sigma^2 \sum_{\kappa\in\mathbf{K}}\sum_{\kappa'\in\mathbf{K}} \alpha_{\kappa,\kappa'}\boldsymbol{C}\left(\alpha_2,\kappa,\kappa'\right)\right)^{-1}\boldsymbol{g}\right]^T \\
&\quad\times\left(\boldsymbol{I} + \sigma^2 \sum_{\kappa\in\mathbf{K}}\sum_{\kappa'\in\mathbf{K}} \alpha_{\kappa,\kappa'}\boldsymbol{C}\left(\alpha_2,\kappa,\kappa'\right)\right) \\
&\quad\times\left[\boldsymbol{f} - \left(\boldsymbol{I} + \sigma^2 \sum_{\kappa\in\mathbf{K}}\sum_{\kappa'\in\mathbf{K}} \alpha_{\kappa,\kappa'}\boldsymbol{C}\left(\alpha_2,\kappa,\kappa'\right)\right)^{-1}\boldsymbol{g}\right] \\
&\quad+\frac{1}{2}\boldsymbol{g}^T\left(\sum_{\kappa\in\mathbf{K}}\sum_{\kappa'\in\mathbf{K}} \alpha_{\kappa,\kappa'}\boldsymbol{C}\left(\alpha_2,\kappa,\kappa'\right)\right)\left(\boldsymbol{I} + \sigma^2 \sum_{\kappa\in\mathbf{K}}\sum_{\kappa'\in\mathbf{K}} \alpha_{\kappa,\kappa'}\boldsymbol{C}\left(\alpha_2,\kappa,\kappa'\right)\right)^{-1}\boldsymbol{g}
\end{aligned}
\tag{3.31}
$$

where we made use of the fact that $\left(\boldsymbol{I} + \sigma^2 \sum_{\kappa\in\mathbf{K}}\sum_{\kappa'\in\mathbf{K}} \alpha_{\kappa,\kappa'}\boldsymbol{C}\left(\alpha_2,\kappa,\kappa'\right)\right)$ is symmetric.

Using equation (3.19) and the eigendecomposition described in (3.21), we can rewrite the second term of (3.31) as follows

$$
\begin{aligned}
&\frac{1}{2}\boldsymbol{g}^T\left(\sum_{\kappa\in\mathbf{K}}\sum_{\kappa'\in\mathbf{K}} \alpha_{\kappa,\kappa'}\boldsymbol{C}\left(\alpha_2,\kappa,\kappa'\right)\right)\left(\boldsymbol{I} + \sigma^2 \sum_{\kappa\in\mathbf{K}}\sum_{\kappa'\in\mathbf{K}} \alpha_{\kappa,\kappa'}\boldsymbol{C}\left(\alpha_2,\kappa,\kappa'\right)\right)^{-1}\boldsymbol{g} \\
=&\frac{1}{2}\boldsymbol{g}^T\left(\sum_{\kappa\in\mathbf{K}}\sum_{\kappa'\in\mathbf{K}} \alpha_{\kappa,\kappa'}\left(\boldsymbol{U}^{-1}\boldsymbol{\Lambda}\boldsymbol{U}\right)\otimes\boldsymbol{J}^{\kappa,\kappa'}\right)\left(\boldsymbol{I} + \sigma^2 \sum_{\kappa\in\mathbf{K}}\sum_{\kappa'\in\mathbf{K}} \alpha_{\kappa,\kappa'}\left(\boldsymbol{U}^{-1}\boldsymbol{\Lambda}\boldsymbol{U}\right)\otimes\boldsymbol{J}^{\kappa,\kappa'}\right)^{-1}\boldsymbol{g} \\
=&\frac{1}{2}\boldsymbol{g}^T\left(\left(\boldsymbol{U}^{-1}\boldsymbol{\Lambda}\boldsymbol{U}\right)\otimes\sum_{\kappa\in\mathbf{K}}\sum_{\kappa'\in\mathbf{K}} \alpha_{\kappa,\kappa'}\boldsymbol{J}^{\kappa,\kappa'}\right)\left(\boldsymbol{I} + \sigma^2\left(\boldsymbol{U}^{-1}\boldsymbol{\Lambda}\boldsymbol{U}\right)\otimes\sum_{\kappa\in\mathbf{K}}\sum_{\kappa'\in\mathbf{K}} \alpha_{\kappa,\kappa'}\boldsymbol{J}^{\kappa,\kappa'}\right)^{-1}\boldsymbol{g} \\
=&\frac{1}{2}\boldsymbol{g}^T\left[\left(\boldsymbol{U}^{-1}\boldsymbol{\Lambda}\boldsymbol{U}\right)\otimes\boldsymbol{\alpha}\right]\left[\boldsymbol{I} + \sigma^2\left(\boldsymbol{U}^{-1}\boldsymbol{\Lambda}\boldsymbol{U}\right)\otimes\boldsymbol{\alpha}\right]^{-1}\boldsymbol{g} \\
=&\frac{1}{2}\boldsymbol{g}^T\left[\left(\boldsymbol{U}^{-1}\boldsymbol{\Lambda}\boldsymbol{U}\right)\otimes(\boldsymbol{e}\boldsymbol{\alpha}\boldsymbol{e})\right]\left[\boldsymbol{I} + \sigma^2\left(\boldsymbol{U}^{-1}\boldsymbol{\Lambda}\boldsymbol{U}\right)\otimes(\boldsymbol{e}\boldsymbol{\alpha}\boldsymbol{e})\right]^{-1}\boldsymbol{g} \\
=&\frac{1}{2}\boldsymbol{g}^T\left[\left(\boldsymbol{U}^{-1}\otimes\boldsymbol{e}\right)(\boldsymbol{\Lambda}\otimes\boldsymbol{\alpha})(\boldsymbol{U}\otimes\boldsymbol{e})\right] \\
&\times\left[\left(\boldsymbol{U}^{-1}\otimes\boldsymbol{e}\right)\boldsymbol{I}(\boldsymbol{U}\otimes\boldsymbol{e}) + \sigma^2\left(\boldsymbol{U}^{-1}\otimes\boldsymbol{e}\right)(\boldsymbol{\Lambda}\otimes\boldsymbol{\alpha})(\boldsymbol{U}\otimes\boldsymbol{e})\right]^{-1}\boldsymbol{g} \\
=&\frac{1}{2}\boldsymbol{g}^T\left[\left(\boldsymbol{U}^{-1}\otimes\boldsymbol{e}\right)(\boldsymbol{\Lambda}\otimes\boldsymbol{\alpha})(\boldsymbol{U}\otimes\boldsymbol{e})\right]\left[\left(\boldsymbol{U}^{-1}\otimes\boldsymbol{e}\right)\left\{\boldsymbol{I} + \sigma^2(\boldsymbol{\Lambda}\otimes\boldsymbol{\alpha})\right\}(\boldsymbol{U}\otimes\boldsymbol{e})\right]^{-1}\boldsymbol{g} \\
=&\frac{1}{2}\boldsymbol{g}^T\left(\boldsymbol{U}^{-1}\otimes\boldsymbol{e}\right)(\boldsymbol{\Lambda}\otimes\boldsymbol{\alpha})(\boldsymbol{U}\otimes\boldsymbol{e})\left(\boldsymbol{U}^{-1}\otimes\boldsymbol{e}\right)\left[\boldsymbol{I} + \sigma^2(\boldsymbol{\Lambda}\otimes\boldsymbol{\alpha})\right]^{-1}(\boldsymbol{U}\otimes\boldsymbol{e})\,\boldsymbol{g} \\
=&\frac{1}{2}\boldsymbol{g}^T\left(\boldsymbol{U}^{-1}\otimes\boldsymbol{e}\right)(\boldsymbol{\Lambda}\otimes\boldsymbol{\alpha})\left[\boldsymbol{I} + \sigma^2(\boldsymbol{\Lambda}\otimes\boldsymbol{\alpha})\right]^{-1}(\boldsymbol{U}\otimes\boldsymbol{e})\,\boldsymbol{g} \\
=&\frac{1}{2}\left[{\boldsymbol{g}_r}^T\otimes(1,0,0) + {\boldsymbol{g}_g}^T\otimes(0,1,0) + {\boldsymbol{g}_b}^T\otimes(0,0,1)\right]\left(\boldsymbol{U}^{-1}\otimes\boldsymbol{e}\right) \\
&\times\left(\sum_{(p,q)\in\mathbf{V}}\lambda(\alpha_2,p,q)\boldsymbol{J}^{pq,pq}\otimes\boldsymbol{\alpha}\right)\left(\sum_{(p,q)\in\mathbf{V}}\boldsymbol{J}^{pq,pq}\otimes\boldsymbol{e} + \sigma^2\lambda(\alpha_2,p,q)\boldsymbol{J}^{pq,pq}\otimes\boldsymbol{\alpha}\right)^{-1} \\
&\times(\boldsymbol{U}\otimes\boldsymbol{e})\left[\boldsymbol{g}_r\otimes\begin{pmatrix}1\\0\\0\end{pmatrix} + \boldsymbol{g}_g\otimes\begin{pmatrix}0\\1\\0\end{pmatrix} + \boldsymbol{g}_b\otimes\begin{pmatrix}0\\0\\1\end{pmatrix}\right]
\end{aligned}
$$

$$
\begin{aligned}
=&\frac{1}{2}\left[\left({\boldsymbol{g}_r}^T\boldsymbol{U}^{-1}\right)\otimes(1,0,0)+\left({\boldsymbol{g}_g}^T\boldsymbol{U}^{-1}\right)\otimes(0,1,0)+\left({\boldsymbol{g}_b}^T\boldsymbol{U}^{-1}\right)\otimes(0,0,1)\right]\\
&\times\left(\sum_{(p,q)\in\mathbf{V}}\boldsymbol{J}^{pq,pq}\otimes\lambda(\alpha_2,p,q)\boldsymbol{\alpha}\right)\left(\sum_{(p,q)\in\mathbf{V}}\boldsymbol{J}^{pq,pq}\otimes\left[\boldsymbol{e}+\sigma^2\lambda(\alpha_2,p,q)\boldsymbol{\alpha}\right]\right)^{-1}\\
&\times\left[(\boldsymbol{U}\boldsymbol{g}_r)\otimes\begin{pmatrix}1\\0\\0\end{pmatrix}+(\boldsymbol{U}\boldsymbol{g}_g)\otimes\begin{pmatrix}0\\1\\0\end{pmatrix}+(\boldsymbol{U}\boldsymbol{g}_b)\otimes\begin{pmatrix}0\\0\\1\end{pmatrix}\right]\\
=&\frac{1}{2}\left[{\boldsymbol{G}_r}^\dagger\otimes(1,0,0)+{\boldsymbol{G}_g}^\dagger\otimes(0,1,0)+{\boldsymbol{G}_b}^\dagger\otimes(0,0,1)\right]\\
&\times\sum_{(p,q)\in\mathbf{V}}\boldsymbol{J}^{pq,pq}\otimes\lambda(\alpha_2,p,q)\boldsymbol{\alpha}\left(\boldsymbol{e}+\sigma^2\lambda(\alpha_2,p,q)\boldsymbol{\alpha}\right)^{-1}\\
&\times\left[\boldsymbol{G}_r\otimes\begin{pmatrix}1\\0\\0\end{pmatrix}+\boldsymbol{G}_g\otimes\begin{pmatrix}0\\1\\0\end{pmatrix}+\boldsymbol{G}_b\otimes\begin{pmatrix}0\\0\\1\end{pmatrix}\right]\\
=&\frac{1}{2}\sum_{(p,q)\in\mathbf{V}}{G_r}^\dagger(p,q)G_r(p,q)\,(1,0,0)\,\lambda(\alpha_2,p,q)\boldsymbol{\alpha}\left(\boldsymbol{e}+\sigma^2\lambda(\alpha_2,p,q)\boldsymbol{\alpha}\right)^{-1}\begin{pmatrix}1\\0\\0\end{pmatrix}\\
&+{G_r}^\dagger(p,q)G_g(p,q)\,(1,0,0)\,\lambda(\alpha_2,p,q)\boldsymbol{\alpha}\left(\boldsymbol{e}+\sigma^2\lambda(\alpha_2,p,q)\boldsymbol{\alpha}\right)^{-1}\begin{pmatrix}0\\1\\0\end{pmatrix}\\
&+{G_r}^\dagger(p,q)G_b(p,q)\,(1,0,0)\,\lambda(\alpha_2,p,q)\boldsymbol{\alpha}\left(\boldsymbol{e}+\sigma^2\lambda(\alpha_2,p,q)\boldsymbol{\alpha}\right)^{-1}\begin{pmatrix}0\\0\\1\end{pmatrix}\\
&+{G_g}^\dagger(p,q)G_r(p,q)\,(0,1,0)\,\lambda(\alpha_2,p,q)\boldsymbol{\alpha}\left(\boldsymbol{e}+\sigma^2\lambda(\alpha_2,p,q)\boldsymbol{\alpha}\right)^{-1}\begin{pmatrix}1\\0\\0\end{pmatrix}\\
&+{G_g}^\dagger(p,q)G_g(p,q)\,(0,1,0)\,\lambda(\alpha_2,p,q)\boldsymbol{\alpha}\left(\boldsymbol{e}+\sigma^2\lambda(\alpha_2,p,q)\boldsymbol{\alpha}\right)^{-1}\begin{pmatrix}0\\1\\0\end{pmatrix}\\
&+{G_g}^\dagger(p,q)G_b(p,q)\,(0,1,0)\,\lambda(\alpha_2,p,q)\boldsymbol{\alpha}\left(\boldsymbol{e}+\sigma^2\lambda(\alpha_2,p,q)\boldsymbol{\alpha}\right)^{-1}\begin{pmatrix}0\\0\\1\end{pmatrix}\\
&+{G_b}^\dagger(p,q)G_r(p,q)\,(0,0,1)\,\lambda(\alpha_2,p,q)\boldsymbol{\alpha}\left(\boldsymbol{e}+\sigma^2\lambda(\alpha_2,p,q)\boldsymbol{\alpha}\right)^{-1}\begin{pmatrix}1\\0\\0\end{pmatrix}\\
&+{G_b}^\dagger(p,q)G_g(p,q)\,(0,0,1)\,\lambda(\alpha_2,p,q)\boldsymbol{\alpha}\left(\boldsymbol{e}+\sigma^2\lambda(\alpha_2,p,q)\boldsymbol{\alpha}\right)^{-1}\begin{pmatrix}0\\1\\0\end{pmatrix}\\
&+{G_b}^\dagger(p,q)G_b(p,q)\,(0,0,1)\,\lambda(\alpha_2,p,q)\boldsymbol{\alpha}\left(\boldsymbol{e}+\sigma^2\lambda(\alpha_2,p,q)\boldsymbol{\alpha}\right)^{-1}\begin{pmatrix}0\\0\\1\end{pmatrix}
\end{aligned}
$$

$$
\begin{aligned}
=&\frac{1}{2}\sum_{(p,q)\in\mathbf{V}}\left[{G_r}^{\dagger}(p,q)\,(1,0,0)+{G_g}^{\dagger}(p,q)\,(0,1,0)+{G_b}^{\dagger}(p,q)\,(0,0,1)\right]\\
&\times\lambda(\alpha_2,p,q)\boldsymbol{\alpha}\left(\boldsymbol{e}+\sigma^2\lambda(\alpha_2,p,q)\boldsymbol{\alpha}\right)^{-1}\left[G_r(p,q)\begin{pmatrix}1\\0\\0\end{pmatrix}+G_g(p,q)\begin{pmatrix}0\\1\\0\end{pmatrix}+G_b(p,q)\begin{pmatrix}0\\0\\1\end{pmatrix}\right]\\
=&\frac{1}{2}\sum_{(p,q)\in\mathbf{V}}\overrightarrow{G}^{\dagger}(p,q)\lambda(\alpha_2,p,q)\boldsymbol{\alpha}\left(\boldsymbol{e}+\sigma^2\lambda(\alpha_2,p,q)\boldsymbol{\alpha}\right)^{-1}\overrightarrow{G}^{\dagger}(p,q)
\end{aligned}
\tag{3.32}
$$

where $\boldsymbol{e}$ is the 3x3 identity matrix,

$$
\overrightarrow{G}(p,q)\quad=\quad\begin{pmatrix}G_{\text{red}}(p,q)\\G_{\text{green}}(p,q)\\G_{\text{blue}}(p,q)\end{pmatrix}\quad\equiv\quad\frac{1}{\sqrt{|\mathbf{V}|}}\sum_{(x,y)\in\mathbf{V}}\begin{pmatrix}g_{x,y,\text{red}}\\g_{x,y,\text{green}}\\g_{x,y,\text{blue}}\end{pmatrix}\exp\left(-2\pi i\left(\frac{px}{V_x}+\frac{qy}{V_y}\right)\right)\tag{3.33}
$$

and

$$
\overrightarrow{G}^{\dagger}(p,q)=\begin{pmatrix}G^{\dagger}_{\text{red}}(p,q)\\G^{\dagger}_{\text{green}}(p,q)\\G^{\dagger}_{\text{blue}}(p,q)\end{pmatrix}^{T}\equiv\frac{1}{\sqrt{|\mathbf{V}|}}\sum_{(x,y)\in\mathbf{V}}(g_{x,y,\text{red}},g_{x,y,\text{green}},g_{x,y,\text{blue}})\exp\left(2\pi i\left(\frac{px}{V_x}+\frac{qy}{V_y}\right)\right).\tag{3.34}
$$

Here we note that $G_\kappa(p,q)$ corresponds to $(\boldsymbol{U}\boldsymbol{g}_\kappa)_{p,q}$ where $(\boldsymbol{U}\boldsymbol{g}_\kappa)$ is the DFT of the vector made from only the κ color component of $\boldsymbol{g}$. Similarly for $\overrightarrow{G}^{\dagger}$ using $(\boldsymbol{g}_\kappa^T\boldsymbol{U}^{-1})$, the inverse DFT.

From the above, we conclude that

$$
\begin{aligned}
H\left(\boldsymbol{f}|\boldsymbol{g},\boldsymbol{\alpha},\alpha_2,\sigma\right)=&\frac{1}{2\sigma^2}\left[\boldsymbol{f}-\left(\boldsymbol{I}+\sigma^2\sum_{\kappa\in\mathbf{K}}\sum_{\kappa'\in\mathbf{K}}\alpha_{\kappa,\kappa'}\boldsymbol{C}\left(\alpha_2,\kappa,\kappa'\right)\right)^{-1}\boldsymbol{g}\right]^T\\
&\times\left(\boldsymbol{I}+\sigma^2\sum_{\kappa\in\mathbf{K}}\sum_{\kappa'\in\mathbf{K}}\alpha_{\kappa,\kappa'}\boldsymbol{C}\left(\alpha_2,\kappa,\kappa'\right)\right)\left[\boldsymbol{f}-\left(\boldsymbol{I}+\sigma^2\sum_{\kappa\in\mathbf{K}}\sum_{\kappa'\in\mathbf{K}}\alpha_{\kappa,\kappa'}\boldsymbol{C}\left(\alpha_2,\kappa,\kappa'\right)\right)^{-1}\boldsymbol{g}\right]\\
&+\frac{1}{2}\sum_{(p,q)\in\mathbf{V}}\left\{\overrightarrow{G}^{\dagger}(p,q)\lambda(\alpha_2,p,q)\boldsymbol{\alpha}\left(\boldsymbol{e}+\sigma^2\lambda(\alpha_2,p,q)\boldsymbol{\alpha}\right)^{-1}\overrightarrow{G}(p,q)\right\}.
\end{aligned}
\tag{3.35}
$$

Using the variable substitution $\boldsymbol{x}=\left[\boldsymbol{z}-\left(\boldsymbol{I}+\sigma^2\sum_{\kappa\in\mathbf{K}}\sum_{\kappa'\in\mathbf{K}}\alpha_{\kappa,\kappa'}\boldsymbol{C}\left(\alpha_2,\kappa,\kappa'\right)\right)^{-1}\boldsymbol{g}\right]$ and $d\boldsymbol{z}=d\boldsymbol{x}$, $Z_{\text{posterior}}$ can be rewritten as

$$
\begin{aligned}
Z_{\text{posterior}}=\int\exp\Bigg\{&\frac{-1}{2\sigma^2}\boldsymbol{x}^T\left(\boldsymbol{I}+\sigma^2\sum_{\kappa\in\mathbf{K}}\sum_{\kappa'\in\mathbf{K}}\alpha_{\kappa,\kappa'}\boldsymbol{C}\left(\alpha_2,\kappa,\kappa'\right)\right)\boldsymbol{x}\\
&-\frac{1}{2}\sum_{(p,q)\in\mathbf{V}}\left[\overrightarrow{G}^{\dagger}(p,q)\lambda(\alpha_2,p,q)\boldsymbol{\alpha}\left(\boldsymbol{e}+\sigma^2\lambda(\alpha_2,p,q)\boldsymbol{\alpha}\right)^{-1}\overrightarrow{G}(p,q)\right]\Bigg\}d\boldsymbol{x}
\end{aligned}
\tag{3.36}
$$

which, using the multidimensional Gaussian integral becomes

$$
\begin{aligned}
Z_{\text{posterior}}=&\left(2\pi\sigma^2\right)^{\frac{3|\mathbf{V}|}{2}}\left\{\det\left(\boldsymbol{I}+\sigma^2\sum_{\kappa\in\mathbf{K}}\sum_{\kappa'\in\mathbf{K}}\alpha_{\kappa,\kappa'}\boldsymbol{C}\left(\alpha_2,\kappa,\kappa'\right)\right)\right\}^{-\frac{1}{2}}\\
&\times\exp\left\{-\frac{1}{2}\sum_{(p,q)\in\mathbf{V}}\left[\overrightarrow{G}^{\dagger}(p,q)\lambda(\alpha_2,p,q)\boldsymbol{\alpha}\left(\boldsymbol{e}+\sigma^2\lambda(\alpha_2,p,q)\boldsymbol{\alpha}\right)^{-1}\overrightarrow{G}(p,q)\right]\right\}.
\end{aligned}
\tag{3.37}
$$

Using the same eigendecomposition as in (3.25), the determinant in equation (3.37) can be rewritten as follows:

$$
\det\left(\boldsymbol{I}+\sigma^2\sum_{\kappa\in\mathbf{K}}\sum_{\kappa'\in\mathbf{K}}\alpha_{\kappa,\kappa'}\boldsymbol{C}\left(\alpha_2,\kappa,\kappa'\right)\right)
$$

$$
\begin{aligned}
&= \det\left[\boldsymbol{I} + \sigma^2\left(\boldsymbol{U}^{-1}\boldsymbol{\Lambda}\boldsymbol{U}\right)\otimes\boldsymbol{\alpha}\right] \\
&= \det\left[\boldsymbol{I}\otimes\boldsymbol{e} + \sigma^2\left(\boldsymbol{U}^{-1}\boldsymbol{\Lambda}\boldsymbol{U}\right)\otimes\boldsymbol{\alpha}\right] \\
&= \det\left[\boldsymbol{U}^{-1}\boldsymbol{U}\otimes\boldsymbol{e}\boldsymbol{e} + \sigma^2\left(\boldsymbol{U}^{-1}\boldsymbol{\Lambda}\boldsymbol{U}\right)\otimes\boldsymbol{e}\boldsymbol{\alpha}\boldsymbol{e}\right] \\
&= \det\left[\left(\boldsymbol{U}^{-1}\otimes\boldsymbol{e}\right)\left(\boldsymbol{U}\otimes\boldsymbol{e}\right) + \sigma^2\left(\boldsymbol{U}^{-1}\otimes\boldsymbol{e}\right)\left(\boldsymbol{\Lambda}\otimes\boldsymbol{\alpha}\right)\left(\boldsymbol{U}\otimes\boldsymbol{e}\right)\right] \\
&= \det\left[\left(\boldsymbol{U}^{-1}\otimes\boldsymbol{e}\right)\left\{\boldsymbol{I} + \sigma^2\left(\boldsymbol{\Lambda}\otimes\boldsymbol{\alpha}\right)\right\}\left(\boldsymbol{U}\otimes\boldsymbol{e}\right)\right] \\
&= \det\left[\boldsymbol{I} + \sigma^2\left(\boldsymbol{\Lambda}\otimes\boldsymbol{\alpha}\right)\right]. \qquad (3.38)
\end{aligned}
$$

Here we notice that $\boldsymbol{I} + \sigma^2\left(\boldsymbol{\Lambda}\otimes\boldsymbol{\alpha}\right)$ is a block diagonal matrix, so we can rewrite the previous line as

$$
\begin{aligned}
\det\left[\boldsymbol{I} + \sigma^2\left(\boldsymbol{\Lambda}\otimes\boldsymbol{\alpha}\right)\right] &= \det\left[\operatorname{diag}\left(\boldsymbol{A}_{11}, \boldsymbol{A}_{12}, \ldots, \boldsymbol{A}_{V_x V_y}\right)\right] \text{ with } \boldsymbol{A}_{pq} = \boldsymbol{e} + \sigma^2\lambda(\alpha_2, p, q)\boldsymbol{\alpha} \\
&= \prod_{(p,q)\in\mathbf{V}} \det\left(\boldsymbol{e} + \sigma^2\lambda(\alpha_2, p, q)\boldsymbol{\alpha}\right) \qquad (3.39)
\end{aligned}
$$

where $\operatorname{diag}(\boldsymbol{A}_1, ..., \boldsymbol{A}_n)$ means creating a block diagonal matrix whose diagonal entries starting in the upper left corner are matrices $\boldsymbol{A}_1, ..., \boldsymbol{A}_n$. So equation (3.37) can be transformed into

$$
\begin{aligned}
Z_{\text{posterior}}\left(\boldsymbol{g}, \boldsymbol{\alpha}, \alpha_2, \sigma\right) = \left(2\pi\sigma^2\right)^{\frac{3|\mathbf{V}|}{2}} &\prod_{(p,q)\in\mathbf{V}} \left[\det\left(\boldsymbol{e} + \sigma^2\lambda(\alpha_2, p, q)\boldsymbol{\alpha}\right)\right]^{-\frac{1}{2}} \\
&\times \exp\left\{-\frac{1}{2}\sum_{(p,q)\in\mathbf{V}}\left[\overrightarrow{G}^{\dagger}(p,q)\lambda(\alpha_2, p, q)\boldsymbol{\alpha}\left(\boldsymbol{e} + \sigma^2\lambda(\alpha_2, p, q)\boldsymbol{\alpha}\right)^{-1}\overrightarrow{G}(p,q)\right]\right\}. \qquad (3.40)
\end{aligned}
$$

3.2.5 Restored Image Equation

In our model, the estimated restored image configuration is given by the expected value of the a posteriori probability function. This gives us the following restored image equation:

$$
\widehat{\boldsymbol{f}} \equiv \int \boldsymbol{z}\Pr\left\{\boldsymbol{F} = \boldsymbol{z} | \boldsymbol{G} = \boldsymbol{g}, \boldsymbol{\alpha}, \alpha_2, \sigma\right\} d\boldsymbol{z} \qquad (3.41)
$$

where the integral is performed over every image configuration $\boldsymbol{z}$ (range of $]-\infty, +\infty[$ for each colour component) and $\widehat{\boldsymbol{f}}$ is our restored image.

Using equation (3.28) we obtain

$$
\widehat{\boldsymbol{f}} = \frac{1}{Z_{\text{posterior}}\left(\boldsymbol{g}, \boldsymbol{\alpha}, \alpha_2, \sigma\right)}\int \boldsymbol{z}\exp\left[-H\left(\boldsymbol{z}|\boldsymbol{g}, \boldsymbol{\alpha}, \alpha_2, \sigma\right)\right] d\boldsymbol{z} \qquad (3.42)
$$

which, using the results of equations (3.35) and (3.37) is rewritten as

$$
\begin{aligned}
\widehat{\boldsymbol{f}} = &\\
&\frac{1}{\left(2\pi\sigma^2\right)^{\frac{3|\mathbf{V}|}{2}}\det\left(\sigma^2\boldsymbol{\Sigma}^{-1}\right)^{-\frac{1}{2}}\exp\left\{-\frac{1}{2}\sum_{(p,q)\in\mathbf{V}}\overrightarrow{G}^{\dagger}(p,q)\lambda(\alpha_2, p, q)\boldsymbol{\alpha}\left(\boldsymbol{e} + \sigma^2\lambda(\alpha_2, p, q)\boldsymbol{\alpha}\right)^{-1}\overrightarrow{G}(p,q)\right\}} \\
&\times\int \boldsymbol{z}\exp\left(-\frac{1}{2\sigma^2}\left[\boldsymbol{z}-\boldsymbol{\mu}\right]^T\sigma^2\boldsymbol{\Sigma}^{-1}\left[\boldsymbol{z}-\boldsymbol{\mu}\right]\right. \\
&\left.-\frac{1}{2}\sum_{(p,q)\in\mathbf{V}}\left[\overrightarrow{G}^{\dagger}(p,q)\lambda(\alpha_2, p, q)\boldsymbol{\alpha}\left(\boldsymbol{e} + \sigma^2\lambda(\alpha_2, p, q)\boldsymbol{\alpha}\right)^{-1}\overrightarrow{G}(p,q)\right]\right) d\boldsymbol{z} \\
&= \frac{1}{\left(2\pi\sigma^2\right)^{\frac{3|\mathbf{V}|}{2}}\left(\sigma^2\right)^{-\frac{3|\mathbf{V}|}{2}}\det\left(\boldsymbol{\Sigma}\right)^{\frac{1}{2}}}\int \boldsymbol{z}\exp\left(-\frac{1}{2}\left[\boldsymbol{z}-\boldsymbol{\mu}\right]^T\boldsymbol{\Sigma}^{-1}\left[\boldsymbol{z}-\boldsymbol{\mu}\right]\right) d\boldsymbol{z} \\
&= \frac{1}{\left(2\pi\right)^{\frac{3|\mathbf{V}|}{2}}\det\left(\boldsymbol{\Sigma}\right)^{\frac{1}{2}}}\int \boldsymbol{z}\exp\left(-\frac{1}{2}\left[\boldsymbol{z}-\boldsymbol{\mu}\right]^T\boldsymbol{\Sigma}^{-1}\left[\boldsymbol{z}-\boldsymbol{\mu}\right]\right) d\boldsymbol{z} \qquad (3.43)
\end{aligned}
$$

with $\boldsymbol{\mu} \equiv \left(\boldsymbol{I} + \sigma^2 \sum_{\kappa \in \mathbf{K}} \sum_{\kappa' \in \mathbf{K}} \alpha_{\kappa,\kappa'} \boldsymbol{C}(\alpha_2, \kappa, \kappa') \right)^{-1} \boldsymbol{g}$

and $\boldsymbol{\Sigma}^{-1} \equiv \frac{1}{\sigma^2} \left(\boldsymbol{I} + \sigma^2 \sum_{\kappa \in \mathbf{K}} \sum_{\kappa' \in \mathbf{K}} \alpha_{\kappa,\kappa'} \boldsymbol{C}(\alpha_2, \kappa, \kappa') \right)$

which corresponds to the expected value equation of a multivariate Gaussian distribution. Using that fact, we conclude that

$$\widehat{\boldsymbol{f}} = \mathbf{E}[\boldsymbol{z}] = \boldsymbol{\mu} = \left(\boldsymbol{I} + \sigma^2 \sum_{\kappa \in \mathbf{K}} \sum_{\kappa' \in \mathbf{K}} \alpha_{\kappa,\kappa'} \boldsymbol{C}(\alpha_2, \kappa, \kappa') \right)^{-1} \boldsymbol{g}. \tag{3.44}$$

However, it is impractical to compute the inverse of such a large matrix, so we use the same eigendecomposition as in (3.25) to simplify the equation as follows:

$$\begin{aligned}
\widehat{\boldsymbol{f}} &= \left[\boldsymbol{I} + \sigma^2 \left(\boldsymbol{U}^{-1} \boldsymbol{\Lambda} \boldsymbol{U} \right) \otimes \boldsymbol{\alpha} \right]^{-1} \boldsymbol{g} \\
&= \left[\boldsymbol{U}^{-1} \boldsymbol{U} \otimes \boldsymbol{e}\boldsymbol{e} + \sigma^2 \left(\boldsymbol{U}^{-1} \boldsymbol{\Lambda} \boldsymbol{U} \right) \otimes \boldsymbol{e}\boldsymbol{\alpha}\boldsymbol{e} \right]^{-1} \boldsymbol{g} \\
&= \left[\left(\boldsymbol{U}^{-1} \otimes \boldsymbol{e} \right) \left(\boldsymbol{U} \otimes \boldsymbol{e} \right) + \sigma^2 \left(\boldsymbol{U}^{-1} \otimes \boldsymbol{e} \right) \left(\boldsymbol{\Lambda} \otimes \boldsymbol{\alpha} \right) \left(\boldsymbol{U} \otimes \boldsymbol{e} \right) \right]^{-1} \boldsymbol{g} \\
&= \left(\boldsymbol{U}^{-1} \otimes \boldsymbol{e} \right) \left[\boldsymbol{I} + \sigma^2 \left(\boldsymbol{\Lambda} \otimes \boldsymbol{\alpha} \right) \right]^{-1} \left(\boldsymbol{U} \otimes \boldsymbol{e} \right) \boldsymbol{g} \\
&= \left(\boldsymbol{U}^{-1} \otimes \boldsymbol{e} \right) \left[\sum_{(p,q) \in \mathbf{V}} \boldsymbol{J}^{pq,pq} \otimes \left(\boldsymbol{e} + \sigma^2 \lambda \left(\alpha_2, p, q \right) \boldsymbol{\alpha} \right) \right]^{-1} \left(\boldsymbol{U} \otimes \boldsymbol{e} \right) \boldsymbol{g} \\
&= \sum_{(p,q) \in \mathbf{V}} \left(\boldsymbol{U}^{-1} \left(p, q \right) \otimes \left(\boldsymbol{e} + \sigma^2 \lambda \left(\alpha_2, p, q \right) \boldsymbol{\alpha} \right)^{-1} \right) \overrightarrow{G} \left(p, q \right)
\end{aligned} \tag{3.45}$$

so that we have

$$\widehat{\mathbf{f}}_{x,y} = \sum_{(p,q) \in \mathbf{V}} U^{-1}_{(x,y),(p,q)} \left(\boldsymbol{e} + \sigma^2 \lambda \left(\alpha_2, p, q \right) \boldsymbol{\alpha} \right)^{-1} \overrightarrow{G} \left(p, q \right). \tag{3.46}$$

Here we note that this corresponds to the inverse DFT of $\left(\boldsymbol{e} + \sigma^2 \lambda \left(\alpha_2, p, q \right) \boldsymbol{\alpha} \right)^{-1} \overrightarrow{G} \left(p, q \right)$ where $\overrightarrow{G}(p, q)$ itself is the DFT of the degraded image.

3.2.6 Hyperparameters Estimation

As we saw in section 3.2.5, the restored image equation depends on the values of the hyperparameters σ, $\boldsymbol{\alpha}$ and α_2. The selection of those values shall be done by fixing the value of α_2 and choosing values for σ and $\boldsymbol{\alpha}$ that maximize the evidence (or likelihood) of equation (3.26). Such a method is known as Maximum Likelihood Estimation (MLE).

Using equation (3.26) with (3.1), (3.10) and (3.28), we find that the evidence is given by

$$\begin{aligned}
\Pr\left\{ \boldsymbol{G} = \boldsymbol{g} | \boldsymbol{\alpha}, \alpha_2, \sigma \right\} &= \frac{\Pr\left\{ \boldsymbol{G} = \boldsymbol{g} | \boldsymbol{F} = \boldsymbol{f}, \sigma \right\} \Pr\left\{ \boldsymbol{F} = \boldsymbol{f} | \boldsymbol{\alpha}, \alpha_2 \right\}}{\Pr\left\{ \boldsymbol{F} = \boldsymbol{f} | \boldsymbol{G} = \boldsymbol{g}, \boldsymbol{\alpha}, \alpha_2, \sigma \right\}} \\
&= \frac{\frac{1}{Z_{\text{noise}}(\sigma)} \exp\left(-\frac{1}{2\sigma^2} \left\| \boldsymbol{g} - \boldsymbol{f} \right\|^2 \right) \frac{1}{Z_{\text{prior}}(\boldsymbol{\alpha}, \alpha_2)} \exp\left(-\frac{1}{2} \sum_{\kappa \in \mathbf{K}} \sum_{\kappa' \in \mathbf{K}} \alpha_{\kappa,\kappa'} \boldsymbol{f}^T \boldsymbol{C}\left(\alpha_2, \kappa, \kappa' \right) \boldsymbol{f} \right)}{\frac{1}{Z_{\text{posterior}}(\boldsymbol{g}, \boldsymbol{\alpha}, \alpha_2, \sigma)} \exp\left[-\frac{1}{2\sigma^2} \left\| \boldsymbol{g} - \boldsymbol{f} \right\|^2 - \frac{1}{2} \sum_{\kappa \in \mathbf{K}} \sum_{\kappa' \in \mathbf{K}} \alpha_{\kappa,\kappa'} \boldsymbol{f}^T \boldsymbol{C}\left(\alpha_2, \kappa, \kappa' \right) \boldsymbol{f} \right]} \\
&= \frac{Z_{\text{posterior}}(\boldsymbol{g}, \boldsymbol{\alpha}, \alpha_2, \sigma)}{Z_{\text{noise}}(\sigma) Z_{\text{prior}}(\boldsymbol{\alpha}, \alpha_2)}
\end{aligned} \tag{3.47}$$

We can simplify the calculations by finding the maximum of the log of the evidence, which gives us

$$(\widehat{\boldsymbol{\alpha}}, \widehat{\sigma}) = \arg \max_{\boldsymbol{\alpha}, \sigma} \left[\ln Z_{\text{posterior}}(\boldsymbol{g}, \boldsymbol{\alpha}, \alpha_2, \sigma) - \ln Z_{\text{noise}}(\sigma) - \ln Z_{\text{prior}}(\boldsymbol{\alpha}, \alpha_2) \right]$$

$$
\begin{aligned}
&= \arg\ \max_{\boldsymbol{\alpha},\sigma}\Bigg[\frac{3\,|\mathbf{V}|}{2}\ln(2\pi\sigma^2) - \frac{1}{2}\sum_{(p,q)\in\mathbf{V}}\ln\left(\det\left[\boldsymbol{e}+\sigma^2\lambda(\alpha_2,p,q)\boldsymbol{\alpha}\right]\right)\\
&\quad - \frac{1}{2}\sum_{(p,q)\in\mathbf{V}}\overrightarrow{G}^{\dagger}(p,q)\lambda(\alpha_2,p,q)\boldsymbol{\alpha}\left[\boldsymbol{e}+\sigma^2\lambda(\alpha_2,p,q)\boldsymbol{\alpha}\right]^{-1}\overrightarrow{G}(p,q) - \frac{3\,|\mathbf{V}|}{2}\ln(2\pi\sigma^2)\\
&\quad - \frac{3\,|\mathbf{V}|}{2}\ln(2\pi) + \frac{1}{2}\sum_{(p,q)\in\mathbf{V}}\ln\left(\det\left[\lambda(\alpha_2,p,q)\boldsymbol{\alpha}\right]\right)\Bigg]\\
&= \arg\ \max_{\boldsymbol{\alpha},\sigma}\Bigg[-\frac{3\,|\mathbf{V}|}{2}\ln(2\pi) - \frac{1}{2}\sum_{(p,q)\in\mathbf{V}}\ln\left(\det\left[\boldsymbol{e}+\sigma^2\lambda(\alpha_2,p,q)\boldsymbol{\alpha}\right]\right)\\
&\quad - \frac{1}{2}\sum_{(p,q)\in\mathbf{V}}\overrightarrow{G}^{\dagger}(p,q)\lambda(\alpha_2,p,q)\boldsymbol{\alpha}\left[\boldsymbol{e}+\sigma^2\lambda(\alpha_2,p,q)\boldsymbol{\alpha}\right]^{-1}\overrightarrow{G}(p,q)\\
&\quad + \frac{1}{2}\sum_{(p,q)\in\mathbf{V}}\ln\left(\det\left[\lambda(\alpha_2,p,q)\boldsymbol{\alpha}\right]\right)\Bigg]\\
&= \arg\ \max_{\boldsymbol{\alpha},\sigma}\Bigg[-\frac{3\,|\mathbf{V}|}{2}\ln(2\pi) - \frac{1}{2}\sum_{(p,q)\in\mathbf{V}}\ln\left(\det\left[\boldsymbol{e}+\sigma^2\lambda(\alpha_2,p,q)\boldsymbol{\alpha}\right]\right)\\
&\quad - \frac{1}{2}\sum_{(p,q)\in\mathbf{V}}\overrightarrow{G}^{\dagger}(p,q)\lambda(\alpha_2,p,q)\boldsymbol{\alpha}\left[\boldsymbol{e}+\sigma^2\lambda(\alpha_2,p,q)\boldsymbol{\alpha}\right]^{-1}\overrightarrow{G}(p,q)\\
&\quad + \frac{1}{2}\sum_{(p,q)\in\mathbf{V}}\ln\left(\lambda(\alpha_2,p,q)^3\det\boldsymbol{\alpha}\right)\Bigg]\\
&= \arg\ \max_{\boldsymbol{\alpha},\sigma}\Bigg[-\frac{3\,|\mathbf{V}|}{2}\ln(2\pi) - \frac{1}{2}\sum_{(p,q)\in\mathbf{V}}\ln\left(\det\left[\boldsymbol{e}+\sigma^2\lambda(\alpha_2,p,q)\boldsymbol{\alpha}\right]\right)\\
&\quad - \frac{1}{2}\sum_{(p,q)\in\mathbf{V}}\overrightarrow{G}^{\dagger}(p,q)\lambda(\alpha_2,p,q)\boldsymbol{\alpha}\left[\boldsymbol{e}+\sigma^2\lambda(\alpha_2,p,q)\boldsymbol{\alpha}\right]^{-1}\overrightarrow{G}(p,q) \qquad (3.48)\\
&\quad + \frac{|\mathbf{V}|}{2}\ln\left(\det\boldsymbol{\alpha}\right) + \frac{3}{2}\sum_{(p,q)\in\mathbf{V}}\ln\left[\lambda(\alpha_2,p,q)\right]\Bigg]
\end{aligned}
$$

where $\widehat{\boldsymbol{\alpha}}$ and $\widehat{\sigma}$ are the estimated values of the hyperparameters $\boldsymbol{\alpha}$ and σ respectively.

We showed in equation (2.63) that last term of equation (3.48) imposes the restriction $\alpha_2 \geq -\frac{1}{2}$.

Using equation (3.48), we find the value of $\widehat{\sigma}$ by solving the equation $\frac{d}{d\widehat{\sigma}^2}\ln(\Pr\{\boldsymbol{G}=\boldsymbol{g}|\widehat{\boldsymbol{\alpha}},\alpha_2,\widehat{\sigma}\}) = 0$ as follows

$$
\begin{aligned}
0 &= -\frac{1}{2}\sum_{(p,q)\in\mathbf{V}}\operatorname{tr}\left(\lambda(\alpha_2,p,q)\widehat{\boldsymbol{\alpha}}\left[\boldsymbol{e}+\widehat{\sigma}^2\lambda(\alpha_2,p,q)\widehat{\boldsymbol{\alpha}}\right]^{-1}\right)\\
&\quad - \frac{1}{2}\sum_{(p,q)\in\mathbf{V}}\overrightarrow{G}^{\dagger}(p,q)\lambda(\alpha_2,p,q)\widehat{\boldsymbol{\alpha}}\\
&\quad \times\left(-\left[\boldsymbol{e}+\widehat{\sigma}^2\lambda(\alpha_2,p,q)\widehat{\boldsymbol{\alpha}}\right]^{-1}\left(\lambda(\alpha_2,p,q)\widehat{\boldsymbol{\alpha}}\right)\left[\boldsymbol{e}+\widehat{\sigma}^2\lambda(\alpha_2,p,q)\widehat{\boldsymbol{\alpha}}\right]^{-1}\right)\overrightarrow{G}(p,q)\\
&= -\frac{1}{2\widehat{\sigma}^2}\sum_{(p,q)\in\mathbf{V}}\operatorname{tr}\left(\widehat{\sigma}^2\lambda(\alpha_2,p,q)\widehat{\boldsymbol{\alpha}}\left(\boldsymbol{e}+\widehat{\sigma}^2\lambda(\alpha_2,p,q)\widehat{\boldsymbol{\alpha}}\right)^{-1}\right)\\
&\quad + \frac{1}{2}\sum_{(p,q)\in\mathbf{V}}\overrightarrow{G}^{\dagger}(p,q)\left(\lambda(\alpha_2,p,q)\widehat{\boldsymbol{\alpha}}\left[\boldsymbol{e}+\widehat{\sigma}^2\lambda(\alpha_2,p,q)\widehat{\boldsymbol{\alpha}}\right]^{-1}\right)^2\overrightarrow{G}(p,q)\\
&= -\frac{1}{2\widehat{\sigma}^2}\sum_{(p,q)\in\mathbf{V}}\operatorname{tr}\left[\left(-\boldsymbol{e}+\boldsymbol{e}+\widehat{\sigma}^2\lambda(\alpha_2,p,q)\widehat{\boldsymbol{\alpha}}\right)\left(\boldsymbol{e}+\widehat{\sigma}^2\lambda(\alpha_2,p,q)\widehat{\boldsymbol{\alpha}}\right)^{-1}\right]\\
&\quad + \frac{1}{2}\sum_{(p,q)\in\mathbf{V}}\overrightarrow{G}^{\dagger}(p,q)\left(\lambda(\alpha_2,p,q)\widehat{\boldsymbol{\alpha}}\left[\boldsymbol{e}+\widehat{\sigma}^2\lambda(\alpha_2,p,q)\widehat{\boldsymbol{\alpha}}\right]^{-1}\right)^2\overrightarrow{G}(p,q)
\end{aligned}
$$

$$
\begin{aligned}
&= -\frac{1}{2\widehat{\sigma}^2}\sum_{(p,q)\in\mathbf{V}}\mathrm{tr}\left[-\boldsymbol{e}\left(\boldsymbol{e}+\widehat{\sigma}^2\lambda(\alpha_2,p,q)\widehat{\boldsymbol{\alpha}}\right)^{-1}\right]-\frac{1}{2\widehat{\sigma}^2}\sum_{(p,q)\in\mathbf{V}}\mathrm{tr}\left(\boldsymbol{e}\right)\\
&\quad+\frac{1}{2}\sum_{(p,q)\in\mathbf{V}}\overrightarrow{G}^{\dagger}(p,q)\left(\lambda(\alpha_2,p,q)\widehat{\boldsymbol{\alpha}}\left[\boldsymbol{e}+\widehat{\sigma}^2\lambda(\alpha_2,p,q)\widehat{\boldsymbol{\alpha}}\right]^{-1}\right)^2\overrightarrow{G}(p,q)\\
\frac{3\left|\mathbf{V}\right|}{2\widehat{\sigma}^2} &= \frac{1}{2\widehat{\sigma}^2}\sum_{(p,q)\in\mathbf{V}}\mathrm{tr}\left(\boldsymbol{e}+\widehat{\sigma}^2\lambda(\alpha_2,p,q)\widehat{\boldsymbol{\alpha}}\right)^{-1}\\
&\quad+\frac{1}{2}\sum_{(p,q)\in\mathbf{V}}\overrightarrow{G}^{\dagger}(p,q)\left(\lambda(\alpha_2,p,q)\widehat{\boldsymbol{\alpha}}\left[\boldsymbol{e}+\widehat{\sigma}^2\lambda(\alpha_2,p,q)\widehat{\boldsymbol{\alpha}}\right]^{-1}\right)^2\overrightarrow{G}(p,q)\\
\widehat{\sigma}^2 &= \frac{\widehat{\sigma}^2}{3\left|\mathbf{V}\right|}\sum_{(p,q)\in\mathbf{V}}\Bigg[\mathrm{tr}\left(\boldsymbol{e}+\widehat{\sigma}^2\lambda(\alpha_2,p,q)\widehat{\boldsymbol{\alpha}}\right)^{-1}\\
&\quad+\widehat{\sigma}^2\overrightarrow{G}^{\dagger}(p,q)\left(\lambda(\alpha_2,p,q)\widehat{\boldsymbol{\alpha}}\left[\boldsymbol{e}+\widehat{\sigma}^2\lambda(\alpha_2,p,q)\widehat{\boldsymbol{\alpha}}\right]^{-1}\right)^2\overrightarrow{G}(p,q)\Bigg].
\end{aligned}
\tag{3.49}
$$

Similarly, we find the value $\widehat{\boldsymbol{\alpha}}$ by solving the equation $\frac{d}{d\widehat{\boldsymbol{\alpha}}}\ln(\Pr\{\boldsymbol{G}=\boldsymbol{g}|\widehat{\boldsymbol{\alpha}},\alpha_2,\widehat{\sigma}\})=0$. Here we shall make use of the following properties of matrix derivatives taken from [16]:
For a symmetric matrix $\boldsymbol{X}$,

$$
\frac{d\ln\det\left(\boldsymbol{X}\right)}{d\boldsymbol{X}}=2\boldsymbol{X}^{-1}-\left(\boldsymbol{X}^{-1}\circ\boldsymbol{I}\right)
\tag{3.50}
$$

and

$$
\frac{d\boldsymbol{X}}{dX_{ij}}=\boldsymbol{J}^{ij}+\boldsymbol{J}^{ji}-\boldsymbol{J}^{ij}\boldsymbol{J}^{ji}
\tag{3.51}
$$

where $\circ$ means the Hadamard product so that $\boldsymbol{X}\circ\boldsymbol{I}=\mathrm{diag}(\boldsymbol{X})$ where $\mathrm{diag}(\boldsymbol{X})$ means the diagonal matrix made from only the main diagonal of $\boldsymbol{X}$. Also, for a general matrix,

$$
\partial\left(\boldsymbol{X}^{-1}\right)=-\boldsymbol{X}^{-1}\left(\partial\boldsymbol{X}\right)\boldsymbol{X}^{-1}.
\tag{3.52}
$$

Using these, we obtain

$$
\begin{aligned}
0 &= -\frac{1}{2}\sum_{(p,q)\in\mathbf{V}}\widehat{\sigma}^2\lambda(\alpha_2,p,q)\left(2\left[\boldsymbol{e}+\widehat{\sigma}^2\lambda(\alpha_2,p,q)\widehat{\boldsymbol{\alpha}}\right]^{-1}-\mathrm{diag}\left\{\left[\boldsymbol{e}+\widehat{\sigma}^2\lambda(\alpha_2,p,q)\widehat{\boldsymbol{\alpha}}\right]^{-1}\right\}\right)\\
&\quad+\frac{\left|\mathbf{V}\right|}{2}\left[2\widehat{\boldsymbol{\alpha}}^{-1}-\mathrm{diag}\left(\widehat{\boldsymbol{\alpha}}^{-1}\right)\right]\\
&\quad-\frac{1}{2}\sum_{(p,q)\in\mathbf{V}}\overrightarrow{G}^{\dagger}(p,q)\lambda(\alpha_2,p,q)\frac{d}{d\widehat{\boldsymbol{\alpha}}}\left\{\widehat{\boldsymbol{\alpha}}\left[\boldsymbol{e}+\widehat{\sigma}^2\lambda(\alpha_2,p,q)\widehat{\boldsymbol{\alpha}}\right]^{-1}\right\}\overrightarrow{G}(p,q)\\
&= -\sum_{(p,q)\in\mathbf{V}}\widehat{\sigma}^2\lambda(\alpha_2,p,q)\left(2\left[\boldsymbol{e}+\widehat{\sigma}^2\lambda(\alpha_2,p,q)\widehat{\boldsymbol{\alpha}}\right]^{-1}-\mathrm{diag}\left\{\left[\boldsymbol{e}+\widehat{\sigma}^2\lambda(\alpha_2,p,q)\widehat{\boldsymbol{\alpha}}\right]^{-1}\right\}\right)\\
&\quad+2|\mathbf{V}|\widehat{\boldsymbol{\alpha}}^{-1}-|\mathbf{V}|\mathrm{diag}\left(\widehat{\boldsymbol{\alpha}}^{-1}\right)\\
&\quad-\sum_{(p,q)\in\mathbf{V}}\overrightarrow{G}^{\dagger}(p,q)\lambda(\alpha_2,p,q)\frac{d}{d\widehat{\boldsymbol{\alpha}}}\left\{\widehat{\boldsymbol{\alpha}}\left[\boldsymbol{e}+\widehat{\sigma}^2\lambda(\alpha_2,p,q)\widehat{\boldsymbol{\alpha}}\right]^{-1}\right\}\overrightarrow{G}(p,q)\\
2|\mathbf{V}|\widehat{\boldsymbol{\alpha}}^{-1} &= \sum_{(p,q)\in\mathbf{V}}\widehat{\sigma}^2\lambda(\alpha_2,p,q)\left(2\left[\boldsymbol{e}+\widehat{\sigma}^2\lambda(\alpha_2,p,q)\widehat{\boldsymbol{\alpha}}\right]^{-1}-\mathrm{diag}\left\{\left[\boldsymbol{e}+\widehat{\sigma}^2\lambda(\alpha_2,p,q)\widehat{\boldsymbol{\alpha}}\right]^{-1}\right\}\right)\\
&\quad+|\mathbf{V}|\mathrm{diag}\left(\widehat{\boldsymbol{\alpha}}^{-1}\right)+\sum_{(p,q)\in\mathbf{V}}\overrightarrow{G}^{\dagger}(p,q)\lambda(\alpha_2,p,q)\frac{d}{d\widehat{\boldsymbol{\alpha}}}\left\{\widehat{\boldsymbol{\alpha}}\left[\boldsymbol{e}+\widehat{\sigma}^2\lambda(\alpha_2,p,q)\widehat{\boldsymbol{\alpha}}\right]^{-1}\right\}\overrightarrow{G}(p,q)
\end{aligned}
$$

$$
\begin{aligned}
\widehat{\boldsymbol{\alpha}}^{-1} &= \frac{1}{2|\mathbf{V}|} \\
&\quad \times \sum_{(p,q)\in\mathbf{V}} \widehat{\sigma}^2\lambda(\alpha_2,p,q)\left(2\left[\boldsymbol{e}+\widehat{\sigma}^2\lambda(\alpha_2,p,q)\widehat{\boldsymbol{\alpha}}\right]^{-1} - \mathrm{diag}\left\{\left[\boldsymbol{e}+\widehat{\sigma}^2\lambda(\alpha_2,p,q)\widehat{\boldsymbol{\alpha}}\right]^{-1}\right\}\right) \\
&\quad + \frac{1}{2}\mathrm{diag}\left(\widehat{\boldsymbol{\alpha}}^{-1}\right) \\
&\quad + \frac{1}{2|\mathbf{V}|}\sum_{(p,q)\in\mathbf{V}} \overrightarrow{G}^{\dagger}(p,q)\lambda(\alpha_2,p,q)\frac{d}{d\widehat{\boldsymbol{\alpha}}}\left\{\widehat{\boldsymbol{\alpha}}\left[\boldsymbol{e}+\widehat{\sigma}^2\lambda(\alpha_2,p,q)\widehat{\boldsymbol{\alpha}}\right]^{-1}\right\}\overrightarrow{G}(p,q) \\
\widehat{\boldsymbol{\alpha}}^{-1} &= \frac{1}{2|\mathbf{V}|} \\
&\quad \times \sum_{(p,q)\in\mathbf{V}} \widehat{\sigma}^2\lambda(\alpha_2,p,q)\left(2\left[\boldsymbol{e}+\widehat{\sigma}^2\lambda(\alpha_2,p,q)\widehat{\boldsymbol{\alpha}}\right]^{-1} - \mathrm{diag}\left\{\left[\boldsymbol{e}+\widehat{\sigma}^2\lambda(\alpha_2,p,q)\widehat{\boldsymbol{\alpha}}\right]^{-1}\right\}\right) \\
&\quad + \frac{1}{2}\mathrm{diag}\left(\widehat{\boldsymbol{\alpha}}^{-1}\right) + \frac{1}{2|\mathbf{V}|}\sum_{\kappa\in\mathbf{K}}\sum_{\kappa'\in\mathbf{K}}\boldsymbol{J}^{\kappa,\kappa'} \\
&\quad \times \sum_{(p,q)\in\mathbf{V}} \overrightarrow{G}^{\dagger}(p,q)\lambda(\alpha_2,p,q)\frac{d}{d\widehat{\alpha}_{\kappa,\kappa'}}\left\{\left[\widehat{\boldsymbol{\alpha}}^{-1}+\widehat{\sigma}^2\lambda(\alpha_2,p,q)\boldsymbol{e}\right]^{-1}\right\}\overrightarrow{G}(p,q) \\
\widehat{\boldsymbol{\alpha}}^{-1} &= \frac{1}{2|\mathbf{V}|} \\
&\quad \times \sum_{(p,q)\in\mathbf{V}} \widehat{\sigma}^2\lambda(\alpha_2,p,q)\left(2\left[\boldsymbol{e}+\widehat{\sigma}^2\lambda(\alpha_2,p,q)\widehat{\boldsymbol{\alpha}}\right]^{-1} - \mathrm{diag}\left\{\left[\boldsymbol{e}+\widehat{\sigma}^2\lambda(\alpha_2,p,q)\widehat{\boldsymbol{\alpha}}\right]^{-1}\right\}\right) \\
&\quad + \frac{1}{2}\mathrm{diag}\left(\widehat{\boldsymbol{\alpha}}^{-1}\right) \\
&\quad + \frac{1}{2|\mathbf{V}|}\sum_{\kappa\in\mathbf{K}}\sum_{\kappa'\in\mathbf{K}}\boldsymbol{J}^{\kappa,\kappa'}\sum_{(p,q)\in\mathbf{V}} \overrightarrow{G}^{\dagger}(p,q)\lambda(\alpha_2,p,q)\Bigg\{-\left[\widehat{\boldsymbol{\alpha}}^{-1}+\widehat{\sigma}^2\lambda(\alpha_2,p,q)\boldsymbol{e}\right]^{-1} \\
&\quad \times \left(\frac{d}{d\widehat{\alpha}_{\kappa,\kappa'}}\left[\widehat{\boldsymbol{\alpha}}^{-1}+\widehat{\sigma}^2\lambda(\alpha_2,p,q)\boldsymbol{e}\right]\right)\left[\widehat{\boldsymbol{\alpha}}^{-1}+\widehat{\sigma}^2\lambda(\alpha_2,p,q)\boldsymbol{e}\right]^{-1}\Bigg\}\overrightarrow{G}(p,q) \\
\widehat{\boldsymbol{\alpha}}^{-1} &= \frac{1}{2|\mathbf{V}|} \\
&\quad \times \sum_{(p,q)\in\mathbf{V}} \widehat{\sigma}^2\lambda(\alpha_2,p,q)\left(2\left[\boldsymbol{e}+\widehat{\sigma}^2\lambda(\alpha_2,p,q)\widehat{\boldsymbol{\alpha}}\right]^{-1} - \mathrm{diag}\left\{\left[\boldsymbol{e}+\widehat{\sigma}^2\lambda(\alpha_2,p,q)\widehat{\boldsymbol{\alpha}}\right]^{-1}\right\}\right) \\
&\quad + \frac{1}{2}\mathrm{diag}\left(\widehat{\boldsymbol{\alpha}}^{-1}\right) \\
&\quad + \frac{1}{2|\mathbf{V}|}\sum_{\kappa\in\mathbf{K}}\sum_{\kappa'\in\mathbf{K}}\boldsymbol{J}^{\kappa,\kappa'}\sum_{(p,q)\in\mathbf{V}} \overrightarrow{G}^{\dagger}(p,q)\lambda(\alpha_2,p,q)\Bigg\{-\left[\widehat{\boldsymbol{\alpha}}^{-1}+\widehat{\sigma}^2\lambda(\alpha_2,p,q)\boldsymbol{e}\right]^{-1} \\
&\quad \times \left[-\widehat{\boldsymbol{\alpha}}^{-1}\left(\boldsymbol{J}^{\kappa,\kappa'}+\boldsymbol{J}^{\kappa',\kappa}-\boldsymbol{J}^{\kappa,\kappa'}\boldsymbol{J}^{\kappa',\kappa}\right)\widehat{\boldsymbol{\alpha}}^{-1}\right]\left[\widehat{\boldsymbol{\alpha}}^{-1}+\widehat{\sigma}^2\lambda(\alpha_2,p,q)\boldsymbol{e}\right]^{-1}\Bigg\}\overrightarrow{G}(p,q) \\
\widehat{\boldsymbol{\alpha}}^{-1} &= \frac{1}{2|\mathbf{V}|} \\
&\quad \times \sum_{(p,q)\in\mathbf{V}} \widehat{\sigma}^2\lambda(\alpha_2,p,q)\left(2\left[\boldsymbol{e}+\widehat{\sigma}^2\lambda(\alpha_2,p,q)\widehat{\boldsymbol{\alpha}}\right]^{-1} - \mathrm{diag}\left\{\left[\boldsymbol{e}+\widehat{\sigma}^2\lambda(\alpha_2,p,q)\widehat{\boldsymbol{\alpha}}\right]^{-1}\right\}\right) \\
&\quad + \frac{1}{2}\mathrm{diag}\left(\widehat{\boldsymbol{\alpha}}^{-1}\right) \\
&\quad + \frac{1}{2|\mathbf{V}|}\sum_{\kappa\in\mathbf{K}}\sum_{\kappa'\in\mathbf{K}}\boldsymbol{J}^{\kappa,\kappa'}\sum_{(p,q)\in\mathbf{V}} \overrightarrow{G}^{\dagger}(p,q)\lambda(\alpha_2,p,q)\left[\boldsymbol{e}+\widehat{\sigma}^2\lambda(\alpha_2,p,q)\widehat{\boldsymbol{\alpha}}\right]^{-1} \\
&\quad \times \left(\boldsymbol{J}^{\kappa,\kappa'}+\boldsymbol{J}^{\kappa',\kappa}-\boldsymbol{J}^{\kappa,\kappa'}\boldsymbol{J}^{\kappa',\kappa}\right)\left[\boldsymbol{e}+\widehat{\sigma}^2\lambda(\alpha_2,p,q)\widehat{\boldsymbol{\alpha}}\right]^{-1}\overrightarrow{G}(p,q)
\end{aligned}
\tag{3.53}
$$

so that we have

$$\widehat{\boldsymbol{\alpha}}^{-1} - \frac{1}{2}\mathrm{diag}\left(\widehat{\boldsymbol{\alpha}}^{-1}\right) = \frac{1}{2\left|\mathbf{V}\right|} \times \sum_{(p,q)\in\mathbf{V}} \Bigg(\widehat{\sigma}^2\lambda(\alpha_2,p,q)\left\{2\left[\boldsymbol{e}+\widehat{\sigma}^2\lambda(\alpha_2,p,q)\widehat{\boldsymbol{\alpha}}\right]^{-1} - \mathrm{diag}\left(\left[\boldsymbol{e}+\widehat{\sigma}^2\lambda(\alpha_2,p,q)\widehat{\boldsymbol{\alpha}}\right]^{-1}\right)\right\} + \sum_{\kappa\in\mathbf{K}}\sum_{\kappa'\in\mathbf{K}}\Big[\boldsymbol{J}^{\kappa,\kappa'}\overrightarrow{G}^{\dagger}(p,q)\lambda(\alpha_2,p,q)\left[\boldsymbol{e}+\widehat{\sigma}^2\lambda(\alpha_2,p,q)\widehat{\boldsymbol{\alpha}}\right]^{-1}\left(\boldsymbol{J}^{\kappa,\kappa'}+\boldsymbol{J}^{\kappa',\kappa}-\boldsymbol{J}^{\kappa,\kappa'}\boldsymbol{J}^{\kappa,\kappa'}\right) \times \left[\boldsymbol{e}+\widehat{\sigma}^2\lambda(\alpha_2,p,q)\widehat{\boldsymbol{\alpha}}\right]^{-1}\overrightarrow{G}(p,q)\Big]\Bigg). \quad (3.54)$$

When actually computing the value of the log of the evidence given in equation (3.48), we notice that the value of the last term diverges when $\lambda(\alpha_2,p,q)=0$. As shown in section 2.2.6 using equation (2.66), we can get around this problem by using the following approximation:

$$\frac{3}{2}\sum_{(p,q)\in\mathbf{V}}\ln\left[\lambda(\alpha_2,p,q)\right] \approx \frac{3V_x^2}{2}\ln\frac{1}{4} + \frac{3V_x}{2}\sum_{p=0}^{V_x-1}\ln\Bigg[2-\cos\left(\frac{2\pi p}{V_x}\right)+2\alpha_2 + \sqrt{\left(2-\cos\left(\frac{2\pi p}{V_x}\right)+2\alpha_2\right)^2-\left(1+2\alpha_2\cos\left(\frac{2\pi p}{V_x}\right)\right)^2}\Bigg]. \quad (3.55)$$

We also concluded in the same section that we should restrict the range of α_2 to $-0.5<\alpha_2<0.5$.

3.3 Algorithm

In this section, we describe an image restoration algorithm based on our image restoration model. We use a fixed point iteration algorithm [12] to find our maximum likelihood estimates for the hyperparameters $\boldsymbol{\alpha}$ and σ. As we saw in section 3.2.6, the extremum values for the hyperparameters $\boldsymbol{\alpha}$ and σ can be expressed in the form of the simultaneous recursive equations $\alpha(r)=f(\boldsymbol{\alpha}(r-1),\sigma(r-1))$ and $\sigma(r)=g(\alpha(r-1),\sigma(r-1))$. Therefore, in our algorithm, we find new values of $\widehat{\boldsymbol{\alpha}}$ and $\widehat{\sigma}$ by applying their current values to equations (3.49) and (3.54) and repeat that process until the algorithm converges. We shall assume that the algorithm has converged once we achieve the following 2 halting criteria:

$$e_1(r) = \left\{\sum_{\kappa\in\mathbf{K}}\sum_{\kappa'\in\mathbf{K}}\left|\frac{a_{\kappa,\kappa'}(r)-a_{\kappa,\kappa'}(r-1)}{a_{\kappa,\kappa'}(r-1)}\right|\right\} + \left|\frac{b(r)-b(r-1)}{b(r-1)}\right| < 10^{-4} \quad (3.56)$$

$$e_2(r) = \left|\frac{c(r)-c(r-1)}{c(r-1)}\right| < 10^{-4} \quad (3.57)$$

where $a_{\kappa,\kappa'}(x)$, $b(x)$ and $c(x)$ are the values of $\widehat{\alpha}_{\kappa,\kappa'}$, $\widehat{\sigma}^2$ and the log of evidence, respectively, at iteration x of the algorithm and r and $r-1$ are the current and previous iterations of the algorithm, respectively.

3.3.1 Algorithm Steps

Following are the steps of the practical algorithm.

Step 1.

(i) Compute the DFT of the degraded image to obtain the value of $\overrightarrow{G}$. We note here that $\overrightarrow{G}^{\dagger}$ is simply the complex conjugate of $\overrightarrow{G}$ so it does not need to be computed explicitly.

(ii) Compute the values of $\lambda(\alpha_2,p,q)$ using (3.24)

(iii) Initialize $\boldsymbol{a}(0)$ to $\begin{pmatrix} 1 & 1/2 & 1/2 \\ 1/2 & 1 & 1/2 \\ 1/2 & 1/2 & 1 \end{pmatrix}$.

(iv) Initialize $b(0)$ to 1.

(v) Initialize r to 0.

Step 2.

(i) Update $r \leftarrow r+1$.

(ii) Compute the right side of equation (3.54) given by

$$\begin{aligned}\boldsymbol{x} = \frac{1}{2\,|\mathbf{V}|} \sum_{(p,q)\in\mathbf{V}} \Big(& b(r-1)\lambda(\alpha_2,p,q)\Big\{2\left[\boldsymbol{e}+b(r-1)\lambda(\alpha_2,p,q)\boldsymbol{a}(r-1)\right]^{-1} \\ & - \operatorname{diag}\left(\left[\boldsymbol{e}+b(r-1)\lambda(\alpha_2,p,q)\boldsymbol{a}(r-1)\right]^{-1}\right)\Big\} \\ & + \sum_{\kappa\in\mathbf{K}}\sum_{\kappa'\in\mathbf{K}}\Big[\boldsymbol{J}^{\kappa,\kappa'}\overrightarrow{G}^{\dagger}(p,q)\lambda(\alpha_2,p,q)\left[\boldsymbol{e}+b(r-1)\lambda(\alpha_2,p,q)\boldsymbol{a}(r-1)\right]^{-1} \\ & \times\left(\boldsymbol{J}^{\kappa,\kappa'}+\boldsymbol{J}^{\kappa',\kappa}-\boldsymbol{J}^{\kappa,\kappa'}\boldsymbol{J}^{\kappa,\kappa'}\right)\left[\boldsymbol{e}+b(r-1)\lambda(\alpha_2,p,q)\boldsymbol{a}(r-1)\right]^{-1}\overrightarrow{G}(p,q)\Big]\Big). \end{aligned} \tag{3.58}$$

(iii) Using equation (3.54), update $\boldsymbol{a}(r) \leftarrow (\boldsymbol{x}+\operatorname{diag}(\boldsymbol{x}))^{-1}$.

(iv) Using equation (3.49), update

$$\begin{aligned} b(r) \leftarrow \frac{b(r-1)}{3\,|\mathbf{V}|} \sum_{(p,q)\in\mathbf{V}} \Big[& \operatorname{tr}\left(\boldsymbol{e}+b(r-1)\lambda(\alpha_2,p,q)\boldsymbol{a}(r-1)\right)^{-1} \\ & + b(r-1)\overrightarrow{G}^{\dagger}(p,q)\left(\lambda(\alpha_2,p,q)\boldsymbol{a}(r-1)\left[\boldsymbol{e}+b(r-1)\lambda(\alpha_2,p,q)\boldsymbol{a}(r-1)\right]^{-1}\right)^2\overrightarrow{G}(p,q)\Big]. \end{aligned} \tag{3.59}$$

(v) Using equations (3.48) and (3.55), update

$$\begin{aligned} c(r) \leftarrow & -\frac{3\,|\mathbf{V}|}{2}\ln(2\pi) - \frac{1}{2}\sum_{(p,q)\in\mathbf{V}} \ln\left(\det\left[\boldsymbol{e}+b(r-1)\lambda(\alpha_2,p,q)\boldsymbol{a}(r-1)\right]\right) \\ & - \frac{1}{2}\sum_{(p,q)\in\mathbf{V}} \overrightarrow{G}^{\dagger}(p,q)\lambda(\alpha_2,p,q)\boldsymbol{a}(r-1)\left[\boldsymbol{e}+b(r-1)\lambda(\alpha_2,p,q)\boldsymbol{a}(r-1)\right]^{-1}\overrightarrow{G}(p,q) \\ & + \frac{|\mathbf{V}|}{2}\ln\left(\det\boldsymbol{a}(r-1)\right) + \frac{3V_x^2}{2}\ln\frac{1}{4} + \frac{3V_x}{2}\sum_{p=0}^{V_x-1}\ln\Bigg[2-\cos\left(\frac{2\pi p}{V_x}\right)+2\alpha_2 \\ & + \sqrt{\left(2-\cos\left(\frac{2\pi p}{V_x}\right)+2\alpha_2\right)^2-\left(1+2\alpha_2\cos\left(\frac{2\pi p}{V_x}\right)\right)^2}\Bigg] \end{aligned} \tag{3.60}$$

Here we note that since $\overrightarrow{G}^{\dagger}(p,q)$ is the conjugate transpose of $\overrightarrow{G}(p,q)$ and that, since $\boldsymbol{a}(r)$ is a symmetric matrix, the matrices involved in their multiplications are all symmetric, the imaginary terms of those multiplications will vanish.

Step 3.

(i) Check the termination conditions of equations (3.56) and (3.57).

(ii) If the termination conditions are fulfilled, proceed to step 4. Otherwise go back to step 2.

Step 4.

(i) Update $\widehat{\boldsymbol{\alpha}} \leftarrow \boldsymbol{a}(r)$.

(ii) Update $\widehat{\sigma} \leftarrow \sqrt{b(r)}$.

(iii) Compute the values of $\left(\mathbf{e}+\widehat{\sigma}^2\lambda\left(\alpha_2,p,q\right)\widehat{\boldsymbol{\alpha}}\right)^{-1}\overrightarrow{G}\left(p,q\right)$ for each p and q.

(iv) Apply the inverse DFT to the above values to obtain the restored image as described in (3.46).

3.3.2 Computational Complexity

We now analyse the complexity of our algorithm using the Big O notation. Here n is the number of pixels in the image, so $n = |\mathbf{V}|$.

Step 1 DFT computation using the FFT algorithm: $O(n \log n)$.

Step 2 Computation of $\widehat{\boldsymbol{\alpha}}(r)$: $O(n)$.
Computation of $\widehat{\sigma}(r)$: $O(n)$.
Computation of the log of evidence: $O(n)$.
Total: $O(n)$.

Step 3 Computation of $e_1(r)$: $O(1)$.
Computation of $e_2(r)$: $O(1)$.
Total: $O(1)$.

Step 4 Computation of the values to be used in the inverse DFT: $O(n)$.
Restored image computation using the FFT algorithm: $O(n \log n)$.
Total: $O(n \log n)$.

This gives a total complexity of $O(n \log n)$.

3.4 Numerical Experiments

In this section, we present the numerical experiments we performed to evaluate our model as well as the results of these experiments. We also discuss these results.

3.4.1 Experiments

We applied our program to the original 512x512 pixels 24-bit truecolor images $\boldsymbol{f}$ presented in Fig.3.1. We first degraded the original images using additive white Gaussian noise with mean 0 and standard deviation $\sigma = 20$ and $\sigma = 40$ to produce 10 degraded images $\boldsymbol{g}$ for each original image and noise value. Examples of the degraded images are presented in Fig.3.2. We then applied our restoration algorithm to the degraded images to obtain the restored images $\widehat{\boldsymbol{f}}$. Examples of the resulting restored images are shown in Fig.3.15 to Fig.3.25.

(a) Peppers. (b) Lenna. (c) Mandrill.

Figure 3.1: Original images $\boldsymbol{f}$ used for the experiments.

(a) Peppers, $\sigma = 20$. (b) Peppers, $\sigma = 40$.

(c) Lenna, $\sigma = 20$. (d) Lenna, $\sigma = 40$.

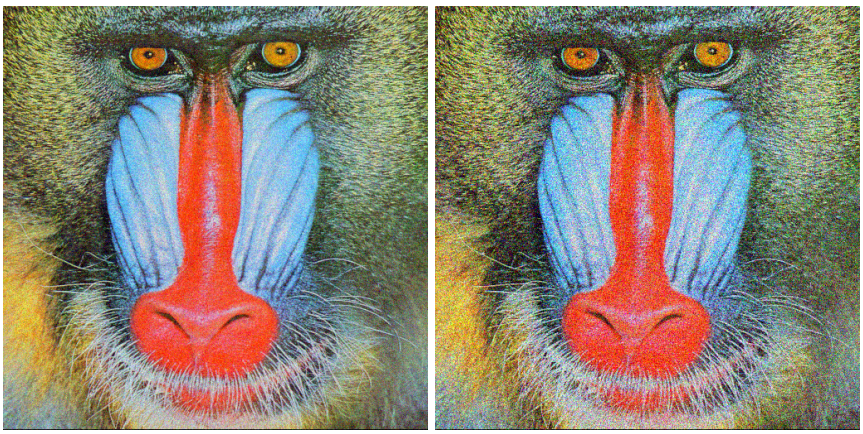

(e) Mandrill $\sigma = 20$. (f) Mandrill $\sigma = 40$.

Figure 3.2: Degraded images $\boldsymbol{g}$ used for the experiments. Degradation process is additive white Gaussian noise with mean 0 and standard deviation σ. (a) and (b) are generated from the original image in Figure 3.1a by setting $\sigma = 20$ and $\sigma = 40$, respectively. (c) and (d) are generated from the original image in Figure 3.1b. (e) and (f) are generated from the original image in Figure 3.1c.

3.4.2 Experimental Results

Our results are generated by fixing the value of α_2 (we remember that $\boldsymbol{\alpha}' = \alpha_2\boldsymbol{\alpha}$) and applying our model to restore each set of 10 degraded images described in section 3.4.1 to obtain restored image sets containing 10 restored images for each value of α_2, σ and each original image.

We then measure the value of the the mean square error (MSE) and the mean structural similarity index (MSSIM) between the original image and the restored image as well as the log of evidence for each restored image. These measurements allow us to calculate the sample mean and sample standard deviation (s) of the MSE, MSSIM and log of evidence for each set of restored images. The sample standard deviation is defined in equation (2.82).

The MSE is used as a measure of the efficiency of our correction. The MSE between two colour images $\boldsymbol{x}$ and $\boldsymbol{y}$ is defined as

$$\mathrm{MSE}(\mathrm{x},\mathrm{y}) \equiv \frac{1}{3|\mathbf{V}|}\sum_{\mathrm{i}\in\mathbf{V}}\sum_{\kappa\in\mathbf{K}}\left(\mathrm{x}_{\mathrm{i},\kappa}-\mathrm{y}_{\mathrm{i},\kappa}\right)^2. \tag{3.61}$$

The MSSIM is also used as a measure of the efficiency of our correction. Since there is no formal definition of a method to compute the MSSIM for colour images, we compute it as follows:

(i) Generate 3 images, where each image is a monochrome image corresponding to one of the colour components of the initial image (red, green or blue component).

(ii) Compute the MSSIM for each image generated previously using the same method as in 2.4.2 to obtain the values $\mathrm{MSSIM}_{\mathrm{red}}$, $\mathrm{MSSIM}_{\mathrm{green}}$ and $\mathrm{MSSIM}_{\mathrm{blue}}$.

(iii) The value of the MSSIM for the colour image is obtained by taking the average of the 3 colour components of the MSSIM:

$$\mathrm{MSSIM} = \frac{1}{3}\left(\mathrm{MSSIM}_{\mathrm{red}} + \mathrm{MSSIM}_{\mathrm{green}} + \mathrm{MSSIM}_{\mathrm{blue}}\right). \tag{3.62}$$

More details about the MSE and MSSIM can be found in section 2.4.2.

Figures 3.3, 3.4 and 3.5 show superpositions of 2 curves. The first curve shows, for various values of α_2, the values of the sample mean for the MSE, with error bars representing s. The second curve shows the same statistics for the log of the evidence. By looking at these figures, we observe that an increase of the evidence is generally accompanied by a decrease of the MSE for all images. However, in the case of the Lenna and Mandrill images, we observe a rise in the values of the MSE for highly negative values of α_2, even though the log of evidence also continues to rise. These results are very similar for the two noise levels used for our experiments.

Figures 3.6 to 3.11 show the effect of α_2 on the estimated values of the components of $\widehat{\boldsymbol{\alpha}}$. By looking at these figures, we observe that as the value of α_2 increases, the values of all the components of $\widehat{\boldsymbol{\alpha}}$ move towards 0 (their absolute value decreases) for all images and noise levels. We also observe that the values and behaviour of $\widehat{\boldsymbol{\alpha}}$ are very similar between the two noise levels for the same image.

Figures 3.12, 3.13 and 3.14 show superpositions of 2 curves. The first curve (+ marks) shows, for various values of α_2, the values of the sample mean for the MSE, with error bars representing s. The second curve (x marks) shows the same statistics for the estimated values of $\widehat{\sigma}^2$. By looking at these figures, we observe that an increase of the value of α_2 is accompanied by a decrease of $\widehat{\sigma}^2$ for all images and noise levels. We also observe that the lowest values of the MSE occur for the values of α_2 where the estimated value of $\widehat{\sigma}^2$ is close to the actual value of σ^2 for all images and noise levels.

Figures 3.15 to 3.25 show some results of the application of the next neighbour extension algorithm to the Peppers, Lenna and Mandrill colour images for noise values of $\sigma = 20$ and $\sigma = 40$.

We only show the results for values of α_2 of -0.49, +0.49, 0.0, for the value producing the smallest MSE, namely $\alpha_2 = -0.49$ for Peppers, $\alpha_2 = -0.45$ for Lenna, $\alpha_2 = -0.25$ and $\alpha_2 = -0.3$ for Mandrill with noise levels $\sigma = 20$ and $\sigma = 40$ respectively, as well as for the value producing the highest MSSIM, namely $\alpha_2 = -0.49$ for Peppers and Lenna, as well as $\alpha_2 = -0.4$ and $\alpha_2 = -0.35$ for Mandrill with noise levels of $\sigma = 20$ and $\sigma = 40$ respectively. Also, only one restored image from the set of 10 is shown.

We observe that the resulting images are more blurry for low values of α_2 and that they become gradually less blurry, but more noisy, as α_2 increases. This can be explained by the previous observations where we saw that, as α_2 increases, the approximated absolute values of the components of $\widehat{\boldsymbol{\alpha}}$ and the value of $\widehat{\sigma}$ decrease, causing our model to assume that the noise level is lower and that correlation between

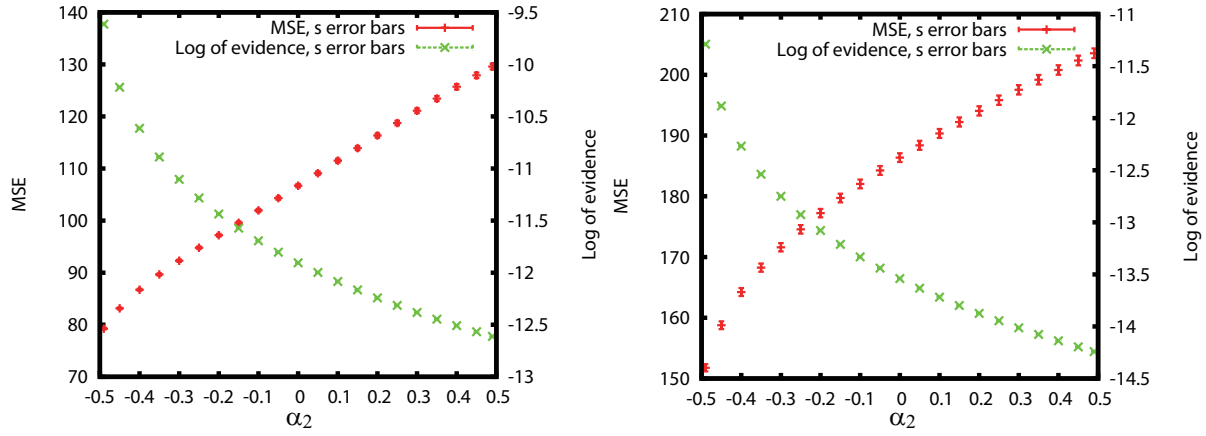

(a) $\sigma = 20$. (b) $\sigma = 40$.

Figure 3.3: Mean square error MSE$(\boldsymbol{f}, \widehat{\boldsymbol{f}})$ (+ marks) and the log of evidence $\log \Pr\{\boldsymbol{G} = \boldsymbol{g} | \widehat{\boldsymbol{\alpha}}, \alpha_2, \widehat{\sigma}\}$ (x marks) for the restored versions of the Peppers image (Fig. 3.1a). The degraded images were generated with noise levels of $\sigma = 20$ in (a) and $\sigma = 40$ in (b). The estimates $\widehat{\boldsymbol{\alpha}}$ and $\widehat{\sigma}$ are obtained by maximizing $\log \Pr\{\boldsymbol{G} = \boldsymbol{g} | \boldsymbol{\alpha}, \alpha_2, \sigma\}$ with respect to $\boldsymbol{\alpha}$ and σ for each fixed value of α_2. Here, the restored image $\widehat{\boldsymbol{f}}$ is defined as $\widehat{\boldsymbol{f}}(\widehat{\boldsymbol{\alpha}}, \alpha_2, \widehat{\sigma})$ for each value of α_2. The values shown are the sample mean values $(\overline{x})$ of the 10 degraded images for each noise level with error bars corresponding to the sample standard deviation (s).

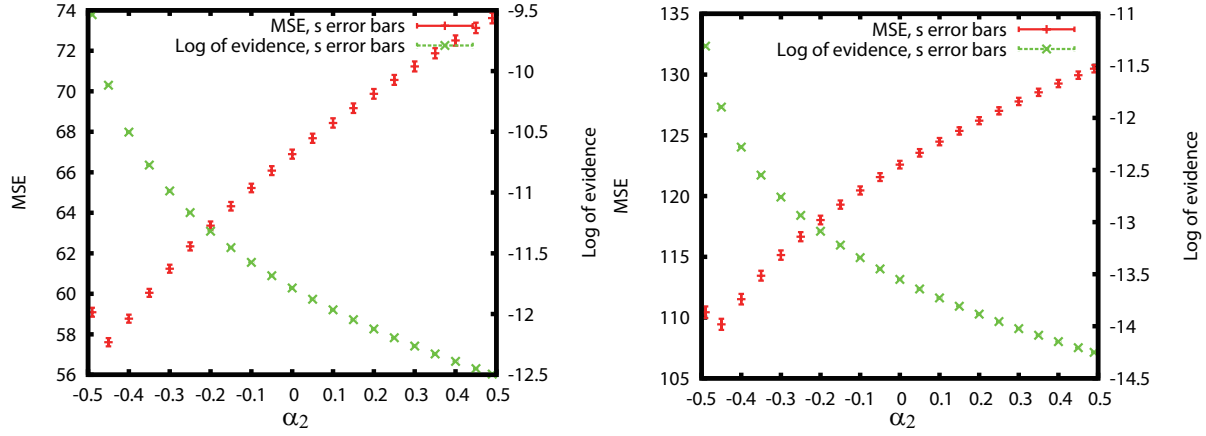

(a) $\sigma = 20$. (b) $\sigma = 40$.

Figure 3.4: Mean square error MSE$(\boldsymbol{f}, \widehat{\boldsymbol{f}})$ (+ marks) and the log of evidence $\log \Pr\{\boldsymbol{G} = \boldsymbol{g} | \widehat{\boldsymbol{\alpha}}, \alpha_2, \widehat{\sigma}\}$ (x marks) for the restored versions of the Lenna image (Fig. 3.1b). The degraded images were generated with noise levels of $\sigma = 20$ in (a) and $\sigma = 40$ in (b). The estimates $\widehat{\boldsymbol{\alpha}}$ and $\widehat{\sigma}$ are obtained by maximizing $\log \Pr\{\boldsymbol{G} = \boldsymbol{g} | \boldsymbol{\alpha}, \alpha_2, \sigma\}$ with respect to $\boldsymbol{\alpha}$ and σ for each fixed value of α_2. Here, the restored image $\widehat{\boldsymbol{f}}$ is defined as $\widehat{\boldsymbol{f}}(\widehat{\boldsymbol{\alpha}}, \alpha_2, \widehat{\sigma})$ for each value of α_2. The values shown are the sample mean values $(\overline{x})$ of the 10 degraded images for each noise level with error bars corresponding to the sample standard deviation (s).

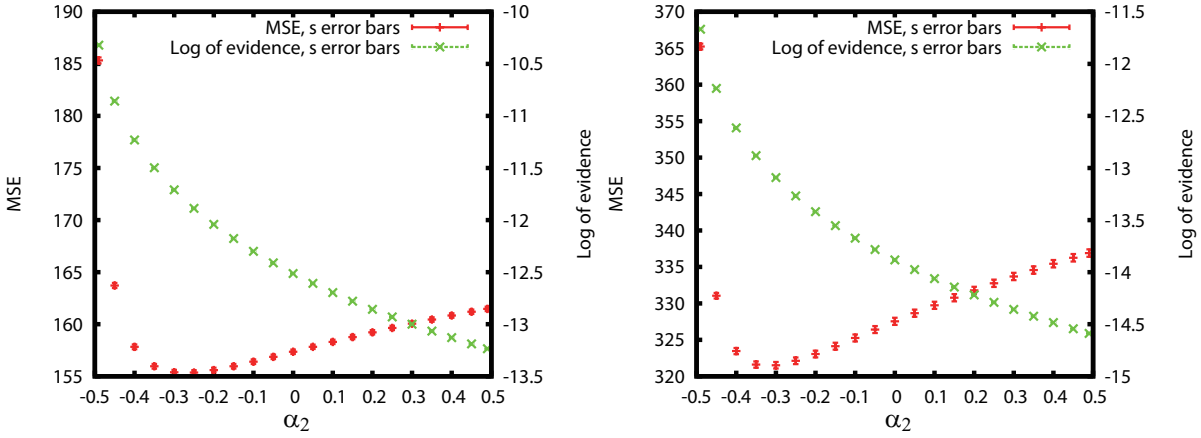

(a) $\sigma = 20$. (b) $\sigma = 40$.

Figure 3.5: Mean square error $\mathrm{MSE}(\boldsymbol{f}, \widehat{\boldsymbol{f}})$ (+ marks) and the log of evidence $\log \Pr\{\boldsymbol{G} = \boldsymbol{g} | \widehat{\boldsymbol{\alpha}}, \alpha_2, \widehat{\sigma}\}$ (x marks) for the restored versions of the Mandrill image (Fig. 3.1c). The degraded images were generated with noise levels of $\sigma = 20$ in (a) and $\sigma = 40$ in (b). The estimates $\widehat{\boldsymbol{\alpha}}$ and $\widehat{\sigma}$ are obtained by maximizing $\log \Pr\{\boldsymbol{G} = \boldsymbol{g} | \boldsymbol{\alpha}, \alpha_2, \sigma\}$ with respect to $\boldsymbol{\alpha}$ and σ for each fixed value of α_2. Here, the restored image $\widehat{\boldsymbol{f}}$ is defined as $\widehat{\boldsymbol{f}}(\widehat{\boldsymbol{\alpha}}, \alpha_2, \widehat{\sigma})$ for each value of α_2. The values shown are the sample mean values ($\overline{x}$) of the 10 degraded images for each noise level with error bars corresponding to the sample standard deviation (s).

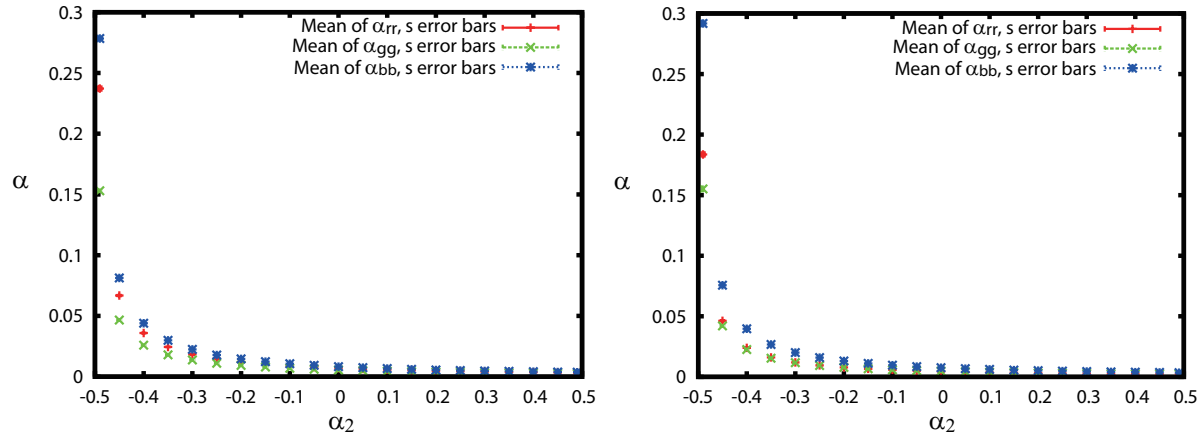

(a) $\sigma = 20$. (b) $\sigma = 40$.

Figure 3.6: Estimates $\widehat{\alpha}_{\mathrm{red,red}}$ (+ marks), $\widehat{\alpha}_{\mathrm{green,green}}$ (x marks) and $\widehat{\alpha}_{\mathrm{blue,blue}}$ (* marks) obtained from the degraded versions of the Peppers image (Fig. 3.1a) for various values of α_2. The degraded images were generated with noise levels of $\sigma = 20$ in (a) and $\sigma = 40$ in (b). The estimates are determined so as to maximize $\log \Pr\{\boldsymbol{G} = \boldsymbol{g} | \boldsymbol{\alpha}, \alpha_2, \sigma\}$ with respect to $\boldsymbol{\alpha}$ and σ for each fixed value of α_2. The values shown are the sample mean values ($\overline{x}$) of the 10 degraded images for each noise level with error bars corresponding to the sample standard deviation (s).

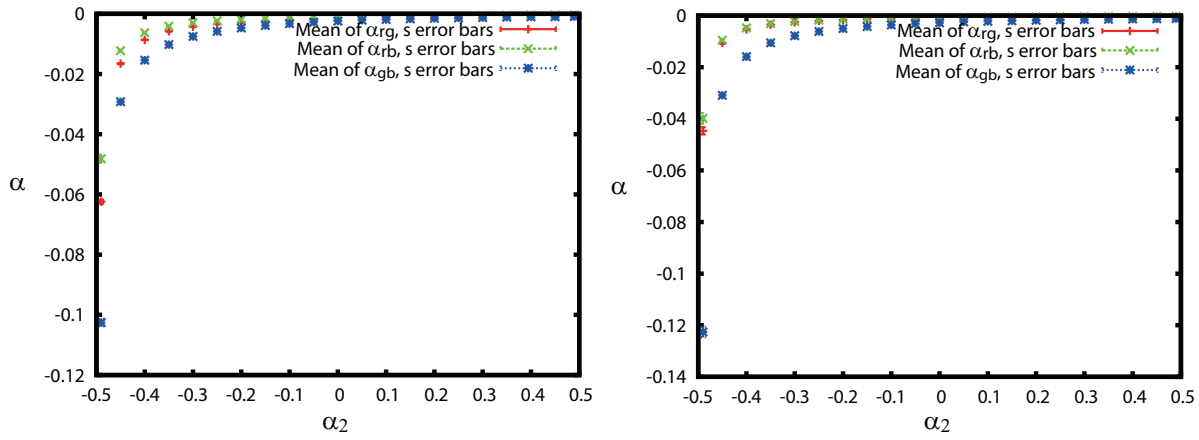

(a) $\sigma = 20$. (b) $\sigma = 40$.

Figure 3.7: Estimates $\widehat{\alpha}_{\text{red,green}}$ (+ marks), $\widehat{\alpha}_{\text{red,blue}}$ (x marks) and $\widehat{\alpha}_{\text{green,blue}}$ (* marks) obtained from the degraded versions of the Peppers image (Fig. 3.1a) for various values of α_2. The degraded images were generated with noise levels of $\sigma = 20$ in (a) and $\sigma = 40$ in (b). The estimates are determined so as to maximize $\log \Pr\{\boldsymbol{G} = \boldsymbol{g}|\boldsymbol{\alpha}, \alpha_2, \sigma\}$ with respect to $\boldsymbol{\alpha}$ and σ for each fixed value of α_2. The values shown are the sample mean values ($\overline{x}$) of the 10 degraded images for each noise level with error bars corresponding to the sample standard deviation (s).

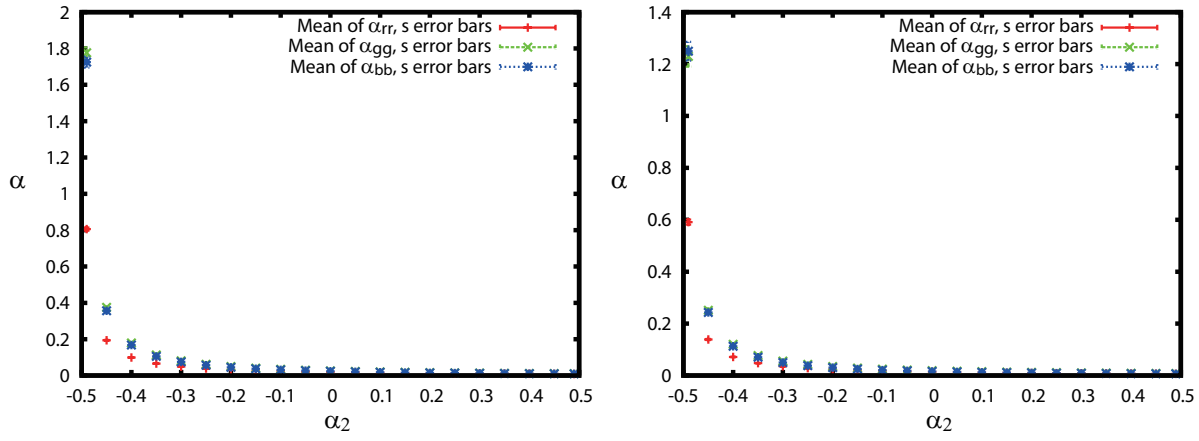

(a) $\sigma = 20$. (b) $\sigma = 40$.

Figure 3.8: Estimates $\widehat{\alpha}_{\text{red,red}}$ (+ marks), $\widehat{\alpha}_{\text{green,green}}$ (x marks) and $\widehat{\alpha}_{\text{blue,blue}}$ (* marks) obtained from the degraded versions of the Lenna image (Fig. 3.1b) for various values of α_2. The degraded images were generated with noise levels of $\sigma = 20$ in (a) and $\sigma = 40$ in (b). The estimates are determined so as to maximize $\log \Pr\{\boldsymbol{G} = \boldsymbol{g}|\boldsymbol{\alpha}, \alpha_2, \sigma\}$ with respect to $\boldsymbol{\alpha}$ and σ for each fixed value of α_2. The values shown are the sample mean values ($\overline{x}$) of the 10 degraded images for each noise level with error bars corresponding to the sample standard deviation (s).

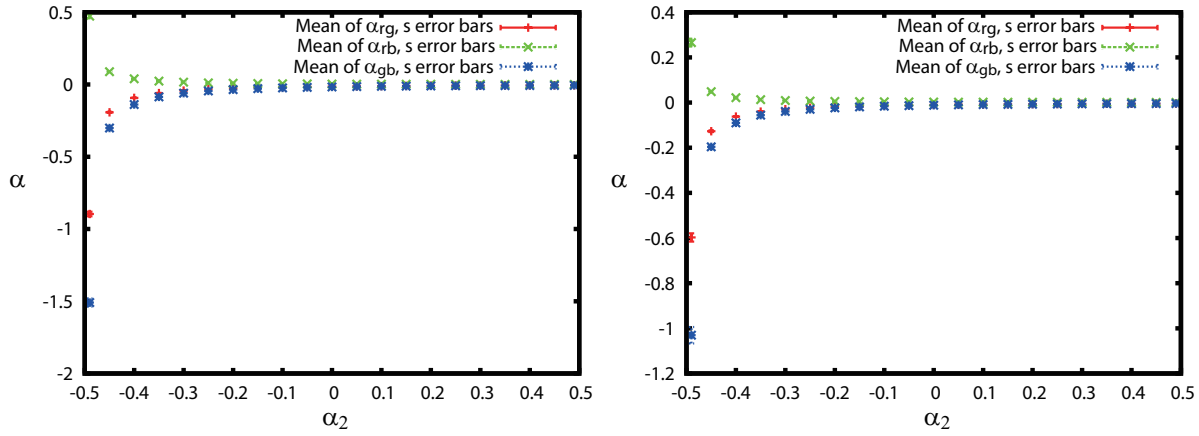

(a) $\sigma = 20$. (b) $\sigma = 40$.

Figure 3.9: Estimates $\widehat{\alpha}_{\text{red,green}}$ (+ marks), $\widehat{\alpha}_{\text{red,blue}}$ (x marks) and $\widehat{\alpha}_{\text{green,blue}}$ (* marks) obtained from the degraded versions of the Lenna image (Fig. 3.1b) for various values of α_2. The degraded images were generated with noise levels of $\sigma = 20$ in (a) and $\sigma = 40$ in (b). The estimates are determined so as to maximize $\log \Pr\{\boldsymbol{G} = \boldsymbol{g}|\boldsymbol{\alpha}, \alpha_2, \sigma\}$ with respect to $\boldsymbol{\alpha}$ and σ for each fixed value of α_2. The values shown are the sample mean values ($\overline{x}$) of the 10 degraded images for each noise level with error bars corresponding to the sample standard deviation (s).

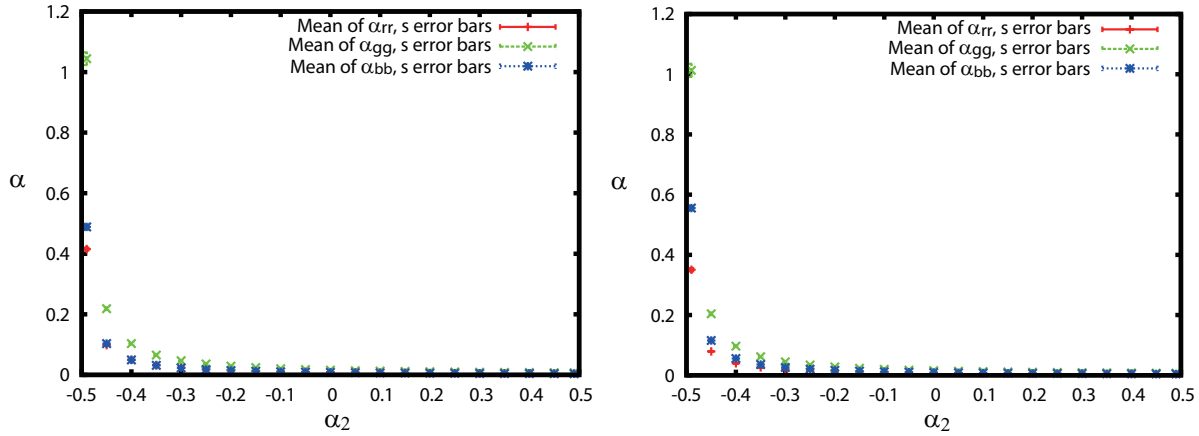

(a) $\sigma = 20$. (b) $\sigma = 40$.

Figure 3.10: Estimates $\widehat{\alpha}_{\text{red,red}}$ (+ marks), $\widehat{\alpha}_{\text{green,green}}$ (x marks) and $\widehat{\alpha}_{\text{blue,blue}}$ (* marks) obtained from the degraded versions of the Mandrill image (Fig. 3.1c) for various values of α_2. The degraded images were generated with noise levels of $\sigma = 20$ in (a) and $\sigma = 40$ in (b). The estimates are determined so as to maximize $\log \Pr\{\boldsymbol{G} = \boldsymbol{g}|\boldsymbol{\alpha}, \alpha_2, \sigma\}$ with respect to $\boldsymbol{\alpha}$ and σ for each fixed value of α_2. The values shown are the sample mean values ($\overline{x}$) of the 10 degraded images for each noise level with error bars corresponding to the sample standard deviation (s).

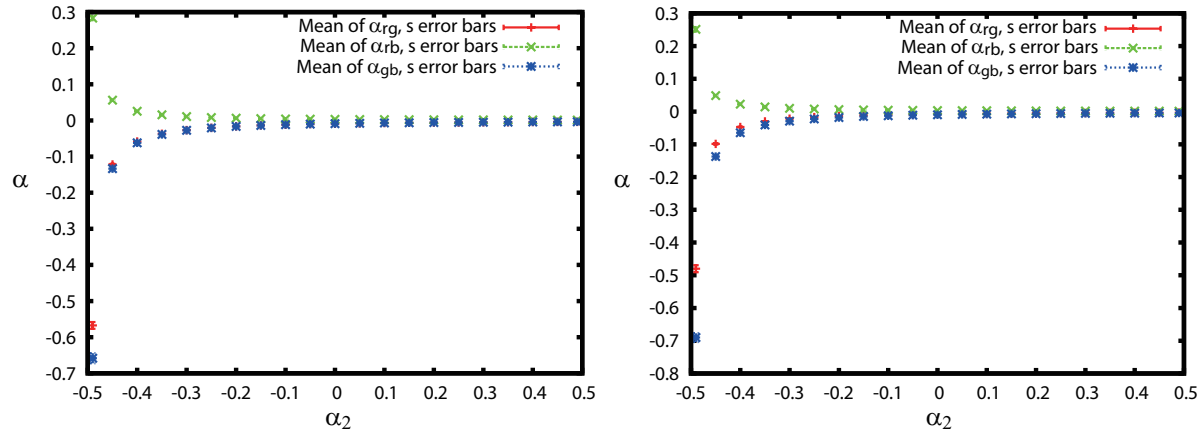

(a) $\sigma = 20$. (b) $\sigma = 40$.

Figure 3.11: Estimates $\widehat{\alpha}_{\text{red,green}}$ (+ marks), $\widehat{\alpha}_{\text{red,blue}}$ (x marks) and $\widehat{\alpha}_{\text{green,blue}}$ (* marks) obtained from the degraded versions of the Mandrill image (Fig. 3.1c) for various values of α_2. The degraded images were generated with noise levels of $\sigma = 20$ in (a) and $\sigma = 40$ in (b). The estimates are determined so as to maximize $\log \Pr\{\boldsymbol{G} = \boldsymbol{g}|\boldsymbol{\alpha}, \alpha_2, \sigma\}$ with respect to $\boldsymbol{\alpha}$ and σ for each fixed value of α_2. The values shown are the sample mean values ($\overline{x}$) of the 10 degraded images for each noise level with error bars corresponding to the sample standard deviation (s).

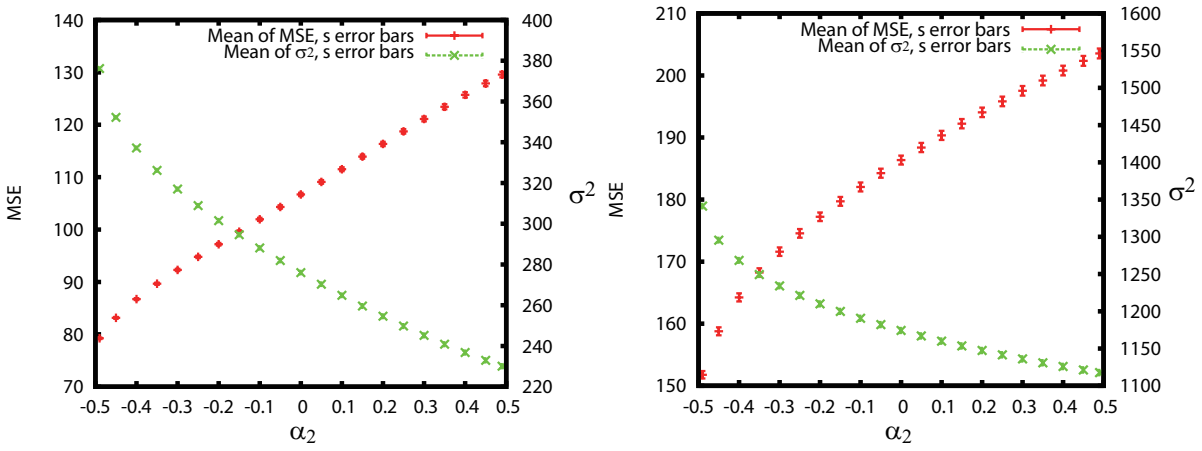

(a) $\sigma = 20$. (b) $\sigma = 40$.

Figure 3.12: Mean square error $\text{MSE}(\boldsymbol{f}, \widehat{\boldsymbol{f}})$ (+ marks) and estimate $\widehat{\sigma}^2$ (x marks) for the restored versions of the Peppers image (Fig. 3.1a). The degraded images were generated with noise levels of $\sigma = 20$ in (a) and $\sigma = 40$ in (b). The estimate $\widehat{\sigma}$ is obtained by maximizing $\log \Pr\{\boldsymbol{G} = \boldsymbol{g}|\boldsymbol{\alpha}, \alpha_2, \sigma\}$ with respect to $\boldsymbol{\alpha}$ and σ for each fixed value of α_2. Here, the restored image $\widehat{\boldsymbol{f}}$ is defined as $\widehat{\boldsymbol{f}}(\widehat{\boldsymbol{\alpha}}, \alpha_2, \widehat{\sigma})$ for each value of α_2. The values shown are the sample mean values ($\overline{x}$) of the 10 degraded images for each noise level with error bars corresponding to the sample standard deviation (s).

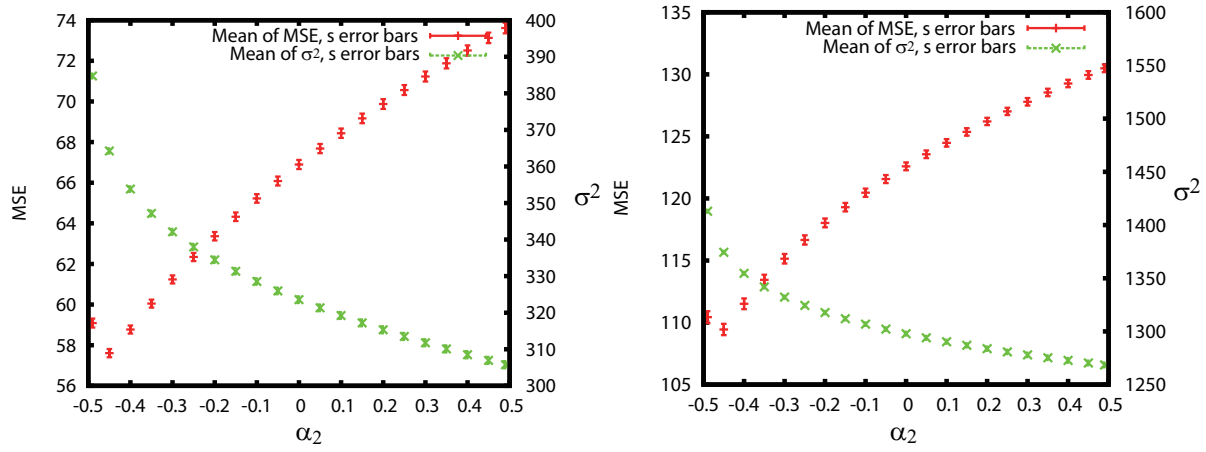

(a) $\sigma = 20$. (b) $\sigma = 40$.

Figure 3.13: Mean square error MSE($\boldsymbol{f}, \widehat{\boldsymbol{f}}$) (+ marks) and estimate $\widehat{\sigma}^2$ (x marks) for the restored versions of the Lenna image (Fig. 3.1b). The degraded images were generated with noise levels of $\sigma = 20$ in (a) and $\sigma = 40$ in (b). The estimate $\widehat{\sigma}$ is obtained by maximizing $\log \Pr\{\boldsymbol{G} = \boldsymbol{g} | \boldsymbol{\alpha}, \alpha_2, \sigma\}$ with respect to $\boldsymbol{\alpha}$ and σ for each fixed value of α_2. Here, the restored image $\widehat{\boldsymbol{f}}$ is defined as $\widehat{\boldsymbol{f}}\,(\widehat{\boldsymbol{\alpha}}, \alpha_2, \widehat{\sigma})$ for each value of α_2. The values shown are the sample mean values ($\overline{x}$) of the 10 degraded images for each noise level with error bars corresponding to the sample standard deviation (s).

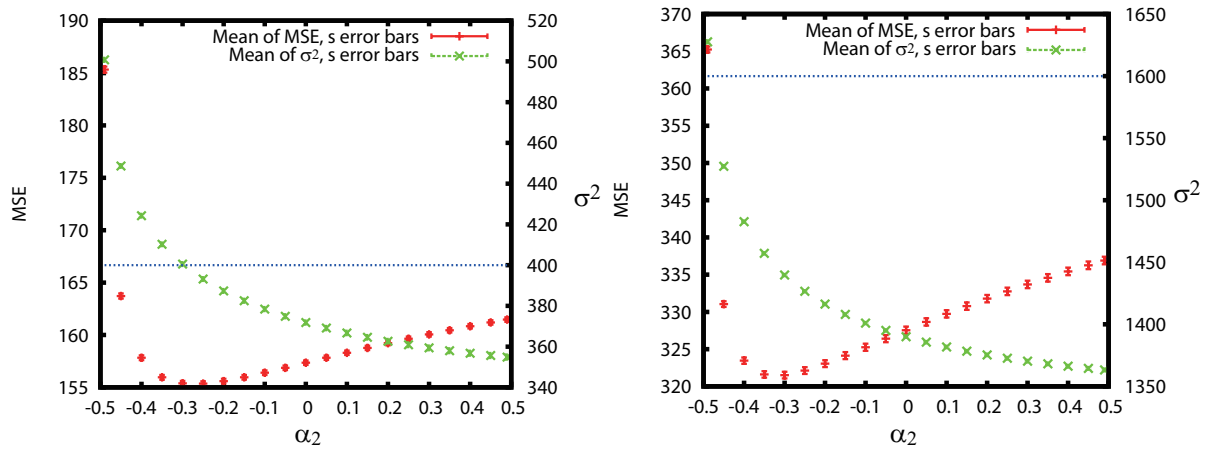

(a) $\sigma = 20$. (b) $\sigma = 40$.

Figure 3.14: Mean square error MSE($\boldsymbol{f}, \widehat{\boldsymbol{f}}$) (+ marks) and estimate $\widehat{\sigma}^2$ (x marks) for the restored versions of the Mandrill image (Fig. 3.1c). The degraded images were generated with noise levels of $\sigma = 20$ in (a) and $\sigma = 40$ in (b). The estimate $\widehat{\sigma}$ is obtained by maximizing $\log \Pr\{\boldsymbol{G} = \boldsymbol{g} | \boldsymbol{\alpha}, \alpha_2, \sigma\}$ with respect to $\boldsymbol{\alpha}$ and σ for each fixed value of α_2. Here, the restored image $\widehat{\boldsymbol{f}}$ is defined as $\widehat{\boldsymbol{f}}\,(\widehat{\boldsymbol{\alpha}}, \alpha_2, \widehat{\sigma})$ for each value of α_2. The values shown are the sample mean values ($\overline{x}$) of the 10 degraded images for each noise level with error bars corresponding to the sample standard deviation (s).

neighbouring pixels is also low. As a consequence, less correction is applied, causing less blurring, but also leaving more noise in the corrected image. We also notice some improved horizontal and vertical edge preservation accompanied by grid-like artefacts in the restored images with a value of α_2 lower than -0.4. This is due to the fact that in such cases, our model approaches the superantiferromagnetic state, as shown in Fig. 1.1c.

(a) Degraded Image. MSE=367. MSSIM=0.6716.

(b) Restored. $\alpha_2 = -0.49$. MSE=79. MSSIM=0.8557.

(c) Restored. $\alpha_2 = 0.0$. MSE=107. MSSIM=0.8065.

(d) Restored. $\alpha_2 = 0.49$. MSE=130. MSSIM=0.7854.

Figure 3.15: Restored images $\widehat{\boldsymbol{f}}(\boldsymbol{g}, \widehat{\boldsymbol{\alpha}}, \alpha_2, \widehat{\sigma})$ obtained by means of the proposed Gauss-Markov random field model for one of the degraded versions of the Peppers image (Fig. 3.1a). The degraded image was generated with a noise level of $\sigma = 20$, has $\mathrm{MSE}(\boldsymbol{f}, \boldsymbol{g}) = 367$, $\mathrm{MSSIM}(\boldsymbol{f}, \boldsymbol{g}) = 0.6716$ and is shown in (a). (b) $\alpha_2 = -0.49$, $\mathrm{MSE}(\boldsymbol{f}, \widehat{\boldsymbol{f}}(\boldsymbol{g}, \widehat{\boldsymbol{\alpha}}, \alpha_2, \widehat{\sigma})) = 79$, $\mathrm{MSSIM}(\boldsymbol{f}, \widehat{\boldsymbol{f}}(\boldsymbol{g}, \widehat{\boldsymbol{\alpha}}, \alpha_2, \widehat{\sigma})) = 0.8557$. (c) $\alpha_2 = 0.0$, $\mathrm{MSE}(\boldsymbol{f}, \widehat{\boldsymbol{f}}(\boldsymbol{g}, \widehat{\boldsymbol{\alpha}}, \alpha_2, \widehat{\sigma})) = 107$, $\mathrm{MSSIM}(\boldsymbol{f}, \widehat{\boldsymbol{f}}(\boldsymbol{g}, \widehat{\boldsymbol{\alpha}}, \alpha_2, \widehat{\sigma})) = 0.8065$. (d) $\alpha_2 = 0.49$, $\mathrm{MSE}(\boldsymbol{f}, \widehat{\boldsymbol{f}}(\boldsymbol{g}, \widehat{\boldsymbol{\alpha}}, \alpha_2, \widehat{\sigma})) = 130$, $\mathrm{MSSIM}(\boldsymbol{f}, \widehat{\boldsymbol{f}}(\boldsymbol{g}, \widehat{\boldsymbol{\alpha}}, \alpha_2, \widehat{\sigma})) = 0.7854$.

(a) Original Image.

(b) Degraded Image. MSE=367. MSSIM=0.6716.

(c) Restored. $\alpha_2 = -0.49$. MSE=79. MSSIM=0.8557.

(d) Restored. $\alpha_2 = 0.0$. MSE=107. MSSIM=0.8065.

(e) Restored. $\alpha_2 = 0.49$. MSE=130. MSSIM=0.7854.

Figure 3.16: Details of the original image $\boldsymbol{f}$ in Fig. 3.1a, the degraded image $\boldsymbol{g}$ in Fig. 3.15a and the restored images $\widehat{\boldsymbol{f}}(\boldsymbol{g}, \widehat{\boldsymbol{\alpha}}, \alpha_2, \widehat{\sigma})$ in Fig. 3.15. (a) Original image $\boldsymbol{f}$ in Fig. 3.1a. (b) Degraded image $\boldsymbol{g}$ in Fig. 3.15a. (c) Restored image $\widehat{\boldsymbol{f}}(\boldsymbol{g}, \widehat{\boldsymbol{\alpha}}, \alpha_2, \widehat{\sigma})$ in Fig. 3.15b. (d) Restored image $\widehat{\boldsymbol{f}}(\boldsymbol{g}, \widehat{\boldsymbol{\alpha}}, \alpha_2, \widehat{\sigma})$ in Fig. 3.15c. (e) Restored image $\widehat{\boldsymbol{f}}(\boldsymbol{g}, \widehat{\boldsymbol{\alpha}}, \alpha_2, \widehat{\sigma})$ in Fig. 3.15d.

(a) Degraded Image. MSE=1367. MSSIM=0.4247.

(b) Restored. $\alpha_2 = -0.49$. MSE=151. MSSIM=0.7664.

(c) Restored. $\alpha_2 = 0.0$. MSE=186. MSSIM=0.7104.

(d) Restored. $\alpha_2 = 0.49$. MSE=203. MSSIM=0.6958.

Figure 3.17: Restored images $\widehat{\boldsymbol{f}}(\boldsymbol{g}, \widehat{\boldsymbol{\alpha}}, \alpha_2, \widehat{\sigma})$ obtained by means of the proposed Gauss-Markov random field model for one of the degraded versions of the Peppers image (Fig. 3.1a). The degraded image was generated with a noise level of $\sigma = 40$, has $\mathrm{MSE}(\boldsymbol{f}, \boldsymbol{g}) = 1367$, $\mathrm{MSSIM}(\boldsymbol{f}, \boldsymbol{g}) = 0.4247$ and is shown in (a). (b) $\alpha_2 = -0.49$, $\mathrm{MSE}(\boldsymbol{f}, \widehat{\boldsymbol{f}}(\boldsymbol{g}, \widehat{\boldsymbol{\alpha}}, \alpha_2, \widehat{\sigma})) = 151$, $\mathrm{MSSIM}(\boldsymbol{f}, \widehat{\boldsymbol{f}}(\boldsymbol{g}, \widehat{\boldsymbol{\alpha}}, \alpha_2, \widehat{\sigma})) = 0.7664$. (c) $\alpha_2 = 0.0$, $\mathrm{MSE}(\boldsymbol{f}, \widehat{\boldsymbol{f}}(\boldsymbol{g}, \widehat{\boldsymbol{\alpha}}, \alpha_2, \widehat{\sigma})) = 186$, $\mathrm{MSSIM}(\boldsymbol{f}, \widehat{\boldsymbol{f}}(\boldsymbol{g}, \widehat{\boldsymbol{\alpha}}, \alpha_2, \widehat{\sigma})) = 0.7104$. (d) $\alpha_2 = 0.49$, $\mathrm{MSE}(\boldsymbol{f}, \widehat{\boldsymbol{f}}(\boldsymbol{g}, \widehat{\boldsymbol{\alpha}}, \alpha_2, \widehat{\sigma})) = 203$, $\mathrm{MSSIM}(\boldsymbol{f}, \widehat{\boldsymbol{f}}(\boldsymbol{g}, \widehat{\boldsymbol{\alpha}}, \alpha_2, \widehat{\sigma})) = 0.6958$.

(a) Original Image.

(b) Degraded Image. MSE=1367. MSSIM=0.4247.

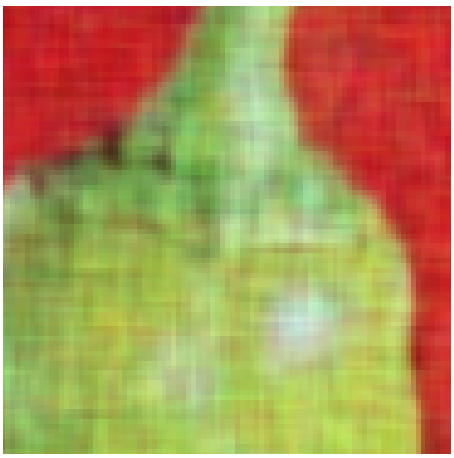

(c) Restored. $\alpha_2 = -0.49$. MSE=151. MSSIM=0.7664.

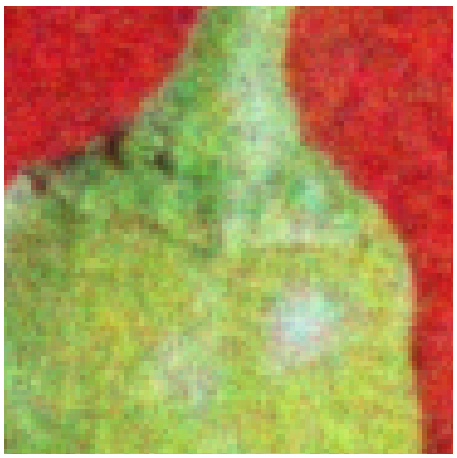

(d) Restored. $\alpha_2 = 0.0$. MSE=186. MSSIM=0.7104.

(e) Restored. $\alpha_2 = 0.49$. MSE=203. MSSIM=0.6958.

Figure 3.18: Details of the original image $\boldsymbol{f}$ in Fig. 3.1a, the degraded image $\boldsymbol{g}$ in Fig. 3.17a and the restored images $\widehat{\boldsymbol{f}}(\boldsymbol{g}, \widehat{\boldsymbol{\alpha}}, \alpha_2, \widehat{\sigma})$ in Fig. 3.17. (a) Original image $\boldsymbol{f}$ in Fig. 3.1a. (b) Degraded image $\boldsymbol{g}$ in Fig. 3.17a. (c) Restored image $\widehat{\boldsymbol{f}}(\boldsymbol{g}, \widehat{\boldsymbol{\alpha}}, \alpha_2, \widehat{\sigma})$ in Fig. 3.17b. (d) Restored image $\widehat{\boldsymbol{f}}(\boldsymbol{g}, \widehat{\boldsymbol{\alpha}}, \alpha_2, \widehat{\sigma})$ in Fig. 3.17c. (e) Restored image $\widehat{\boldsymbol{f}}(\boldsymbol{g}, \widehat{\boldsymbol{\alpha}}, \alpha_2, \widehat{\sigma})$ in Fig. 3.17d.

(a) Degraded Image. MSE=373. MSSIM=0.6796.

(b) Restored. $\alpha_2 = -0.49$. MSE=59. MSSIM=0.8871.

(c) Restored. $\alpha_2 = -0.45$. MSE=58. MSSIM=0.8810.

(d) Restored. $\alpha_2 = 0.0$. MSE=67. MSSIM=0.8660.

(e) Restored. $\alpha_2 = 0.49$. MSE=73. MSSIM=0.8589.

Figure 3.19: Restored images $\widehat{\boldsymbol{f}}(\boldsymbol{g}, \widehat{\boldsymbol{\alpha}}, \alpha_2, \widehat{\sigma})$ obtained by means of the proposed Gauss-Markov random field model for one of the degraded versions of the Lenna image (Fig. 3.1b). The degraded image was generated with a noise level of $\sigma = 20$, has $\mathrm{MSE}(\boldsymbol{f}, \boldsymbol{g}) = 373$, $\mathrm{MSSIM}(\boldsymbol{f}, \boldsymbol{g}) = 0.6796$ and is shown in (a). (b) $\alpha_2 = -0.49$, $\mathrm{MSE}(\boldsymbol{f}, \widehat{\boldsymbol{f}}(\boldsymbol{g}, \widehat{\boldsymbol{\alpha}}, \alpha_2, \widehat{\sigma})) = 59$, $\mathrm{MSSIM}(\boldsymbol{f}, \widehat{\boldsymbol{f}}(\boldsymbol{g}, \widehat{\boldsymbol{\alpha}}, \alpha_2, \widehat{\sigma})) = 0.8871$. (c) $\alpha_2 = -0.45$, $\mathrm{MSE}(\boldsymbol{f}, \widehat{\boldsymbol{f}}(\boldsymbol{g}, \widehat{\boldsymbol{\alpha}}, \alpha_2, \widehat{\sigma})) = 58$, $\mathrm{MSSIM}(\boldsymbol{f}, \widehat{\boldsymbol{f}}(\boldsymbol{g}, \widehat{\boldsymbol{\alpha}}, \alpha_2, \widehat{\sigma})) = 0.8810$. (d) $\alpha_2 = 0.0$, $\mathrm{MSE}(\boldsymbol{f}, \widehat{\boldsymbol{f}}(\boldsymbol{g}, \widehat{\boldsymbol{\alpha}}, \alpha_2, \widehat{\sigma})) = 67$, $\mathrm{MSSIM}(\boldsymbol{f}, \widehat{\boldsymbol{f}}(\boldsymbol{g}, \widehat{\boldsymbol{\alpha}}, \alpha_2, \widehat{\sigma})) = 0.8660$. (e) $\alpha_2 = 0.49$, $\mathrm{MSE}(\boldsymbol{f}, \widehat{\boldsymbol{f}}(\boldsymbol{g}, \widehat{\boldsymbol{\alpha}}, \alpha_2, \widehat{\sigma})) = 73$, $\mathrm{MSSIM}(\boldsymbol{f}, \widehat{\boldsymbol{f}}(\boldsymbol{g}, \widehat{\boldsymbol{\alpha}}, \alpha_2, \widehat{\sigma})) = 0.8589$.

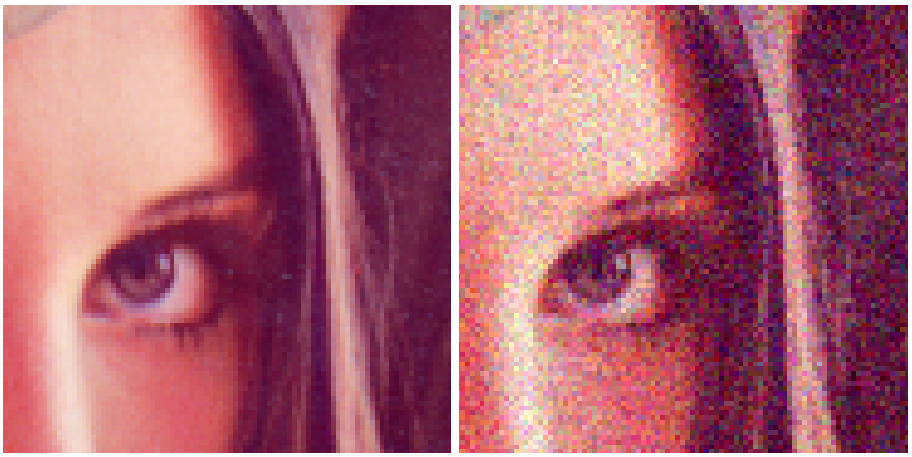

(a) Original Image. (b) Degraded Image. MSE=373. MSSIM=0.6796.

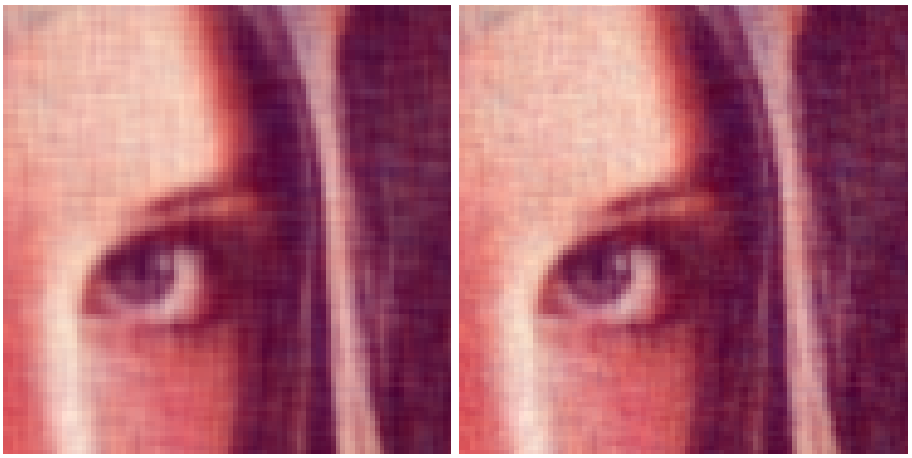

(c) Restored. $\alpha_2 = -0.49$. MSE=59. MSSIM=0.8871. (d) Restored. $\alpha_2 = -0.45$. MSE=58. MSSIM=0.8810.

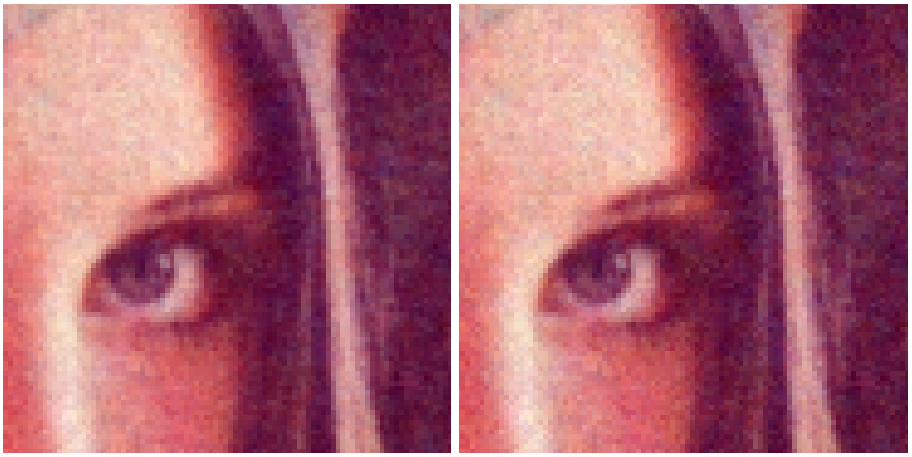

(e) Restored. $\alpha_2 = 0.0$. MSE=67. MSSIM=0.8660. (f) Restored. $\alpha_2 = 0.49$. MSE=73. MSSIM=0.8589.

Figure 3.20: Details of the original image $\boldsymbol{f}$ in Fig. 3.1b, the degraded image $\boldsymbol{g}$ in Fig. 3.19a and the restored images $\widehat{\boldsymbol{f}}(\boldsymbol{g}, \widehat{\boldsymbol{\alpha}}, \alpha_2, \widehat{\sigma})$ in Fig. 3.19. (a) Original image $\boldsymbol{f}$ in Fig. 3.1b. (b) Degraded image $\boldsymbol{g}$ in Fig. 3.19a. (c) Restored image $\widehat{\boldsymbol{f}}(\boldsymbol{g}, \widehat{\boldsymbol{\alpha}}, \alpha_2, \widehat{\sigma})$ in Fig. 3.19b. (d) Restored image $\widehat{\boldsymbol{f}}(\boldsymbol{g}, \widehat{\boldsymbol{\alpha}}, \alpha_2, \widehat{\sigma})$ in Fig. 3.19c. (e) Restored image $\widehat{\boldsymbol{f}}(\boldsymbol{g}, \widehat{\boldsymbol{\alpha}}, \alpha_2, \widehat{\sigma})$ in Fig. 3.19d. (f) Restored image $\widehat{\boldsymbol{f}}(\boldsymbol{g}, \widehat{\boldsymbol{\alpha}}, \alpha_2, \widehat{\sigma})$ in Fig. 3.19e.

(a) Degraded Image. MSE=1418. MSSIM=0.4310.

(b) Restored. $\alpha_2 = -0.49$. MSE=110. MSSIM=0.8080.

(c) Restored. $\alpha_2 = -0.45$. MSE=109. MSSIM=0.7976.

(d) Restored. $\alpha_2 = 0.0$. MSE=122. MSSIM=0.7778.

(e) Restored. $\alpha_2 = 0.49$. MSE=130. MSSIM=0.7714.

Figure 3.21: Restored images $\widehat{\boldsymbol{f}}(\boldsymbol{g}, \widehat{\boldsymbol{\alpha}}, \alpha_2, \widehat{\sigma})$ obtained by means of the proposed Gauss-Markov random field model for one of the degraded versions of the Lenna image (Fig. 3.1b). The degraded image was generated with a noise level of $\sigma = 40$, has $\mathrm{MSE}(\boldsymbol{f}, \boldsymbol{g}) = 1418$, $\mathrm{MSSIM}(\boldsymbol{f}, \boldsymbol{g}) = 0.4310$ and is shown in (a). (b) $\alpha_2 = -0.49$, $\mathrm{MSE}(\boldsymbol{f}, \widehat{\boldsymbol{f}}(\boldsymbol{g}, \widehat{\boldsymbol{\alpha}}, \alpha_2, \widehat{\sigma})) = 110$, $\mathrm{MSSIM}(\boldsymbol{f}, \widehat{\boldsymbol{f}}(\boldsymbol{g}, \widehat{\boldsymbol{\alpha}}, \alpha_2, \widehat{\sigma})) = 0.8080$. (c) $\alpha_2 = -0.45$, $\mathrm{MSE}(\boldsymbol{f}, \widehat{\boldsymbol{f}}(\boldsymbol{g}, \widehat{\boldsymbol{\alpha}}, \alpha_2, \widehat{\sigma})) = 109$, $\mathrm{MSSIM}(\boldsymbol{f}, \widehat{\boldsymbol{f}}(\boldsymbol{g}, \widehat{\boldsymbol{\alpha}}, \alpha_2, \widehat{\sigma})) = 0.7976$. (d) $\alpha_2 = 0.0$, $\mathrm{MSE}(\boldsymbol{f}, \widehat{\boldsymbol{f}}(\boldsymbol{g}, \widehat{\boldsymbol{\alpha}}, \alpha_2, \widehat{\sigma})) = 122$, $\mathrm{MSSIM}(\boldsymbol{f}, \widehat{\boldsymbol{f}}(\boldsymbol{g}, \widehat{\boldsymbol{\alpha}}, \alpha_2, \widehat{\sigma})) = 0.7778$. (e) $\alpha_2 = 0.49$, $\mathrm{MSE}(\boldsymbol{f}, \widehat{\boldsymbol{f}}(\boldsymbol{g}, \widehat{\boldsymbol{\alpha}}, \alpha_2, \widehat{\sigma})) = 130$, $\mathrm{MSSIM}(\boldsymbol{f}, \widehat{\boldsymbol{f}}(\boldsymbol{g}, \widehat{\boldsymbol{\alpha}}, \alpha_2, \widehat{\sigma})) = 0.7714$.

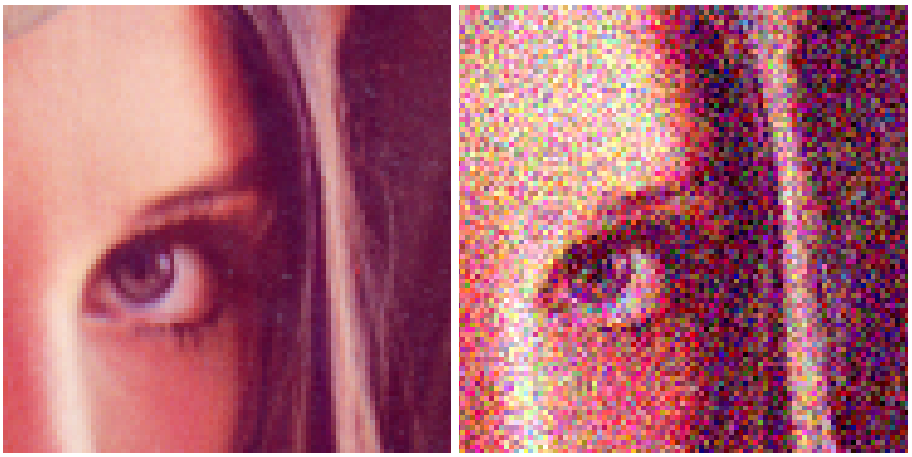

(a) Original Image. (b) Degraded Image. MSE=1418. MSSIM=0.4310.

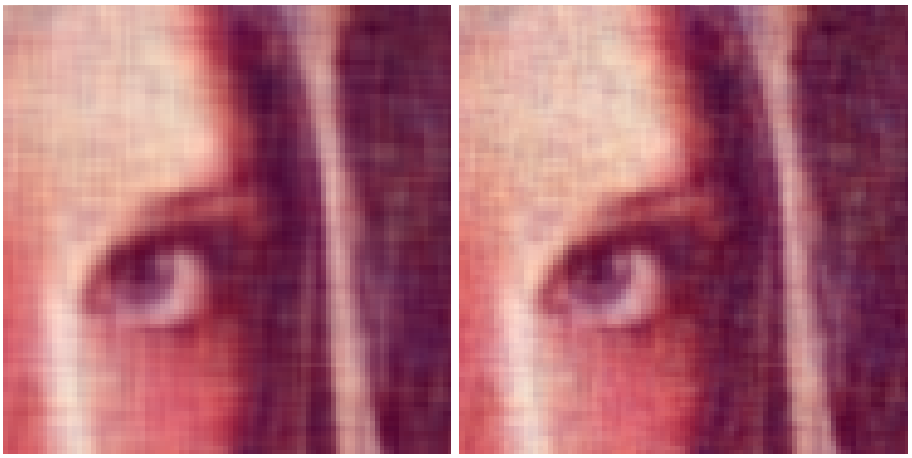

(c) Restored. $\alpha_2 = -0.49$. MSE=110. MSSIM=0.8080. (d) Restored. $\alpha_2 = -0.45$. MSE=109. MSSIM=0.7976.

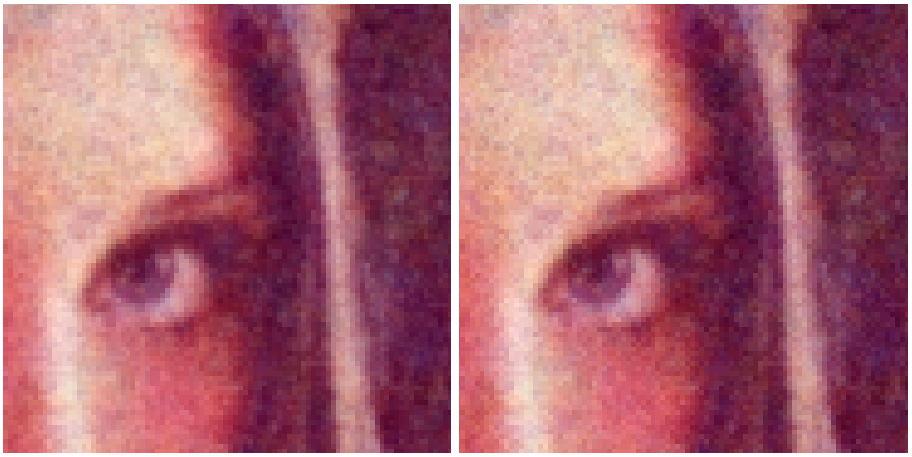

(e) Restored. $\alpha_2 = 0.0$. MSE=122. MSSIM=0.7778. (f) Restored. $\alpha_2 = 0.49$. MSE=130. MSSIM=0.7714.

Figure 3.22: Details of the original image $\boldsymbol{f}$ in Fig. 3.1b, the degraded image $\boldsymbol{g}$ in Fig. 3.21a and the restored images $\widehat{\boldsymbol{f}}(\boldsymbol{g}, \widehat{\boldsymbol{\alpha}}, \alpha_2, \widehat{\sigma})$ in Fig. 3.21. (a) Original image $\boldsymbol{f}$ in Fig. 3.1b. (b) Degraded image $\boldsymbol{g}$ in Fig. 3.21a. (c) Restored image $\widehat{\boldsymbol{f}}(\boldsymbol{g}, \widehat{\boldsymbol{\alpha}}, \alpha_2, \widehat{\sigma})$ in Fig. 3.21b. (d) Restored image $\widehat{\boldsymbol{f}}(\boldsymbol{g}, \widehat{\boldsymbol{\alpha}}, \alpha_2, \widehat{\sigma})$ in Fig. 3.21c. (e) Restored image $\widehat{\boldsymbol{f}}(\boldsymbol{g}, \widehat{\boldsymbol{\alpha}}, \alpha_2, \widehat{\sigma})$ in Fig. 3.21d. (f) Restored image $\widehat{\boldsymbol{f}}(\boldsymbol{g}, \widehat{\boldsymbol{\alpha}}, \alpha_2, \widehat{\sigma})$ in Fig. 3.21e.

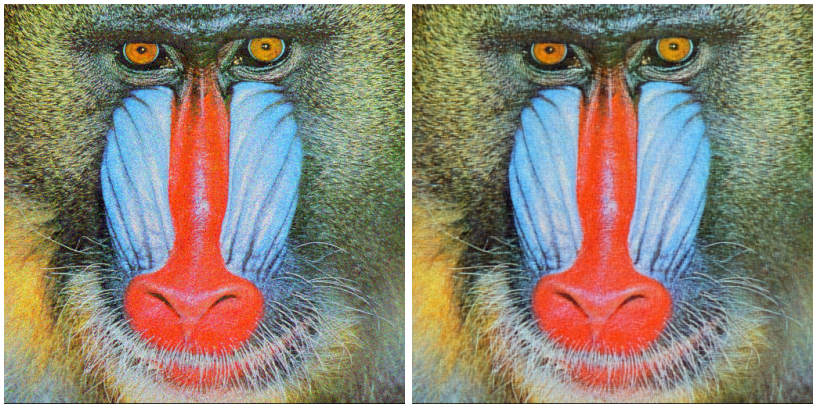

(a) Degraded Image. MSE=375. MSSIM=0.8518.

(b) Restored. $\alpha_2 = -0.49$. MSE=186. MSSIM=0.9055.

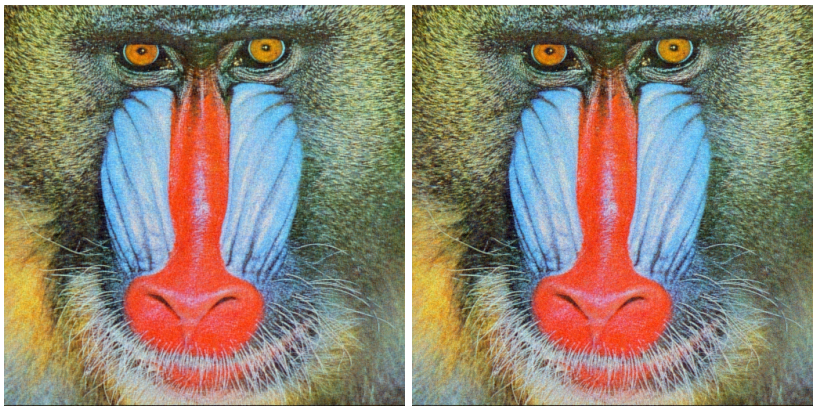

(c) Restored. $\alpha_2 = -0.4$. MSE=158. MSSIM=0.9112.

(d) Restored. $\alpha_2 = -0.25$. MSE=156. MSSIM=0.9108.

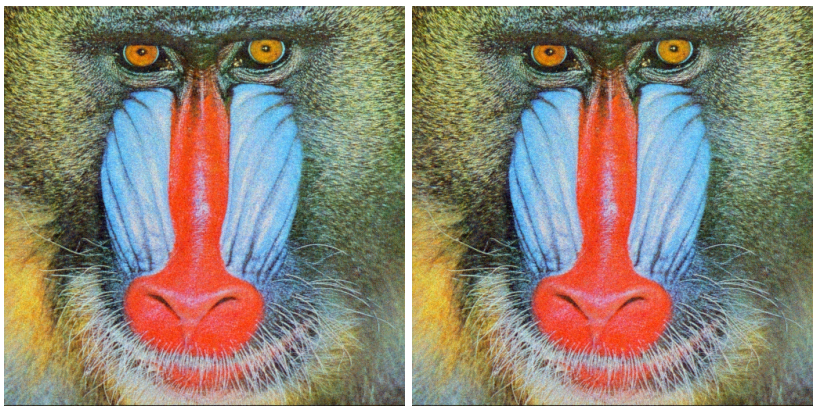

(e) Restored. $\alpha_2 = 0.0$. MSE=157. MSSIM=0.9099.

(f) Restored. $\alpha_2 = 0.49$. MSE=162. MSSIM=0.9089.

Figure 3.23: Restored images $\widehat{\boldsymbol{f}}(\boldsymbol{g}, \widehat{\boldsymbol{\alpha}}, \alpha_2, \widehat{\sigma})$ obtained by means of the proposed Gauss-Markov random field model for one of the degraded versions of the Mandrill image (Fig. 3.1c). The degraded image was generated with a noise level of $\sigma = 20$, has $\text{MSE}(\boldsymbol{f}, \boldsymbol{g}) = 375$, $\text{MSSIM}(\boldsymbol{f}, \boldsymbol{g}) = 0.8518$ and is shown in (a). (b) $\alpha_2 = -0.49$, $\text{MSE}(\boldsymbol{f}, \widehat{\boldsymbol{f}}(\boldsymbol{g}, \widehat{\boldsymbol{\alpha}}, \alpha_2, \widehat{\sigma})) = 186$, $\text{MSSIM}(\boldsymbol{f}, \widehat{\boldsymbol{f}}(\boldsymbol{g}, \widehat{\boldsymbol{\alpha}}, \alpha_2, \widehat{\sigma})) = 0.9055$. (c) $\alpha_2 = -0.4$, $\text{MSE}(\boldsymbol{f}, \widehat{\boldsymbol{f}}(\boldsymbol{g}, \widehat{\boldsymbol{\alpha}}, \alpha_2, \widehat{\sigma})) = 158$, $\text{MSSIM}(\boldsymbol{f}, \widehat{\boldsymbol{f}}(\boldsymbol{g}, \widehat{\boldsymbol{\alpha}}, \alpha_2, \widehat{\sigma})) = 0.9112$. (d) $\alpha_2 = -0.25$, $\text{MSE}(\boldsymbol{f}, \widehat{\boldsymbol{f}}(\boldsymbol{g}, \widehat{\boldsymbol{\alpha}}, \alpha_2, \widehat{\sigma})) = 156$, $\text{MSSIM}(\boldsymbol{f}, \widehat{\boldsymbol{f}}(\boldsymbol{g}, \widehat{\boldsymbol{\alpha}}, \alpha_2, \widehat{\sigma})) = 0.9108$. (e) $\alpha_2 = 0.0$, $\text{MSE}(\boldsymbol{f}, \widehat{\boldsymbol{f}}(\boldsymbol{g}, \widehat{\boldsymbol{\alpha}}, \alpha_2, \widehat{\sigma})) = 157$, $\text{MSSIM}(\boldsymbol{f}, \widehat{\boldsymbol{f}}(\boldsymbol{g}, \widehat{\boldsymbol{\alpha}}, \alpha_2, \widehat{\sigma})) = 0.9099$. (f) $\alpha_2 = 0.49$, $\text{MSE}(\boldsymbol{f}, \widehat{\boldsymbol{f}}(\boldsymbol{g}, \widehat{\boldsymbol{\alpha}}, \alpha_2, \widehat{\sigma})) = 162$, $\text{MSSIM}(\boldsymbol{f}, \widehat{\boldsymbol{f}}(\boldsymbol{g}, \widehat{\boldsymbol{\alpha}}, \alpha_2, \widehat{\sigma})) = 0.9089$.

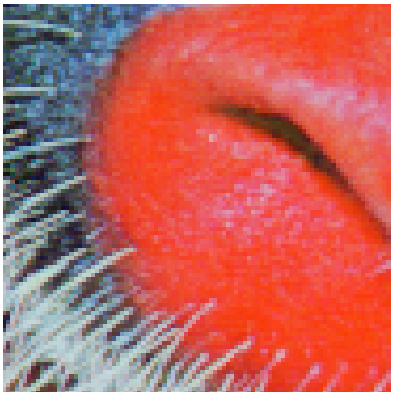

(a) Original Image.

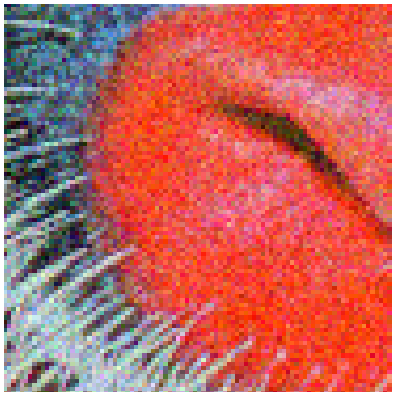

(b) Degraded Image. MSE=375. MSSIM=0.8518.

(c) Restored. $\alpha_2 = -0.49$. MSE=186. MSSIM=0.9055.

(d) Restored. $\alpha_2 = -0.4$. MSE=158. MSSIM=0.9112.

(e) Restored. $\alpha_2 = -0.25$. MSE=156. MSSIM=0.9108.

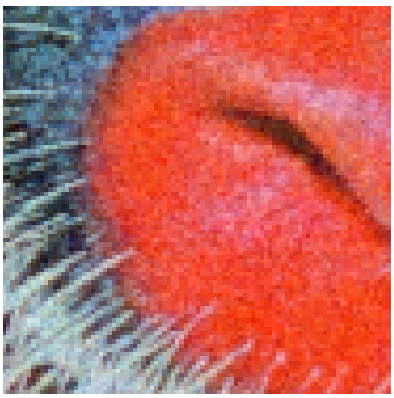

(f) Restored. $\alpha_2 = 0.0$. MSE=157. MSSIM=0.9099.

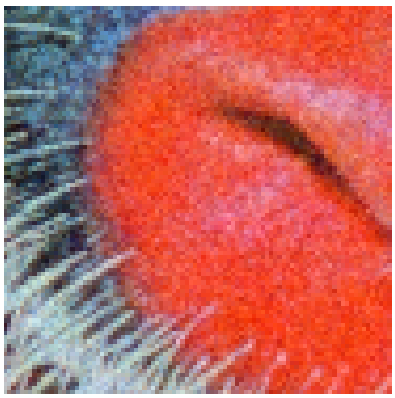

(g) Restored. $\alpha_2 = 0.49$. MSE=162. MSSIM=0.9089.

Figure 3.24: Details of the original image $\boldsymbol{f}$ in Fig. 3.1c, the degraded image $\boldsymbol{g}$ in Fig. 3.23a and the restored images $\widehat{\boldsymbol{f}}(\boldsymbol{g}, \widehat{\boldsymbol{\alpha}}, \alpha_2, \widehat{\sigma})$ in Fig. 3.23. (a) Original image $\boldsymbol{f}$ in Fig. 3.1c. (b) Degraded image $\boldsymbol{g}$ in Fig. 3.23a. (c) Restored image $\widehat{\boldsymbol{f}}(\boldsymbol{g}, \widehat{\boldsymbol{\alpha}}, \alpha_2, \widehat{\sigma})$ in Fig. 3.23b. (d) Restored image $\widehat{\boldsymbol{f}}(\boldsymbol{g}, \widehat{\boldsymbol{\alpha}}, \alpha_2, \widehat{\sigma})$ in Fig. 3.23c. (e) Restored image $\widehat{\boldsymbol{f}}(\boldsymbol{g}, \widehat{\boldsymbol{\alpha}}, \alpha_2, \widehat{\sigma})$ in Fig. 3.23d. (f) Restored image $\widehat{\boldsymbol{f}}(\boldsymbol{g}, \widehat{\boldsymbol{\alpha}}, \alpha_2, \widehat{\sigma})$ in Fig. 3.23e. (g) Restored image $\widehat{\boldsymbol{f}}(\boldsymbol{g}, \widehat{\boldsymbol{\alpha}}, \alpha_2, \widehat{\sigma})$ in Fig. 3.23f.

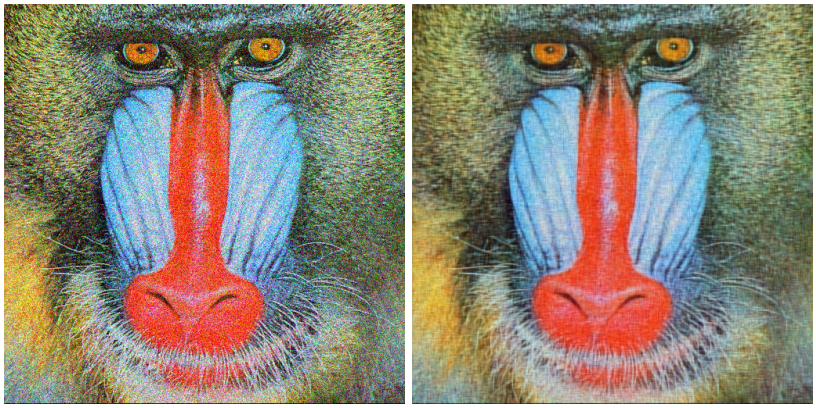

(a) Degraded Image. MSE=1436. MSSIM=0.6468.

(b) Restored. $\alpha_2 = -0.49$. MSE=365. MSSIM=0.7976.

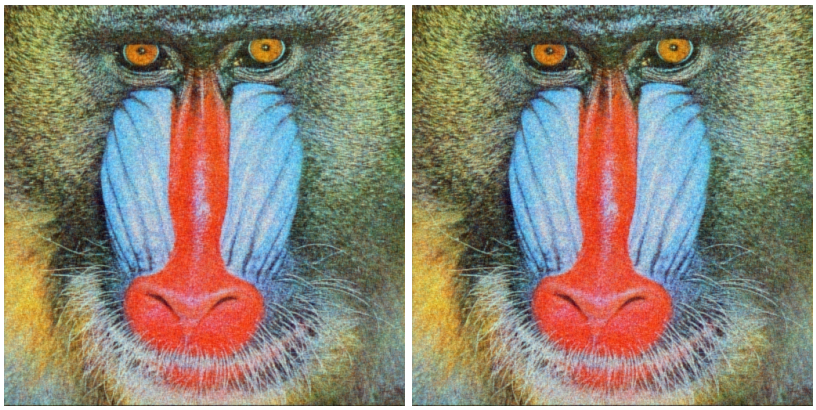

(c) Restored. $\alpha_2 = -0.35$. MSE=320.8. MSSIM=0.8116.

(d) Restored. $\alpha_2 = -0.30$. MSE=320.7. MSSIM=0.8114.

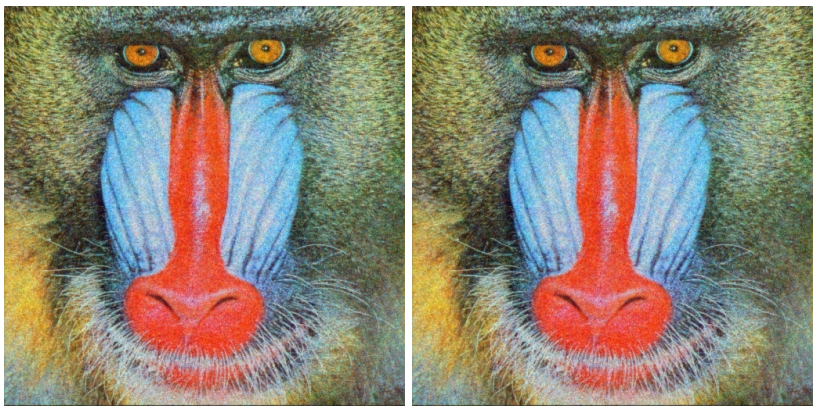

(e) Restored. $\alpha_2 = 0.0$. MSE=327. MSSIM=0.8098.

(f) Restored. $\alpha_2 = 0.49$. MSE=336. MSSIM=0.8083.

Figure 3.25: Restored images $\widehat{\boldsymbol{f}}(\boldsymbol{g}, \widehat{\boldsymbol{\alpha}}, \alpha_2, \widehat{\sigma})$ obtained by means of the proposed Gauss-Markov random field model for one of the degraded versions of the Mandrill image (Fig. 3.1c). The degraded image was generated with a noise level of $\sigma = 40$, has $\text{MSE}(\boldsymbol{f}, \boldsymbol{g}) = 1436$, $\text{MSSIM}(\boldsymbol{f}, \boldsymbol{g}) = 0.6468$ and is shown in (a). (b) $\alpha_2 = -0.49$, $\text{MSE}(\boldsymbol{f}, \widehat{\boldsymbol{f}}(\boldsymbol{g}, \widehat{\boldsymbol{\alpha}}, \alpha_2, \widehat{\sigma})) = 365$, $\text{MSSIM}(\boldsymbol{f}, \widehat{\boldsymbol{f}}(\boldsymbol{g}, \widehat{\boldsymbol{\alpha}}, \alpha_2, \widehat{\sigma})) = 0.7976$. (c) $\alpha_2 = -0.35$, $\text{MSE}(\boldsymbol{f}, \widehat{\boldsymbol{f}}(\boldsymbol{g}, \widehat{\boldsymbol{\alpha}}, \alpha_2, \widehat{\sigma})) = 320.8$, $\text{MSSIM}(\boldsymbol{f}, \widehat{\boldsymbol{f}}(\boldsymbol{g}, \widehat{\boldsymbol{\alpha}}, \alpha_2, \widehat{\sigma})) = 0.8116$. (d) $\alpha_2 = -0.30$, $\text{MSE}(\boldsymbol{f}, \widehat{\boldsymbol{f}}(\boldsymbol{g}, \widehat{\boldsymbol{\alpha}}, \alpha_2, \widehat{\sigma})) = 320.7$, $\text{MSSIM}(\boldsymbol{f}, \widehat{\boldsymbol{f}}(\boldsymbol{g}, \widehat{\boldsymbol{\alpha}}, \alpha_2, \widehat{\sigma})) = 0.8114$. (e) $\alpha_2 = 0.0$, $\text{MSE}(\boldsymbol{f}, \widehat{\boldsymbol{f}}(\boldsymbol{g}, \widehat{\boldsymbol{\alpha}}, \alpha_2, \widehat{\sigma})) = 327$, $\text{MSSIM}(\boldsymbol{f}, \widehat{\boldsymbol{f}}(\boldsymbol{g}, \widehat{\boldsymbol{\alpha}}, \alpha_2, \widehat{\sigma})) = 0.8098$. (f) $\alpha_2 = 0.49$, $\text{MSE}(\boldsymbol{f}, \widehat{\boldsymbol{f}}(\boldsymbol{g}, \widehat{\boldsymbol{\alpha}}, \alpha_2, \widehat{\sigma})) = 336$, $\text{MSSIM}(\boldsymbol{f}, \widehat{\boldsymbol{f}}(\boldsymbol{g}, \widehat{\boldsymbol{\alpha}}, \alpha_2, \widehat{\sigma})) = 0.8083$.

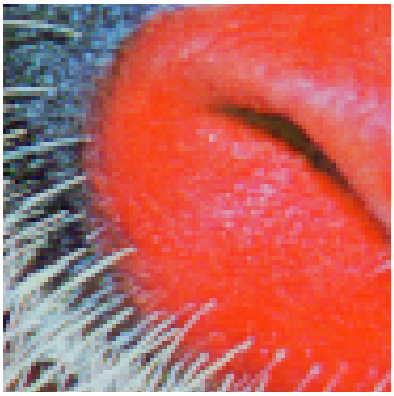

(a) Original Image.

(b) Degraded Image. MSE=1436. MSSIM=0.6468.

(c) Restored. $\alpha_2 = -0.49$. MSE=365. MSSIM=0.7976.

(d) Restored. $\alpha_2 = -0.35$. MSE=320.8. MSSIM=0.8116.

(e) Restored. $\alpha_2 = -0.30$. MSE=320.7. MSSIM=0.8114.

(f) Restored. $\alpha_2 = 0.0$. MSE=327. MSSIM=0.8098.

(g) Restored. $\alpha_2 = 0.49$. MSE=336. MSSIM=0.8083.

Figure 3.26: Details of the original image $\boldsymbol{f}$ in Fig. 3.1c, the degraded image $\boldsymbol{g}$ in Fig. 3.25a and the restored images $\widehat{\boldsymbol{f}}(\boldsymbol{g}, \widehat{\boldsymbol{\alpha}}, \alpha_2, \widehat{\sigma})$ in Fig. 3.25. (a) Original image $\boldsymbol{f}$ in Fig. 3.1c. (b) Degraded image $\boldsymbol{g}$ in Fig. 3.25a. (c) Restored image $\widehat{\boldsymbol{f}}(\boldsymbol{g}, \widehat{\boldsymbol{\alpha}}, \alpha_2, \widehat{\sigma})$ in Fig. 3.25b. (d) Restored image $\widehat{\boldsymbol{f}}(\boldsymbol{g}, \widehat{\boldsymbol{\alpha}}, \alpha_2, \widehat{\sigma})$ in Fig. 3.25c. (e) Restored image $\widehat{\boldsymbol{f}}(\boldsymbol{g}, \widehat{\boldsymbol{\alpha}}, \alpha_2, \widehat{\sigma})$ in Fig. 3.25d. (f) Restored image $\widehat{\boldsymbol{f}}(\boldsymbol{g}, \widehat{\boldsymbol{\alpha}}, \alpha_2, \widehat{\sigma})$ in Fig. 3.25e. (g) Restored image $\widehat{\boldsymbol{f}}(\boldsymbol{g}, \widehat{\boldsymbol{\alpha}}, \alpha_2, \widehat{\sigma})$ in Fig. 3.25f.

3.5 Chapter Summary

In this chapter, we described our solvable probabilistic model for colour images using second-neighbour pixel interactions. We derived the mathematical expressions related to this model and proposed an algorithm based on these results. Finally, we presented the results of numerical experiments using our algorithm and confirmed that, with a good choice of the hyperparameter α_2, we can obtain better image correction results by using our extension to the second-neighbour pixel interactions than by using the original model which only takes the next-neighbour pixel interactions into account. In particular, we saw that by using negative values of α_2, this model allows a better preservation of horizontal and vertical edges in the images, but at the same time, it introduces horizontal and vertical line artefacts in the images.

Chapter 4

Solvable Probabilistic Model with Third-Neighbour Interaction for Grayscale Image Restoration

4.1 Chapter Outline

In this chapter, we shall describe the extension to the third-neighbour pixel interactions of the solvable probabilistic model for greyscale images originally proposed by Tanaka in [3]. We start with a detailed description of the model as well as the calculations involved in its formation. This is followed by the presentation of an image correction algorithm based on this model before concluding with a description of the numerical experiments we performed to evaluate this model.

4.2 Model Description

In this section we describe in detail the equations that form the basis of our solvable probabilistic model with third-neighbour interaction for grayscale image restoration. From these equations, we also derive mathematical expressions that can be used to implement an efficient image correction algorithm. We shall use the same image and degradation process models as those for the second-neighbour extension model described in Sections 2.2.1 and 2.2.2 respectively.

4.2.1 A Priori Probability Density Function

We define the a priori probability density function (prior) that the original image $\boldsymbol{F}$ has a given configuration $\boldsymbol{f}$ as

$$\begin{aligned}\Pr\{\boldsymbol{F}=\boldsymbol{f}|\alpha,\alpha',\alpha''\}\equiv\\ \frac{1}{Z_{\text{prior}}(\alpha,\alpha',\alpha'')}\exp\Bigg\{-\frac{1}{8}\Bigg(\alpha\sum_{(x,y)\in\mathbf{V}}\left[(f_{x,y}-f_{x+1,y})^2+(f_{x,y}-f_{x,y+1})^2\right]\\ +\alpha'\sum_{(x,y)\in\mathbf{V}}\left[(f_{x,y}-f_{x+1,y+1})^2+(f_{x,y}-f_{x+1,y-1})^2\right]\\ +\alpha''\sum_{(x,y)\in\mathbf{V}}\left[(f_{x,y}-f_{x+2,y})^2+(f_{x,y}-f_{x,y+2})^2\right]\Bigg)\Bigg\}\end{aligned}\tag{4.1}$$

where α defines the correlation between nearest neighbour pixels, α' defines the correlation between second-neighbour pixels, α'' defines the correlation between third-neighbour pixels and

$$Z_{\text{prior}}(\alpha,\alpha',\alpha'')\equiv\int\exp\Bigg\{-\frac{1}{8}\Bigg(\alpha\sum_{(x,y)\in\mathbf{V}}\left[(z_{x,y}-z_{x+1,y})^2+(z_{x,y}-z_{x,y+1})^2\right]$$

$$+\alpha'\sum_{(x,y)\in\mathbf{V}}\left[(z_{x,y}-z_{x+1,y+1})^2+(z_{x,y}-z_{x+1,y-1})^2\right]$$
$$+\alpha''\sum_{(x,y)\in\mathbf{V}}\left[(f_{x,y}-f_{x+2,y})^2+(f_{x,y}-f_{x,y+2})^2\right]\Bigg)\Bigg\}d\boldsymbol{z}, \quad (4.2)$$

with $\int d\boldsymbol{z}\equiv\int_{-\infty}^{+\infty}\int_{-\infty}^{+\infty}\cdots\int_{-\infty}^{+\infty}\prod_{(x,y)\in\mathbf{V}}dz_{x,y}$, is the normalization constant.

The prior can be rewritten using matrix notation as follows:

$$\begin{aligned}
&\Pr\{\boldsymbol{F}=\boldsymbol{f}|\alpha,\alpha',\alpha''\}\\
&=\frac{1}{Z_{\text{prior}}(\alpha,\alpha',\alpha'')}\exp\Bigg\{-\frac{1}{8}\Bigg(\alpha\sum_{(x,y)\in\mathbf{V}}\left[(f_{x,y}-f_{x+1,y})^2+(f_{x,y}-f_{x,y+1})^2\right.\\
&\quad\left.+\frac{\alpha'}{\alpha}\left\{(f_{x,y}-f_{x+1,y+1})^2+(f_{x,y}-f_{x+1,y-1})^2\right\}\right]\Bigg)\\
&\quad-\frac{1}{8}\alpha''\sum_{(x,y)\in\mathbf{V}}\left[(f_{x,y}-f_{x+2,y})^2+(f_{x,y}-f_{x,y+2})^2\right]\Bigg\}\\
&=\frac{1}{Z_{\text{prior}}(\alpha,\alpha',\alpha'')}\exp\Bigg\{-\frac{1}{8}\Bigg(\alpha\sum_{(x,y)\in\mathbf{V}}\left[4f_{x,y}^2-f_{x,y}f_{x+1,y}-f_{x,y}f_{x-1,y}\right.\\
&\quad-f_{x,y}f_{x,y+1}-f_{x,y}f_{x,y-1}\\
&\quad\left.+\frac{\alpha'}{\alpha}\left(4f_{x,y}^2-f_{x,y}f_{x+1,y+1}-f_{x,y}f_{x-1,y-1}-f_{x,y}f_{x+1,y-1}-f_{x,y}f_{x-1,y+1}\right)\right]\Bigg)\\
&\quad-\frac{1}{8}\alpha''\sum_{(x,y)\in\mathbf{V}}\left[(f_{x,y}-f_{x+2,y})^2+(f_{x,y}-f_{x,y+2})^2\right]\Bigg\},
\end{aligned} \quad (4.3)$$

where we used the results of equation (2.7). The summation in the last term of the exponential can be rewritten in the following way:

$$\begin{aligned}
&\sum_{(x,y)\in\mathbf{V}}\left[(f_{x,y}-f_{x+2,y})^2+(f_{x,y}-f_{x,y+2})^2\right]\\
&=\sum_{(x,y)\in\mathbf{V}}\left[f_{x,y}^2-2f_{x,y}f_{x+2,y}+f_{x+2,y}^2+f_{x,y}^2-2f_{x,y}f_{x,y+2}+f_{x,y+2}^2\right]\\
&=\sum_{(x,y)\in\mathbf{V}}\left[4f_{x,y}^2-2f_{x,y}f_{x+2,y}-2f_{x,y}f_{x,y+2}\right]\\
&=\sum_{(x,y)\in\mathbf{V}}\left[4f_{x,y}^2-f_{x,y}f_{x+2,y}-f_{x,y}f_{x-2,y}-f_{x,y}f_{x,y+2}-f_{x,y}f_{x,y-2}\right].
\end{aligned} \quad (4.4)$$

By inserting (4.4) into (4.3), we have

$$\begin{aligned}
&\Pr\{\boldsymbol{F}=\boldsymbol{f}|\alpha,\alpha',\alpha''\}\\
&=\frac{1}{Z_{\text{prior}}(\alpha,\alpha',\alpha'')}\exp\Bigg\{-\frac{1}{8}\Bigg(\alpha\\
&\quad\times\sum_{(x,y)\in\mathbf{V}}\left[4f_{x,y}^2-f_{x,y}f_{x+1,y}-f_{x,y}f_{x-1,y}-f_{x,y}f_{x,y+1}-f_{x,y}f_{x,y-1}\right.\\
&\quad\left.+\frac{\alpha'}{\alpha}\left(4f_{x,y}^2-f_{x,y}f_{x+1,y+1}-f_{x,y}f_{x-1,y-1}-f_{x,y}f_{x+1,y-1}-f_{x,y}f_{x-1,y+1}\right)\right]\Bigg)\\
&\quad-\frac{1}{8}\alpha''\sum_{(x,y)\in\mathbf{V}}\left[4f_{x,y}^2-f_{x,y}f_{x+2,y}-f_{x,y}f_{x-2,y}-f_{x,y}f_{x,y+2}-f_{x,y}f_{x,y-2}\right]\Bigg\}
\end{aligned}$$

$$
\begin{aligned}
=&\frac{1}{Z_{\text{prior}}\left(\alpha,\alpha',\alpha''\right)}\exp\Bigg\{-\frac{1}{8}\Bigg(\alpha\\
&\times\sum_{(x,y)\in\mathbf{V}}\left[4f_{x,y}^2-f_{x,y}f_{x+1,y}-f_{x,y}f_{x-1,y}-f_{x,y}f_{x,y+1}-f_{x,y}f_{x,y-1}\right.\\
&+\frac{\alpha'}{\alpha}\left(4f_{x,y}^2-f_{x,y}f_{x+1,y+1}-f_{x,y}f_{x-1,y-1}-f_{x,y}f_{x+1,y-1}-f_{x,y}f_{x-1,y+1}\right)\\
&\left.+\frac{\alpha''}{\alpha}\left(4f_{x,y}^2-f_{x,y}f_{x+2,y}-f_{x,y}f_{x-2,y}-f_{x,y}f_{x,y+2}-f_{x,y}f_{x,y-2}\right)\right]\Bigg)\Bigg\}\\
=&\frac{1}{Z_{\text{prior}}\left(\alpha,\alpha',\alpha''\right)}\exp\left\{-\frac{1}{2}\alpha\boldsymbol{f}^T\boldsymbol{C}\left(\alpha,\alpha',\alpha''\right)\boldsymbol{f}\right\}
\end{aligned}
\tag{4.5}
$$

where $\boldsymbol{C}\left(\alpha,\alpha',\alpha''\right)$ is a $|\mathbf{V}|\times|\mathbf{V}|$ matrix where the $(x,y|x',y')$ elements are defined by

$$
\begin{aligned}
\langle x,y|x',y'\rangle\equiv&\,\delta_{x,x'}\delta_{y,y'}-\frac{1}{4}\delta_{x,x'+1}\delta_{y,y'}-\frac{1}{4}\delta_{x,x'-1}\delta_{y,y'}-\frac{1}{4}\delta_{x,x'}\delta_{y,y'+1}-\frac{1}{4}\delta_{x,x'}\delta_{y,y'-1}\\
&+\alpha_2\left[\delta_{x,x'}\delta_{y,y'}-\frac{1}{4}\delta_{x,x'+1}\delta_{y,y'+1}-\frac{1}{4}\delta_{x,x'-1}\delta_{y,y'-1}-\frac{1}{4}\delta_{x,x'+1}\delta_{y,y'-1}-\frac{1}{4}\delta_{x,x'-1}\delta_{y,y'+1}\right]\\
+\alpha_3\Big[\delta_{x,x'}\delta_{y,y'}-\frac{1}{4}\delta_{x,x'+2}\delta_{y,y'}-\frac{1}{4}\delta_{x,x'-2}\delta_{y,y'}-\frac{1}{4}\delta_{x,x'}\delta_{y,y'+2}-\frac{1}{4}\delta_{x,x'}\delta_{y,y'-2}\Big]&\,[(x,y),(x',y')\in\mathbf{V}]
\end{aligned}
\tag{4.6}
$$

where $\delta_{a,b}$ is the Kronecker delta and we defined $\alpha_2\equiv\alpha'/\alpha$ and $\alpha_3\equiv\alpha''/\alpha$ to simplify notations, so that we can write $\boldsymbol{C}\left(\alpha,\alpha',\alpha''\right)\equiv\boldsymbol{C}\left(\alpha_2,\alpha_3\right)$.

Similarly, $Z_{\text{prior}}\left(\alpha,\alpha',\alpha''\right)$ can be rewritten using matrix notation as

$$
Z_{\text{prior}}\left(\alpha,\alpha_2,\alpha_3\right)\equiv\int\exp\left\{-\frac{1}{2}\alpha\boldsymbol{z}^T\boldsymbol{C}\left(\alpha_2,\alpha_3\right)\boldsymbol{z}\right\}d\boldsymbol{z}
\tag{4.7}
$$

and subsequently, it can be simplified using the multidimensional Gaussian integral to give

$$
Z_{\text{prior}}\left(\alpha,\alpha_2,\alpha_3\right)=\sqrt{\frac{(2\pi)^{|\mathbf{V}|}}{\alpha^{|\mathbf{V}|}\det\left(\boldsymbol{C}\left(\alpha_2,\alpha_3\right)\right)}}.
\tag{4.8}
$$

This model corresponds to an extension to the third-neighbour of the CAR model proposed by Molina in [1] and its energy function is:

$$
\begin{aligned}
\frac{1}{8}\Bigg(\alpha\sum_{(x,y)\in\mathbf{V}}\left[(f_{x,y}-f_{x+1,y})^2+(f_{x,y}-f_{x,y+1})^2\right]+\alpha'\sum_{(x,y)\in\mathbf{V}}\left[(f_{x,y}-f_{x+1,y+1})^2+(f_{x,y}-f_{x+1,y-1})^2\right]\\
+\alpha''\sum_{(x,y)\in\mathbf{V}}\left[(f_{x,y}-f_{x+2,y})^2+(f_{x,y}-f_{x,y+2})^2\right]\Bigg)
\end{aligned}
\tag{4.9}
$$

We note that $\boldsymbol{f}$ is a Gaussian Markov random field (GMRF) with mean $\mathbf{0}$ and precision matrix $\boldsymbol{Q}=\alpha\boldsymbol{C}\left(\alpha_2,\alpha_3\right)$, so that by using the properties of GMRFs described in section 2.2.3, we obtain the following properties for our model:

$$
\begin{aligned}
\mathrm{E}(f_{(x,y)}|\boldsymbol{f}_{-(x,y)})=&\,\mu_{(x,y)}-\frac{1}{Q_{(x,y),(x,y)}}\sum_{(i,j):(i,j)\sim(x,y)}Q_{(x,y),(i,j)}(f_{(i,j)}-\mu_{(i,j)})\\
=&-\frac{1}{\alpha+\alpha'+\alpha''}\sum_{(i,j):(i,j)\sim(x,y)}Q_{(x,y),(i,j)}f_{(i,j)}\\
=&-\frac{1}{\alpha+\alpha'+\alpha''}\Bigg[-\alpha\left(\frac{1}{4}f_{(x+1,y)}+\frac{1}{4}f_{(x-1,y)}+\frac{1}{4}f_{(x,y+1)}+\frac{1}{4}f_{(x,y-1)}\right)\\
&-\alpha'\left(\frac{1}{4}f_{(x+1,y+1)}+\frac{1}{4}f_{(x-1,y-1)}+\frac{1}{4}f_{(x+1,y-1)}+\frac{1}{4}f_{(x-1,y+1)}\right)\\
&-\alpha''\left(\frac{1}{4}f_{(x+2,y)}+\frac{1}{4}f_{(x-2,y)}+\frac{1}{4}f_{(x,y+2)}+\frac{1}{4}f_{(x,y-2)}\right)\Bigg]
\end{aligned}
$$

$$= \frac{1}{4(\alpha+\alpha'+\alpha'')}\Big[\alpha\left(f_{(x+1,y)}+f_{(x-1,y)}+f_{(x,y+1)}+f_{(x,y-1)}\right) + \alpha'\left(f_{(x+1,y+1)}+f_{(x-1,y-1)}+f_{(x+1,y-1)}+f_{(x-1,y+1)}\right) + \alpha''\left(f_{(x+2,y)}+f_{(x-2,y)}+f_{(x,y+2)}+f_{(x,y-2)}\right)\Big] \tag{4.10}$$

and

$$\text{Prec}(f_{(x,y)}|\boldsymbol{f}_{-(x,y)}) = \alpha+\alpha'+\alpha'' \tag{4.11}$$

so that we have

$$\Pr(f_{(x,y)}|\boldsymbol{f}_{-(x,y)}) \sim N\Bigg(\frac{1}{4(\alpha+\alpha'+\alpha'')}\Big[\alpha\left(f_{(x+1,y)}+f_{(x-1,y)}+f_{(x,y+1)}+f_{(x,y-1)}\right) + \alpha'\left(f_{(x+1,y+1)}+f_{(x-1,y-1)}+f_{(x+1,y-1)}+f_{(x-1,y+1)}\right) + \alpha''\left(f_{(x+2,y)}+f_{(x-2,y)}+f_{(x,y+2)}+f_{(x,y-2)}\right)\Big], \frac{1}{\alpha+\alpha'+\alpha''}\Bigg). \tag{4.12}$$

Since $\boldsymbol{C}(\alpha_2,\alpha_3)$ is a real symmetric matrix, it can be eigendecomposed to obtain

$$\boldsymbol{C}(\alpha_2,\alpha_3) = \left(\boldsymbol{U}^{-1}\boldsymbol{\Lambda}\boldsymbol{U}\right) \tag{4.13}$$

where $\boldsymbol{U}$ is a unitary matrix with the eigenvectors of $\boldsymbol{C}(\alpha_2,\alpha_3)$ as its column vectors. We shall use the DFT matrix defined as

$$\langle x,y|\boldsymbol{U}|p,q\rangle \equiv \frac{1}{\sqrt{|\mathbf{V}|}}\exp\left[-2\pi i\left(\frac{px}{V_x}+\frac{qy}{V_y}\right)\right], \tag{4.14}$$

$\boldsymbol{U}^{-1}$ is the conjugate transpose of $\boldsymbol{U}$, known as the inverse DFT matrix and defined as

$$\left\langle x,y|\boldsymbol{U}^{-1}|p,q\right\rangle \equiv \frac{1}{\sqrt{|\mathbf{V}|}}\exp\left[2\pi i\left(\frac{px}{V_x}+\frac{qy}{V_y}\right)\right] \tag{4.15}$$

and $\boldsymbol{\Lambda}$ is the diagonal matrix of the eigenvalues $\lambda(\alpha_2,\alpha_3,p,q)$ of $\boldsymbol{C}(\alpha_2,\alpha_3)$.

We shall now find the value of $\boldsymbol{\Lambda}$ for $\boldsymbol{U}$ by using the eigenvalue equation

$$\boldsymbol{M}\boldsymbol{u}_{(x,y)} = \lambda(x,y)\boldsymbol{u}_{(x,y)} \tag{4.16}$$

for every $(x,y)\in\mathbf{V}$. Here $\boldsymbol{u}_{(x,y)}$ is the column vector (x,y) of $\boldsymbol{U}$ and $\lambda(x,y)$ is the corresponding eigenvalue. To simplify our calculations, we shall split $\boldsymbol{C}(\alpha_2,\alpha_3)$ into the sum of matrices $\boldsymbol{A}$, $\boldsymbol{B}$ and $\boldsymbol{D}$ as follows

$$\langle x,y|\boldsymbol{A}|x',y'\rangle \equiv \delta_{x,x'}\delta_{y,y'} - \frac{1}{4}\delta_{x,x'+1}\delta_{y,y'} - \frac{1}{4}\delta_{x,x'-1}\delta_{y,y'} - \frac{1}{4}\delta_{x,x'}\delta_{y,y'+1} - \frac{1}{4}\delta_{x,x'}\delta_{y,y'-1}, \tag{4.17}$$

$$\langle x,y|\boldsymbol{B}|x',y'\rangle \equiv \alpha_2\Big[\delta_{x,x'}\delta_{y,y'} - \frac{1}{4}\delta_{x,x'+1}\delta_{y,y'+1} - \frac{1}{4}\delta_{x,x'-1}\delta_{y,y'-1} - \frac{1}{4}\delta_{x,x'+1}\delta_{y,y'-1} - \frac{1}{4}\delta_{x,x'-1}\delta_{y,y'+1}\Big], \tag{4.18}$$

$$\langle x,y|\boldsymbol{D}|x',y'\rangle \equiv \alpha_3\Big[\delta_{x,x'}\delta_{y,y'} - \frac{1}{4}\delta_{x,x'+2}\delta_{y,y'} - \frac{1}{4}\delta_{x,x'-2}\delta_{y,y'} - \frac{1}{4}\delta_{x,x'}\delta_{y,y'+2} - \frac{1}{4}\delta_{x,x'}\delta_{y,y'-2}\Big]. \tag{4.19}$$

We then have

$$\begin{aligned}\boldsymbol{C}(\alpha_2,\alpha_3) &= \boldsymbol{A}+\boldsymbol{B}+\boldsymbol{D}\\ \boldsymbol{U}^{-1}\boldsymbol{\Lambda}\boldsymbol{U} &= \boldsymbol{A}+\boldsymbol{B}+\boldsymbol{D}\\ \boldsymbol{\Lambda} &= \boldsymbol{U}(\boldsymbol{A}+\boldsymbol{B}+\boldsymbol{D})\boldsymbol{U}^{-1}\end{aligned}$$

$$\begin{aligned}\boldsymbol{\Lambda} &= \boldsymbol{U}\boldsymbol{A}\boldsymbol{U}^{-1} + \boldsymbol{U}\boldsymbol{B}\boldsymbol{U}^{-1} + \boldsymbol{U}\boldsymbol{D}\boldsymbol{U}^{-1} \\ \boldsymbol{\Lambda} &= \boldsymbol{\Lambda}_A + \boldsymbol{\Lambda}_B + \boldsymbol{\Lambda}_D, \end{aligned} \tag{4.20}$$

so we can find the value of $\boldsymbol{\Lambda}$ by finding the values of $\boldsymbol{\Lambda}_A$, $\boldsymbol{\Lambda}_B$ and $\boldsymbol{\Lambda}_D$.

We already found the values of $\boldsymbol{\Lambda}_A$ and $\boldsymbol{\Lambda}_B$ in equations (2.28) and (2.31) respectively. We apply a similar method to find the values of $\boldsymbol{\Lambda}_D$ by using the fact that the elements of $\boldsymbol{D}$ are such that

$$d_{(p,q),(r,s)} = \begin{cases} \alpha_3 & \text{if } (p,q) = (r,s), \\ -\frac{1}{4}\alpha_3 & \text{if } (p,q) = (r-2,s), \\ -\frac{1}{4}\alpha_3 & \text{if } (p,q) = (r+2,s), \\ -\frac{1}{4}\alpha_3 & \text{if } (p,q) = (r,s-2), \\ -\frac{1}{4}\alpha_3 & \text{if } (p,q) = (r,s+2), \\ 0 & \text{for every other case.} \end{cases} \tag{4.21}$$

Line (r,s) of equation (4.16) can be rewritten as follows:

$$\sum_{(p,q)\in\mathbf{V}} d_{(p,q),(r,s)} u_{(x,y),(p,q)} = \lambda_d(x,y) u_{(x,y),(r,s)} \tag{4.22}$$

so by using the values of (4.21) into equation (4.22) we obtain

$$\begin{aligned} \alpha_3 u_{(x,y),(r,s)} - \left(\frac{\alpha_3}{4}u_{(x,y),(r-2,s)} + \frac{\alpha_3}{4}u_{(x,y),(r+2,s)} + \frac{\alpha_3}{4}u_{(x,y),(r,s-2)} + \frac{\alpha_3}{4}u_{(x,y),(r,s+2)}\right) \\ = \lambda_d(x,y)u_{(x,y),(r,s)} \\ \therefore -\frac{\alpha_3}{4}\left(u_{(x,y),(r-2,s)} + u_{(x,y),(r+2,s)} + u_{(x,y),(r,s-2)} + u_{(x,y),(r,s+2)}\right) = \left(\lambda_d(x,y) - \alpha_3\right) u_{(x,y),(r,s)} \\ \therefore -\frac{\alpha_3}{4\sqrt{|\mathbf{V}|}}\left\{\exp\left[-2\pi i\left(\frac{x(r-2)}{V_x} + \frac{ys}{V_y}\right)\right] + \exp\left[-2\pi i\left(\frac{x(r+2)}{V_x} + \frac{ys}{V_y}\right)\right]\right. \\ \left. + \exp\left[-2\pi i\left(\frac{xr}{V_x} + \frac{y(s-2)}{V_y}\right)\right] + \exp\left[-2\pi i\left(\frac{xr}{V_x} + \frac{y(s+2)}{V_y}\right)\right]\right\} \\ = \left(\lambda_d(x,y) - \alpha_3\right)\frac{1}{\sqrt{|\mathbf{V}|}}\exp\left[-2\pi i\left(\frac{xr}{V_x} + \frac{ys}{V_y}\right)\right] \\ \therefore -\frac{\alpha_3}{4}\exp\left[2\pi i\left(\frac{xr}{V_x} + \frac{ys}{V_y}\right)\right]\left\{\exp\left[-2\pi i\left(\frac{x(r-2)}{V_x} + \frac{ys}{V_y}\right)\right] + \exp\left[-2\pi i\left(\frac{x(r+2)}{V_x} + \frac{ys}{V_y}\right)\right]\right. \\ \left. + \exp\left[-2\pi i\left(\frac{xr}{V_x} + \frac{y(s-2)}{V_y}\right)\right] + \exp\left[-2\pi i\left(\frac{xr}{V_x} + \frac{y(s+2)}{V_y}\right)\right]\right\} \\ = \lambda_d(x,y) - \alpha_3 \\ \therefore -\frac{\alpha_3}{4}\left\{\exp\left[-2\pi i\frac{-2x}{V_x}\right] + \exp\left[-2\pi i\frac{2x}{V_x}\right] + \exp\left[-2\pi i\frac{-2y}{V_y}\right] + \exp\left[-2\pi i\frac{2y}{V_y}\right]\right\} \\ = \lambda_d(x,y) - \alpha_3 \\ \therefore \alpha_3 - \frac{\alpha_3}{4}\left\{\cos\left(\frac{4\pi x}{V_x}\right) + i\sin\left(\frac{4\pi x}{V_x}\right) + \cos\left(-\frac{4\pi x}{V_x}\right) + i\sin\left(-\frac{4\pi x}{V_x}\right)\right. \\ \left. + \cos\left(\frac{4\pi y}{V_y}\right) + i\sin\left(\frac{4\pi y}{V_y}\right) + \cos\left(-\frac{4\pi y}{V_y}\right) + i\sin\left(-\frac{4\pi y}{V_y}\right)\right\} \\ = \lambda_d(x,y) \\ \therefore \lambda_d(x,y) = \alpha_3\left[1 - \frac{1}{2}\cos\left(\frac{4\pi x}{V_x}\right) - \frac{1}{2}\cos\left(\frac{4\pi y}{V_y}\right)\right]. \end{aligned} \tag{4.23}$$

Using the results of (2.28), (2.31) and (4.23), we find

$$\lambda(p,q) = \lambda_a(p,q) + \lambda_b(p,q) + \lambda_d(p,q)$$

$$
\begin{aligned}
&= 1 - \frac{1}{2}\cos\left(\frac{2\pi p}{V_x}\right) - \frac{1}{2}\cos\left(\frac{2\pi q}{V_y}\right) \\
&\quad + \alpha_2\left[1 - \frac{1}{2}\cos\left(2\pi(\frac{p}{V_x} + \frac{q}{V_y})\right) - \frac{1}{2}\cos\left(2\pi(\frac{p}{V_x} - \frac{q}{V_y})\right)\right] \\
&\quad + \alpha_3\left[1 - \frac{1}{2}\cos\left(\frac{4\pi p}{V_x}\right) - \frac{1}{2}\cos\left(\frac{4\pi q}{V_y}\right)\right]
\end{aligned} \tag{4.24}
$$

so we have

$$
\begin{aligned}
\boldsymbol{\Lambda} \equiv \sum_{(p,q)\in\mathbf{V}} \Bigg(& 1 - \frac{1}{2}\cos\left(\frac{2\pi p}{V_x}\right) - \frac{1}{2}\cos\left(\frac{2\pi q}{V_y}\right) \\
& + \alpha_2\left[1 - \frac{1}{2}\cos\left(2\pi(\frac{p}{V_x} + \frac{q}{V_y})\right) - \frac{1}{2}\cos\left(2\pi(\frac{p}{V_x} - \frac{q}{V_y})\right)\right] \\
& + \alpha_3\left[1 - \frac{1}{2}\cos\left(\frac{4\pi p}{V_x}\right) - \frac{1}{2}\cos\left(\frac{4\pi q}{V_y}\right)\right]\Bigg)\boldsymbol{J}^{pq,pq}
\end{aligned} \tag{4.25}
$$

which is the diagonal matrix of the eigenvalues $\lambda(\alpha_2, \alpha_3, p, q)$ of $\boldsymbol{C}(\alpha_2, \alpha_3)$ where $\boldsymbol{J}^{pq,pq}$ is the $|\boldsymbol{V}| \times |\boldsymbol{V}|$ single-entry matrix.

Using the results of this eigendecomposition, we can rewrite the expression of $Z_{\text{prior}}(\alpha, \alpha_2, \alpha_3)$ given in (4.8) as

$$
Z_{\text{prior}}(\alpha, \alpha_2, \alpha_3) = \left(\frac{2\pi}{\alpha}\right)^{\frac{|\mathbf{V}|}{2}} \prod_{(p,q)\in\mathbf{V}} \lambda(\alpha_2, \alpha_3, p, q)^{-\frac{1}{2}} \tag{4.26}
$$

4.2.2 A Posteriori Probability Density Function

The a posteriori probability density function of having an original image configuration $\boldsymbol{f}$ given a degraded image $\boldsymbol{g}$ is found by applying Bayes' theorem as follows:

$$
\begin{aligned}
\Pr\{\boldsymbol{F} = \boldsymbol{f}|\boldsymbol{G} = \boldsymbol{g}, \alpha, \alpha_2, \alpha_3, \sigma\} &= \frac{\Pr\{\boldsymbol{G} = \boldsymbol{g}|\boldsymbol{F} = \boldsymbol{f}, \sigma\}\Pr\{\boldsymbol{F} = \boldsymbol{f}|\alpha, \alpha_2, \alpha_3\}}{\Pr\{\boldsymbol{G} = \boldsymbol{g}|\alpha, \alpha_2, \alpha_3, \sigma\}} \\
&= \frac{\Pr\{\boldsymbol{G} = \boldsymbol{g}|\boldsymbol{F} = \boldsymbol{f}, \sigma\}\Pr\{\boldsymbol{F} = \boldsymbol{f}|\alpha, \alpha_2, \alpha_3\}}{\int \Pr\{\boldsymbol{G} = \boldsymbol{g}|\boldsymbol{F} = \boldsymbol{z}, \sigma\}\Pr\{\boldsymbol{F} = \boldsymbol{z}|\alpha, \alpha_2, \alpha_3\}\, d\boldsymbol{z}}
\end{aligned} \tag{4.27}
$$

where $\Pr\{\boldsymbol{G} = \boldsymbol{g}|\alpha, \alpha_2, \alpha_3, \sigma\} = \int \Pr\{\boldsymbol{G} = \boldsymbol{g}|\boldsymbol{F} = \boldsymbol{z}, \sigma\}\Pr\{\boldsymbol{F} = \boldsymbol{z}|\alpha, \alpha_2, \alpha_3\}\, d\boldsymbol{z}$ is called the evidence.

Using (2.1) and (4.5), the function can be rewritten as follows:

$$
\begin{aligned}
&\Pr\{\boldsymbol{F} = \boldsymbol{f}|\boldsymbol{G} = \boldsymbol{g}, \alpha, \alpha_2, \alpha_3, \sigma\} = \\
&\frac{\frac{1}{Z_{\text{noise}}(\sigma)}\exp\left(-\frac{1}{2\sigma^2}\sum_{(x,y)\in\mathbf{V}}(g_{x,y} - f_{x,y})^2\right) \times \frac{1}{Z_{\text{prior}}(\alpha,\alpha_2,\alpha_3)}\exp\left\{-\frac{1}{2}\alpha\boldsymbol{f}^T\boldsymbol{C}(\alpha_2, \alpha_3)\,\boldsymbol{f}\right\}}{\int \frac{1}{Z_{\text{noise}}(\sigma)}\exp\left(-\frac{1}{2\sigma^2}\sum_{(x,y)\in\mathbf{V}}(g_{x,y} - z_{x,y})^2\right) \times \frac{1}{Z_{\text{prior}}(\alpha,\alpha_2,\alpha_3)}\exp\left\{-\frac{1}{2}\alpha\boldsymbol{z}^T\boldsymbol{C}(\alpha_2, \alpha_3)\,\boldsymbol{z}\right\} d\boldsymbol{z}}.
\end{aligned} \tag{4.28}
$$

Since Z_{noise} and Z_{prior} are not dependant on $\boldsymbol{z}$, they can be taken out of the integral in the denominator and cancel out with the numerator, so we have

$$
\Pr\{\boldsymbol{F} = \boldsymbol{f}|\boldsymbol{G} = \boldsymbol{g}, \alpha, \alpha_2, \alpha_3, \sigma\} = \frac{1}{Z_{\text{posterior}}(\boldsymbol{g}, \alpha, \alpha_2, \alpha_3, \sigma)}\exp\left[-H(\boldsymbol{f}|\boldsymbol{g}, \alpha, \alpha_2, \alpha_3, \sigma)\right] \tag{4.29}
$$

where

$$
Z_{\text{posterior}}(\boldsymbol{g}, \alpha, \alpha_2, \alpha_3, \sigma) = \int \exp\left[-H(\boldsymbol{z}|\boldsymbol{g}, \alpha, \alpha_2, \alpha_3, \sigma)\right] d\boldsymbol{z} \tag{4.30}
$$

and

$$
H(\boldsymbol{f}|\boldsymbol{g}, \alpha, \alpha_2, \alpha_3, \sigma) = \frac{1}{2\sigma^2}\sum_{(x,y)\in\mathbf{V}}(g_{x,y} - f_{x,y})^2 + \frac{1}{2}\alpha\boldsymbol{f}^T\boldsymbol{C}(\alpha_2, \alpha_3)\,\boldsymbol{f}. \tag{4.31}
$$

We can simplify calculations by grouping all element of $\boldsymbol{f}$ in H in one single term in the same manner as in equation (2.40) to obtain

$$H\left(\boldsymbol{f}|\boldsymbol{g},\alpha,\alpha_2,\alpha_3,\sigma\right)=\frac{1}{2\sigma^2}\left[\boldsymbol{f}-\left(\boldsymbol{I}+\sigma^2\alpha\boldsymbol{C}\left(\alpha_2,\alpha_3\right)\right)^{-1}\boldsymbol{g}\right]^T\left(\boldsymbol{I}+\sigma^2\alpha\boldsymbol{C}\left(\alpha_2,\alpha_3\right)\right)$$
$$\times\left[\boldsymbol{f}-\left(\boldsymbol{I}+\sigma^2\alpha\boldsymbol{C}\left(\alpha_2,\alpha_3\right)\right)^{-1}\boldsymbol{g}\right]+\frac{1}{2}\boldsymbol{g}^T\alpha\boldsymbol{C}\left(\alpha_2,\alpha_3\right)\left(\boldsymbol{I}+\sigma^2\alpha\boldsymbol{C}\left(\alpha_2,\alpha_3\right)\right)^{-1}\boldsymbol{g}. \quad (4.32)$$

Using the eigendecomposition described in (4.13), we can rewrite the second term of (4.32) as

$$\frac{1}{2}\boldsymbol{g}^T\alpha\boldsymbol{C}\left(\alpha_2,\alpha_3\right)\left(\boldsymbol{I}+\sigma^2\alpha\boldsymbol{C}\left(\alpha_2,\alpha_3\right)\right)^{-1}\boldsymbol{g}=\frac{1}{2}\sum_{(p,q)\in\mathbf{V}}G^{\dagger}_{p,q}\alpha\lambda\left(\alpha_2,\alpha_3,p,q\right)\left(1+\sigma^2\alpha\lambda\left(\alpha_2,\alpha_3,p,q\right)\right)^{-1}G_{p,q} \quad (4.33)$$

where

$$G_{p,q}\equiv\frac{1}{\sqrt{|\mathbf{V}|}}\sum_{(x,y)\in\mathbf{V}}g_{x,y}\exp\left[-2\pi i\left(\frac{px}{V_x}+\frac{qy}{V_y}\right)\right] \quad (4.34)$$

and

$$G^{\dagger}_{p,q}\equiv\frac{1}{\sqrt{|\mathbf{V}|}}\sum_{(x,y)\in\mathbf{V}}g_{x,y}\exp\left[2\pi i\left(\frac{px}{V_x}+\frac{qy}{V_y}\right)\right]. \quad (4.35)$$

The detailed computations can be found at (2.41). Here we note that $G_{p,q}$ corresponds to $(\boldsymbol{U}\boldsymbol{g})_{p,q}$ where $(\boldsymbol{U}\boldsymbol{g})$ is the DFT of $\boldsymbol{g}$. Similarly for $\overrightarrow{G}^{\dagger}$ using $(\boldsymbol{g}^T\boldsymbol{U}^{-1})$, the inverse DFT.

From the above, we conclude that

$$H\left(\boldsymbol{f}|\boldsymbol{g},\alpha,\alpha_2,\alpha_3,\sigma\right)=\frac{1}{2\sigma^2}\left[\boldsymbol{f}-\left(\boldsymbol{I}+\sigma^2\alpha\boldsymbol{C}\left(\alpha_2,\alpha_3\right)\right)^{-1}\boldsymbol{g}\right]^T\left(\boldsymbol{I}+\sigma^2\alpha\boldsymbol{C}\left(\alpha_2,\alpha_3\right)\right)$$
$$\times\left[\boldsymbol{f}-\left(\boldsymbol{I}+\sigma^2\alpha\boldsymbol{C}\left(\alpha_2,\alpha_3\right)\right)^{-1}\boldsymbol{g}\right]+\frac{1}{2}\sum_{(p,q)\in\mathbf{V}}G^{\dagger}_{p,q}\alpha\lambda\left(\alpha_2,\alpha_3,p,q\right)\left(1+\sigma^2\alpha\lambda\left(\alpha_2,\alpha_3,p,q\right)\right)^{-1}G_{p,q}. \quad (4.36)$$

Using the variable substitution $\boldsymbol{x}=\left[\boldsymbol{z}-\left(\boldsymbol{I}+\sigma^2\alpha\boldsymbol{C}\left(\alpha_2,\alpha_3\right)\right)^{-1}\boldsymbol{g}\right]$ and $d\boldsymbol{z}=d\boldsymbol{x}$, $Z_{\text{posterior}}$ can be rewritten as

$$Z_{\text{posterior}}=\int\exp\Bigg\{-\frac{1}{2\sigma^2}\boldsymbol{x}^T\left(\boldsymbol{I}+\sigma^2\alpha\boldsymbol{C}\left(\alpha_2,\alpha_3\right)\right)\boldsymbol{x}$$
$$-\frac{1}{2}\sum_{(p,q)\in\mathbf{V}}G^{\dagger}_{p,q}\alpha\lambda\left(\alpha_2,\alpha_3,p,q\right)\left(1+\sigma^2\alpha\lambda\left(\alpha_2,\alpha_3,p,q\right)\right)^{-1}G_{p,q}\Bigg\}d\boldsymbol{x} \quad (4.37)$$

which, using the multidimensional Gaussian integral becomes

$$Z_{\text{posterior}}=\left(2\pi\sigma^2\right)^{\frac{|\mathbf{V}|}{2}}\left\{\det\left(\boldsymbol{I}+\sigma^2\alpha\boldsymbol{C}\left(\alpha_2,\alpha_3\right)\right)\right\}^{-\frac{1}{2}}$$
$$\times\exp\left\{-\frac{1}{2}\sum_{(p,q)\in\mathbf{V}}G^{\dagger}_{p,q}\alpha\lambda\left(\alpha_2,\alpha_3,p,q\right)\left(1+\sigma^2\alpha\lambda\left(\alpha_2,\alpha_3,p,q\right)\right)^{-1}G_{p,q}\right\}. \quad (4.38)$$

The determinant in equation (4.38) can be rewritten as

$$\det\left(\boldsymbol{I}+\alpha\sigma^2\boldsymbol{C}\left(\alpha_2,\alpha_3\right)\right)=\prod_{(p,q)\in\mathbf{V}}\left(1+\alpha\sigma^2\lambda(\alpha_2,\alpha_3,p,q)\right)\quad\text{(See equation (2.47)).} \quad (4.39)$$

So equation (4.38) can be transformed into

$$Z_{\text{posterior}}=\left(2\pi\sigma^2\right)^{\frac{|\mathbf{V}|}{2}}\left\{\prod_{(p,q)\in\mathbf{V}}\left(1+\alpha\sigma^2\lambda(\alpha_2,\alpha_3,p,q)\right)\right\}^{-\frac{1}{2}}$$
$$\times\exp\left\{-\frac{1}{2}\sum_{(p,q)\in\mathbf{V}}G^{\dagger}_{p,q}\alpha\lambda\left(\alpha_2,\alpha_3,p,q\right)\left(1+\sigma^2\alpha\lambda\left(\alpha_2,\alpha_3,p,q\right)\right)^{-1}G_{p,q}\right\}. \quad (4.40)$$

4.2.3 Restored Image Equation

In our model, the estimated restored image configuration is given by the expected value of the a posteriori probability function. This gives us the following restored image equation:

$$\widehat{\boldsymbol{f}} \equiv \int \boldsymbol{z} \Pr\left\{\boldsymbol{F} = \boldsymbol{z} | \boldsymbol{G} = \boldsymbol{g}, \alpha, \alpha_2, \alpha_3, \sigma\right\} d\boldsymbol{z} \tag{4.41}$$

where the integral is performed over every image configuration $\boldsymbol{z}$ (range of $]-\infty, +\infty[$ for each pixel element) and $\widehat{\boldsymbol{f}}$ is our restored image.

Using (4.29) we obtain

$$\widehat{\boldsymbol{f}} = \frac{1}{Z_{\text{posterior}}\left(\boldsymbol{g}, \alpha, \alpha_2, \alpha_3, \sigma\right)} \int \boldsymbol{z} \exp\left[-H\left(\boldsymbol{z} | \boldsymbol{g}, \alpha, \alpha_2, \alpha_3, \sigma\right)\right] d\boldsymbol{z} \tag{4.42}$$

which, using the results of (4.36) and (4.38) is rewritten as

$$\begin{aligned}
\widehat{\boldsymbol{f}} = & \frac{1}{\left(2\pi\sigma^2\right)^{\frac{|\mathbf{V}|}{2}} \det\left(\sigma^2 \boldsymbol{\Sigma}^{-1}\right)^{-1/2}} \\
& \times \frac{1}{\exp\left\{-\frac{1}{2} \sum\limits_{(p,q)\in\mathbf{V}} \left[G^{\dagger}_{p,q} \alpha\lambda(\alpha_2, \alpha_3, p, q) \left(1 + \sigma^2 \alpha\lambda(\alpha_2, \alpha_3, p, q)\right)^{-1} G_{p,q}\right]\right\}} \\
& \times \int \boldsymbol{z} \exp\Bigg(-\frac{1}{2\sigma^2} \left[\boldsymbol{z} - \boldsymbol{\mu}\right]^T \sigma^2 \boldsymbol{\Sigma}^{-1} \left[\boldsymbol{z} - \boldsymbol{\mu}\right] \\
& \quad - \frac{1}{2} \sum_{(p,q)\in\mathbf{V}} \left[G^{\dagger}_{p,q} \alpha\lambda(\alpha_2, \alpha_3, p, q) \left(1 + \sigma^2 \alpha\lambda(\alpha_2, \alpha_3, p, q)\right)^{-1} G_{p,q}\right] \Bigg) d\boldsymbol{z} \\
= & \frac{1}{\left(2\pi\right)^{\frac{|\mathbf{V}|}{2}} \det\left(\boldsymbol{\Sigma}\right)^{1/2}} \int \boldsymbol{z} \exp\left(-\frac{1}{2} \left[\boldsymbol{z} - \boldsymbol{\mu}\right]^T \boldsymbol{\Sigma}^{-1} \left[\boldsymbol{z} - \boldsymbol{\mu}\right] \right) d\boldsymbol{z}
\end{aligned} \tag{4.43}$$

with $\boldsymbol{\mu} \equiv \left(\boldsymbol{I} + \sigma^2 \alpha \boldsymbol{C}\left(\alpha_2, \alpha_3\right)\right)^{-1} \boldsymbol{g}$ and $\boldsymbol{\Sigma}^{-1} \equiv \frac{1}{\sigma^2}\left(\boldsymbol{I} + \sigma^2 \alpha \boldsymbol{C}\left(\alpha_2, \alpha_3\right)\right)$, which corresponds to the expected value equation of a multivariate Gaussian distribution. Using that fact, we conclude that

$$\widehat{\boldsymbol{f}} = \mathbf{E}[\boldsymbol{z}] = \boldsymbol{\mu} = \left(\boldsymbol{I} + \sigma^2 \alpha \boldsymbol{C}\left(\alpha_2, \alpha_3\right)\right)^{-1} \boldsymbol{g}. \tag{4.44}$$

However, it is impractical to compute the inverse of such a large matrix, so we use the eigendecomposition of (4.13) to simplify the equation as follows:

$$\begin{aligned}
\widehat{\boldsymbol{f}} &= \left[\boldsymbol{I} + \sigma^2 \alpha \left(\boldsymbol{U}^{-1} \boldsymbol{\Lambda} \boldsymbol{U}\right)\right]^{-1} \boldsymbol{g} \\
&= \boldsymbol{U}^{-1} \left(\boldsymbol{I} + \sigma^2 \alpha \boldsymbol{\Lambda}\right)^{-1} \boldsymbol{U} \boldsymbol{g} \\
&= \boldsymbol{U}^{-1} \left(\boldsymbol{I} + \sigma^2 \alpha \boldsymbol{\Lambda}\right)^{-1} \overrightarrow{G}
\end{aligned} \tag{4.45}$$

Here we note that this corresponds to the inverse DFT of $\left(\boldsymbol{I} + \sigma^2 \alpha \boldsymbol{\Lambda}\right)^{-1} \overrightarrow{G}$ where $\overrightarrow{G}$ is itself the DFT of the degraded image. $\left(\boldsymbol{I} + \sigma^2 \alpha \boldsymbol{\Lambda}\right)^{-1}$ can also easily be computed since it is the inverse of a diagonal matrix.

4.2.4 Hyperparameters Estimation

As we saw in section 4.2.3, the restored image equation depends on the values of the hyperparameters σ, α, α_2 and α_3. The selection of those values shall be done by fixing the values of α_2 and α_3 and then choosing values for σ and α that maximize the evidence (or likelihood) of equation (4.27). Such a method is known as Maximum Likelihood Estimation (MLE).

Using (4.27) with (2.1), (4.5) and (4.29), we find that the evidence is given by

$$\Pr\left\{\boldsymbol{G} = \boldsymbol{g} | \alpha, \alpha_2, \alpha_3, \sigma\right\} = \frac{\Pr\left\{\boldsymbol{G} = \boldsymbol{g} | \boldsymbol{F} = \boldsymbol{f}, \sigma\right\} \Pr\left\{\boldsymbol{F} = \boldsymbol{f} | \alpha, \alpha_2, \alpha_3\right\}}{\Pr\left\{\boldsymbol{F} = \boldsymbol{f} | \boldsymbol{G} = \boldsymbol{g}, \alpha, \alpha_2, \alpha_3, \sigma\right\}}$$

$$= \frac{\frac{1}{Z_{\text{noise}}(\sigma)} \exp\left(-\frac{1}{2\sigma^2}\left\|\boldsymbol{g}-\boldsymbol{f}\right\|^2\right) \frac{1}{Z_{\text{prior}}(\alpha,\alpha_2,\alpha_3)} \exp\left\{-\frac{1}{2}\alpha \boldsymbol{f}^T \boldsymbol{C}\left(\alpha_2,\alpha_3\right)\boldsymbol{f}\right\}}{\frac{1}{Z_{\text{posterior}}(\boldsymbol{g},\alpha,\alpha_2,\alpha_3,\sigma)} \exp\left\{-\frac{1}{2\sigma^2}\left\|\boldsymbol{g}-\boldsymbol{f}\right\|^2 - \frac{1}{2}\alpha \boldsymbol{f}^T \boldsymbol{C}\left(\alpha_2,\alpha_3\right)\boldsymbol{f}\right\}}$$
$$= \frac{Z_{\text{posterior}}(\boldsymbol{g},\alpha,\alpha_2,\alpha_3,\sigma)}{Z_{\text{noise}}(\sigma) Z_{\text{prior}}(\alpha,\alpha_2,\alpha_3)}. \tag{4.46}$$

We can simplify the calculations by finding the maximum of the log of the evidence, which gives us

$$\begin{aligned}(\widehat{\alpha},\widehat{\sigma}) &= \arg\ \max_{\alpha,\sigma}\left[\ln Z_{\text{posterior}}(\boldsymbol{g},\alpha,\alpha_2,\alpha_3,\sigma) - \ln Z_{\text{noise}}(\sigma) - \ln Z_{\text{prior}}(\alpha,\alpha_2,\alpha_3)\right] \\ &= \arg\ \max_{\alpha,\sigma}\Bigg[-\frac{|\mathbf{V}|}{2}\ln(2\pi) + \frac{|\mathbf{V}|}{2}\ln\alpha - \frac{1}{2}\sum_{(p,q)\in\mathbf{V}} \ln\left(1+\alpha\sigma^2\lambda(\alpha_2,\alpha_3,p,q)\right) \\ &\quad - \frac{1}{2}\sum_{(p,q)\in\mathbf{V}} G^{\dagger}_{p,q}\alpha\lambda(\alpha_2,\alpha_3,p,q)\left(1+\sigma^2\alpha\lambda(\alpha_2,\alpha_3,p,q)\right)^{-1} G_{p,q} \\ &\quad + \frac{1}{2}\sum_{(p,q)\in\mathbf{V}} \ln\lambda(\alpha_2,\alpha_3,p,q)\Bigg].\end{aligned} \tag{4.47}$$

where $\widehat{\alpha}$ and $\widehat{\sigma}$ are the estimated values of the hyperparameters α and σ respectively.

Using the above, we find the value of $\widehat{\sigma}$ by solving the equation $\frac{d}{d\widehat{\sigma}^2}\ln(\Pr\{\boldsymbol{G}=\boldsymbol{g}|\widehat{\alpha},\alpha_2,\alpha_3,\widehat{\sigma}\}) = 0$ to obtain

$$\widehat{\sigma}^2 = \frac{\widehat{\sigma}^2}{|\mathbf{V}|}\sum_{(p,q)\in\mathbf{V}}\left\{\frac{1}{1+\widehat{\alpha}\widehat{\sigma}^2\lambda(\alpha_2,\alpha_3,p,q)} + \widehat{\sigma}^2 G^{\dagger}_{p,q}\left(\frac{\widehat{\alpha}\lambda(\alpha_2,\alpha_3,p,q)}{1+\widehat{\alpha}\widehat{\sigma}^2\lambda(\alpha_2,\alpha_3,p,q)}\right)^2 G_{p,q}\right\}. \tag{4.48}$$

The details of the computation are the same as in equation (2.64).

Similarly, we find the value $\widehat{\alpha}$ by solving the equation $\frac{d}{d\widehat{\alpha}}\ln(\Pr\{\boldsymbol{G}=\boldsymbol{g}|\widehat{\alpha},\alpha_2,\alpha_3,\widehat{\sigma}\}) = 0$ to obtain

$$\widehat{\alpha}^{-1} = \frac{1}{|\mathbf{V}|}\sum_{(p,q)\in\mathbf{V}}\left\{\frac{\widehat{\sigma}^2\lambda(\alpha_2,\alpha_3,p,q)}{1+\widehat{\alpha}\widehat{\sigma}^2\lambda(\alpha_2,\alpha_3,p,q)} + \frac{G^{\dagger}_{p,q}\lambda(\alpha_2,\alpha_3,p,q)G_{p,q}}{\left(1+\widehat{\alpha}\widehat{\sigma}^2\lambda(\alpha_2,\alpha_3,p,q)\right)^2}\right\} \tag{4.49}$$

Refer to equation (2.65) for the detailed computation.

When actually computing the value of the log of the evidence given in (4.47), we notice that the value of the last term diverges when $\lambda(\alpha_2,\alpha_3,p,q)=0$. We have not yet found a way to get around this problem, so we do not compute the value of the evidence in our algorithm. This is not a major problem since our algorithm depends on the derivates of the evidence and not on the actual value of the evidence.

4.3 Algorithm

In this section, we describe an image restoration algorithm based on our image restoration model. We use a fixed point iteration algorithm [12] to find our maximum likelihood estimates for the hyperparameters α and σ. As we saw in section 4.2.4, the extremum values for the hyperparameters α and σ can be expressed in the form of the simultaneous recursive equations $\alpha(r) = f(\alpha(r-1),\sigma(r-1))$ and $\sigma(r) = g(\alpha(r-1),\sigma(r-1))$. Therefore, in our algorithm, we find new values of $\widehat{\alpha}$ and $\widehat{\sigma}$ by applying their current values to equations (4.48) and (4.49) and repeat that process until the algorithm converges. We shall assume that the algorithm has converged once we achieve the following halting criterion:

$$e_1(r) = \left|\frac{a(r)-a(r-1)}{a(r-1)}\right| + \left|\frac{b(r)-b(r-1)}{b(r-1)}\right| < 10^{-4} \tag{4.50}$$

where $a(x)$ and $b(x)$ are the values of $\widehat{\alpha}$ and $\widehat{\sigma}^2$, respectively, at iteration x of the algorithm and r and $r-1$ are the current and previous iterations of the algorithm, respectively.

4.3.1 Algorithm Steps

Following are the steps of the practical algorithm.

Step 1.

(i) Compute the DFT of the degraded image to obtain the value of G. We note here that $G^\dagger$ is simply the complex conjugate of G so it does not need to be computed explicitly.

(ii) Compute the values of $\lambda(\alpha_2, \alpha_3, p, q)$ using equation (4.25).

(iii) Initialize $a(0)$ to 0.0001

(iv) Initialize $b(0)$ to 10000.

(v) Initialize r to 0.

Step 2.

(i) Update $r \leftarrow r + 1$.

(ii) Using equation (4.49), update

$$a(r) \leftarrow \left(\frac{1}{|\mathbf{V}|} \times \sum_{(p,q)\in\mathbf{V}} \left\{ \frac{b(r-1)\lambda(\alpha_2,\alpha_3,p,q)}{1+a(r-1)b(r-1)\lambda(\alpha_2,\alpha_3,p,q)} + \frac{G^\dagger_{p,q}G_{p,q}\lambda(\alpha_2,\alpha_3,p,q)}{(1+a(r-1)b(r-1)\lambda(\alpha_2,\alpha_3,p,q))^2} \right\} \right)^{-1}. \tag{4.51}$$

(iii) Using equation (4.48), update

$$b(r) \leftarrow \frac{b(r-1)}{|\mathbf{V}|} \sum_{(p,q)\in\mathbf{V}} \left\{ \frac{1}{1+a(r-1)b(r-1)\lambda(\alpha_2,\alpha_3,p,q)} + b(r-1)G^\dagger_{p,q}G_{p,q} \left(\frac{a(r-1)\lambda(\alpha_2,\alpha_3,p,q)}{1+a(r-1)b(r-1)\lambda(\alpha_2,\alpha_3,p,q)} \right)^2 \right\}. \tag{4.52}$$

Here we note that since $\overrightarrow{G}^\dagger$ is the conjugate transpose of $\overrightarrow{G}$, we can write $G_{p,q} = a + bi$ and $G^\dagger_{p,q} = a - bi$, so that $G^\dagger_{p,q}G_{p,q}$ is simply $a^2 + b^2$.

Step 3.

(i) Check the termination condition of equation (4.50).

(ii) If the termination condition is fulfilled, proceed to step 4. Otherwise go back to step 2.

Step 4.

(i) Update $\widehat{\alpha} \leftarrow a(r)$.

(ii) Update $\widehat{\sigma} \leftarrow \sqrt{b(r)}$.

(iii) Compute the values of $\left(1 + \widehat{\sigma}^2\lambda\left(\alpha_2, \alpha_3, p, q\right)\widehat{\alpha}\right)^{-1} G_{p,q}$ for each p and q.

(iv) Apply the inverse DFT to the above values to obtain the restored image as described in (4.45).

4.3.2 Computational Complexity

We now analyse the complexity of our algorithm using the Big O notation. Here n is the number of pixels in the image, so $n = |\mathbf{V}|$.

Step 1 DFT computation using the FFT algorithm: $O(n \log n)$.

Step 2 Computation of $\widehat{\alpha}(r)$: $O(n)$.
Computation of $\widehat{\sigma}(r)$: $O(n)$.
Total: $O(n)$.

Step 3 Computation of $e_1(r)$: $O(1)$.
Total: $O(1)$.

Step 4 Computation of the values to be used in the inverse DFT: $O(n)$.
Restored image computation using the FFT algorithm: $O(n \log n)$.
Total: $O(n \log n)$.

This gives a total complexity of $O(n \log n)$.

4.4 Numerical Experiments

In this section, we present the numerical experiments we performed to evaluate our model as well as the results of these experiments. We also discuss these results.

4.4.1 Experiments

We tested our algorithm against the original 256x256 pixels 8-bit grayscale images $\boldsymbol{f}$ presented in Fig.2.1, using the same degraded images $\boldsymbol{g}$ as those introduced in section 2.4.1. Examples of the degraded images are presented in Fig.2.2. We then applied our restoration algorithm to the degraded images to obtain the restored images $\widehat{\boldsymbol{f}}$. Examples of the resulting restored images are shown in Fig.4.10 to Fig.4.20.

4.4.2 Experimental Results

Our results are generated by fixing the values of $\alpha_2 = \frac{\widehat{\alpha}'}{\widehat{\alpha}}$ and $\alpha_3 = \frac{\widehat{\alpha}''}{\widehat{\alpha}}$ and applying our model to restore each set of 10 degraded images described in section 2.4.1 to obtain restored image sets containing 10 restored images for each combination of the values of α_2 and α_3, σ and each original image. We apply that procedure for values of α_2 and α_3 in the range of $]-0.5, 0.5[$ with a step of 0.1 (we use the values -0.49 and 0.49 as the higher and lower bounds).

We then measure the value of the the mean square error (MSE) and the mean structural similarity index (MSSIM) between the original image and the restored image for each restored image. These measurements allow us to calculate the sample mean of the MSE and MSSIM for each set of restored images. The MSE is used as a measure of the efficiency of our correction and is defined in equation (2.81). The MSSIM is also used as a measure of the efficiency of our correction and is described in section 2.4.2. More details about the MSE and MSSIM can be found in section 2.4.2.

Figures 4.1, 4.2 and 4.3 show, for various values of α_2 and α_3, the values of the sample mean for the MSE. By looking at these figures, we observe that the MSE has similar levels along the lines of direction $\alpha_3 = -\frac{\alpha_2}{2} + b$ for all images and noise levels. We also notice that the values of the MSE suddenly become very large in the region $\alpha_3 < -\frac{\alpha_2}{2} - 0.25$ for all images and noise levels. In the case of the Boat and Lenna images, we observe the lowest values of the MSE in the region around the line $\alpha_3 = -\frac{\alpha_2}{2} - 0.25$, right next to the limit where the MSE suddenly increases dramatically. In the case of the Mandrill image, the lowest MSE is more to the right, in the region around the line $\alpha_3 = -\frac{\alpha_2}{2} + 0.1$ for both noise levels.

Figures 4.4, 4.5 and 4.6 show, for various values of $\widehat{\alpha_2}$ and α_3, the values of the sample mean for the estimated values of $\widehat{\alpha}$. By looking at these figures, we observe that the values of $\widehat{\alpha}$ become very large or even negative in the region $\alpha_3 < -\frac{\alpha_2}{2} - 0.25$ for all images and noise levels. We believe that this is due to a diverging value of the evidence in that region.

Figures 4.7, 4.8 and 4.9 show, for various values of α_2 and α_3, the values of the sample mean for the estimated values of $\widehat{\sigma}^2$. By looking at these figures, we observe again that the values of $\widehat{\sigma}^2$ become very large or even negative in the region $\alpha_3 < -\frac{\alpha_2}{2} - 0.25$ for all images and noise levels. As for $\widehat{\alpha}$, we believe that this is due to a diverging value of the evidence in that region.

Figures 4.10 to 4.20 show some results of the application of the third neighbour extension algorithm to the Boat, Lenna and Mandrill greyscale images for noise values of $\sigma = 20$ and $\sigma = 40$.

We only show the results for values of (α_2, α_3) of $(-0.2, -0.1)$ and $(-0.3, -0.1)$, since we expect these values to approach the Mexican Hat weighting function shown in Fig 1.2, the combinations producing the smallest MSE, namely $(-0.49, 0.0)$ for Boat, $(0.49, -0.49)$ and $(0.4, -0.4)$ for Lenna with $\sigma = 20$ and $\sigma = 40$ respectively, and $(-0.1, 0.0)$ for Mandrill, as well as the combinations producing the highest MSSIM, namely $(-0.3, -0.1)$ for Boat and Lenna, $(-0.1, 0)$ and $(0, 0)$ for Mandrill with $\sigma = 20$ and $\sigma = 40$ respectively. Also, only one restored image from the set of 10 is shown.

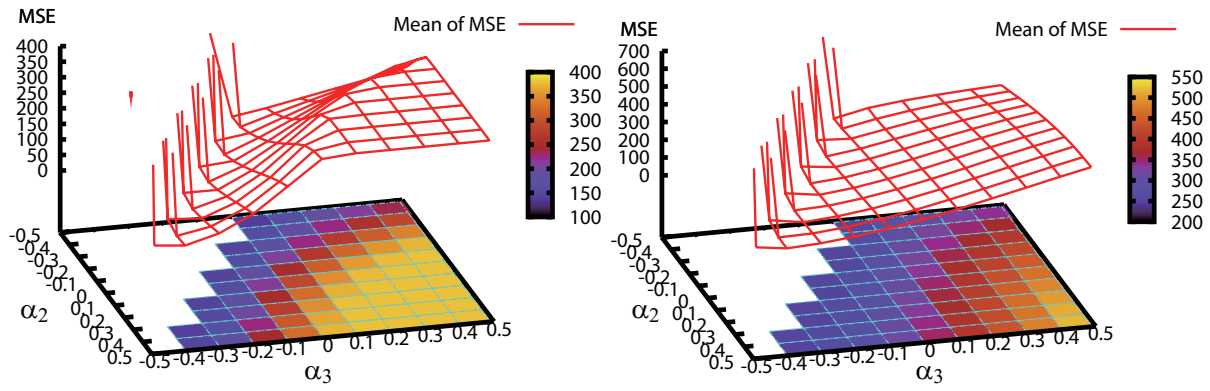

(a) $\sigma = 20$. (b) $\sigma = 40$.

Figure 4.1: Mean square error MSE($\boldsymbol{f}, \widehat{\boldsymbol{f}}$) for the restored versions of the Boat image (Fig. 2.1a). The degraded images were generated with noise levels of $\sigma = 20$ in (a) and $\sigma = 40$ in (b). The estimates $\widehat{\alpha}$ and $\widehat{\sigma}$ are obtained by maximizing $\log \Pr\{\boldsymbol{G} = \boldsymbol{g} | \alpha, \alpha_2, \alpha_3, \sigma\}$ with respect to α and σ for each fixed value of α_2 and α_3. Here, the restored image $\widehat{\boldsymbol{f}}$ is defined as $\widehat{\boldsymbol{f}}\,(\widehat{\alpha}, \alpha_2, \alpha_3, \widehat{\sigma})$ for each value of α_2 and α_3. The values shown are the sample mean values ($\overline{x}$) of the 10 degraded images for each noise level.

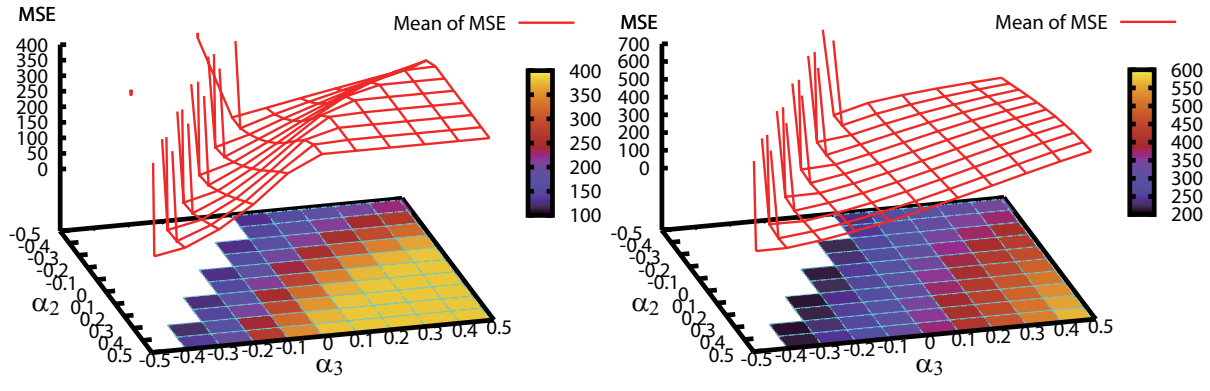

(a) $\sigma = 20$. (b) $\sigma = 40$.

Figure 4.2: Mean square error MSE($\boldsymbol{f}, \widehat{\boldsymbol{f}}$) for the restored versions of the Lenna image (Fig. 2.1b). The degraded images were generated with noise levels of $\sigma = 20$ in (a) and $\sigma = 40$ in (b). The estimates $\widehat{\alpha}$ and $\widehat{\sigma}$ are obtained by maximizing $\log \Pr\{\boldsymbol{G} = \boldsymbol{g} | \alpha, \alpha_2, \alpha_3, \sigma\}$ with respect to α and σ for each fixed value of α_2 and α_3. Here, the restored image $\widehat{\boldsymbol{f}}$ is defined as $\widehat{\boldsymbol{f}}\,(\widehat{\alpha}, \alpha_2, \alpha_3, \widehat{\sigma})$ for each value of α_2 and α_3. The values shown are the sample mean values ($\overline{x}$) of the 10 degraded images for each noise level.

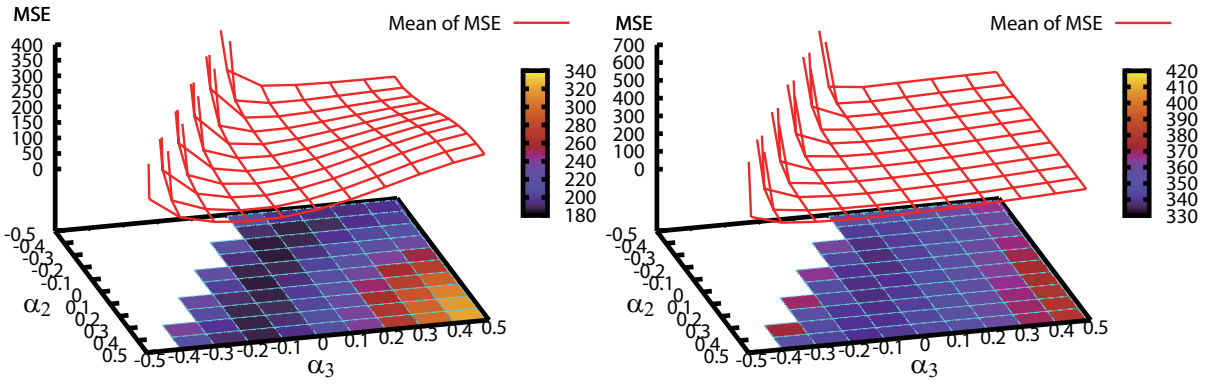

(a) $\sigma = 20$. (b) $\sigma = 40$.

Figure 4.3: Mean square error MSE($\boldsymbol{f}, \widehat{\boldsymbol{f}}$) for the restored versions of the Mandrill image (Fig. 2.1c). The degraded images were generated with noise levels of $\sigma = 20$ in (a) and $\sigma = 40$ in (b). The estimates $\widehat{\alpha}$ and $\widehat{\sigma}$ are obtained by maximizing $\log \Pr\{\boldsymbol{G} = \boldsymbol{g}|\alpha, \alpha_2, \alpha_3, \sigma\}$ with respect to α and σ for each fixed value of α_2 and α_3. Here, the restored image $\widehat{\boldsymbol{f}}$ is defined as $\widehat{\boldsymbol{f}}(\widehat{\alpha}, \alpha_2, \alpha_3, \widehat{\sigma})$ for each value of α_2 and α_3. The values shown are the sample mean values ($\overline{x}$) of the 10 degraded images for each noise level.

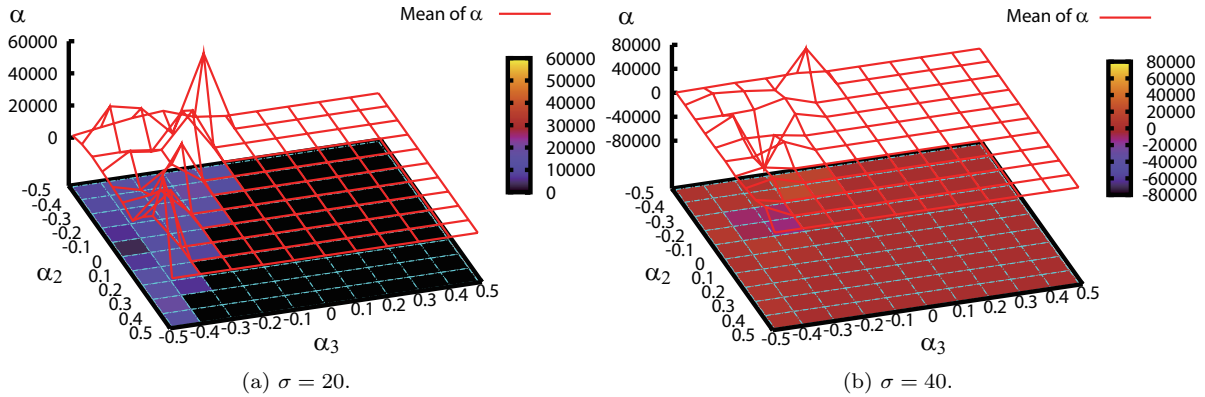

(a) $\sigma = 20$. (b) $\sigma = 40$.

Figure 4.4: Estimate $\widehat{\alpha}$ obtained from the degraded versions of the Boat image (Fig. 2.1a) for various combinations of values of α_2 and α_3. The degraded images were generated with noise levels of $\sigma = 20$ in (a) and $\sigma = 40$ in (b). The estimates are determined so as to maximize $\log \Pr\{\boldsymbol{G} = \boldsymbol{g}|\alpha, \alpha_2, \alpha_3, \sigma\}$ with respect to α and σ for each combination of the fixed values of α_2 and α_3. The values shown are the sample mean values ($\overline{x}$) of the 10 degraded images for each noise level.

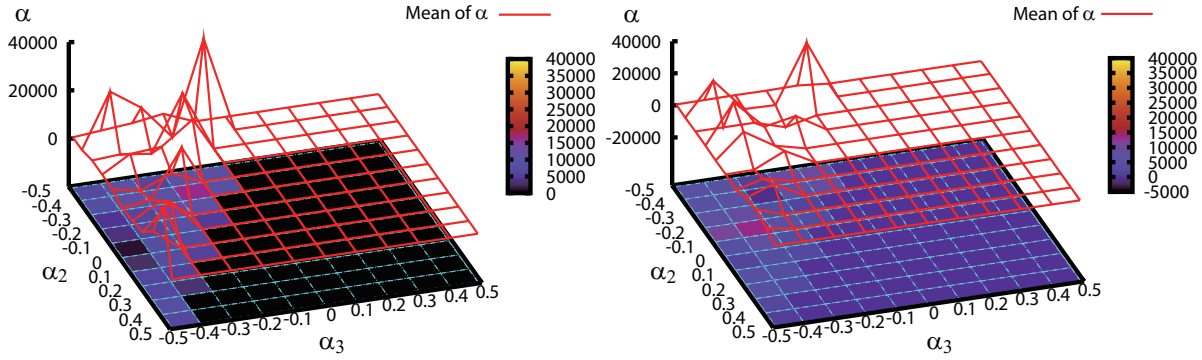

(a) $\sigma = 20$. (b) $\sigma = 40$.

Figure 4.5: Estimate $\widehat{\alpha}$ obtained from the degraded versions of the Lenna image (Fig. 2.1b) for various combinations of values of α_2 and α_3. The degraded images were generated with noise levels of $\sigma = 20$ in (a) and $\sigma = 40$ in (b). The estimates are determined so as to maximize $\log \Pr\{\boldsymbol{G} = \boldsymbol{g} | \alpha, \alpha_2, \alpha_3, \sigma\}$ with respect to α and σ for each combination of the fixed values of α_2 and α_3. The values shown are the sample mean values ($\overline{x}$) of the 10 degraded images for each noise level.

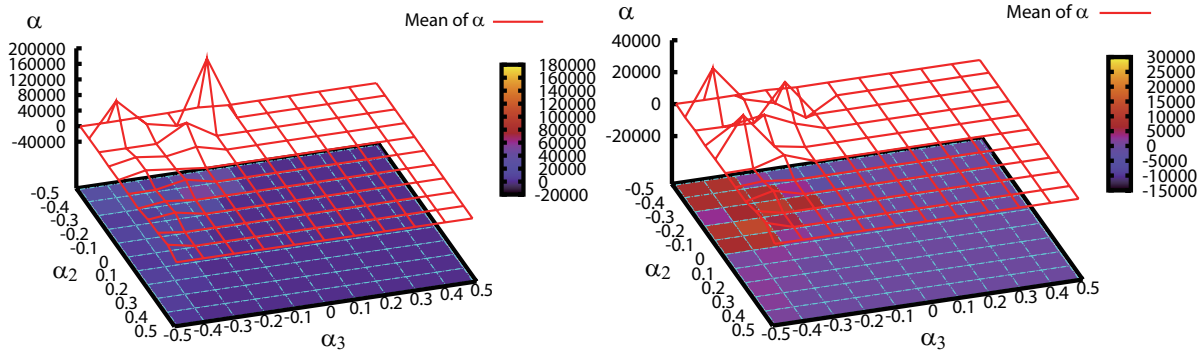

(a) $\sigma = 20$. (b) $\sigma = 40$.

Figure 4.6: Estimate $\widehat{\alpha}$ obtained from the degraded versions of the Mandrill image (Fig. 2.1c) for various combinations of values of α_2 and α_3. The degraded images were generated with noise levels of $\sigma = 20$ in (a) and $\sigma = 40$ in (b). The estimates are determined so as to maximize $\log \Pr\{\boldsymbol{G} = \boldsymbol{g} | \alpha, \alpha_2, \alpha_3, \sigma\}$ with respect to α and σ for each combination of the fixed values of α_2 and α_3. The values shown are the sample mean values ($\overline{x}$) of the 10 degraded images for each noise level.

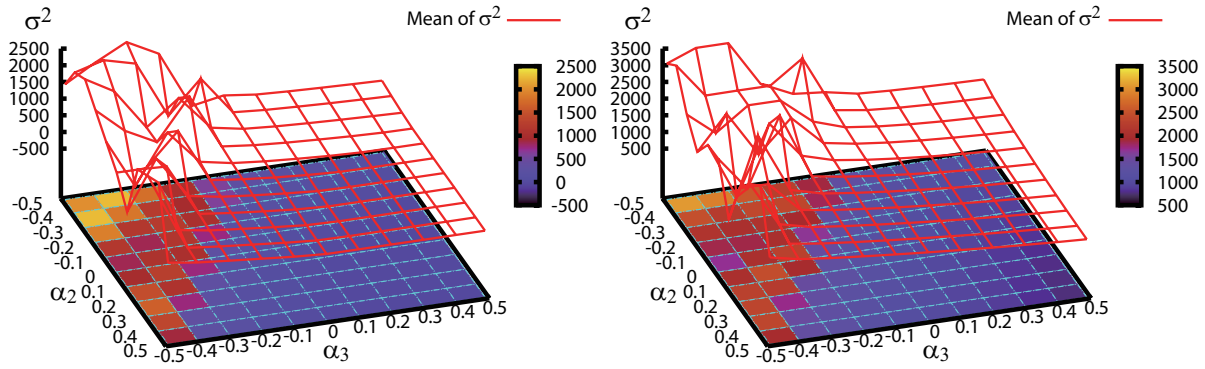

(a) $\sigma = 20$. (b) $\sigma = 40$.

Figure 4.7: Estimate $\widehat{\sigma}^2$ for the restored versions of the Boat image (Fig. 2.1a). The degraded images were generated with noise levels of $\sigma = 20$ in (a) and $\sigma = 40$ in (b). The estimate $\widehat{\sigma}$ is obtained by maximizing $\log \Pr\{\boldsymbol{G} = \boldsymbol{g} | \alpha, \alpha_2, \alpha_3, \sigma\}$ with respect to α and σ for each combination of the fixed values of α_2 and α_3. The values shown are the sample mean values ($\overline{x}$) of the 10 degraded images for each noise level.

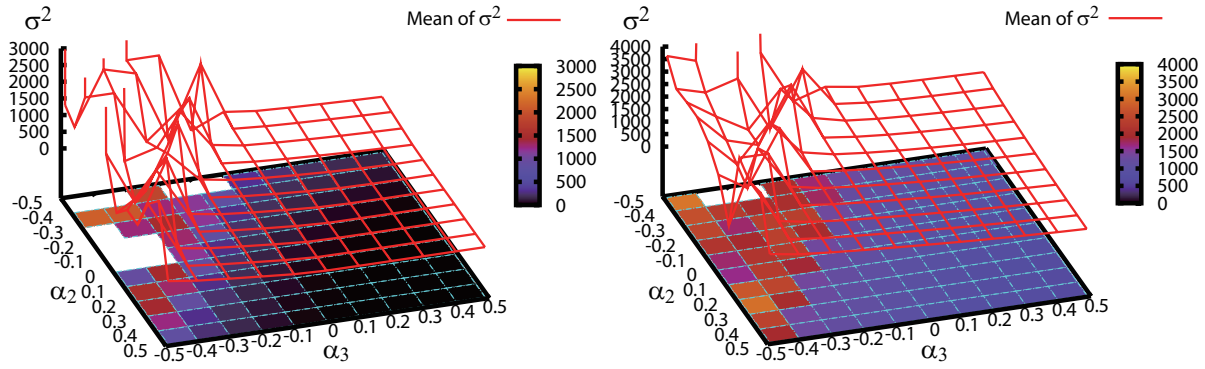

(a) $\sigma = 20$. (b) $\sigma = 40$.

Figure 4.8: Estimate $\widehat{\sigma}^2$ for the restored versions of the Lenna image (Fig. 2.1b). The degraded images were generated with noise levels of $\sigma = 20$ in (a) and $\sigma = 40$ in (b). The estimate $\widehat{\sigma}$ is obtained by maximizing $\log \Pr\{\boldsymbol{G} = \boldsymbol{g} | \alpha, \alpha_2, \alpha_3, \sigma\}$ with respect to α and σ for each combination of the fixed values of α_2 and α_3. The values shown are the sample mean values ($\overline{x}$) of the 10 degraded images for each noise level.

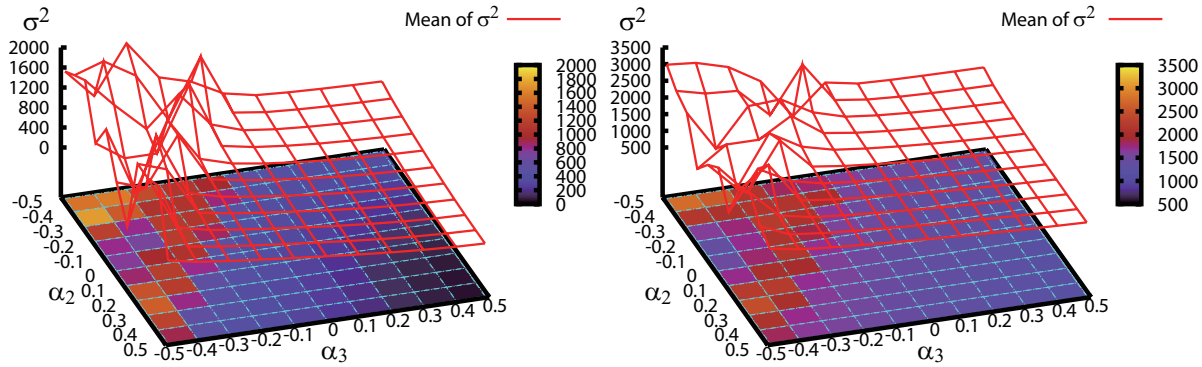

(a) $\sigma = 20$. (b) $\sigma = 40$.

Figure 4.9: Estimate $\widehat{\sigma}^2$ for the restored versions of the Mandrill image (Fig. 2.1c). The degraded images were generated with noise levels of $\sigma = 20$ in (a) and $\sigma = 40$ in (b). The estimate $\widehat{\sigma}$ is obtained by maximizing $\log \Pr\{\boldsymbol{G} = \boldsymbol{g}|\alpha, \alpha_2, \alpha_3, \sigma\}$ with respect to α and σ for each combination of the fixed values of α_2 and α_3. The values shown are the sample mean values ($\overline{x}$) of the 10 degraded images for each noise level.

A visual inspection of the corrected images for Boat (Figs 4.10 - 4.13) and Lenna (Figs 4.14 - 4.17) reveals that, although it does not produce the lowest MSE nor the highest MSSIM, the best correction, from a human perception point of view, is achieved with values of $(\alpha_2, \alpha_3) = (-0.2, -0.1)$. Indeed that choice of values offers good noise reduction with less blurring than with $(\alpha_2, \alpha_3) = (-0.3, -0.1)$ and without the introduction of artefacts such as the horizontal-vertical grid-like artefacts observed in the boat images with the lowest MSE as well as the diagonal grid-like artefacts observed in the Lenna images with the lowest MSE. However, in the case of the Mandrill images (Figs 4.18 - 4.21), the best correction from a human perception point of view matches the image with the highest MSSIM and is obtained with values of $(\alpha_2, \alpha_3) = (0.0, 0.0)$. This is probably due to the fact that a stronger correction (larger absolute values of α_2 and α_3) tends to blur the texture of the fur too much. Also, from a visual point of view, it is difficult to distinguish the noise from the texture of the fur.

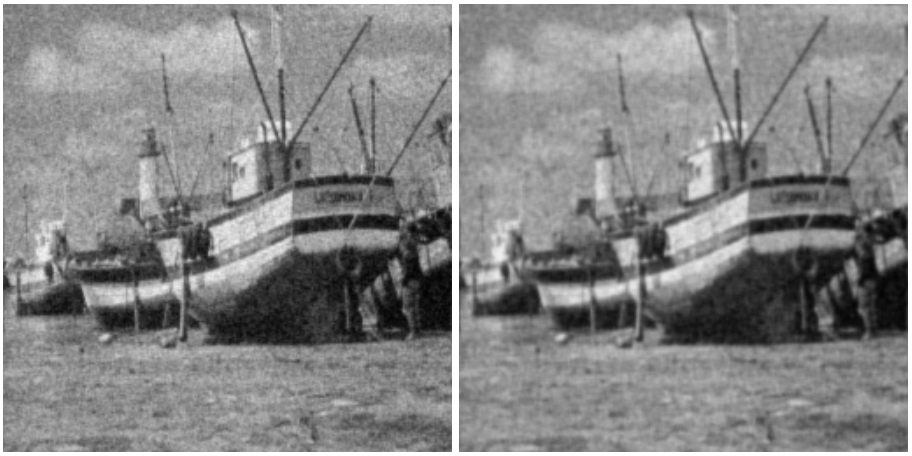

(a) $(\alpha_2, \alpha_3) = (-0.2, -0.1)$. MSE=127. MSSIM=0.7078.

(b) $(\alpha_2, \alpha_3) = (-0.3, -0.1)$. MSE=130. MSSIM=0.7550.

(c) $(\alpha_2, \alpha_3) = (-0.49, 0.0)$. MSE=124. MSSIM=0.7461.

Figure 4.10: Restored images $\widehat{\boldsymbol{f}}(\boldsymbol{g}, \widehat{\alpha}, \alpha_2, \alpha_3, \widehat{\sigma})$ obtained by means of the proposed Gauss-Markov random field model for one of the degraded versions of the Boat image (Fig. 2.1a). The degraded image was generated with a noise level of $\sigma = 20$ and is shown in Fig. 2.12a. (a) $\alpha_2 = -0.2$, $\alpha_3 = -0.1$, $\mathrm{MSE}(\boldsymbol{f}, \widehat{\boldsymbol{f}}(\boldsymbol{g}, \widehat{\alpha}, \alpha_2, \alpha_3, \widehat{\sigma})) = 127$, $\mathrm{MSSIM}(\boldsymbol{f}, \widehat{\boldsymbol{f}}(\boldsymbol{g}, \widehat{\alpha}, \alpha_2, \alpha_3, \widehat{\sigma})) = 0.7078$. (b) $\alpha_2 = -0.3$, $\alpha_3 = -0.1$, $\mathrm{MSE}(\boldsymbol{f}, \widehat{\boldsymbol{f}}(\boldsymbol{g}, \widehat{\alpha}, \alpha_2, \alpha_3, \widehat{\sigma})) = 130$, $\mathrm{MSSIM}(\boldsymbol{f}, \widehat{\boldsymbol{f}}(\boldsymbol{g}, \widehat{\alpha}, \alpha_2, \alpha_3, \widehat{\sigma})) = 0.7550$. (c) $\alpha_2 = -0.49$, $\alpha_3 = 0.0$, $\mathrm{MSE}(\boldsymbol{f}, \widehat{\boldsymbol{f}}(\boldsymbol{g}, \widehat{\alpha}, \alpha_2, \alpha_3, \widehat{\sigma})) = 124$, $\mathrm{MSSIM}(\boldsymbol{f}, \widehat{\boldsymbol{f}}(\boldsymbol{g}, \widehat{\alpha}, \alpha_2, \alpha_3, \widehat{\sigma})) = 0.7461$.

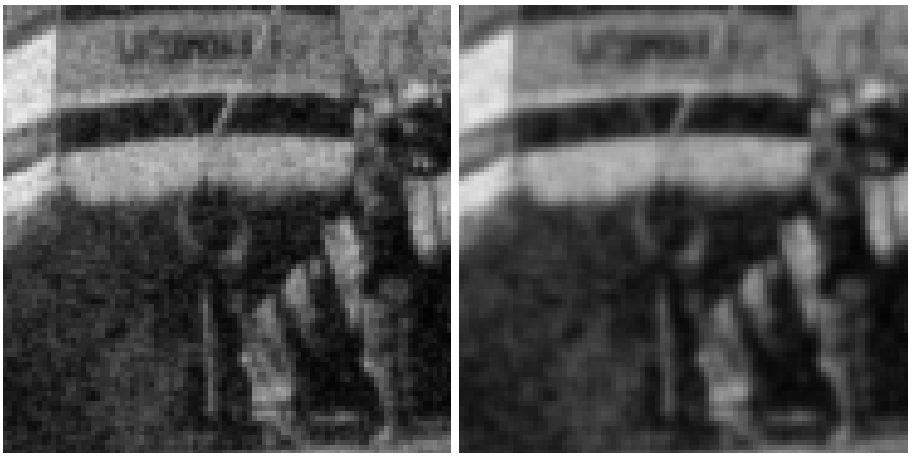

(a) $(\alpha_2, \alpha_3) = (-0.2, -0.1)$. MSE=127. MSSIM=0.7078.

(b) $(\alpha_2, \alpha_3) = (-0.3, -0.1)$. MSE=130. MSSIM=0.7550.

(c) $(\alpha_2, \alpha_3) = (-0.49, 0.0)$. MSE=124. MSSIM=0.7461.

Figure 4.11: Details of the restored images $\widehat{\boldsymbol{f}}(\boldsymbol{g}, \widehat{\alpha}, \alpha_2, \alpha_3, \widehat{\sigma})$ in Fig. 4.10. (a) Restored image $\widehat{\boldsymbol{f}}(\boldsymbol{g}, \widehat{\alpha}, \alpha_2, \alpha_3, \widehat{\sigma})$ in Fig. 4.10a. (b) Restored image $\widehat{\boldsymbol{f}}(\boldsymbol{g}, \widehat{\alpha}, \alpha_2, \alpha_3, \widehat{\sigma})$ in Fig. 4.10b. (c) Restored image $\widehat{\boldsymbol{f}}(\boldsymbol{g}, \widehat{\alpha}, \alpha_2, \alpha_3, \widehat{\sigma})$ in Fig. 4.10c.

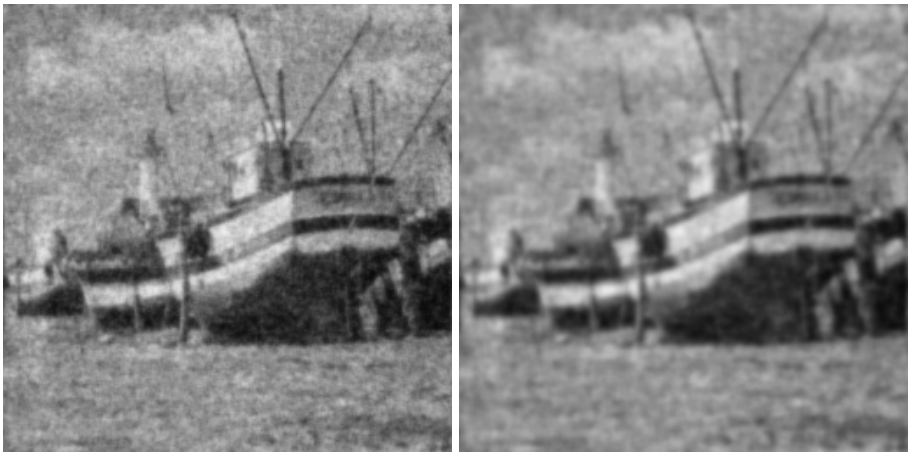

(a) $(\alpha_2, \alpha_3) = (-0.2, -0.1)$. MSE=239. MSSIM=0.6049.

(b) $(\alpha_2, \alpha_3) = (-0.3, -0.1)$. MSE=263. MSSIM=0.6246.

(c) $(\alpha_2, \alpha_3) = (-0.49, 0.0)$. MSE=236. MSSIM=0.6189.

Figure 4.12: Restored images $\widehat{\boldsymbol{f}}(\boldsymbol{g}, \widehat{\alpha}, \alpha_2, \alpha_3, \widehat{\sigma})$ obtained by means of the proposed Gauss-Markov random field model for one of the degraded versions of the Boat image (Fig. 2.1a). The degraded image was generated with a noise level of $\sigma = 40$ and is shown in Fig. 2.14a. (a) $\alpha_2 = -0.2$, $\alpha_3 = -0.1$, $\mathrm{MSE}(\boldsymbol{f}, \widehat{\boldsymbol{f}}(\boldsymbol{g}, \widehat{\alpha}, \alpha_2, \alpha_3, \widehat{\sigma})) = 239$, $\mathrm{MSSIM}(\boldsymbol{f}, \widehat{\boldsymbol{f}}(\boldsymbol{g}, \widehat{\alpha}, \alpha_2, \alpha_3, \widehat{\sigma})) = 0.6049$. (b) $\alpha_2 = -0.3$, $\alpha_3 = -0.1$, $\mathrm{MSE}(\boldsymbol{f}, \widehat{\boldsymbol{f}}(\boldsymbol{g}, \widehat{\alpha}, \alpha_2, \alpha_3, \widehat{\sigma})) = 263$, $\mathrm{MSSIM}(\boldsymbol{f}, \widehat{\boldsymbol{f}}(\boldsymbol{g}, \widehat{\alpha}, \alpha_2, \alpha_3, \widehat{\sigma})) = 0.6246$. (c) $\alpha_2 = -0.49$, $\alpha_3 = 0.0$, $\mathrm{MSE}(\boldsymbol{f}, \widehat{\boldsymbol{f}}(\boldsymbol{g}, \widehat{\alpha}, \alpha_2, \alpha_3, \widehat{\sigma})) = 236$, $\mathrm{MSSIM}(\boldsymbol{f}, \widehat{\boldsymbol{f}}(\boldsymbol{g}, \widehat{\alpha}, \alpha_2, \alpha_3, \widehat{\sigma})) = 0.6189$.

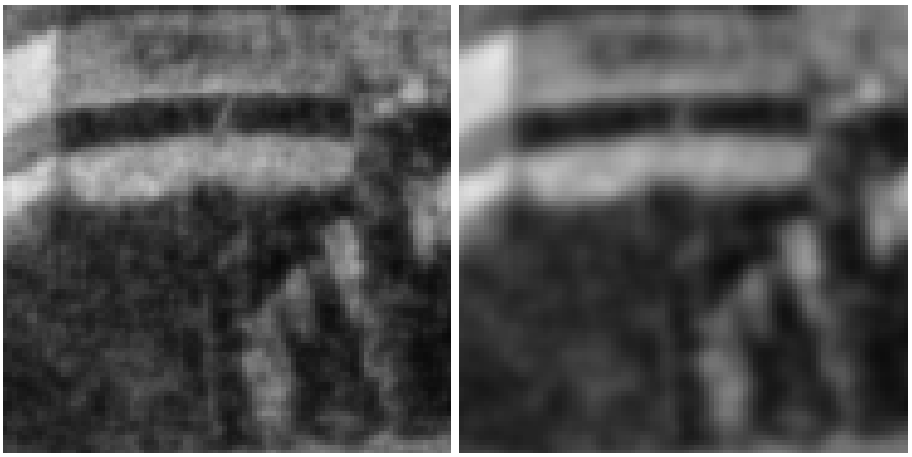

(a) $(\alpha_2, \alpha_3) = (-0.2, -0.1)$. MSE=239. MSSIM=0.6049.

(b) $(\alpha_2, \alpha_3) = (-0.3, -0.1)$. MSE=263. MSSIM=0.6246.

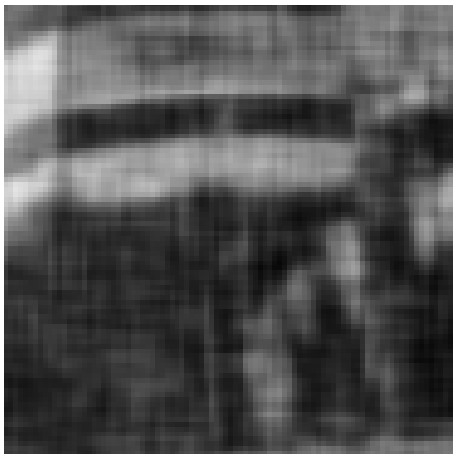

(c) $(\alpha_2, \alpha_3) = (-0.49, 0.0)$. MSE=236. MSSIM=0.6189.

Figure 4.13: Details of the restored images $\widehat{\boldsymbol{f}}(\boldsymbol{g}, \widehat{\alpha}, \alpha_2, \alpha_3, \widehat{\sigma})$ in Fig. 4.12. (a) Restored image $\widehat{\boldsymbol{f}}(\boldsymbol{g}, \widehat{\alpha}, \alpha_2, \alpha_3, \widehat{\sigma})$ in Fig. 4.12a. (b) Restored image $\widehat{\boldsymbol{f}}(\boldsymbol{g}, \widehat{\alpha}, \alpha_2, \alpha_3, \widehat{\sigma})$ in Fig. 4.12b. (c) Restored image $\widehat{\boldsymbol{f}}(\boldsymbol{g}, \widehat{\alpha}, \alpha_2, \alpha_3, \widehat{\sigma})$ in Fig. 4.12c.

(a) $(\alpha_2, \alpha_3) = (-0.2, -0.1)$. MSE=113. MSSIM=0.6938.

(b) $(\alpha_2, \alpha_3) = (-0.3, -0.1)$. MSE=105. MSSIM=0.7799.

(c) $(\alpha_2, \alpha_3) = (0.49, -0.49)$. MSE=104. MSSIM=0.7675.

Figure 4.14: Restored images $\widehat{\boldsymbol{f}}(\boldsymbol{g}, \widehat{\alpha}, \alpha_2, \alpha_3, \widehat{\sigma})$ obtained by means of the proposed Gauss-Markov random field model for one of the degraded versions of the Lenna image (Fig. 2.1b). The degraded image was generated with a noise level of $\sigma = 20$ and is shown in Fig. 2.16a. (a) $\alpha_2 = -0.2$, $\alpha_3 = -0.1$, $\mathrm{MSE}(\boldsymbol{f}, \widehat{\boldsymbol{f}}(\boldsymbol{g}, \widehat{\alpha}, \alpha_2, \alpha_3, \widehat{\sigma})) = 113$, $\mathrm{MSSIM}(\boldsymbol{f}, \widehat{\boldsymbol{f}}(\boldsymbol{g}, \widehat{\alpha}, \alpha_2, \alpha_3, \widehat{\sigma})) = 0.6938$. (b) $\alpha_2 = -0.3$, $\alpha_3 = -0.1$, $\mathrm{MSE}(\boldsymbol{f}, \widehat{\boldsymbol{f}}(\boldsymbol{g}, \widehat{\alpha}, \alpha_2, \alpha_3, \widehat{\sigma})) = 105$, $\mathrm{MSSIM}(\boldsymbol{f}, \widehat{\boldsymbol{f}}(\boldsymbol{g}, \widehat{\alpha}, \alpha_2, \alpha_3, \widehat{\sigma})) = 0.7799$. (c) $\alpha_2 = 0.49$, $\alpha_3 = -0.49$, $\mathrm{MSE}(\boldsymbol{f}, \widehat{\boldsymbol{f}}(\boldsymbol{g}, \widehat{\alpha}, \alpha_2, \alpha_3, \widehat{\sigma})) = 104$, $\mathrm{MSSIM}(\boldsymbol{f}, \widehat{\boldsymbol{f}}(\boldsymbol{g}, \widehat{\alpha}, \alpha_2, \alpha_3, \widehat{\sigma})) = 0.7675$.

(a) $(\alpha_2, \alpha_3) = (-0.2, -0.1)$. MSE=113. MSSIM=0.6938.

(b) $(\alpha_2, \alpha_3) = (-0.3, -0.1)$. MSE=105. MSSIM=0.7799.

(c) $(\alpha_2, \alpha_3) = (0.49, -0.49)$. MSE=104. MSSIM=0.7675.

Figure 4.15: Details of the restored images $\widehat{\boldsymbol{f}}(\boldsymbol{g}, \widehat{\alpha}, \alpha_2, \alpha_3, \widehat{\sigma})$ in Fig. 4.14. (a) Restored image $\widehat{\boldsymbol{f}}(\boldsymbol{g}, \widehat{\alpha}, \alpha_2, \alpha_3, \widehat{\sigma})$ in Fig. 4.14a. (b) Restored image $\widehat{\boldsymbol{f}}(\boldsymbol{g}, \widehat{\alpha}, \alpha_2, \alpha_3, \widehat{\sigma})$ in Fig. 4.14b. (c) Restored image $\widehat{\boldsymbol{f}}(\boldsymbol{g}, \widehat{\alpha}, \alpha_2, \alpha_3, \widehat{\sigma})$ in Fig. 4.14c.

(a) $(\alpha_2, \alpha_3) = (-0.2, -0.1)$. MSE=207. MSSIM=0.6151.

(b) $(\alpha_2, \alpha_3) = (-0.3, -0.1)$. MSE=211. MSSIM=0.6910.

(c) $(\alpha_2, \alpha_3) = (0.4, -0.4)$. MSE=203. MSSIM=0.6379.

Figure 4.16: Restored images $\widehat{\boldsymbol{f}}(\boldsymbol{g}, \widehat{\alpha}, \alpha_2, \alpha_3, \widehat{\sigma})$ obtained by means of the proposed Gauss-Markov random field model for one of the degraded versions of the Lenna image (Fig. 2.1b). The degraded image was generated with a noise level of $\sigma = 40$ and is shown in Fig. 2.18a. (a) $\alpha_2 = -0.2$, $\alpha_3 = -0.1$, $\mathrm{MSE}(\boldsymbol{f}, \widehat{\boldsymbol{f}}(\boldsymbol{g}, \widehat{\alpha}, \alpha_2, \alpha_3, \widehat{\sigma})) = 207$, $\mathrm{MSSIM}(\boldsymbol{f}, \widehat{\boldsymbol{f}}(\boldsymbol{g}, \widehat{\alpha}, \alpha_2, \alpha_3, \widehat{\sigma})) = 0.6151$. (b) $\alpha_2 = -0.3$, $\alpha_3 = -0.1$, $\mathrm{MSE}(\boldsymbol{f}, \widehat{\boldsymbol{f}}(\boldsymbol{g}, \widehat{\alpha}, \alpha_2, \alpha_3, \widehat{\sigma})) = 211$, $\mathrm{MSSIM}(\boldsymbol{f}, \widehat{\boldsymbol{f}}(\boldsymbol{g}, \widehat{\alpha}, \alpha_2, \alpha_3, \widehat{\sigma})) = 0.6910$. (c) $\alpha_2 = 0.40$, $\alpha_3 = -0.40$, $\mathrm{MSE}(\boldsymbol{f}, \widehat{\boldsymbol{f}}(\boldsymbol{g}, \widehat{\alpha}, \alpha_2, \alpha_3, \widehat{\sigma})) = 203$, $\mathrm{MSSIM}(\boldsymbol{f}, \widehat{\boldsymbol{f}}(\boldsymbol{g}, \widehat{\alpha}, \alpha_2, \alpha_3, \widehat{\sigma})) = 0.6379$.

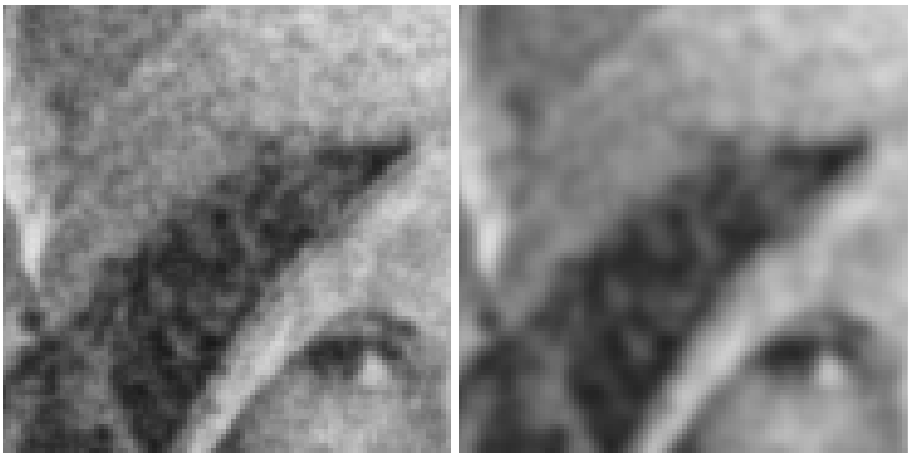

(a) $(\alpha_2, \alpha_3) = (-0.2, -0.1)$. MSE=207. MSSIM=0.6151.

(b) $(\alpha_2, \alpha_3) = (-0.3, -0.1)$. MSE=211. MSSIM=0.6910.

(c) $(\alpha_2, \alpha_3) = (0.4, -0.4)$. MSE=203. MSSIM=0.6379.

Figure 4.17: Details of the restored images $\widehat{\boldsymbol{f}}(\boldsymbol{g}, \widehat{\alpha}, \alpha_2, \alpha_3, \widehat{\sigma})$ in Fig. 4.16. (a) Restored image $\widehat{\boldsymbol{f}}(\boldsymbol{g}, \widehat{\alpha}, \alpha_2, \alpha_3, \widehat{\sigma})$ in Fig. 4.16a. (b) Restored image $\widehat{\boldsymbol{f}}(\boldsymbol{g}, \widehat{\alpha}, \alpha_2, \alpha_3, \widehat{\sigma})$ in Fig. 4.16b. (c) Restored image $\widehat{\boldsymbol{f}}(\boldsymbol{g}, \widehat{\alpha}, \alpha_2, \alpha_3, \widehat{\sigma})$ in Fig. 4.16c.

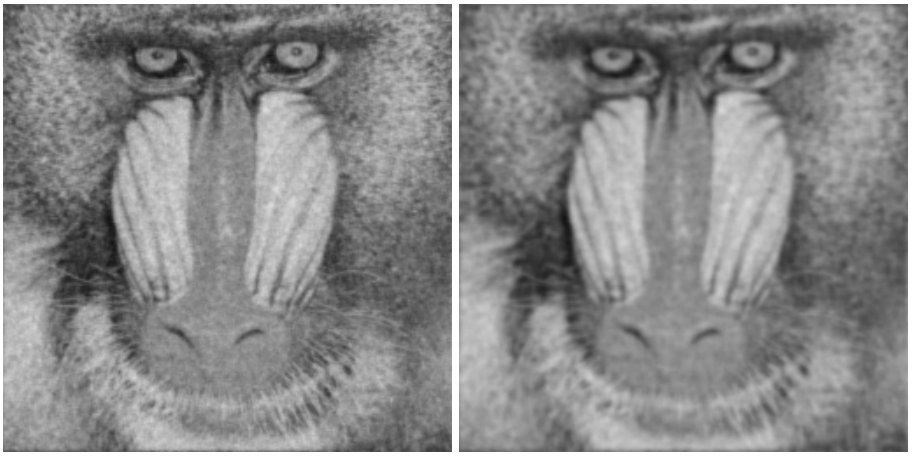

(a) $(\alpha_2, \alpha_3) = (-0.2, -0.1)$. MSE=216. MSSIM=0.6879.

(b) $(\alpha_2, \alpha_3) = (-0.3, -0.1)$. MSE=297. MSSIM=0.5868.

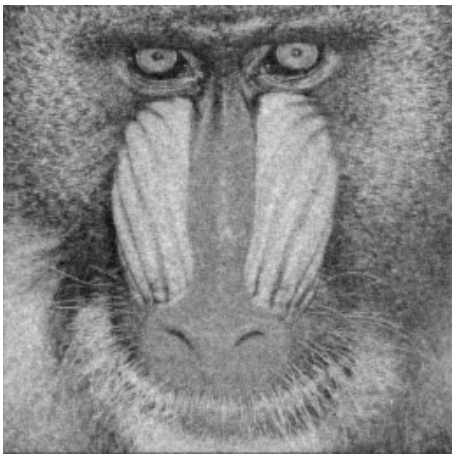

(c) $(\alpha_2, \alpha_3) = (-0.1, 0.0)$. MSE=185. MSSIM=0.7150.

Figure 4.18: Restored images $\widehat{\boldsymbol{f}}(\boldsymbol{g}, \widehat{\alpha}, \alpha_2, \alpha_3, \widehat{\sigma})$ obtained by means of the proposed Gauss-Markov random field model for one of the degraded versions of the Mandrill image (Fig. 2.1c). The degraded image was generated with a noise level of $\sigma = 20$ and is shown in Fig. 2.20a. (a) $\alpha_2 = -0.2$, $\alpha_3 = -0.1$, $\mathrm{MSE}(\boldsymbol{f}, \widehat{\boldsymbol{f}}(\boldsymbol{g}, \widehat{\alpha}, \alpha_2, \alpha_3, \widehat{\sigma})) = 216$, $\mathrm{MSSIM}(\boldsymbol{f}, \widehat{\boldsymbol{f}}(\boldsymbol{g}, \widehat{\alpha}, \alpha_2, \alpha_3, \widehat{\sigma})) = 0.6879$. (b) $\alpha_2 = -0.3$, $\alpha_3 = -0.1$, $\mathrm{MSE}(\boldsymbol{f}, \widehat{\boldsymbol{f}}(\boldsymbol{g}, \widehat{\alpha}, \alpha_2, \alpha_3, \widehat{\sigma})) = 297$, $\mathrm{MSSIM}(\boldsymbol{f}, \widehat{\boldsymbol{f}}(\boldsymbol{g}, \widehat{\alpha}, \alpha_2, \alpha_3, \widehat{\sigma})) = 0.5868$. (c) $\alpha_2 = -0.1$, $\alpha_3 = 0.0$, $\mathrm{MSE}(\boldsymbol{f}, \widehat{\boldsymbol{f}}(\boldsymbol{g}, \widehat{\alpha}, \alpha_2, \alpha_3, \widehat{\sigma})) = 185$, $\mathrm{MSSIM}(\boldsymbol{f}, \widehat{\boldsymbol{f}}(\boldsymbol{g}, \widehat{\alpha}, \alpha_2, \alpha_3, \widehat{\sigma})) = 0.7150$.

(a) $(\alpha_2, \alpha_3) = (-0.2, -0.1)$. MSE=216. MSSIM=0.6879.

(b) $(\alpha_2, \alpha_3) = (-0.3, -0.1)$. MSE=297. MSSIM=0.5868.

(c) $(\alpha_2, \alpha_3) = (-0.1, 0.0)$. MSE=185. MSSIM=0.7150.

Figure 4.19: Details of the restored images $\widehat{\boldsymbol{f}}(\boldsymbol{g}, \widehat{\alpha}, \alpha_2, \alpha_3, \widehat{\sigma})$ in Fig. 4.18. (a) Restored image $\widehat{\boldsymbol{f}}(\boldsymbol{g}, \widehat{\alpha}, \alpha_2, \alpha_3, \widehat{\sigma})$ in Fig. 4.18a. (b) Restored image $\widehat{\boldsymbol{f}}(\boldsymbol{g}, \widehat{\alpha}, \alpha_2, \alpha_3, \widehat{\sigma})$ in Fig. 4.18b. (c) Restored image $\widehat{\boldsymbol{f}}(\boldsymbol{g}, \widehat{\alpha}, \alpha_2, \alpha_3, \widehat{\sigma})$ in Fig. 4.18c.

(a) $(\alpha_2, \alpha_3) = (-0.2, -0.1)$. MSE=354. MSSIM=0.5202.

(b) $(\alpha_2, \alpha_3) = (-0.3, -0.1)$. MSE=417. MSSIM=0.4367.

(c) $(\alpha_2, \alpha_3) = (-0.1, 0.0)$. MSE=335.21. MSSIM=0.5434.

(d) $(\alpha_2, \alpha_3) = (0.0, 0.0)$. MSE=335.24. MSSIM=0.5440.

Figure 4.20: Restored images $\widehat{\boldsymbol{f}}(\boldsymbol{g}, \widehat{\alpha}, \alpha_2, \alpha_3, \widehat{\sigma})$ obtained by means of the proposed Gauss-Markov random field model for one of the degraded versions of the Mandrill image (Fig. 2.1c). The degraded image was generated with a noise level of $\sigma = 40$ and is shown in Fig. 2.22a. (a) $\alpha_2 = -0.2$, $\alpha_3 = -0.1$, $\mathrm{MSE}(\boldsymbol{f}, \widehat{\boldsymbol{f}}(\boldsymbol{g}, \widehat{\alpha}, \alpha_2, \alpha_3, \widehat{\sigma})) = 354$, $\mathrm{MSSIM}(\boldsymbol{f}, \widehat{\boldsymbol{f}}(\boldsymbol{g}, \widehat{\alpha}, \alpha_2, \alpha_3, \widehat{\sigma})) = 0.5202$. (b) $\alpha_2 = -0.3$, $\alpha_3 = -0.1$, $\mathrm{MSE}(\boldsymbol{f}, \widehat{\boldsymbol{f}}(\boldsymbol{g}, \widehat{\alpha}, \alpha_2, \alpha_3, \widehat{\sigma})) = 417$, $\mathrm{MSSIM}(\boldsymbol{f}, \widehat{\boldsymbol{f}}(\boldsymbol{g}, \widehat{\alpha}, \alpha_2, \alpha_3, \widehat{\sigma})) = 0.4367$. (c) $\alpha_2 = -0.1$, $\alpha_3 = 0.0$, $\mathrm{MSE}(\boldsymbol{f}, \widehat{\boldsymbol{f}}(\boldsymbol{g}, \widehat{\alpha}, \alpha_2, \alpha_3, \widehat{\sigma})) = 335.21$, $\mathrm{MSSIM}(\boldsymbol{f}, \widehat{\boldsymbol{f}}(\boldsymbol{g}, \widehat{\alpha}, \alpha_2, \alpha_3, \widehat{\sigma})) = 0.5434$. (d) $\alpha_2 = 0.0$, $\alpha_3 = 0.0$, $\mathrm{MSE}(\boldsymbol{f}, \widehat{\boldsymbol{f}}(\boldsymbol{g}, \widehat{\alpha}, \alpha_2, \alpha_3, \widehat{\sigma})) = 335.24$, $\mathrm{MSSIM}(\boldsymbol{f}, \widehat{\boldsymbol{f}}(\boldsymbol{g}, \widehat{\alpha}, \alpha_2, \alpha_3, \widehat{\sigma})) = 0.5440$.

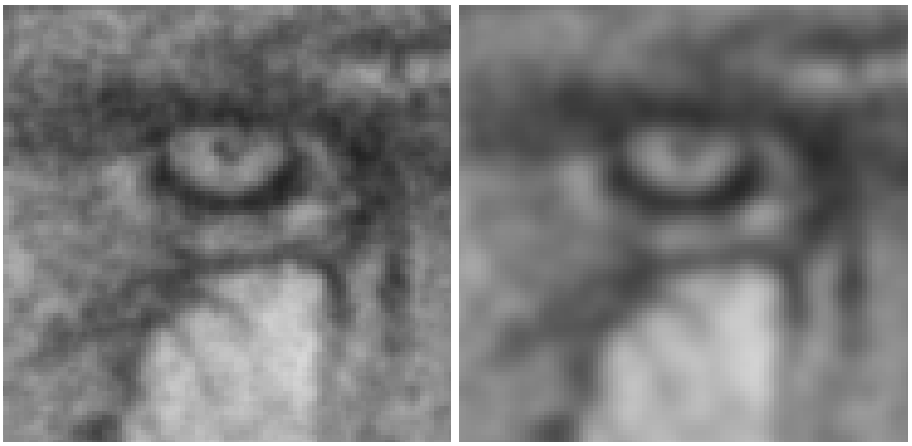

(a) $(\alpha_2, \alpha_3) = (-0.2, -0.1)$. MSE=354. MSSIM=0.5202.

(b) $(\alpha_2, \alpha_3) = (-0.3, -0.1)$. MSE=417. MSSIM=0.4367.

(c) $(\alpha_2, \alpha_3) = (-0.1, 0.0)$. MSE=335.21. MSSIM=0.5434.

(d) $(\alpha_2, \alpha_3) = (0.0, 0.0)$. MSE=335.24. MSSIM=0.5440.

Figure 4.21: Details of the restored images $\widehat{\boldsymbol{f}}(\boldsymbol{g}, \widehat{\alpha}, \alpha_2, \alpha_3, \widehat{\sigma})$ in Fig. 4.20. (a) Restored image $\widehat{\boldsymbol{f}}(\boldsymbol{g}, \widehat{\alpha}, \alpha_2, \alpha_3, \widehat{\sigma})$ in Fig. 4.20a. (b) Restored image $\widehat{\boldsymbol{f}}(\boldsymbol{g}, \widehat{\alpha}, \alpha_2, \alpha_3, \widehat{\sigma})$ in Fig. 4.20b. (c) Restored image $\widehat{\boldsymbol{f}}(\boldsymbol{g}, \widehat{\alpha}, \alpha_2, \alpha_3, \widehat{\sigma})$ in Fig. 4.20c. (d) Restored image $\widehat{\boldsymbol{f}}(\boldsymbol{g}, \widehat{\alpha}, \alpha_2, \alpha_3, \widehat{\sigma})$ in Fig. 4.20d.

4.5 Chapter Summary

In this chapter, we described our solvable probabilistic model for greyscale images using third-neighbour pixel interactions. We derived the mathematical expressions related to this model and proposed an algorithm based on these results. Finally, we presented the results of numerical experiments using our algorithm and confirmed that, with a good combination of the hyperparameters α_2 and α_3, we can generally obtain better image correction results by using our extension to the third-neighbour pixel interactions than by taking only the nearest- and second-neighbour pixel interactions into account. In particular, we saw that, for the Boat and Lenna images, by using values of (α_2, α_3) close to $(-0.2, -0.1)$, this model allows better noise reduction than the second-neighbour model without introducing too much blurring and without creating the horizontal and vertical line artefacts observed with the second-neighbour model.

Chapter 5

Solvable Probabilistic Model with Third-Neighbour Interaction for Colour Image Restoration

5.1 Chapter Outline

In this chapter, we shall describe the extension to the third-neighbour pixel interactions of the solvable probabilistic model for colour images originally proposed by Tanaka and Horiguchi in [4]. We start with a detailed description of the model as well as the calculations involved in its formation. This is followed by the presentation of an image correction algorithm based on this model before concluding with a description of the numerical experiments we performed to evaluate this model. We note that this model constitutes an extension to colour images of the model described in Chapter 4.

5.2 Model Description

In this section we describe in detail the equations that form the basis of our solvable probabilistic model with third-neighbour interaction for colour image restoration. From these equations, we also derive mathematical expressions that can be used to implement an efficient image correction algorithm. We shall use the same image and degradation process models as those for the second-neighbour extension model described in Sections 3.2.1 and 3.2.2 respectively.

5.2.1 A Priori Probability Density Function

We define the a priori probability density function (prior) that the original image $\boldsymbol{F}$ has a given configuration $\boldsymbol{f}$ as

$$\Pr\{\boldsymbol{F}=\boldsymbol{f}|\boldsymbol{\alpha},\boldsymbol{\alpha}',\boldsymbol{\alpha}''\} \equiv \frac{1}{Z_{\text{prior}}(\boldsymbol{\alpha},\boldsymbol{\alpha}',\boldsymbol{\alpha}'')}\exp\Bigg\{-\frac{1}{8}$$
$$\times\sum_{\kappa\in\mathbf{K}}\sum_{\kappa'\in\mathbf{K}}\Bigg(\alpha_{\kappa,\kappa'}\sum_{(x,y)\in\mathbf{V}}[(f_{x,y,\kappa}-f_{x+1,y,\kappa})(f_{x,y,\kappa'}-f_{x+1,y,\kappa'})+(f_{x,y,\kappa}-f_{x,y+1,\kappa})(f_{x,y,\kappa'}-f_{x,y+1,\kappa'})]$$
$$+\alpha'_{\kappa,\kappa'}\sum_{(x,y)\in\mathbf{V}}[(f_{x,y,\kappa}-f_{x+1,y+1,\kappa})(f_{x,y,\kappa'}-f_{x+1,y+1,\kappa'})+(f_{x,y,\kappa}-f_{x+1,y-1,\kappa})(f_{x,y,\kappa'}-f_{x+1,y-1,\kappa'})]$$
$$+\alpha''_{\kappa,\kappa'}\sum_{(x,y)\in\mathbf{V}}[(f_{x,y,\kappa}-f_{x+2,y,\kappa})(f_{x,y,\kappa'}-f_{x+2,y,\kappa'})+(f_{x,y,\kappa}-f_{x,y+2,\kappa})(f_{x,y,\kappa'}-f_{x,y+2,\kappa'})]\Bigg)\Bigg\} \quad (5.1)$$

where

$$\boldsymbol{\alpha} \equiv \begin{pmatrix} \alpha_{red,red} & \alpha_{red,green} & \alpha_{red,blue} \\ \alpha_{green,red} & \alpha_{green,green} & \alpha_{green,blue} \\ \alpha_{blue,red} & \alpha_{blue,green} & \alpha_{blue,blue} \end{pmatrix} \tag{5.2}$$

is a hyperparameter expressing the correlation between the colour components of nearest neighbour pixels and is assumed to be symmetric, $\boldsymbol{\alpha}' \equiv \alpha_2 \boldsymbol{\alpha}$ and $\boldsymbol{\alpha}'' \equiv \alpha_3 \boldsymbol{\alpha}$ are hyperparameters expressing the correlation between the colour components of second- and third-neighbour pixels respectively and

$$\begin{aligned} Z_{\text{prior}}(\boldsymbol{\alpha}, \boldsymbol{\alpha}', \boldsymbol{\alpha}'') \equiv \int \exp\Bigg\{ & -\frac{1}{8} \sum_{\kappa \in \mathbf{K}} \sum_{\kappa' \in \mathbf{K}} \\ & \Bigg(\alpha_{\kappa,\kappa'} \sum_{(x,y) \in \mathbf{V}} \left[(f_{x,y,\kappa} - f_{x+1,y,\kappa})(f_{x,y,\kappa'} - f_{x+1,y,\kappa'}) + (f_{x,y,\kappa} - f_{x,y+1,\kappa})(f_{x,y,\kappa'} - f_{x,y+1,\kappa'}) \right] \\ & + \alpha'_{\kappa,\kappa'} \sum_{(x,y) \in \mathbf{V}} \left[(f_{x,y,\kappa} - f_{x+1,y+1,\kappa})(f_{x,y,\kappa'} - f_{x+1,y+1,\kappa'}) + (f_{x,y,\kappa} - f_{x+1,y-1,\kappa})(f_{x,y,\kappa'} - f_{x+1,y-1,\kappa'}) \right] \\ & + \alpha''_{\kappa,\kappa'} \sum_{(x,y) \in \mathbf{V}} \left[(f_{x,y,\kappa} - f_{x+2,y,\kappa})(f_{x,y,\kappa'} - f_{x+2,y,\kappa'}) + (f_{x,y,\kappa} - f_{x,y+2,\kappa})(f_{x,y,\kappa'} - f_{x,y+2,\kappa'}) \right] \Bigg) \Bigg\} d\boldsymbol{z} \end{aligned} \tag{5.3}$$

with $\int d\boldsymbol{z} \equiv \int_{-\infty}^{+\infty} \int_{-\infty}^{+\infty} \dots \int_{-\infty}^{+\infty} \prod_{(x,y) \in \mathbf{V}} \prod_{\kappa \in \mathbf{K}} dz_{x,y,\kappa}$, is the normalization constant.

The exponential components of equation (5.1) can be rewritten using matrix notation as follows:

$$\begin{aligned} & -\frac{1}{8} \sum_{\kappa \in \mathbf{K}} \sum_{\kappa' \in \mathbf{K}} \\ & \Bigg(\alpha_{\kappa,\kappa'} \sum_{(x,y) \in \mathbf{V}} \left[(f_{x,y,\kappa} - f_{x+1,y,\kappa})(f_{x,y,\kappa'} - f_{x+1,y,\kappa'}) + (f_{x,y,\kappa} - f_{x,y+1,\kappa})(f_{x,y,\kappa'} - f_{x,y+1,\kappa'}) \right] \\ & + \alpha'_{\kappa,\kappa'} \sum_{(x,y) \in \mathbf{V}} \Big[(f_{x,y,\kappa} - f_{x+1,y+1,\kappa})(f_{x,y,\kappa'} - f_{x+1,y+1,\kappa'}) + (f_{x,y,\kappa} - f_{x+1,y-1,\kappa})(f_{x,y,\kappa'} - f_{x+1,y-1,\kappa'}) \\ & + \alpha''_{\kappa,\kappa'} \sum_{(x,y) \in \mathbf{V}} \Big[(f_{x,y,\kappa} - f_{x+2,y,\kappa})(f_{x,y,\kappa'} - f_{x+2,y,\kappa'}) + (f_{x,y,\kappa} - f_{x,y+2,\kappa})(f_{x,y,\kappa'} - f_{x,y+2,\kappa'}) \Big] \Bigg) \\ = & -\frac{1}{8} \sum_{\kappa \in \mathbf{K}} \sum_{\kappa' \in \mathbf{K}} \alpha_{\kappa,\kappa'} \sum_{(x,y) \in \mathbf{V}} 2 f_{x,y,\kappa} f_{x,y,\kappa'} - f_{x,y,\kappa} f_{x+1,y,\kappa'} - f_{x+1,y,\kappa} f_{x,y,\kappa'} + f_{x+1,y,\kappa} f_{x+1,y,\kappa'} \\ & - f_{x,y,\kappa} f_{x,y+1,\kappa'} - f_{x,y+1,\kappa} f_{x,y,\kappa'} + f_{x,y+1,\kappa} f_{x,y+1,\kappa'} \\ & + \alpha_2 \Big[2 f_{x,y,\kappa} f_{x,y,\kappa'} - f_{x,y,\kappa} f_{x+1,y+1,\kappa'} - f_{x+1,y+1,\kappa} f_{x,y,\kappa'} + f_{x+1,y+1,\kappa} f_{x+1,y+1,\kappa'} \\ & - f_{x,y,\kappa} f_{x+1,y-1,\kappa'} - f_{x+1,y-1,\kappa} f_{x,y,\kappa'} + f_{x+1,y-1,\kappa} f_{x+1,y-1,\kappa'} \Big] \\ & + \alpha_3 \Big[2 f_{x,y,\kappa} f_{x,y,\kappa'} - f_{x,y,\kappa} f_{x+2,y,\kappa'} - f_{x+2,y,\kappa} f_{x,y,\kappa'} + f_{x+2,y,\kappa} f_{x+2,y,\kappa'} \\ & - f_{x,y,\kappa} f_{x,y+2,\kappa'} - f_{x,y+2,\kappa} f_{x,y,\kappa'} + f_{x,y+2,\kappa} f_{x,y+2,\kappa'} \Big] \\ = & -\frac{1}{8} \sum_{\kappa \in \mathbf{K}} \sum_{\kappa' \in \mathbf{K}} \alpha_{\kappa,\kappa'} \\ & \times \sum_{(x,y) \in \mathbf{V}} 4 f_{x,y,\kappa} f_{x,y,\kappa'} - f_{x,y,\kappa} f_{x+1,y,\kappa'} - f_{x,y,\kappa} f_{x-1,y,\kappa'} - f_{x,y,\kappa} f_{x,y+1,\kappa'} - f_{x,y,\kappa} f_{x,y-1,\kappa'} \\ & + \alpha_2 \Big[4 f_{x,y,\kappa} f_{x,y,\kappa'} - f_{x,y,\kappa} f_{x+1,y+1,\kappa'} - f_{x,y,\kappa} f_{x-1,y-1,\kappa'} - f_{x,y,\kappa} f_{x+1,y-1,\kappa'} - f_{x,y,\kappa} f_{x-1,y+1,\kappa'} \Big] \\ & + \alpha_3 \Big[4 f_{x,y,\kappa} f_{x,y,\kappa'} - f_{x,y,\kappa} f_{x+2,y,\kappa'} - f_{x,y,\kappa} f_{x-2,y,\kappa'} - f_{x,y,\kappa} f_{x,y+2,\kappa'} - f_{x,y,\kappa} f_{x,y-2,\kappa'} \Big] \\ = & -\frac{1}{2} \sum_{\kappa \in \mathbf{K}} \sum_{\kappa' \in \mathbf{K}} \alpha_{\kappa,\kappa'} \boldsymbol{f}^T \boldsymbol{C}(\alpha_2, \alpha_3, \kappa, \kappa') \boldsymbol{f} \end{aligned} \tag{5.4}$$

where $\boldsymbol{C}(\alpha_2, \alpha_3, \kappa, \kappa')$ is a $3|\mathbf{V}| \times 3|\mathbf{V}|$ matrix where the $(x, y, \mu | x', y', \mu')$ elements are defined by

$$\begin{aligned}\langle x, y, \mu | x', y', \mu' \rangle \equiv \delta_{\kappa,\mu}\delta_{\kappa',\mu'} \Bigg(& \delta_{x,x'}\delta_{y,y'} - \frac{1}{4}\delta_{x,x'+1}\delta_{y,y'} - \frac{1}{4}\delta_{x,x'-1}\delta_{y,y'} - \frac{1}{4}\delta_{x,x'}\delta_{y,y'+1} - \frac{1}{4}\delta_{x,x'}\delta_{y,y'-1} \\ & + \alpha_2 \left[\delta_{x,x'}\delta_{y,y'} - \frac{1}{4}\delta_{x,x'+1}\delta_{y,y'+1} - \frac{1}{4}\delta_{x,x'-1}\delta_{y,y'-1} - \frac{1}{4}\delta_{x,x'+1}\delta_{y,y'-1} - \frac{1}{4}\delta_{x,x'-1}\delta_{y,y'+1} \right] \\ & + \alpha_3 \left[\delta_{x,x'}\delta_{y,y'} - \frac{1}{4}\delta_{x,x'+2}\delta_{y,y'} - \frac{1}{4}\delta_{x,x'-2}\delta_{y,y'} - \frac{1}{4}\delta_{x,x'}\delta_{y,y'+2} - \frac{1}{4}\delta_{x,x'}\delta_{y,y'-2} \right] \Bigg) \\ & [(x, y), (x', y') \in \mathbf{V}, \mu, \mu' \in \mathbf{K}] \end{aligned} \tag{5.5}$$

where $\delta_{a,b}$ is the Kronecker delta.

Thus equation (5.1) can be rewritten as

$$\Pr\{\boldsymbol{F} = \boldsymbol{f} | \boldsymbol{\alpha}, \alpha_2, \alpha_3\} \equiv \frac{1}{Z_{\text{prior}}(\boldsymbol{\alpha}, \alpha_2, \alpha_3)} \exp\left(-\frac{1}{2} \sum_{\kappa \in \mathbf{K}} \sum_{\kappa' \in \mathbf{K}} \alpha_{\kappa,\kappa'} \boldsymbol{f}^T \boldsymbol{C}(\alpha_2, \alpha_3, \kappa, \kappa') \boldsymbol{f} \right) \tag{5.6}$$

with

$$Z_{\text{prior}}(\boldsymbol{\alpha}, \alpha_2, \alpha_3) \equiv \int \exp\left(-\frac{1}{2} \sum_{\kappa \in \mathbf{K}} \sum_{\kappa' \in \mathbf{K}} \alpha_{\kappa,\kappa'} \boldsymbol{z}^T \boldsymbol{C}(\alpha_2, \alpha_3, \kappa, \kappa') \boldsymbol{z} \right) d\boldsymbol{z}. \tag{5.7}$$

This model corresponds to an extension to the third-neighbour interactions of the multichannel CAR model proposed by Tanaka and Horiguchi in [4] and its energy function is

$$\begin{aligned} \frac{1}{8} \sum_{\kappa \in \mathbf{K}} \sum_{\kappa' \in \mathbf{K}} \Bigg(& \alpha_{\kappa,\kappa'} \\ & \times \sum_{(x,y) \in \mathbf{V}} [(f_{x,y,\kappa} - f_{x+1,y,\kappa})(f_{x,y,\kappa'} - f_{x+1,y,\kappa'}) + (f_{x,y,\kappa} - f_{x,y+1,\kappa})(f_{x,y,\kappa'} - f_{x,y+1,\kappa'})] \\ & + \alpha'_{\kappa,\kappa'} \sum_{(x,y) \in \mathbf{V}} \Big[(f_{x,y,\kappa} - f_{x+1,y+1,\kappa})(f_{x,y,\kappa'} - f_{x+1,y+1,\kappa'}) + (f_{x,y,\kappa} - f_{x+1,y-1,\kappa})(f_{x,y,\kappa'} - f_{x+1,y-1,\kappa'}) \Big] \\ & + \alpha''_{\kappa,\kappa'} \sum_{(x,y) \in \mathbf{V}} \Big[(f_{x,y,\kappa} - f_{x+2,y,\kappa})(f_{x,y,\kappa'} - f_{x+2,y,\kappa'}) + (f_{x,y,\kappa} - f_{x,y+2,\kappa})(f_{x,y,\kappa'} - f_{x,y+2,\kappa'}) \Big] \Bigg) \end{aligned} \tag{5.8}$$

We note that $\boldsymbol{f}$ is a Multivariate Gaussian Markov random field with dimension 3 (MGMRF$_3$), with mean $\mathbf{0}$ and precision matrix $\boldsymbol{Q} = \sum_{\kappa \in \mathbf{K}} \sum_{\kappa' \in \mathbf{K}} \alpha_{\kappa,\kappa'} \boldsymbol{C}(\alpha_2, \alpha_3, \kappa, \kappa')$, so that by using the properties of GMRFs described in section 3.2.3, we obtain the following properties for our model:

$$\begin{aligned} \mathrm{E}(\boldsymbol{f}_{(x,y)} | \boldsymbol{f}_{-(x,y)}) &= \boldsymbol{\mu}_{(x,y)} - \boldsymbol{Q}^{-1}_{(x,y),(x,y)} \sum_{(i,j):(i,j)\sim(x,y)} \boldsymbol{Q}_{(x,y),(i,j)} (\boldsymbol{f}_{(i,j)} - \boldsymbol{\mu}_{(i,j)}) \\ &= -(\boldsymbol{\alpha} + \boldsymbol{\alpha}' + \boldsymbol{\alpha}'')^{-1} \sum_{(i,j):(i,j)\sim(x,y)} \boldsymbol{Q}_{(x,y),(i,j)} \boldsymbol{f}_{(i,j)} \\ &= -(\boldsymbol{\alpha} + \boldsymbol{\alpha}' + \boldsymbol{\alpha}'')^{-1} \Bigg[-\boldsymbol{\alpha} \left(\frac{1}{4}\boldsymbol{f}_{(x+1,y)} + \frac{1}{4}\boldsymbol{f}_{(x-1,y)} + \frac{1}{4}\boldsymbol{f}_{(x,y+1)} + \frac{1}{4}\boldsymbol{f}_{(x,y-1)} \right) \\ &\quad - \boldsymbol{\alpha}' \left(\frac{1}{4}\boldsymbol{f}_{(x+1,y+1)} + \frac{1}{4}\boldsymbol{f}_{(x+1,y-1)} + \frac{1}{4}\boldsymbol{f}_{(x-1,y+1)} + \frac{1}{4}\boldsymbol{f}_{(x-1,y-1)} \right) \\ &\quad - \boldsymbol{\alpha}'' \left(\frac{1}{4}\boldsymbol{f}_{(x+2,y)} + \frac{1}{4}\boldsymbol{f}_{(x-2,y)} + \frac{1}{4}\boldsymbol{f}_{(x,y+2)} + \frac{1}{4}\boldsymbol{f}_{(x,y-2)} \right) \Bigg] \\ &= \frac{1}{4}(\boldsymbol{\alpha} + \boldsymbol{\alpha}' + \boldsymbol{\alpha}'')^{-1} \Big[\boldsymbol{\alpha} \left(\boldsymbol{f}_{(x+1,y)} + \boldsymbol{f}_{(x-1,y)} + \boldsymbol{f}_{(x,y+1)} + \boldsymbol{f}_{(x,y-1)} \right) \\ &\quad + \boldsymbol{\alpha}' \left(\boldsymbol{f}_{(x+1,y+1)} + \boldsymbol{f}_{(x+1,y-1)} + \boldsymbol{f}_{(x-1,y+1)} + \boldsymbol{f}_{(x-1,y-1)} \right) \\ &\quad + \boldsymbol{\alpha}'' \left(\boldsymbol{f}_{(x+2,y)} + \boldsymbol{f}_{(x-2,y)} + \boldsymbol{f}_{(x,y+2)} + \boldsymbol{f}_{(x,y-2)} \right) \Big] \end{aligned} \tag{5.9}$$

and

$$\text{Prec}(\boldsymbol{f}_{(x,y)}|\boldsymbol{f}_{-(x,y)}) = \boldsymbol{\alpha} + \boldsymbol{\alpha}' + \boldsymbol{\alpha}'' \tag{5.10}$$

so that we have

$$\begin{aligned}\Pr(\boldsymbol{f}_{(x,y)}|\boldsymbol{f}_{-(x,y)}) \sim N\Bigg(&\frac{1}{4}\left(\boldsymbol{\alpha} + \boldsymbol{\alpha}' + \boldsymbol{\alpha}''\right)^{-1}\Big[\boldsymbol{\alpha}\left(\boldsymbol{f}_{(x+1,y)} + \boldsymbol{f}_{(x-1,y)} + \boldsymbol{f}_{(x,y+1)} + \boldsymbol{f}_{(x,y-1)}\right)\\ &+ \boldsymbol{\alpha}'\left(\boldsymbol{f}_{(x+1,y+1)} + \boldsymbol{f}_{(x+1,y-1)} + \boldsymbol{f}_{(x-1,y+1)} + \boldsymbol{f}_{(x-1,y-1)}\right)\\ &+ \boldsymbol{\alpha}''\left(\boldsymbol{f}_{(x+2,y)} + \boldsymbol{f}_{(x-2,y)} + \boldsymbol{f}_{(x,y+2)} + \boldsymbol{f}_{(x,y-2)}\right)\Big], \left(\boldsymbol{\alpha} + \boldsymbol{\alpha}' + \boldsymbol{\alpha}''\right)^{-1}\Bigg).\end{aligned} \tag{5.11}$$

To simplify calculations, $\boldsymbol{C}(\alpha_2, \alpha_3, \kappa, \kappa')$ can be decomposed as follows:

$$\boldsymbol{C}(\alpha_2, \alpha_3, \kappa, \kappa') = \boldsymbol{D}(\alpha_2, \alpha_3) \otimes \boldsymbol{J}^{\kappa,\kappa'} \tag{5.12}$$

where $\otimes$ is the Kronecker product, $\boldsymbol{J}^{\kappa,\kappa'}$ is the single-entry 3x3 matrix, with 1 at position (κ, κ') and zero elsewhere and $\boldsymbol{D}(\alpha_2, \alpha_3)$ is a $|\mathbf{V}| \times |\mathbf{V}|$ matrix where the $(x, y|x', y')$ elements are defined by

$$\begin{aligned}\langle x, y|x', y'\rangle \equiv\ &\delta_{x,x'}\delta_{y,y'} - \frac{1}{4}\delta_{x,x'+1}\delta_{y,y'} - \frac{1}{4}\delta_{x,x'-1}\delta_{y,y'} - \frac{1}{4}\delta_{x,x'}\delta_{y,y'+1} - \frac{1}{4}\delta_{x,x'}\delta_{y,y'-1}\\ &+ \alpha_2\left(\delta_{x,x'}\delta_{y,y'} - \frac{1}{4}\delta_{x,x'+1}\delta_{y,y'+1} - \frac{1}{4}\delta_{x,x'+1}\delta_{y,y'-1} - \frac{1}{4}\delta_{x,x'-1}\delta_{y,y'+1} - \frac{1}{4}\delta_{x,x'-1}\delta_{y,y'-1}\right)\\ &+ \alpha_3\left(\delta_{x,x'}\delta_{y,y'} - \frac{1}{4}\delta_{x,x'+2}\delta_{y,y'} - \frac{1}{4}\delta_{x,x'-2}\delta_{y,y'} - \frac{1}{4}\delta_{x,x'}\delta_{y,y'+2} - \frac{1}{4}\delta_{x,x'}\delta_{y,y'-2}\right)\\ &[(x, y), (x', y') \in \mathbf{V}].\end{aligned} \tag{5.13}$$

Here, we observe that $\boldsymbol{D}(\alpha_2, \alpha_3)$ is identical to the matrix $\boldsymbol{C}(\alpha_2, \alpha_3)$ defined in equation (4.6). We can then use the eigendecomposition of equation (4.13) to obtain

$$\boldsymbol{D} = \left(\boldsymbol{U}^{-1}\boldsymbol{\Lambda}\boldsymbol{U}\right) \tag{5.14}$$

where $\boldsymbol{U}$ is the DFT matrix defined in equation (4.14), $\boldsymbol{U}^{-1}$ is the conjugate transpose of $\boldsymbol{U}$, known as the inverse DFT matrix and defined in equation (4.15) and $\boldsymbol{\Lambda}$ is the diagonal matrix of the eigenvalues $\lambda(\alpha_2, \alpha_3, p, q)$ of $\boldsymbol{D}$ and is defined in equation (4.25).

We can simplify the expression of Z_{prior} in (5.7) by applying the multidimensional Gaussian integral as shown in equation (3.25) and using the results of the eigendecomposition above to obtain

$$Z_{\text{prior}} = (2\pi)^{\frac{3|\mathbf{V}|}{2}}\left\{\prod_{(p,q)\in\mathbf{V}} \lambda(\alpha_2, \alpha_3, p, q)^3 \det\boldsymbol{\alpha}\right\}^{-\frac{1}{2}}. \tag{5.15}$$

5.2.2 A Posteriori Probability Density Function

The a posteriori probability density function of having an original image configuration $\boldsymbol{f}$ given a degraded image $\boldsymbol{g}$ is found by applying Bayes' theorem as follows:

$$\begin{aligned}\Pr\{\boldsymbol{F} = \boldsymbol{f}|\boldsymbol{G} = \boldsymbol{g}, \boldsymbol{\alpha}, \alpha_2, \alpha_3, \sigma\} &= \frac{\Pr\{\boldsymbol{G} = \boldsymbol{g}|\boldsymbol{F} = \boldsymbol{f}, \sigma\}\Pr\{\boldsymbol{F} = \boldsymbol{f}|\boldsymbol{\alpha}, \alpha_2, \alpha_3\}}{\Pr\{\boldsymbol{G} = \boldsymbol{g}|\boldsymbol{\alpha}, \alpha_2, \alpha_3, \sigma\}}\\ &= \frac{\Pr\{\boldsymbol{G} = \boldsymbol{g}|\boldsymbol{F} = \boldsymbol{f}, \sigma\}\Pr\{\boldsymbol{F} = \boldsymbol{f}|\boldsymbol{\alpha}, \alpha_2, \alpha_3\}}{\int \Pr\{\boldsymbol{G} = \boldsymbol{g}|\boldsymbol{F} = \boldsymbol{z}, \sigma\}\Pr\{\boldsymbol{F} = \boldsymbol{z}|\boldsymbol{\alpha}, \alpha_2, \alpha_3\}\, d\boldsymbol{z}}\end{aligned} \tag{5.16}$$

where $\Pr\{\boldsymbol{G} = \boldsymbol{g}|\boldsymbol{\alpha}, \alpha_2, \alpha_3, \sigma\} = \int \Pr\{\boldsymbol{G} = \boldsymbol{g}|\boldsymbol{F} = \boldsymbol{z}, \sigma\}\Pr\{\boldsymbol{F} = \boldsymbol{z}|\boldsymbol{\alpha}, \alpha_2, \alpha_3\}\, d\boldsymbol{z}$ is called the evidence.

Using (3.1) and (5.6), the function can be rewritten as follows:

$$\Pr\{\boldsymbol{F} = \boldsymbol{f}|\boldsymbol{G} = \boldsymbol{g}, \boldsymbol{\alpha}, \alpha_2, \alpha_3, \sigma\} =$$

$$\frac{1}{Z_{\text{noise}}(\sigma)} \exp\left(-\frac{1}{2\sigma^2} \sum_{(x,y)\in\mathbf{V}} \sum_{\kappa\in\mathbf{K}} (g_{x,y,\kappa} - f_{x,y,\kappa})^2\right)$$
$$\times \frac{1}{Z_{\text{prior}}(\boldsymbol{\alpha}, \alpha_2, \alpha_3)} \exp\left\{-\frac{1}{2} \sum_{\kappa\in\mathbf{K}} \sum_{\kappa'\in\mathbf{K}} \alpha_{\kappa,\kappa'} \boldsymbol{f}^T \boldsymbol{C}(\alpha_2, \alpha_3, \kappa, \kappa') \boldsymbol{f}\right\}$$
$$\div \left[\int \frac{1}{Z_{\text{noise}}(\sigma)} \exp\left(-\frac{1}{2\sigma^2} \sum_{(x,y)\in\mathbf{V}} \sum_{\kappa\in\mathbf{K}} (g_{x,y,\kappa} - z_{x,y,\kappa})^2\right)\right.$$
$$\left. \times \frac{1}{Z_{\text{prior}}(\boldsymbol{\alpha}, \alpha_2, \alpha_3)} \exp\left\{-\frac{1}{2} \sum_{\kappa\in\mathbf{K}} \sum_{\kappa'\in\mathbf{K}} \alpha_{\kappa,\kappa'} \boldsymbol{z}^T \boldsymbol{C}(\alpha_2, \alpha_3, \kappa, \kappa') \boldsymbol{z}\right\} d\boldsymbol{z}\right]. \quad (5.17)$$

Since Z_{noise} and Z_{prior} are not dependant on $\boldsymbol{z}$, they can be taken out of the integral in the denominator and cancel out with the numerator, so we have

$$\Pr\{\boldsymbol{F} = \boldsymbol{f} | \boldsymbol{G} = \boldsymbol{g}, \boldsymbol{\alpha}, \alpha_2, \alpha_3, \sigma\} = \frac{1}{Z_{\text{posterior}}(\boldsymbol{g}, \boldsymbol{\alpha}, \alpha_2, \alpha_3, \sigma)} \exp\left[-H(\boldsymbol{f}|\boldsymbol{g}, \boldsymbol{\alpha}, \alpha_2, \alpha_3, \sigma)\right] \quad (5.18)$$

where

$$Z_{\text{posterior}}(\boldsymbol{g}, \boldsymbol{\alpha}, \alpha_2, \alpha_3, \sigma) = \int \exp\left[-H(\boldsymbol{z}|\boldsymbol{g}, \boldsymbol{\alpha}, \alpha_2, \alpha_3, \sigma)\right] d\boldsymbol{z} \quad (5.19)$$

and

$$H(\boldsymbol{f}|\boldsymbol{g}, \boldsymbol{\alpha}, \alpha_2, \alpha_3, \sigma) = \frac{1}{2\sigma^2} \sum_{(x,y)\in\mathbf{V}} \sum_{\kappa\in\mathbf{K}} (g_{x,y,\kappa} - f_{x,y,\kappa})^2 + \frac{1}{2} \boldsymbol{f}^T \left(\sum_{\kappa\in\mathbf{K}} \sum_{\kappa'\in\mathbf{K}} \alpha_{\kappa,\kappa'} \boldsymbol{C}(\alpha_2, \alpha_3, \kappa, \kappa')\right) \boldsymbol{f}. \quad (5.20)$$

We can simplify calculations by grouping all element of $\boldsymbol{f}$ in H in one single term in the same manner as in equation (3.31) to obtain

$$H(\boldsymbol{f}|\boldsymbol{g}, \boldsymbol{\alpha}, \alpha_2, \alpha_3, \sigma) = \frac{1}{2\sigma^2} \left[\boldsymbol{f} - \left(\boldsymbol{I} + \sigma^2 \sum_{\kappa\in\mathbf{K}} \sum_{\kappa'\in\mathbf{K}} \alpha_{\kappa,\kappa'} \boldsymbol{C}(\alpha_2, \alpha_3, \kappa, \kappa')\right)^{-1} \boldsymbol{g}\right]^T$$
$$\times \left(\boldsymbol{I} + \sigma^2 \sum_{\kappa\in\mathbf{K}} \sum_{\kappa'\in\mathbf{K}} \alpha_{\kappa,\kappa'} \boldsymbol{C}(\alpha_2, \alpha_3, \kappa, \kappa')\right) \left[\boldsymbol{f} - \left(\boldsymbol{I} + \sigma^2 \sum_{\kappa\in\mathbf{K}} \sum_{\kappa'\in\mathbf{K}} \alpha_{\kappa,\kappa'} \boldsymbol{C}(\alpha_2, \alpha_3, \kappa, \kappa')\right)^{-1} \boldsymbol{g}\right]$$
$$+ \frac{1}{2} \boldsymbol{g}^T \left(\sum_{\kappa\in\mathbf{K}} \sum_{\kappa'\in\mathbf{K}} \alpha_{\kappa,\kappa'} \boldsymbol{C}(\alpha_2, \alpha_3, \kappa, \kappa')\right) \left(\boldsymbol{I} + \sigma^2 \sum_{\kappa\in\mathbf{K}} \sum_{\kappa'\in\mathbf{K}} \alpha_{\kappa,\kappa'} \boldsymbol{C}(\alpha_2, \alpha_3, \kappa, \kappa')\right)^{-1} \boldsymbol{g} \quad (5.21)$$

Using the eigendecomposition described in (5.14), we can rewrite the second term of (5.21) as

$$\frac{1}{2} \boldsymbol{g}^T \left(\sum_{\kappa\in\mathbf{K}} \sum_{\kappa'\in\mathbf{K}} \alpha_{\kappa,\kappa'} \boldsymbol{C}(\alpha_2, \alpha_3, \kappa, \kappa')\right) \left(\boldsymbol{I} + \sigma^2 \sum_{\kappa\in\mathbf{K}} \sum_{\kappa'\in\mathbf{K}} \alpha_{\kappa,\kappa'} \boldsymbol{C}(\alpha_2, \alpha_3, \kappa, \kappa')\right)^{-1} \boldsymbol{g}$$
$$= \frac{1}{2} \sum_{(p,q)\in\mathbf{V}} \overrightarrow{G}^{\dagger}(p,q) \lambda(\alpha_2, \alpha_3, p, q) \boldsymbol{\alpha} \left(\boldsymbol{e} + \sigma^2 \lambda(\alpha_2, \alpha_3, p, q) \boldsymbol{\alpha}\right)^{-1} \overrightarrow{G}^{\dagger}(p,q) \quad (5.22)$$

where $\boldsymbol{e}$ is the 3x3 identity matrix and $\overrightarrow{G}(p,q)$ and $\overrightarrow{G}^{\dagger}(p,q)$ are defined in equations (3.33) and (3.34) respectively. The detailed computations can be found at (3.32).

From the above, we conclude that

$$H(\boldsymbol{f}|\boldsymbol{g}, \boldsymbol{\alpha}, \alpha_2, \alpha_3, \sigma) = \frac{1}{2\sigma^2} \left[\boldsymbol{f} - \left(\boldsymbol{I} + \sigma^2 \sum_{\kappa\in\mathbf{K}} \sum_{\kappa'\in\mathbf{K}} \alpha_{\kappa,\kappa'} \boldsymbol{C}(\alpha_2, \alpha_3, \kappa, \kappa')\right)^{-1} \boldsymbol{g}\right]^T$$

$$\times \left(\boldsymbol{I} + \sigma^2 \sum_{\kappa \in \mathbf{K}} \sum_{\kappa' \in \mathbf{K}} \alpha_{\kappa,\kappa'} \boldsymbol{C}\left(\alpha_2, \alpha_3, \kappa, \kappa'\right) \right) \left[\boldsymbol{f} - \left(\boldsymbol{I} + \sigma^2 \sum_{\kappa \in \mathbf{K}} \sum_{\kappa' \in \mathbf{K}} \alpha_{\kappa,\kappa'} \boldsymbol{C}\left(\alpha_2, \alpha_3, \kappa, \kappa'\right) \right)^{-1} \boldsymbol{g} \right]$$
$$+ \frac{1}{2} \sum_{(p,q) \in \mathbf{V}} \left\{ \overrightarrow{G}^{\dagger}(p,q) \lambda(\alpha_2, \alpha_3, p, q) \boldsymbol{\alpha} \left(\boldsymbol{e} + \sigma^2 \lambda(\alpha_2, \alpha_3, p, q) \boldsymbol{\alpha} \right)^{-1} \overrightarrow{G}(p,q) \right\}. \quad (5.23)$$

Using the variable substitution $\boldsymbol{x} = \left[\boldsymbol{z} - \left(\boldsymbol{I} + \sigma^2 \sum_{\kappa \in \mathbf{K}} \sum_{\kappa' \in \mathbf{K}} \alpha_{\kappa,\kappa'} \boldsymbol{C}\left(\alpha_2, \alpha_3, \kappa, \kappa'\right) \right)^{-1} \boldsymbol{g} \right]$ and $d\boldsymbol{z} = d\boldsymbol{x}$, $Z_{\text{posterior}}$ can be rewritten as

$$Z_{\text{posterior}} = \int \exp\left\{ \frac{-1}{2\sigma^2} \boldsymbol{x}^T \left(\boldsymbol{I} + \sigma^2 \sum_{\kappa \in \mathbf{K}} \sum_{\kappa' \in \mathbf{K}} \alpha_{\kappa,\kappa'} \boldsymbol{C}\left(\alpha_2, \alpha_3, \kappa, \kappa'\right) \right) \boldsymbol{x} \right.$$
$$\left. - \frac{1}{2} \sum_{(p,q) \in \mathbf{V}} \left[\overrightarrow{G}^{\dagger}(p,q) \lambda(\alpha_2, \alpha_3, p, q) \boldsymbol{\alpha} \left(\boldsymbol{e} + \sigma^2 \lambda(\alpha_2, \alpha_3, p, q) \boldsymbol{\alpha} \right)^{-1} \overrightarrow{G}(p,q) \right] \right\} d\boldsymbol{x} \quad (5.24)$$

which, using the multidimensional Gaussian integral becomes

$$Z_{\text{posterior}} = \left(2\pi\sigma^2\right)^{\frac{3|\mathbf{V}|}{2}} \left\{ \det \left(\boldsymbol{I} + \sigma^2 \sum_{\kappa \in \mathbf{K}} \sum_{\kappa' \in \mathbf{K}} \alpha_{\kappa,\kappa'} \boldsymbol{C}\left(\alpha_2, \alpha_3, \kappa, \kappa'\right) \right) \right\}^{-\frac{1}{2}}$$
$$\times \exp\left\{ -\frac{1}{2} \sum_{(p,q) \in \mathbf{V}} \left[\overrightarrow{G}^{\dagger}(p,q) \lambda(\alpha_2, \alpha_3, p, q) \boldsymbol{\alpha} \left(\boldsymbol{e} + \sigma^2 \lambda(\alpha_2, \alpha_3, p, q) \boldsymbol{\alpha} \right)^{-1} \overrightarrow{G}(p,q) \right] \right\}. \quad (5.25)$$

The determinant in equation (5.25) can be rewritten as

$$\det \left(\boldsymbol{I} + \sigma^2 \sum_{\kappa \in \mathbf{K}} \sum_{\kappa' \in \mathbf{K}} \alpha_{\kappa,\kappa'} \boldsymbol{C}\left(\alpha_2, \alpha_3, \kappa, \kappa'\right) \right) = \prod_{(p,q) \in \mathbf{V}} \det \left(\boldsymbol{e} + \sigma^2 \lambda(\alpha_2, \alpha_3, p, q) \boldsymbol{\alpha} \right) \quad \text{See equation (3.39).} \quad (5.26)$$

So equation (5.25) can be transformed into

$$Z_{\text{posterior}}\left(\boldsymbol{g}, \boldsymbol{\alpha}, \alpha_2, \alpha_3, \sigma\right) = \left(2\pi\sigma^2\right)^{\frac{3|\mathbf{V}|}{2}} \prod_{(p,q) \in \mathbf{V}} \left[\det \left(\boldsymbol{e} + \sigma^2 \lambda(\alpha_2, \alpha_3, p, q) \boldsymbol{\alpha} \right) \right]^{-\frac{1}{2}}$$
$$\times \exp\left\{ -\frac{1}{2} \sum_{(p,q) \in \mathbf{V}} \left[\overrightarrow{G}^{\dagger}(p,q) \lambda(\alpha_2, \alpha_3, p, q) \boldsymbol{\alpha} \left(\boldsymbol{e} + \sigma^2 \lambda(\alpha_2, \alpha_3, p, q) \boldsymbol{\alpha} \right)^{-1} \overrightarrow{G}(p,q) \right] \right\}. \quad (5.27)$$

5.2.3 Restored Image Equation

In our model, the estimated restored image configuration is given by the expected value of the a posteriori probability function. This gives us the following restored image equation:

$$\widehat{\boldsymbol{f}} \equiv \int \boldsymbol{z} \Pr\left\{ \boldsymbol{F} = \boldsymbol{z} | \boldsymbol{G} = \boldsymbol{g}, \boldsymbol{\alpha}, \alpha_2, \alpha_3, \sigma \right\} d\boldsymbol{z} \quad (5.28)$$

where the integral is performed over every image configuration $\boldsymbol{z}$ (range of $]-\infty, +\infty[$ for each colour component) and $\widehat{\boldsymbol{f}}$ is our restored image.

Using equation (5.18) we obtain

$$\widehat{\boldsymbol{f}} = \frac{1}{Z_{\text{posterior}}\left(\boldsymbol{g}, \boldsymbol{\alpha}, \alpha_2, \alpha_3, \sigma\right)} \int \boldsymbol{z} \exp\left[-H\left(\boldsymbol{z} | \boldsymbol{g}, \boldsymbol{\alpha}, \alpha_2, \alpha_3, \sigma\right) \right] d\boldsymbol{z} \quad (5.29)$$

which, using the results of equations (5.23) and (5.25) is rewritten as

$$\widehat{\boldsymbol{f}} =$$

$$\frac{1}{(2\pi\sigma^2)^{\frac{3|\mathbf{V}|}{2}} \det\left(\sigma^2\boldsymbol{\Sigma}^{-1}\right)^{-\frac{1}{2}} \exp\left\{-\frac{1}{2}\sum_{(p,q)\in\mathbf{V}} \overrightarrow{G}^{\dagger}(p,q)\lambda(\alpha_2,\alpha_3,p,q)\boldsymbol{\alpha}\left(\boldsymbol{e}+\sigma^2\lambda(\alpha_2,\alpha_3,p,q)\boldsymbol{\alpha}\right)^{-1}\overrightarrow{G}(p,q)\right\}}$$

$$\times \int \boldsymbol{z}\exp\Bigg(-\frac{1}{2\sigma^2}\left[\boldsymbol{z}-\boldsymbol{\mu}\right]^T\sigma^2\boldsymbol{\Sigma}^{-1}\left[\boldsymbol{z}-\boldsymbol{\mu}\right]$$

$$-\frac{1}{2}\sum_{(p,q)\in\mathbf{V}}\left[\overrightarrow{G}^{\dagger}(p,q)\lambda(\alpha_2,\alpha_3,p,q)\boldsymbol{\alpha}\left(\boldsymbol{e}+\sigma^2\lambda(\alpha_2,\alpha_3,p,q)\boldsymbol{\alpha}\right)^{-1}\overrightarrow{G}(p,q)\right]\Bigg)d\boldsymbol{z}$$

$$= \frac{1}{(2\pi\sigma^2)^{\frac{3|\mathbf{V}|}{2}}(\sigma^2)^{-\frac{3|\mathbf{V}|}{2}}\det(\boldsymbol{\Sigma})^{\frac{1}{2}}}\int \boldsymbol{z}\exp\left(-\frac{1}{2}\left[\boldsymbol{z}-\boldsymbol{\mu}\right]^T\boldsymbol{\Sigma}^{-1}\left[\boldsymbol{z}-\boldsymbol{\mu}\right]\right)d\boldsymbol{z}$$

$$= \frac{1}{(2\pi)^{\frac{3|\mathbf{V}|}{2}}\det(\boldsymbol{\Sigma})^{\frac{1}{2}}}\int \boldsymbol{z}\exp\left(-\frac{1}{2}\left[\boldsymbol{z}-\boldsymbol{\mu}\right]^T\boldsymbol{\Sigma}^{-1}\left[\boldsymbol{z}-\boldsymbol{\mu}\right]\right)d\boldsymbol{z} \tag{5.30}$$

with $\boldsymbol{\mu} \equiv \left(\boldsymbol{I}+\sigma^2\sum_{\kappa\in\mathbf{K}}\sum_{\kappa'\in\mathbf{K}}\alpha_{\kappa,\kappa'}\boldsymbol{C}(\alpha_2,\alpha_3,\kappa,\kappa')\right)^{-1}\boldsymbol{g}$
and $\boldsymbol{\Sigma}^{-1} \equiv \frac{1}{\sigma^2}\left(\boldsymbol{I}+\sigma^2\sum_{\kappa\in\mathbf{K}}\sum_{\kappa'\in\mathbf{K}}\alpha_{\kappa,\kappa'}\boldsymbol{C}(\alpha_2,\alpha_3,\kappa,\kappa')\right)$
which corresponds to the expected value equation of a multivariate Gaussian distribution. Using that fact, we conclude that

$$\widehat{\boldsymbol{f}} = \mathbf{E}[\boldsymbol{z}] = \boldsymbol{\mu} = \left(\boldsymbol{I}+\sigma^2\sum_{\kappa\in\mathbf{K}}\sum_{\kappa'\in\mathbf{K}}\alpha_{\kappa,\kappa'}\boldsymbol{C}(\alpha_2,\alpha_3,\kappa,\kappa')\right)^{-1}\boldsymbol{g}. \tag{5.31}$$

However, it is impractical to compute the inverse of such a large matrix, so we use the same eigendecomposition as in (5.15) to simplify the equation as shown in (3.45) and obtain

$$\widehat{\mathbf{f}}_{x,y} = \sum_{(p,q)\in\mathbf{V}} U^{-1}_{(x,y),(p,q)}\left(\boldsymbol{e}+\sigma^2\lambda\left(\alpha_2,\alpha_3,p,q\right)\boldsymbol{\alpha}\right)^{-1}\overrightarrow{G}\left(p,q\right). \tag{5.32}$$

Here we note that this corresponds to the inverse DFT of $\left(\boldsymbol{e}+\sigma^2\lambda\left(\alpha_2,\alpha_3,p,q\right)\boldsymbol{\alpha}\right)^{-1}\overrightarrow{G}\left(p,q\right)$ where $\overrightarrow{G}(p,q)$ itself is the DFT of the degraded image.

5.2.4 Hyperparameters Estimation

As we saw in section 5.2.3, the restored image equation depends on the values of the hyperparameters σ, $\boldsymbol{\alpha}$, α_2 and α_3. The selection of those values shall be done by fixing the values of α_2 and α_3 and then choosing values for σ and $\boldsymbol{\alpha}$ that maximize the evidence (or likelihood) of equation (5.16). Such a method is known as Maximum Likelihood Estimation (MLE).

Using equation (5.16) with (3.1), (5.6) and (5.18), we find that the evidence is given by

$$\Pr\left\{\boldsymbol{G}=\boldsymbol{g}|\boldsymbol{\alpha},\alpha_2,\alpha_3,\sigma\right\} = \frac{\Pr\left\{\boldsymbol{G}=\boldsymbol{g}|\boldsymbol{F}=\boldsymbol{f},\sigma\right\}\Pr\left\{\boldsymbol{F}=\boldsymbol{f}|\boldsymbol{\alpha},\alpha_2,\alpha_3\right\}}{\Pr\left\{\boldsymbol{F}=\boldsymbol{f}|\boldsymbol{G}=\boldsymbol{g},\boldsymbol{\alpha},\alpha_2,\alpha_3,\sigma\right\}}$$

$$= \frac{\frac{1}{Z_{\text{noise}}(\sigma)}\exp\left(-\frac{1}{2\sigma^2}\left\|\boldsymbol{g}-\boldsymbol{f}\right\|^2\right)\frac{1}{Z_{\text{prior}}(\boldsymbol{\alpha},\alpha_2,\alpha_3)}\exp\left(-\frac{1}{2}\sum_{\kappa\in\mathbf{K}}\sum_{\kappa'\in\mathbf{K}}\alpha_{\kappa,\kappa'}\boldsymbol{f}^T\boldsymbol{C}\left(\alpha_2,\alpha_3,\kappa,\kappa'\right)\boldsymbol{f}\right)}{\frac{1}{Z_{\text{posterior}}(\boldsymbol{g},\boldsymbol{\alpha},\alpha_2,\alpha_3,\sigma)}\exp\left[-\frac{1}{2\sigma^2}\left\|\boldsymbol{g}-\boldsymbol{f}\right\|^2-\frac{1}{2}\sum_{\kappa\in\mathbf{K}}\sum_{\kappa'\in\mathbf{K}}\alpha_{\kappa,\kappa'}\boldsymbol{f}^T\boldsymbol{C}\left(\alpha_2,\alpha_3,\kappa,\kappa'\right)\boldsymbol{f}\right]}$$

$$= \frac{Z_{\text{posterior}}(\boldsymbol{g},\boldsymbol{\alpha},\alpha_2,\alpha_3,\sigma)}{Z_{\text{noise}}(\sigma)Z_{\text{prior}}(\boldsymbol{\alpha},\alpha_2,\alpha_3)} \tag{5.33}$$

We can simplify the calculations by finding the maximum of the log of the evidence as in equation (3.48), which gives us

$$\begin{aligned}(\widehat{\boldsymbol{\alpha}},\widehat{\sigma}) &= \arg\ \max_{\boldsymbol{\alpha},\sigma}\left[\ln Z_{\text{posterior}}(\boldsymbol{g},\boldsymbol{\alpha},\alpha_2,\alpha_3,\sigma) - \ln Z_{\text{noise}}(\sigma) - \ln Z_{\text{prior}}(\boldsymbol{\alpha},\alpha_2,\alpha_3)\right] \\ &= \arg\ \max_{\boldsymbol{\alpha},\sigma}\Bigg[-\frac{3\,|\mathbf{V}|}{2}\ln(2\pi) - \frac{1}{2}\sum_{(p,q)\in\mathbf{V}}\ln\left(\det\left[\boldsymbol{e}+\sigma^2\lambda(\alpha_2,\alpha_3,p,q)\boldsymbol{\alpha}\right]\right) \\ &\quad - \frac{1}{2}\sum_{(p,q)\in\mathbf{V}}\overrightarrow{G}^{\dagger}(p,q)\lambda(\alpha_2,\alpha_3,p,q)\boldsymbol{\alpha}\left[\boldsymbol{e}+\sigma^2\lambda(\alpha_2,\alpha_3,p,q)\boldsymbol{\alpha}\right]^{-1}\overrightarrow{G}(p,q) \\ &\quad + \frac{|\mathbf{V}|}{2}\ln\left(\det\boldsymbol{\alpha}\right) + \frac{3}{2}\sum_{(p,q)\in\mathbf{V}}\ln\left[\lambda(\alpha_2,\alpha_3,p,q)\right]\Bigg]\end{aligned} \tag{5.34}$$

where $\widehat{\boldsymbol{\alpha}}$ and $\widehat{\sigma}$ are the estimated values of the hyperparameters $\boldsymbol{\alpha}$ and σ respectively.

Using the above, we find the value of $\widehat{\sigma}$ by solving the equation $\frac{d}{d\widehat{\sigma}^2}\ln(\Pr\{\boldsymbol{G}=\boldsymbol{g}|\widehat{\boldsymbol{\alpha}},\alpha_2,\alpha_3,\widehat{\sigma}\}) = 0$ to obtain

$$\begin{aligned}\widehat{\sigma}^2 = \frac{\widehat{\sigma}^2}{3\,|\mathbf{V}|}\sum_{(p,q)\in\mathbf{V}}\Bigg[&\operatorname{tr}\left(\boldsymbol{e}+\widehat{\sigma}^2\lambda(\alpha_2,\alpha_3,p,q)\widehat{\boldsymbol{\alpha}}\right)^{-1} \\ &+ \widehat{\sigma}^2\overrightarrow{G}^{\dagger}(p,q)\left(\lambda(\alpha_2,\alpha_3,p,q)\widehat{\boldsymbol{\alpha}}\left[\boldsymbol{e}+\widehat{\sigma}^2\lambda(\alpha_2,\alpha_3,p,q)\widehat{\boldsymbol{\alpha}}\right]^{-1}\right)^2\overrightarrow{G}(p,q)\Bigg].\end{aligned} \tag{5.35}$$

The details of the computation are the same as in equation (3.49).

Similarly, we find the value $\widehat{\boldsymbol{\alpha}}$ by solving the equation $\frac{d}{d\widehat{\boldsymbol{\alpha}}}\ln(\Pr\{\boldsymbol{G}=\boldsymbol{g}|\widehat{\boldsymbol{\alpha}},\alpha_2,\alpha_3,\widehat{\sigma}\}) = 0$ to obtain

$$\begin{aligned}\widehat{\boldsymbol{\alpha}}^{-1} - \frac{1}{2}\operatorname{diag}\left(\widehat{\boldsymbol{\alpha}}^{-1}\right) &= \frac{1}{2\,|\mathbf{V}|} \\ &\times\sum_{(p,q)\in\mathbf{V}}\Bigg(\widehat{\sigma}^2\lambda(\alpha_2,\alpha_3,p,q)\left\{2\left[\boldsymbol{e}+\widehat{\sigma}^2\lambda(\alpha_2,\alpha_3,p,q)\widehat{\boldsymbol{\alpha}}\right]^{-1} - \operatorname{diag}\left(\left[\boldsymbol{e}+\widehat{\sigma}^2\lambda(\alpha_2,\alpha_3,p,q)\widehat{\boldsymbol{\alpha}}\right]^{-1}\right)\right\} \\ &+\sum_{\kappa\in\mathbf{K}}\sum_{\kappa'\in\mathbf{K}}\Bigg[\boldsymbol{J}^{\kappa,\kappa'}\overrightarrow{G}^{\dagger}(p,q)\lambda(\alpha_2,\alpha_3,p,q)\left[\boldsymbol{e}+\widehat{\sigma}^2\lambda(\alpha_2,\alpha_3,p,q)\widehat{\boldsymbol{\alpha}}\right]^{-1}\left(\boldsymbol{J}^{\kappa,\kappa'}+\boldsymbol{J}^{\kappa',\kappa}-\boldsymbol{J}^{\kappa,\kappa'}\boldsymbol{J}^{\kappa,\kappa'}\right) \\ &\qquad\times\left[\boldsymbol{e}+\widehat{\sigma}^2\lambda(\alpha_2,\alpha_3,p,q)\widehat{\boldsymbol{\alpha}}\right]^{-1}\overrightarrow{G}(p,q)\Bigg]\Bigg).\end{aligned} \tag{5.36}$$

Refer to equation (3.54) for the detailed computation.

When actually computing the value of the log of the evidence given in (5.34), we notice that the value of the last term diverges when $\lambda(\alpha_2,\alpha_3,p,q)=0$. We have not yet found a way to get around this problem, so we do not compute the value of the evidence in our algorithm. This is not a major problem since our algorithm depends on the derivates of the evidence and not on the actual value of the evidence.

5.3 Algorithm

In this section, we describe an image restoration algorithm based on our image restoration model. We use a fixed point iteration algorithm [12] to find our maximum likelihood estimates for the hyperparameters $\boldsymbol{\alpha}$ and σ. As we saw in section 5.2.4, the extremum values for the hyperparameters $\boldsymbol{\alpha}$ and σ can be expressed in the form of the simultaneous recursive equations $\alpha(r) = f(\boldsymbol{\alpha}(r-1),\sigma(r-1))$ and $\sigma(r) = g(\alpha(r-1),\sigma(r-1))$. Therefore, in our algorithm, we find new values of $\widehat{\boldsymbol{\alpha}}$ and $\widehat{\sigma}$ by applying their current values to equations (5.35) and (5.36) and repeat that process until the algorithm converges. We shall assume that the algorithm has converged once we achieve the following halting criterion:

$$e_1(r) = \left\{\sum_{\kappa\in\mathbf{K}}\sum_{\kappa'\in\mathbf{K}}\left|\frac{a_{\kappa,\kappa'}(r)-a_{\kappa,\kappa'}(r-1)}{a_{\kappa,\kappa'}(r-1)}\right|\right\} + \left|\frac{b(r)-b(r-1)}{b(r-1)}\right| < 10^{-4} \tag{5.37}$$

where $a_{\kappa,\kappa'}(x)$ and $b(x)$ are the values of $\widehat{\alpha}_{\kappa,\kappa'}$ and $\widehat{\sigma}^2$, respectively, at iteration x of the algorithm and r and $r-1$ are the current and previous iterations of the algorithm, respectively.

5.3.1 Algorithm Steps

Following are the steps of the practical algorithm.

Step 1.

(i) Compute the DFT of the degraded image to obtain the value of $\overrightarrow{G}$. We note here that $\overrightarrow{G}^{\dagger}$ is simply the complex conjugate of $\overrightarrow{G}$ so it does not need to be computed explicitly.

(ii) Compute the values of $\lambda(\alpha_2, \alpha_3, p, q)$ using (4.25)

(iii) Initialize $\boldsymbol{a}(0)$ to $\begin{pmatrix} 1 & 1/2 & 1/2 \\ 1/2 & 1 & 1/2 \\ 1/2 & 1/2 & 1 \end{pmatrix}$.

(iv) Initialize $b(0)$ to 1.

(v) Initialize r to 0.

Step 2.

(i) Update $r \leftarrow r + 1$.

(ii) Compute the right side of equation (5.36) given by

$$\begin{aligned} \boldsymbol{x} = \frac{1}{2\,|\mathbf{V}|} \sum_{(p,q)\in\mathbf{V}} \Big(& b(r-1)\lambda(\alpha_2,\alpha_3,p,q)\Big\{2\left[\boldsymbol{e} + b(r-1)\lambda(\alpha_2,\alpha_3,p,q)\boldsymbol{a}(r-1)\right]^{-1} \\ & - \operatorname{diag}\left(\left[\boldsymbol{e} + b(r-1)\lambda(\alpha_2,\alpha_3,p,q)\boldsymbol{a}(r-1)\right]^{-1}\right)\Big\} \\ & + \sum_{\kappa\in\mathbf{K}} \sum_{\kappa'\in\mathbf{K}} \Big[\boldsymbol{J}^{\kappa,\kappa'} \overrightarrow{G}^{\dagger}(p,q)\lambda(\alpha_2,\alpha_3,p,q)\left[\boldsymbol{e} + b(r-1)\lambda(\alpha_2,\alpha_3,p,q)\boldsymbol{a}(r-1)\right]^{-1} \\ & \times \left(\boldsymbol{J}^{\kappa,\kappa'} + \boldsymbol{J}^{\kappa',\kappa} - \boldsymbol{J}^{\kappa,\kappa'}\boldsymbol{J}^{\kappa,\kappa'}\right)\left[\boldsymbol{e} + b(r-1)\lambda(\alpha_2,\alpha_3,p,q)\boldsymbol{a}(r-1)\right]^{-1} \overrightarrow{G}(p,q)\Big]\Big). \end{aligned} \tag{5.38}$$

(iii) Using equation (5.36), update $\boldsymbol{a}(r) \leftarrow (\boldsymbol{x} + \operatorname{diag}(\boldsymbol{x}))^{-1}$.

(iv) Using equation (5.35), update

$$\begin{aligned} b(r) \leftarrow \frac{b(r-1)}{3\,|\mathbf{V}|} \sum_{(p,q)\in\mathbf{V}} \Big[& \operatorname{tr}\left(\boldsymbol{e} + b(r-1)\lambda(\alpha_2,\alpha_3,p,q)\boldsymbol{a}(r-1)\right)^{-1} \\ & + b(r-1)\overrightarrow{G}^{\dagger}(p,q)\left(\lambda(\alpha_2,\alpha_3,p,q)\boldsymbol{a}(r-1)\left[\boldsymbol{e} + b(r-1)\lambda(\alpha_2,\alpha_3,p,q)\boldsymbol{a}(r-1)\right]^{-1}\right)^2 \overrightarrow{G}(p,q)\Big]. \end{aligned} \tag{5.39}$$

Here we note that since $\overrightarrow{G}^{\dagger}(p,q)$ is the conjugate transpose of $\overrightarrow{G}(p,q)$ and that, since $\boldsymbol{a}(r)$ is a symmetric matrix, the matrices involved in their multiplications are all symmetric, the imaginary terms of those multiplications will vanish.

Step 3.

(i) Check the termination condition of equation (5.37).

(ii) If the termination condition is fulfilled, proceed to step 4. Otherwise go back to step 2.

Step 4.

(i) Update $\widehat{\boldsymbol{\alpha}} \leftarrow \boldsymbol{a}(r)$.

(ii) Update $\widehat{\sigma} \leftarrow \sqrt{b(r)}$.

(iii) Compute the values of $\left(\mathbf{e} + \widehat{\sigma}^2\lambda\left(\alpha_2,\alpha_3,p,q\right)\widehat{\boldsymbol{\alpha}}\right)^{-1}\overrightarrow{G}\left(p,q\right)$ for each p and q.

(iv) Apply the inverse DFT to the above values to obtain the restored image as described in (5.32).

5.3.2 Computational Complexity

We now analyse the complexity of our algorithm using the Big O notation. Here n is the number of pixels in the image, so $n = |\mathbf{V}|$.

Step 1 DFT computation using the FFT algorithm: $O(n \log n)$.

Step 2 Computation of $\widehat{\boldsymbol{\alpha}}(r)$: $O(n)$.
Computation of $\widehat{\sigma}(r)$: $O(n)$.
Total: $O(n)$.

Step 3 Computation of $e_1(r)$: $O(1)$.
Total: $O(1)$.

Step 4 Computation of the values to be used in the inverse DFT: $O(n)$.
Restored image computation using the FFT algorithm: $O(n \log n)$.
Total: $O(n \log n)$.

This gives a total complexity of $O(n \log n)$.

5.4 Numerical Experiments

In this section, we present the numerical experiments we performed to evaluate our model as well as the results of these experiments. We also discuss these results.

5.4.1 Experiments

We applied our program to the original 512x512 pixels 24-bit truecolor images $\boldsymbol{f}$ presented in Fig.3.1. We first degraded the original images using additive white Gaussian noise with mean 0 and standard deviation $\sigma = 20$ and $\sigma = 40$ to produce 10 degraded images $\boldsymbol{g}$ for each original image and noise value. Examples of the degraded images are presented in Fig.3.2. We then applied our restoration algorithm to the degraded images to obtain the restored images $\widehat{\boldsymbol{f}}$. Examples of the resulting restored images are shown in Fig.5.7 to Fig.5.17.

5.4.2 Experimental Results

Our results are generated by fixing the values of α_2 and α_3 (we remember that $\boldsymbol{\alpha}' = \alpha_2\boldsymbol{\alpha}$ and that $\boldsymbol{\alpha}'' = \alpha_3\boldsymbol{\alpha}$) and applying our model to restore each set of 10 degraded images described in section 5.4.1 to obtain restored image sets containing 10 restored images for each combination of the values of α_2 and α_3, σ and each original image. We apply that procedure for values of α_2 and α_3 in the range of $]-0.5, 0.5[$ with a step of 0.1 (we use the values -0.49 and 0.49 as the higher and lower bounds).

We then measure the value of the the mean square error (MSE) and the mean structural similarity index (MSSIM) between the original image and the restored image for each restored image. These measurements allow us to calculate the sample mean of the MSE and MSSIM for each set of restored images. The MSE is used as a measure of the efficiency of our correction and is defined in equation (3.61). The MSSIM is also used as a measure of the efficiency of our correction and is described in section 3.4.2. Additional details about the MSE and MSSIM can also be found in section 2.4.2.

Figures 5.1, 5.2 and 5.3 show, for various values of α_2 and α_3, the values of the sample mean for the MSE. By looking at these figures, we observe that the MSE has similar levels along the lines of direction $\alpha_3 = -\frac{\alpha_2}{2} + b$ for all images and noise levels. We also notice that the values of the MSE suddenly become very large in the region $\alpha_3 < -\frac{\alpha_2}{2} - 0.25$ for all images and noise levels. In the case of the Peppers and Lenna images, we observe the lowest values of the MSE in the region around the line $\alpha_3 = -\frac{\alpha_2}{2} - 0.25$, right next to the limit where the MSE suddenly increases dramatically. In the case of the Mandrill image, the lowest MSE is more to the right, in the region around $(\alpha_2, \alpha_3) = (-0.2, 0)$ for both noise levels.

Figures 5.4, 5.5 and 5.6 show, for various values of α_2 and α_3, the values of the sample mean for the estimated values of $\widehat{\sigma}^2$. By looking at these figures, we observe that the values of $\widehat{\sigma}^2$ become very large or even negative in the region $\alpha_3 < -\frac{\alpha_2}{2} - 0.25$ for all images and noise levels. We believe that this is due to a diverging value of the evidence in that region.

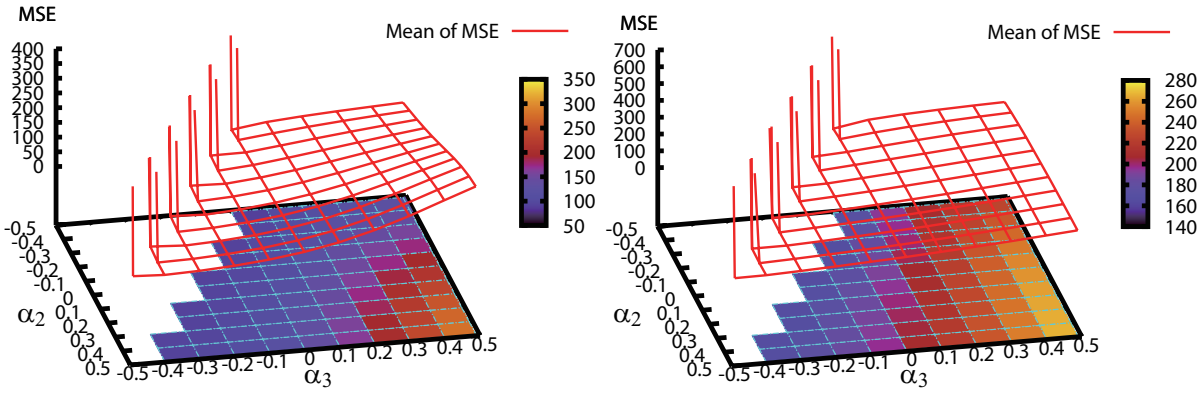

(a) $\sigma = 20$. (b) $\sigma = 40$.

Figure 5.1: Mean square error MSE($\boldsymbol{f}, \widehat{\boldsymbol{f}}$) for the restored versions of the Peppers image (Fig. 3.1a). The degraded images were generated with noise levels of $\sigma = 20$ in (a) and $\sigma = 40$ in (b). The estimates $\widehat{\boldsymbol{\alpha}}$ and $\widehat{\sigma}$ are obtained by maximizing $\log \Pr\{\boldsymbol{G} = \boldsymbol{g}|\boldsymbol{\alpha}, \alpha_2, \alpha_3, \sigma\}$ with respect to $\boldsymbol{\alpha}$ and σ for each fixed value of α_2 and α_3. Here, the restored image $\widehat{\boldsymbol{f}}$ is defined as $\widehat{\boldsymbol{f}}\,(\widehat{\boldsymbol{\alpha}}, \alpha_2, \alpha_3, \widehat{\sigma})$ for each value of α_2 and α_3. The values shown are the sample mean values ($\overline{x}$) of the 10 degraded images for each noise level.

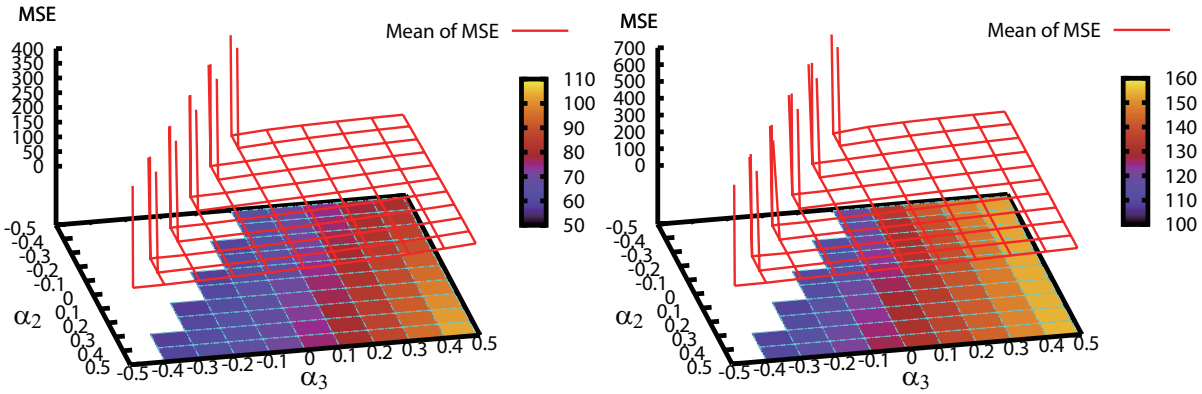

(a) $\sigma = 20$. (b) $\sigma = 40$.

Figure 5.2: Mean square error MSE($\boldsymbol{f}, \widehat{\boldsymbol{f}}$) for the restored versions of the Lenna image (Fig. 3.1b). The degraded images were generated with noise levels of $\sigma = 20$ in (a) and $\sigma = 40$ in (b). The estimates $\widehat{\boldsymbol{\alpha}}$ and $\widehat{\sigma}$ are obtained by maximizing $\log \Pr\{\boldsymbol{G} = \boldsymbol{g}|\boldsymbol{\alpha}, \alpha_2, \alpha_3, \sigma\}$ with respect to $\boldsymbol{\alpha}$ and σ for each fixed value of α_2 and α_3. Here, the restored image $\widehat{\boldsymbol{f}}$ is defined as $\widehat{\boldsymbol{f}}\,(\widehat{\boldsymbol{\alpha}}, \alpha_2, \alpha_3, \widehat{\sigma})$ for each value of α_2 and α_3. The values shown are the sample mean values ($\overline{x}$) of the 10 degraded images for each noise level.

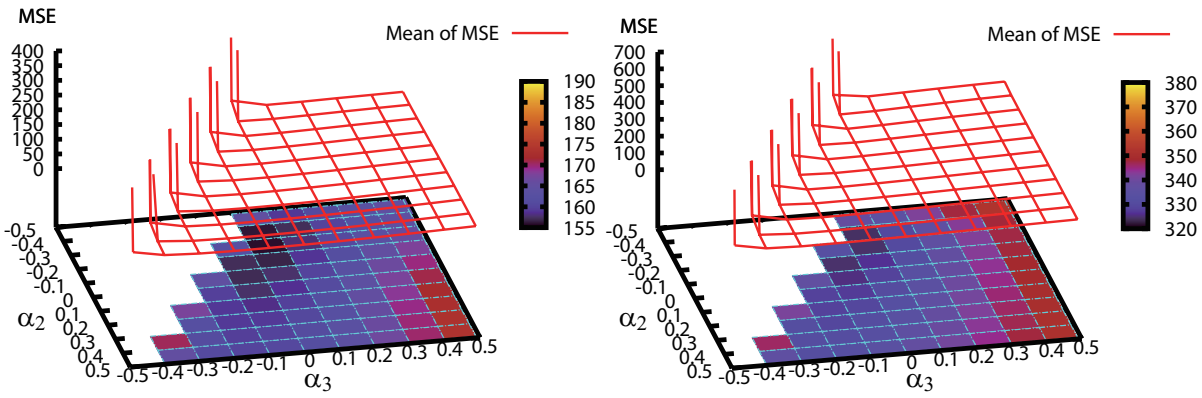

(a) $\sigma = 20$. (b) $\sigma = 40$.

Figure 5.3: Mean square error MSE($\boldsymbol{f}, \widehat{\boldsymbol{f}}$) for the restored versions of the Mandrill image (Fig. 3.1c). The degraded images were generated with noise levels of $\sigma = 20$ in (a) and $\sigma = 40$ in (b). The estimates $\widehat{\boldsymbol{\alpha}}$ and $\widehat{\sigma}$ are obtained by maximizing $\log \Pr\{\boldsymbol{G} = \boldsymbol{g} | \boldsymbol{\alpha}, \alpha_2, \alpha_3, \sigma\}$ with respect to $\boldsymbol{\alpha}$ and σ for each fixed value of α_2 and α_3. Here, the restored image $\widehat{\boldsymbol{f}}$ is defined as $\widehat{\boldsymbol{f}}\,(\widehat{\boldsymbol{\alpha}}, \alpha_2, \alpha_3, \widehat{\sigma})$ for each value of α_2 and α_3. The values shown are the sample mean values ($\overline{x}$) of the 10 degraded images for each noise level.

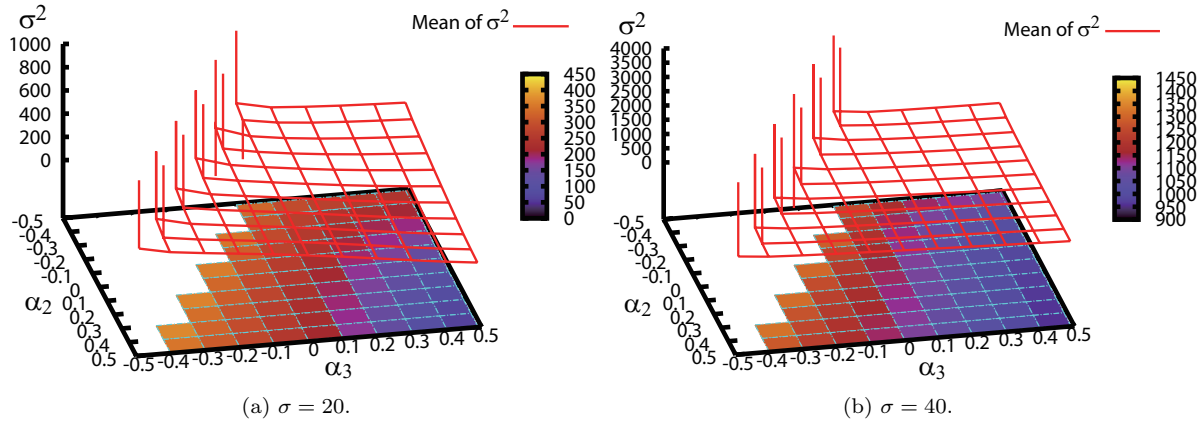

(a) $\sigma = 20$. (b) $\sigma = 40$.

Figure 5.4: Estimate $\widehat{\sigma}^2$ for the restored versions of the Peppers image (Fig. 3.1a). The degraded images were generated with noise levels of $\sigma = 20$ in (a) and $\sigma = 40$ in (b). The estimate $\widehat{\sigma}$ is obtained by maximizing $\log \Pr\{\boldsymbol{G} = \boldsymbol{g} | \boldsymbol{\alpha}, \alpha_2, \alpha_3, \sigma\}$ with respect to $\boldsymbol{\alpha}$ and σ for each combination of the fixed values of α_2 and α_3. The values shown are the sample mean values ($\overline{x}$) of the 10 degraded images for each noise level.

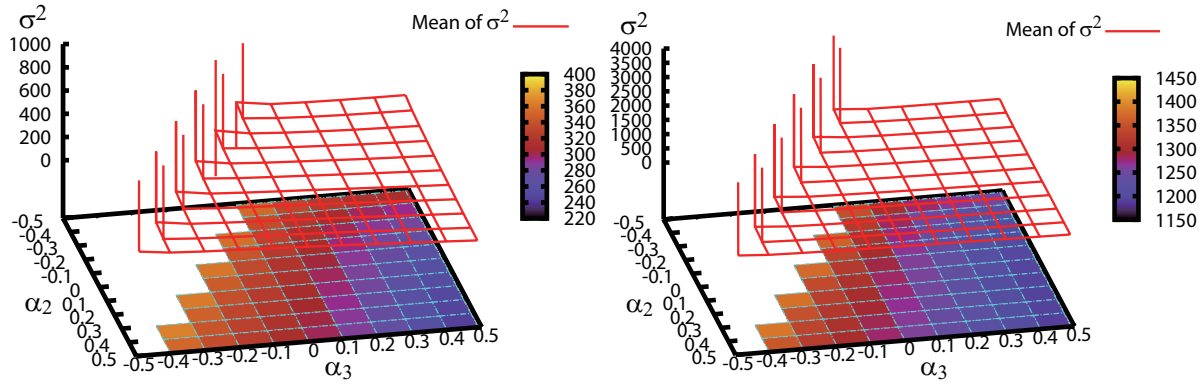

(a) $\sigma = 20$. (b) $\sigma = 40$.

Figure 5.5: Estimate $\widehat{\sigma}^2$ for the restored versions of the Lenna image (Fig. 3.1b). The degraded images were generated with noise levels of $\sigma = 20$ in (a) and $\sigma = 40$ in (b). The estimate $\widehat{\sigma}$ is obtained by maximizing $\log \Pr\{\boldsymbol{G} = \boldsymbol{g}|\boldsymbol{\alpha}, \alpha_2, \alpha_3, \sigma\}$ with respect to $\boldsymbol{\alpha}$ and σ for each combination of the fixed values of α_2 and α_3. The values shown are the sample mean values ($\overline{x}$) of the 10 degraded images for each noise level.

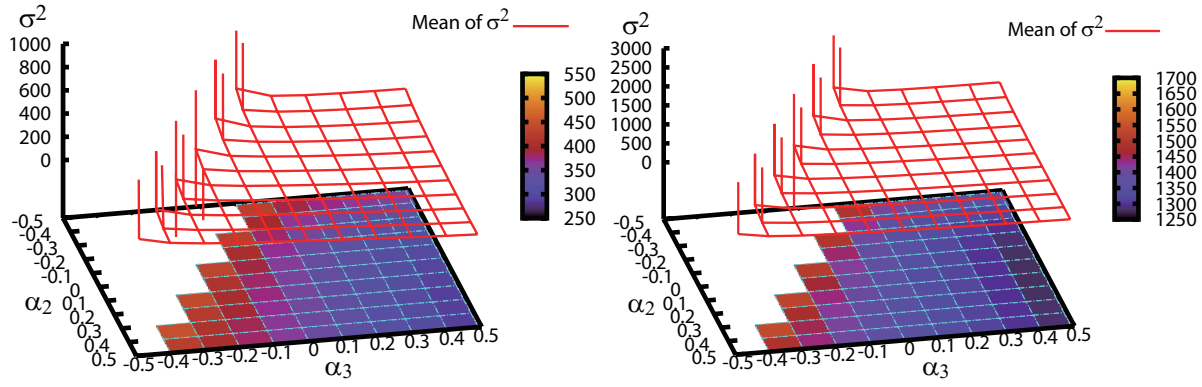

(a) $\sigma = 20$. (b) $\sigma = 40$.

Figure 5.6: Estimate $\widehat{\sigma}^2$ for the restored versions of the Mandrill image (Fig. 3.1c). The degraded images were generated with noise levels of $\sigma = 20$ in (a) and $\sigma = 40$ in (b). The estimate $\widehat{\sigma}$ is obtained by maximizing $\log \Pr\{\boldsymbol{G} = \boldsymbol{g}|\boldsymbol{\alpha}, \alpha_2, \alpha_3, \sigma\}$ with respect to $\boldsymbol{\alpha}$ and σ for each combination of the fixed values of α_2 and α_3. The values shown are the sample mean values ($\overline{x}$) of the 10 degraded images for each noise level.

Figures 5.7 to 5.17 show some results of the application of the third neighbour extension algorithm to the Peppers, Lenna and Mandrill colour images for noise values of $\sigma = 20$ and $\sigma = 40$.

We only show the results for values of (α_2, α_3) of $(-0.2, -0.1)$ and $(-0.3, -0.1)$, since we expect these values to approach the Mexican Hat weighting function shown in Fig 1.2, the combinations producing the smallest MSE, namely $(-0.49, 0.0)$ for Peppers, $(-0.3, -0.1)$ and $(0.4, -0.4)$ for Lenna with $\sigma = 20$ and $\sigma = 40$ respectively, as well as $(-0.25, 0.0)$ and $(-0.3, 0.0)$ for Mandrill with $\sigma = 20$ and $\sigma = 40$ respectively, as well as the combinations producing the highest MSSIM, namely $(-0.3, -0.1)$ for Peppers, $(-0.1, -0.2)$ and $(-0.3, -0.1)$ for Lenna with $\sigma = 20$ and $\sigma = 40$ respectively, as well as $(-0.4, 0.0)$ and $(-0.35, 0.0)$ for Mandrill with $\sigma = 20$ and $\sigma = 40$ respectively. Also, only one restored image from the set of 10 is shown.

A visual inspection of the corrected images reveals that, although it does not produce the lowest MSE nor the highest MSSIM, the best correction, from a human perception point of view, is achieved with values of $(\alpha_2, \alpha_3) = (-0.2, -0.1)$. Indeed that choice of values offers good noise reduction with less blurring than with $(\alpha_2, \alpha_3) = (-0.3, -0.1)$ and without the introduction of artefacts such as the horizontal-vertical grid-like artefacts observed in the Peppers images with the lowest MSE as well as the diagonal grid-like artefacts observed in the Lenna images with the highest MSSIM. In the case of the Mandrill images (Figs 5.15 - 5.18), it is difficult to choose which corrected image is the best one, but in our opinion, the images for values of $(\alpha_2, \alpha_3) = (-0.2, -0.1)$ offer the best compromise between blurring as observed in Fig. 5.17b and residual noise as observed in Figs 5.17c and 5.17d.

(a) $(\alpha_2, \alpha_3) = (-0.2, -0.1)$. MSE=88. MSSIM=0.8421.

(b) $(\alpha_2, \alpha_3) = (-0.3, -0.1)$. MSE=92. MSSIM=0.8733.

(c) $(\alpha_2, \alpha_3) = (-0.49, 0.0)$. MSE=79. MSSIM=0.8557.

Figure 5.7: Restored images $\widehat{\boldsymbol{f}}(\boldsymbol{g}, \widehat{\boldsymbol{\alpha}}, \alpha_2, \alpha_3, \widehat{\sigma})$ obtained by means of the proposed Gauss-Markov random field model for one of the degraded versions of the Peppers image (Fig. 3.1a). The degraded image was generated with a noise level of $\sigma = 20$ and is shown in Fig. 3.15a. (a) $\alpha_2 = -0.2$, $\alpha_3 = -0.1$, $\text{MSE}(\boldsymbol{f}, \widehat{\boldsymbol{f}}(\boldsymbol{g}, \widehat{\boldsymbol{\alpha}}, \alpha_2, \alpha_3, \widehat{\sigma})) = 88$, $\text{MSSIM}(\boldsymbol{f}, \widehat{\boldsymbol{f}}(\boldsymbol{g}, \widehat{\boldsymbol{\alpha}}, \alpha_2, \alpha_3, \widehat{\sigma})) = 0.8421$. (b) $\alpha_2 = -0.3$, $\alpha_3 = -0.1$, $\text{MSE}(\boldsymbol{f}, \widehat{\boldsymbol{f}}(\boldsymbol{g}, \widehat{\boldsymbol{\alpha}}, \alpha_2, \alpha_3, \widehat{\sigma})) = 92$, $\text{MSSIM}(\boldsymbol{f}, \widehat{\boldsymbol{f}}(\boldsymbol{g}, \widehat{\boldsymbol{\alpha}}, \alpha_2, \alpha_3, \widehat{\sigma})) = 0.8733$. (c) $\alpha_2 = -0.49$, $\alpha_3 = 0.0$, $\text{MSE}(\boldsymbol{f}, \widehat{\boldsymbol{f}}(\boldsymbol{g}, \widehat{\boldsymbol{\alpha}}, \alpha_2, \alpha_3, \widehat{\sigma})) = 79$, $\text{MSSIM}(\boldsymbol{f}, \widehat{\boldsymbol{f}}(\boldsymbol{g}, \widehat{\boldsymbol{\alpha}}, \alpha_2, \alpha_3, \widehat{\sigma})) = 0.8557$.

(a) $(\alpha_2, \alpha_3) = (-0.2, -0.1)$. MSE=88. MSSIM=0.8421.

(b) $(\alpha_2, \alpha_3) = (-0.3, -0.1)$. MSE=92. MSSIM=0.8733.

(c) $(\alpha_2, \alpha_3) = (-0.49, 0.0)$. MSE=79. MSSIM=0.8557.

Figure 5.8: Details of the restored images $\widehat{\boldsymbol{f}}(\boldsymbol{g}, \widehat{\boldsymbol{\alpha}}, \alpha_2, \alpha_3, \widehat{\sigma})$ in Fig. 5.7. (a) Restored image $\widehat{\boldsymbol{f}}(\boldsymbol{g}, \widehat{\boldsymbol{\alpha}}, \alpha_2, \alpha_3, \widehat{\sigma})$ in Fig. 5.7a. (b) Restored image $\widehat{\boldsymbol{f}}(\boldsymbol{g}, \widehat{\boldsymbol{\alpha}}, \alpha_2, \alpha_3, \widehat{\sigma})$ in Fig. 5.7b. (c) Restored image $\widehat{\boldsymbol{f}}(\boldsymbol{g}, \widehat{\boldsymbol{\alpha}}, \alpha_2, \alpha_3, \widehat{\sigma})$ in Fig. 5.7c.

(a) $(\alpha_2, \alpha_3) = (-0.2, -0.1)$. MSE=161. MSSIM=0.7469.

(b) $(\alpha_2, \alpha_3) = (-0.3, -0.1)$. MSE=159. MSSIM=0.8024.

(c) $(\alpha_2, \alpha_3) = (-0.49, 0.0)$. MSE=151. MSSIM=0.7664.

Figure 5.9: Restored images $\widehat{\boldsymbol{f}}(\boldsymbol{g}, \widehat{\boldsymbol{\alpha}}, \alpha_2, \alpha_3, \widehat{\sigma})$ obtained by means of the proposed Gauss-Markov random field model for one of the degraded versions of the Peppers image (Fig. 3.1a). The degraded image was generated with a noise level of $\sigma = 40$ and is shown in Fig. 3.17a. (a) $\alpha_2 = -0.2$, $\alpha_3 = -0.1$, $\mathrm{MSE}(\boldsymbol{f}, \widehat{\boldsymbol{f}}(\boldsymbol{g}, \widehat{\boldsymbol{\alpha}}, \alpha_2, \alpha_3, \widehat{\sigma})) = 161$, $\mathrm{MSSIM}(\boldsymbol{f}, \widehat{\boldsymbol{f}}(\boldsymbol{g}, \widehat{\boldsymbol{\alpha}}, \alpha_2, \alpha_3, \widehat{\sigma})) = 0.7469$. (b) $\alpha_2 = -0.3$, $\alpha_3 = -0.1$, $\mathrm{MSE}(\boldsymbol{f}, \widehat{\boldsymbol{f}}(\boldsymbol{g}, \widehat{\boldsymbol{\alpha}}, \alpha_2, \alpha_3, \widehat{\sigma})) = 159$, $\mathrm{MSSIM}(\boldsymbol{f}, \widehat{\boldsymbol{f}}(\boldsymbol{g}, \widehat{\boldsymbol{\alpha}}, \alpha_2, \alpha_3, \widehat{\sigma})) = 0.8024$. (c) $\alpha_2 = -0.49$, $\alpha_3 = 0.0$, $\mathrm{MSE}(\boldsymbol{f}, \widehat{\boldsymbol{f}}(\boldsymbol{g}, \widehat{\boldsymbol{\alpha}}, \alpha_2, \alpha_3, \widehat{\sigma})) = 151$, $\mathrm{MSSIM}(\boldsymbol{f}, \widehat{\boldsymbol{f}}(\boldsymbol{g}, \widehat{\boldsymbol{\alpha}}, \alpha_2, \alpha_3, \widehat{\sigma})) = 0.7664$.

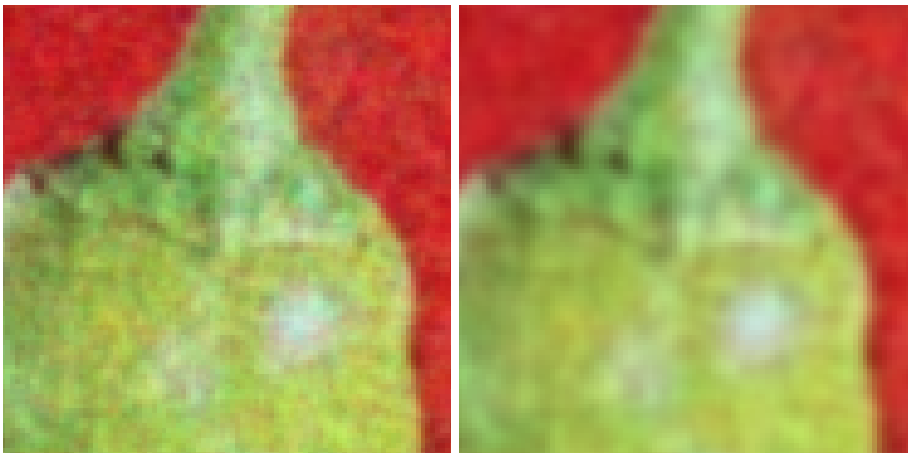

(a) $(\alpha_2, \alpha_3) = (-0.2, -0.1)$. MSE=161. MSSIM=0.7469.

(b) $(\alpha_2, \alpha_3) = (-0.3, -0.1)$. MSE=159. MSSIM=0.8024.

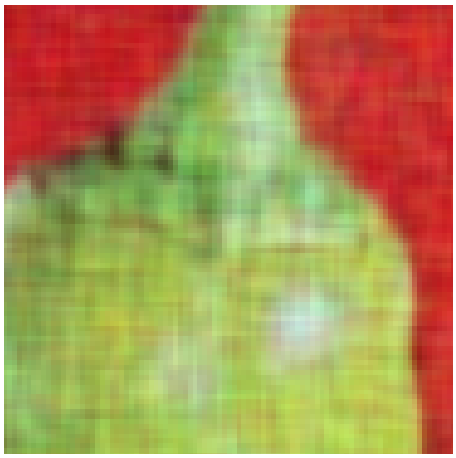

(c) $(\alpha_2, \alpha_3) = (-0.49, 0.0)$. MSE=151. MSSIM=0.7664.

Figure 5.10: Details of the restored images $\widehat{\boldsymbol{f}}(\boldsymbol{g}, \widehat{\boldsymbol{\alpha}}, \alpha_2, \alpha_3, \widehat{\sigma})$ in Fig. 5.9. (a) Restored image $\widehat{\boldsymbol{f}}(\boldsymbol{g}, \widehat{\boldsymbol{\alpha}}, \alpha_2, \alpha_3, \widehat{\sigma})$ in Fig. 5.9a. (b) Restored image $\widehat{\boldsymbol{f}}(\boldsymbol{g}, \widehat{\boldsymbol{\alpha}}, \alpha_2, \alpha_3, \widehat{\sigma})$ in Fig. 5.9b. (c) Restored image $\widehat{\boldsymbol{f}}(\boldsymbol{g}, \widehat{\boldsymbol{\alpha}}, \alpha_2, \alpha_3, \widehat{\sigma})$ in Fig. 5.9c.

(a) $(\alpha_2, \alpha_3) = (-0.2, -0.1)$. MSE=56.5. MSSIM=0.87982.

(b) $(\alpha_2, \alpha_3) = (-0.3, -0.1)$. MSE=55.6. MSSIM=0.89495.

(c) $(\alpha_2, \alpha_3) = (-0.1, -0.2)$. MSE=55.7. MSSIM=0.89498.

Figure 5.11: Restored images $\widehat{\boldsymbol{f}}(\boldsymbol{g}, \widehat{\boldsymbol{\alpha}}, \alpha_2, \alpha_3, \widehat{\sigma})$ obtained by means of the proposed Gauss-Markov random field model for one of the degraded versions of the Lenna image (Fig. 3.1b). The degraded image was generated with a noise level of $\sigma = 20$ and is shown in Fig. 3.19a. (a) $\alpha_2 = -0.2$, $\alpha_3 = -0.1$, $\mathrm{MSE}(\boldsymbol{f}, \widehat{\boldsymbol{f}}(\boldsymbol{g}, \widehat{\boldsymbol{\alpha}}, \alpha_2, \alpha_3, \widehat{\sigma})) = 56.5$, $\mathrm{MSSIM}(\boldsymbol{f}, \widehat{\boldsymbol{f}}(\boldsymbol{g}, \widehat{\boldsymbol{\alpha}}, \alpha_2, \alpha_3, \widehat{\sigma})) = 0.87982$. (b) $\alpha_2 = -0.3$, $\alpha_3 = -0.1$, $\mathrm{MSE}(\boldsymbol{f}, \widehat{\boldsymbol{f}}(\boldsymbol{g}, \widehat{\boldsymbol{\alpha}}, \alpha_2, \alpha_3, \widehat{\sigma})) = 55.6$, $\mathrm{MSSIM}(\boldsymbol{f}, \widehat{\boldsymbol{f}}(\boldsymbol{g}, \widehat{\boldsymbol{\alpha}}, \alpha_2, \alpha_3, \widehat{\sigma})) = 0.89495$. (c) $\alpha_2 = -0.1$, $\alpha_3 = -0.2$, $\mathrm{MSE}(\boldsymbol{f}, \widehat{\boldsymbol{f}}(\boldsymbol{g}, \widehat{\boldsymbol{\alpha}}, \alpha_2, \alpha_3, \widehat{\sigma})) = 55.7$, $\mathrm{MSSIM}(\boldsymbol{f}, \widehat{\boldsymbol{f}}(\boldsymbol{g}, \widehat{\boldsymbol{\alpha}}, \alpha_2, \alpha_3, \widehat{\sigma})) = 0.89498$.

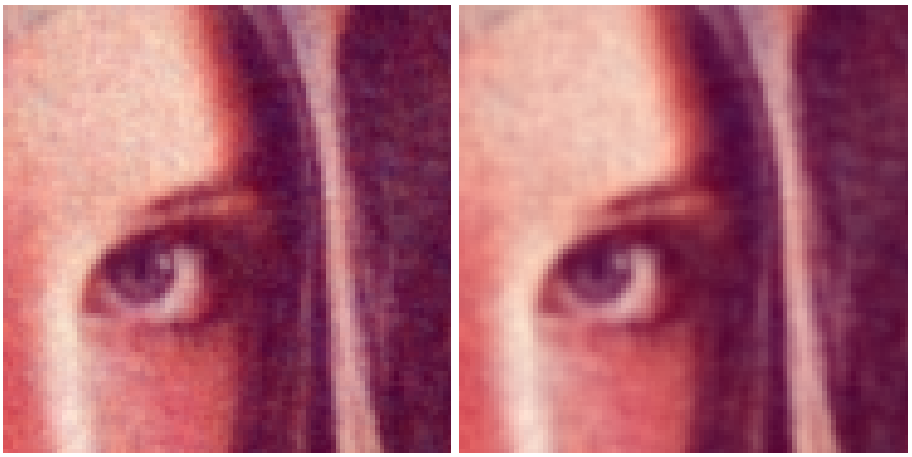

(a) $(\alpha_2, \alpha_3) = (-0.2, -0.1)$. MSE=56.5. MSSIM=0.87982.

(b) $(\alpha_2, \alpha_3) = (-0.3, -0.1)$. MSE=55.6. MSSIM=0.89495.

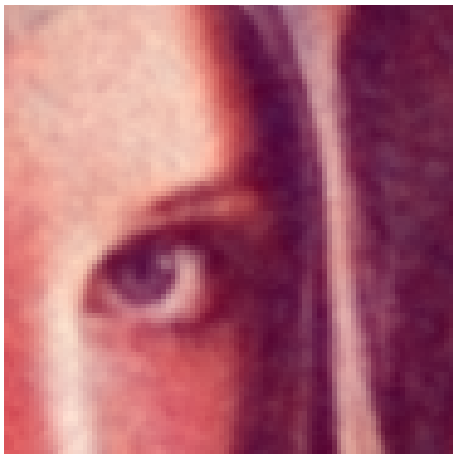

(c) $(\alpha_2, \alpha_3) = (-0.1, -0.2)$. MSE=55.7. MSSIM=0.89498.

Figure 5.12: Details of the restored images $\widehat{\boldsymbol{f}}(\boldsymbol{g}, \widehat{\boldsymbol{\alpha}}, \alpha_2, \alpha_3, \widehat{\sigma})$ in Fig. 5.11. (a) Restored image $\widehat{\boldsymbol{f}}(\boldsymbol{g}, \widehat{\boldsymbol{\alpha}}, \alpha_2, \alpha_3, \widehat{\sigma})$ in Fig. 5.11a. (b) Restored image $\widehat{\boldsymbol{f}}(\boldsymbol{g}, \widehat{\boldsymbol{\alpha}}, \alpha_2, \alpha_3, \widehat{\sigma})$ in Fig. 5.11b. (c) Restored image $\widehat{\boldsymbol{f}}(\boldsymbol{g}, \widehat{\boldsymbol{\alpha}}, \alpha_2, \alpha_3, \widehat{\sigma})$ in Fig. 5.11c.

(a) $(\alpha_2, \alpha_3) = (-0.2, -0.1)$. MSE=106.5. MSSIM=0.7972.

(b) $(\alpha_2, \alpha_3) = (-0.3, -0.1)$. MSE=105.4. MSSIM=0.8291.

(c) $(\alpha_2, \alpha_3) = (0.4, -0.4)$. MSE=104.8. MSSIM=0.8047.

Figure 5.13: Restored images $\widehat{\boldsymbol{f}}(\boldsymbol{g}, \widehat{\boldsymbol{\alpha}}, \alpha_2, \alpha_3, \widehat{\sigma})$ obtained by means of the proposed Gauss-Markov random field model for one of the degraded versions of the Lenna image (Fig. 3.1b). The degraded image was generated with a noise level of $\sigma = 40$ and is shown in Fig. 3.21a. (a) $\alpha_2 = -0.2$, $\alpha_3 = -0.1$, $\mathrm{MSE}(\boldsymbol{f}, \widehat{\boldsymbol{f}}(\boldsymbol{g}, \widehat{\boldsymbol{\alpha}}, \alpha_2, \alpha_3, \widehat{\sigma})) = 106.5$, $\mathrm{MSSIM}(\boldsymbol{f}, \widehat{\boldsymbol{f}}(\boldsymbol{g}, \widehat{\boldsymbol{\alpha}}, \alpha_2, \alpha_3, \widehat{\sigma})) = 0.7972$. (b) $\alpha_2 = -0.3$, $\alpha_3 = -0.1$, $\mathrm{MSE}(\boldsymbol{f}, \widehat{\boldsymbol{f}}(\boldsymbol{g}, \widehat{\boldsymbol{\alpha}}, \alpha_2, \alpha_3, \widehat{\sigma})) = 105.4$, $\mathrm{MSSIM}(\boldsymbol{f}, \widehat{\boldsymbol{f}}(\boldsymbol{g}, \widehat{\boldsymbol{\alpha}}, \alpha_2, \alpha_3, \widehat{\sigma})) = 0.8291$. (c) $\alpha_2 = 0.4$, $\alpha_3 = -0.4$, $\mathrm{MSE}(\boldsymbol{f}, \widehat{\boldsymbol{f}}(\boldsymbol{g}, \widehat{\boldsymbol{\alpha}}, \alpha_2, \alpha_3, \widehat{\sigma})) = 104.8$, $\mathrm{MSSIM}(\boldsymbol{f}, \widehat{\boldsymbol{f}}(\boldsymbol{g}, \widehat{\boldsymbol{\alpha}}, \alpha_2, \alpha_3, \widehat{\sigma})) = 0.8047$.

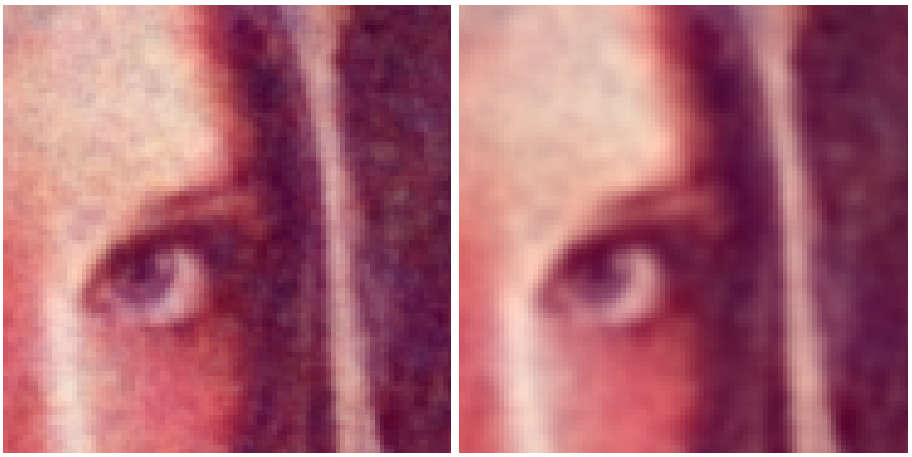

(a) $(\alpha_2, \alpha_3) = (-0.2, -0.1)$. MSE=106.5. MSSIM=0.7972.

(b) $(\alpha_2, \alpha_3) = (-0.3, -0.1)$. MSE=105.4. MSSIM=0.8291.

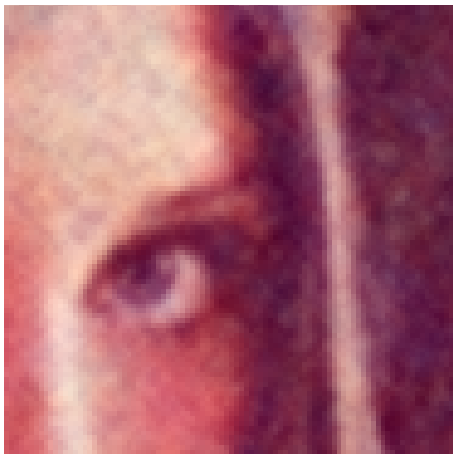

(c) $(\alpha_2, \alpha_3) = (0.4, -0.4)$. MSE=104.8. MSSIM=0.8047.

Figure 5.14: Details of the restored images $\widehat{\boldsymbol{f}}(\boldsymbol{g}, \widehat{\boldsymbol{\alpha}}, \alpha_2, \alpha_3, \widehat{\sigma})$ in Fig. 5.13. (a) Restored image $\widehat{\boldsymbol{f}}(\boldsymbol{g}, \widehat{\boldsymbol{\alpha}}, \alpha_2, \alpha_3, \widehat{\sigma})$ in Fig. 5.13a. (b) Restored image $\widehat{\boldsymbol{f}}(\boldsymbol{g}, \widehat{\boldsymbol{\alpha}}, \alpha_2, \alpha_3, \widehat{\sigma})$ in Fig. 5.13b. (c) Restored image $\widehat{\boldsymbol{f}}(\boldsymbol{g}, \widehat{\boldsymbol{\alpha}}, \alpha_2, \alpha_3, \widehat{\sigma})$ in Fig. 5.13c.

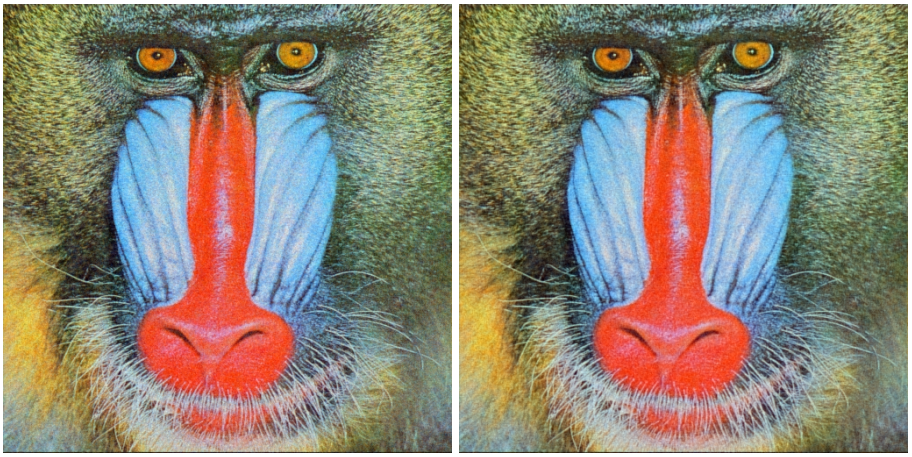

(a) $(\alpha_2, \alpha_3) = (-0.2, -0.1)$. MSE=160. MSSIM=0.9107.

(b) $(\alpha_2, \alpha_3) = (-0.3, -0.1)$. MSE=180. MSSIM=0.9045.

(c) $(\alpha_2, \alpha_3) = (-0.25, 0.0)$. MSE=156. MSSIM=0.9108.

(d) $(\alpha_2, \alpha_3) = (-0.4, 0.0)$. MSE=158. MSSIM=0.9112.

Figure 5.15: Restored images $\widehat{\boldsymbol{f}}(\boldsymbol{g}, \widehat{\boldsymbol{\alpha}}, \alpha_2, \alpha_3, \widehat{\sigma})$ obtained by means of the proposed Gauss-Markov random field model for one of the degraded versions of the Mandrill image (Fig. 3.1c). The degraded image was generated with a noise level of $\sigma = 20$ and is shown in Fig. 3.23a. (a) $\alpha_2 = -0.2$, $\alpha_3 = -0.1$, $\text{MSE}(\boldsymbol{f}, \widehat{\boldsymbol{f}}(\boldsymbol{g}, \widehat{\boldsymbol{\alpha}}, \alpha_2, \alpha_3, \widehat{\sigma})) = 160$, $\text{MSSIM}(\boldsymbol{f}, \widehat{\boldsymbol{f}}(\boldsymbol{g}, \widehat{\boldsymbol{\alpha}}, \alpha_2, \alpha_3, \widehat{\sigma})) = 0.9107$. (b) $\alpha_2 = -0.3$, $\alpha_3 = -0.1$, $\text{MSE}(\boldsymbol{f}, \widehat{\boldsymbol{f}}(\boldsymbol{g}, \widehat{\boldsymbol{\alpha}}, \alpha_2, \alpha_3, \widehat{\sigma})) = 180$, $\text{MSSIM}(\boldsymbol{f}, \widehat{\boldsymbol{f}}(\boldsymbol{g}, \widehat{\boldsymbol{\alpha}}, \alpha_2, \alpha_3, \widehat{\sigma})) = 0.9045$. (c) $\alpha_2 = -0.25$, $\alpha_3 = 0.0$, $\text{MSE}(\boldsymbol{f}, \widehat{\boldsymbol{f}}(\boldsymbol{g}, \widehat{\boldsymbol{\alpha}}, \alpha_2, \alpha_3, \widehat{\sigma})) = 156$, $\text{MSSIM}(\boldsymbol{f}, \widehat{\boldsymbol{f}}(\boldsymbol{g}, \widehat{\boldsymbol{\alpha}}, \alpha_2, \alpha_3, \widehat{\sigma})) = 0.9108$. (d) $\alpha_2 = -0.4$, $\alpha_3 = 0.0$, $\text{MSE}(\boldsymbol{f}, \widehat{\boldsymbol{f}}(\boldsymbol{g}, \widehat{\boldsymbol{\alpha}}, \alpha_2, \alpha_3, \widehat{\sigma})) = 158$, $\text{MSSIM}(\boldsymbol{f}, \widehat{\boldsymbol{f}}(\boldsymbol{g}, \widehat{\boldsymbol{\alpha}}, \alpha_2, \alpha_3, \widehat{\sigma})) = 0.9112$.

(a) $(\alpha_2, \alpha_3) = (-0.2, -0.1)$. MSE=160. MSSIM=0.9107.

(b) $(\alpha_2, \alpha_3) = (-0.3, -0.1)$. MSE=180. MSSIM=0.9045.

(c) $(\alpha_2, \alpha_3) = (-0.25, 0.0)$. MSE=156. MSSIM=0.9108.

(d) $(\alpha_2, \alpha_3) = (-0.4, 0.0)$. MSE=158. MSSIM=0.9112.

Figure 5.16: Details of the restored images $\widehat{\boldsymbol{f}}(\boldsymbol{g}, \widehat{\boldsymbol{\alpha}}, \alpha_2, \alpha_3, \widehat{\sigma})$ in Fig. 5.15. (a) Restored image $\widehat{\boldsymbol{f}}(\boldsymbol{g}, \widehat{\boldsymbol{\alpha}}, \alpha_2, \alpha_3, \widehat{\sigma})$ in Fig. 5.15a. (b) Restored image $\widehat{\boldsymbol{f}}(\boldsymbol{g}, \widehat{\boldsymbol{\alpha}}, \alpha_2, \alpha_3, \widehat{\sigma})$ in Fig. 5.15b. (c) Restored image $\widehat{\boldsymbol{f}}(\boldsymbol{g}, \widehat{\boldsymbol{\alpha}}, \alpha_2, \alpha_3, \widehat{\sigma})$ in Fig. 5.15c. (d) Restored image $\widehat{\boldsymbol{f}}(\boldsymbol{g}, \widehat{\boldsymbol{\alpha}}, \alpha_2, \alpha_3, \widehat{\sigma})$ in Fig. 5.15d.

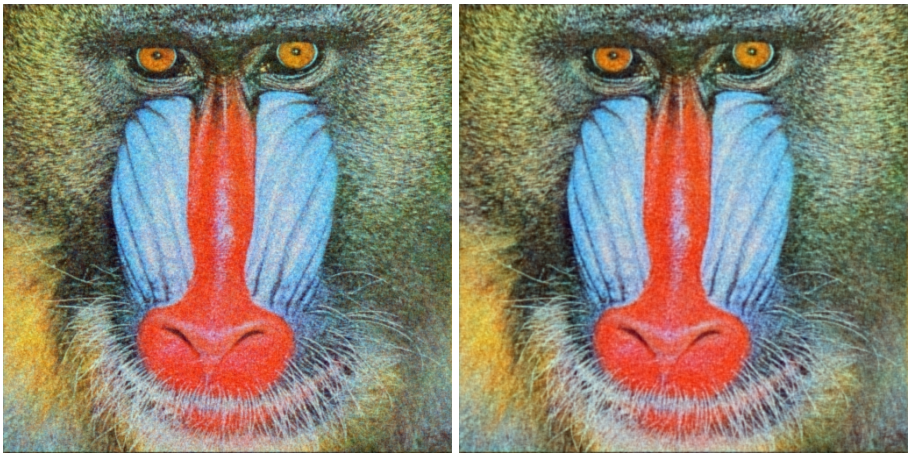

(a) $(\alpha_2, \alpha_3) = (-0.2, -0.1)$. MSE=325.6. MSSIM=0.8115.

(b) $(\alpha_2, \alpha_3) = (-0.3, -0.1)$. MSE=360.8. MSSIM=0.8010.

(c) $(\alpha_2, \alpha_3) = (-0.3, 0.0)$. MSE=320.7. MSSIM=0.8114.

(d) $(\alpha_2, \alpha_3) = (-0.35, 0.0)$. MSE=320.8. MSSIM=0.8116.

Figure 5.17: Restored images $\widehat{\boldsymbol{f}}(\boldsymbol{g}, \widehat{\boldsymbol{\alpha}}, \alpha_2, \alpha_3, \widehat{\sigma})$ obtained by means of the proposed Gauss-Markov random field model for one of the degraded versions of the Mandrill image (Fig. 3.1c). The degraded image was generated with a noise level of $\sigma = 40$ and is shown in Fig. 3.25a. (a) $\alpha_2 = -0.2$, $\alpha_3 = -0.1$, $\text{MSE}(\boldsymbol{f}, \widehat{\boldsymbol{f}}(\boldsymbol{g}, \widehat{\boldsymbol{\alpha}}, \alpha_2, \alpha_3, \widehat{\sigma})) = 325.6$, $\text{MSSIM}(\boldsymbol{f}, \widehat{\boldsymbol{f}}(\boldsymbol{g}, \widehat{\boldsymbol{\alpha}}, \alpha_2, \alpha_3, \widehat{\sigma})) = 0.8115$. (b) $\alpha_2 = -0.3$, $\alpha_3 = -0.1$, $\text{MSE}(\boldsymbol{f}, \widehat{\boldsymbol{f}}(\boldsymbol{g}, \widehat{\boldsymbol{\alpha}}, \alpha_2, \alpha_3, \widehat{\sigma})) = 360.8$, $\text{MSSIM}(\boldsymbol{f}, \widehat{\boldsymbol{f}}(\boldsymbol{g}, \widehat{\boldsymbol{\alpha}}, \alpha_2, \alpha_3, \widehat{\sigma})) = 0.8010$. (c) $\alpha_2 = -0.3$, $\alpha_3 = 0.0$, $\text{MSE}(\boldsymbol{f}, \widehat{\boldsymbol{f}}(\boldsymbol{g}, \widehat{\boldsymbol{\alpha}}, \alpha_2, \alpha_3, \widehat{\sigma})) = 320.7$, $\text{MSSIM}(\boldsymbol{f}, \widehat{\boldsymbol{f}}(\boldsymbol{g}, \widehat{\boldsymbol{\alpha}}, \alpha_2, \alpha_3, \widehat{\sigma})) = 0.8114$. (d) $\alpha_2 = -0.35$, $\alpha_3 = 0.0$, $\text{MSE}(\boldsymbol{f}, \widehat{\boldsymbol{f}}(\boldsymbol{g}, \widehat{\boldsymbol{\alpha}}, \alpha_2, \alpha_3, \widehat{\sigma})) = 320.8$, $\text{MSSIM}(\boldsymbol{f}, \widehat{\boldsymbol{f}}(\boldsymbol{g}, \widehat{\boldsymbol{\alpha}}, \alpha_2, \alpha_3, \widehat{\sigma})) = 0.8116$.

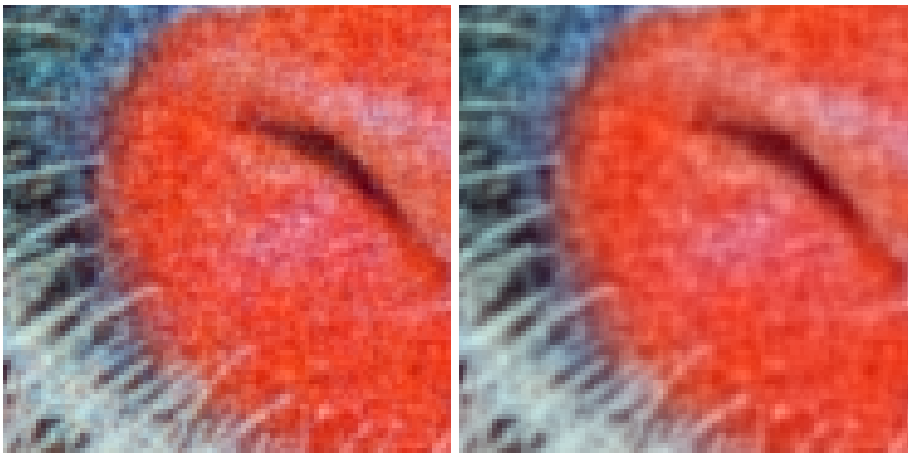

(a) $(\alpha_2, \alpha_3) = (-0.2, -0.1)$. MSE=325.6. MSSIM=0.8115.

(b) $(\alpha_2, \alpha_3) = (-0.3, -0.1)$. MSE=360.8. MSSIM=0.8010.

(c) $(\alpha_2, \alpha_3) = (-0.3, 0.0)$. MSE=320.7. MSSIM=0.8114.

(d) $(\alpha_2, \alpha_3) = (-0.35, 0.0)$. MSE=320.8. MSSIM=0.8116.

Figure 5.18: Details of the restored images $\widehat{\boldsymbol{f}}(\boldsymbol{g}, \widehat{\boldsymbol{\alpha}}, \alpha_2, \alpha_3, \widehat{\sigma})$ in Fig. 5.17. (a) Restored image $\widehat{\boldsymbol{f}}(\boldsymbol{g}, \widehat{\boldsymbol{\alpha}}, \alpha_2, \alpha_3, \widehat{\sigma})$ in Fig. 5.17a. (b) Restored image $\widehat{\boldsymbol{f}}(\boldsymbol{g}, \widehat{\boldsymbol{\alpha}}, \alpha_2, \alpha_3, \widehat{\sigma})$ in Fig. 5.17b. (c) Restored image $\widehat{\boldsymbol{f}}(\boldsymbol{g}, \widehat{\boldsymbol{\alpha}}, \alpha_2, \alpha_3, \widehat{\sigma})$ in Fig. 5.17c. (d) Restored image $\widehat{\boldsymbol{f}}(\boldsymbol{g}, \widehat{\boldsymbol{\alpha}}, \alpha_2, \alpha_3, \widehat{\sigma})$ in Fig. 5.17d.

5.5 Chapter Summary

In this chapter, we described our solvable probabilistic model for colour images using third-neighbour pixel interactions. We derived the mathematical expressions related to this model and proposed an algorithm based on these results. Finally, we presented the results of numerical experiments using our algorithm and confirmed that, with a good combination of the hyperparameters α_2 and α_3, we can generally obtain better image correction results by using our extension to the third-neighbour pixel interactions than by taking only the nearest- and second-neighbour pixel interactions into account. In particular, we saw that by using values of (α_2, α_3) close to $(-0.2, -0.1)$, this model allows better noise reduction than the second-neighbour model without introducing too much blurring and without creating the horizontal and vertical line artefacts observed with the second-neighbour model.

Chapter 6

Conclusion

6.1 Summary and Concluding Remarks

In this thesis, we investigated the extension to second- and third-neighbour pixel interactions of the CAR model defined by Molina in [1] and developed by Tanaka and Inoue in [2], by Tanaka in [3] as well as by Tanaka and Horiguchi in [4] in the context of noise correction in digital images. We defined an extension to the second-neighbour pixel interactions for greyscale images in chapter 2 and for colour images in chapter 3. We then proposed extensions to the third-neighbour pixel interactions for greyscale images in chapter 4 and for colour images in chapter 5. In each of these chapters, we also proposed algorithms based on the described models and performed numerical experiments using these algorithms to evaluate the quality of the resulting image correction. We used the MSE and MSSIM as tools to evaluate the performance of our algorithms and the results showed that, with a good choice of the hyperparameters controlling the models, the second-neighbour model has a better performance than the original model and that the third-neighbour model has a better performance than the second-neighbour model. Visual inspection of the results also revealed that the second-neighbour model allows a good preservation of horizontal and vertical edges in the images, but that it also introduces horizontal and vertical line artefacts. On the other hand, the third-neighbour model manages to reduce significantly the noise level without causing too much blurring and without introducing visible artefacts. We also calculated the computational complexity for each algorithm and saw that, if we ignore the problem of the selection of the hyperparameters α_2 and α_3, the extension of the models to the second- and third-neighbour pixel interactions has no significant impact on the complexity of the algorithms.

6.2 Future Problems

As mentioned above, we did not investigate the problem of the selection of the hyperparameters α_2 and α_3 controlling our models. Indeed, in our experiments, we tried numerous combinations of these parameters and then compared the results obtained. Such a method is computationally intensive. For instance, it took more than 2 weeks of continuous processing to produce the 7260 result images for the numerical experiment of chapter 5 (we had 3 original images x 2 noise levels x 10 degraded image versions x 11 values of α_2 x 11 values of α_3). Therefore, it would be interesting to investigate a way of selecting automatically good estimates for the values of these hyperparameters. Such a method could potentially find more precise values for these hyperparameters while simultaneously reducing the computational load.

Acknowledgements

First and foremost, I am very much indebted to my research supervisor, Professor Kazuyuki Tanaka for welcoming me in his laboratory and helping me to adapt to and enjoy life in Japan. His never-failing guidance and advice were invaluable for this research. I am also grateful to Professor Takafumi Aoki and Professor Mitsuyuki Nakao for taking time away from their busy schedules to act as reviewers for my Master's thesis and for their precious comments and advice. I would also like to express my gratitude to Professor Yuji Waizumi for his precious guidance and generosity. I also thank Assistant-Professor Muneki Yasuda whose informal and friendly style of supervision I especially appreciated. I would also like to thank the students of the Tanaka-Waizumi laboratory, including students who already graduated, for providing various advice regarding my research and creating a friendly research atmosphere. Finally, I wish to extend my sincere gratitude to the Japanese government and its Ministry of Education, Culture, Sports, Science and Technology (MEXT) for providing me with the scholarship that allowed me to study and perform research in Japan.

Bibliography

[1] R. Molina, "On the hierarchical Bayesian approach to image restoration: applications to astronomical images", *Pattern Analysis and Machine Intelligence, IEEE Transactions on*, vol.16, no.11, pp.1122-1128, November 1994.

[2] K. Tanaka and J. Inoue, "Maximum Likelihood Hyperparameter Estimation for Solvable Markov Random Field Model in Image Restoration", *IEICE Transactions on Information and Systems*, vol.E85-D, No.3, pp.546-557, March 2002.

[3] K. Tanaka, "Statistical-Mechanical Approach to Image Processing (Topical Review)", *Journal of Physics A: Mathematical and General*, Vol.35, No.37, pp.R81-R150, September 2002.

[4] K. Tanaka and T. Horiguchi, "Solvable Markov random field model in color image restoration" *Physical review. E, Statistical, nonlinear, and soft matter physics*, Vol.65, No.4, pp.046142.1-046142.18, April 2002.

[5] H. Nishimori, *Statistical Physics of Spin Glasses and Information Processing, An Introduction* (Oxford University Press, 2001).

[6] C. Fan and F. Y. Wu, "Ising Model with Second-Neighbor Interaction. I. Some Exact Results and an Approximate Solution", *Physical Review* Vol.179, No.2, pp.560-569, March 1969.

[7] S. Amari, "Dynamics of Pattern Formation in Lateral-Inhibition Type Neural Fields", *Biological Cybernetics*, Vol.27, pp.77-87, June 1977.

[8] D. C. Somers, S. B. Nelson and M. Sur, "An emergent model of orientation selectivity in cat visual cortical simple cells", *Journal of Neuroscience*, Vol.15, pp.5448-5465, August 1995.

[9] K. Takiyama, Y. Naruse, M. Okada, "Statistical Mechanics of Mexican-Hat-Type Horizontal Connection", *Journal of the Physical Society of Japan*, Vol.78, No.6, pp.064002.1-064002.6, May 2009.

[10] H. Rue and L. Held, *Gaussian Markov random fields : theory and applications* (Chapman & Hall/CRC, 2005).

[11] S. Moriguchi, K. Udagawa and S. Hitotumatu, *Iwanami Suugaku Koushiki I* (Iwanami Shoten, 2005) (in Japanese).

[12] Yu. A. Shashkin, *Fixed Points* (American Mathematical Society, 1991).

[13] Z. Wang and A. C. Bovik, "Mean Squared Error: Love It or Leave It? A new look at Signal Fidelity Measures", *Signal Processing Magazine, IEEE*, vol.26, no.1, pp.98-117, Jan. 2009.

[14] Z. Wang and A. C. Bovik, "Image quality assessment: from error visibility to structural similarity", *Image Processing, IEEE Transactions on*, vol.13, no.4, pp.600-612, April 2004.

[15] Z. Wang, A. C. Bovik, H. R. Sheikh and E. P. Simoncelli, *The SSIM Index for Image Quality Assessment*, (http://www.ece.uwaterloo.ca/ z70wang/research/ssim/, December 1, 2009).

[16] K.B. Petersen and M.S. Pedersen, *The Matrix Cookbook*, (http://matrixcookbook.com/, February 16, 2008).

Research Achievements

Research Papers

Kazuyuki Tanaka, Nicolas Morin, Muneki Yasuda and D. M. Titterington: Probabilistic image processing by extended Gauss-Markov random fields, Proceedings of IEEE/SP 15th Workshop on Statistical Signal Processing (August 31-September 3, 2009, University of Cardiff, Wales, UK), pp.618-621.